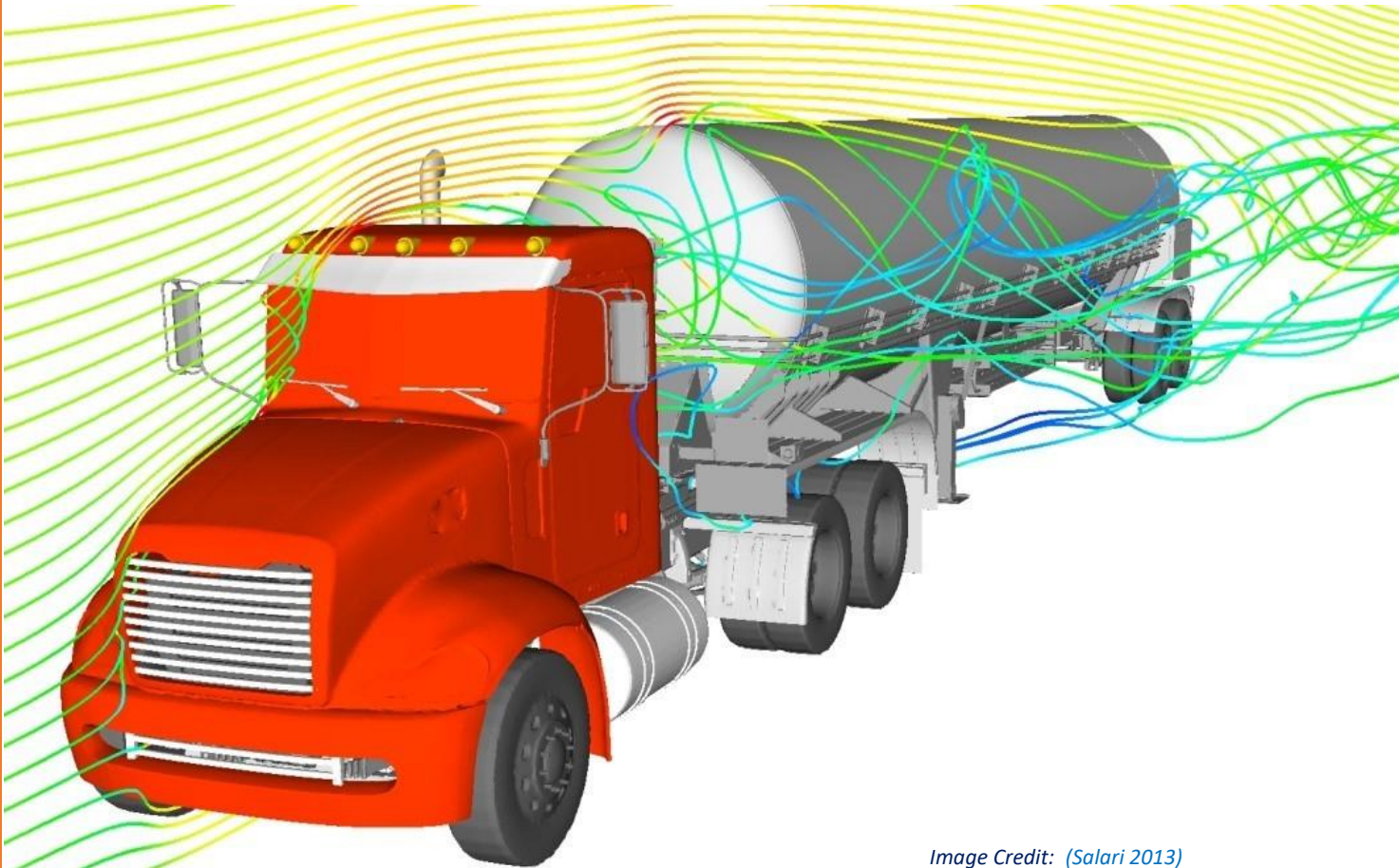


OCTOBER 11, 2023

# NUMERICAL SIMULATION ON THE AERODYNAMIC PERFORMANCE OF A SEMI- TRAILER TANKER UNDER CROSSWINDS



*Image Credit: (Salari 2013)*

PREPARED BY

**Uy Ngo**

Student ID: [REDACTED]

University of Southern Queensland

Course: ENG4111 & ENG4112

Supervisor: Dr Ahmad Sharifian-Barforoush

11 October 2023

**University of Southern Queensland**  
**Faculty of Health, Engineering and Sciences**

*Numerical simulation on the Aerodynamic performance of a  
semi-trailer tanker under crosswinds*

A dissertation submitted by

**Mr Uy Truong Ngo**

in fulfilment of the requirements of

**Courses ENG4111 and ENG4112 Research Project**

towards the degree of

**Bachelor of Engineering (Mechanical Engineering)**

Submitted October 2023

**University of Southern Queensland**  
**Faculty of Health, Engineering and Sciences**

**ENG4111/ENG4112 Research Project**

**LIMITATION OF USE**

The Council of the University of Southern Queensland, its Faculty of Health, Engineering & Sciences, and the University of Southern Queensland staff do not accept any responsibility for the truth, accuracy or completeness of material contained within or associated with this dissertation.

Persons using all or any part of this material do so at their own risk and not at the risk of the Council of the University of Southern Queensland, its Faculty of Health, Engineering & Sciences or the staff of the University of Southern Queensland.


This dissertation reports an educational exercise and has no purpose or validity beyond this exercise. The sole purpose of the course pair entitled "Research Project" is to contribute to the general education within the student's chosen degree program. This document, the associated hardware, software, drawings, and other material in the related appendices should not be used for any other purpose. It is entirely at the user's risk if they are used.

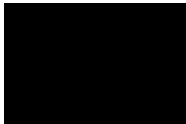
## CERTIFICATION OF DISSERTATION

I certify that this dissertation's ideas, designs, experimental work, results, analyses and conclusions are entirely my effort, except where otherwise indicated and acknowledged.

I also certify that the work is original and has not been previously submitted for assessment in any other course or institution except where specifically stated.

Uy Truong Ngo

Student Number: 



\_\_\_\_\_  
Signature

\_\_\_\_\_  
11/10/2023

Date



## ACKNOWLEDGEMENTS

The author, Uy Truong Ngo, wishes to express sincere gratitude to the following individuals:

First and foremost, I extend my most profound appreciation to Dr. Ahmad Sharifian-Barforoush for his unwavering support, invaluable guidance, and dedication throughout this project. Dr. Sharifian-Barforoush was an exceptional supervisor and played a pivotal role in enhancing my comprehension of Computational Fluid Dynamics. His expertise in ANSYS proved indispensable in weaving together all the facets of this research.

Additionally, I would like to acknowledge Mr. Mark Skinner for his generosity in providing crucial technical data related to the semi-trailer tanker. His contributions played a vital role in conducting preliminary calculations and laid the foundation for the success of this project.

Finally, I also wish to express my gratitude to Associate Professor Andrew Wandel for his assistance with the installation and licensing issues related to the Ansys Software during the project. His expertise with the Ansys Software was invaluable in saving time and effort.

The contributions of these individuals, both in terms of mentorship and technical support, have been instrumental in shaping the course of this research and have had a lasting impact on my personal and academic growth.

## ABSTRACT

The liquid transportation industry relies heavily on road tankers to transport hazardous and non-hazardous liquids efficiently and safely, playing a pivotal role in the global economy. However, road tankers face a significant challenge due to aerodynamic resistance, resulting in high fuel consumption rates compared to passenger vehicles (ABS 2020).

Previous studies have shown that installing aerodynamic devices, such as side skirts and gap fairings, significantly reduces drag forces under headwinds. However, generating aerodynamic resistance, or drag force, during crosswind scenarios presents a substantial risk, potentially leading to accidents such as rollovers, sideslips, and rotations. This risk is particularly elevated for vehicles transporting hazardous materials, as road tankers carry unfixed loads, possessing significant size, weight, and a high centre of gravity. These crosswind-induced accidents can be catastrophic and may lead to explosions or fires (Batista & Perkovič 2014).

This research investigates methods to improve semitrailer tankers' aerodynamic performance and stability when subjected to crosswind conditions. The study encompasses comprehensive simulations and analysis, focusing on the impact of various aerodynamic devices and design modifications on the vehicle's behaviour.

The research begins with headwind and crosswind simulations, encompassing wind angles ranging from 15 to 90 degrees. Results indicate that adding specific aerodynamic enhancements, such as tractor side skirts, tractor-trailer gap fairings, and trailer side skirts, substantially reduces the drag coefficient by up to 18%, aligning with prior research findings.

Safety assessments highlight the potential increase in lateral drag and the rotational and rollover moments caused by these enhancements, particularly at wind angles of 15 and 30 degrees, posing challenges to vehicle stability. The analysis concludes that the aerodynamic tanker is unlikely to experience sideslip, rotation, or rollover accidents under typical crosswind conditions. However, the increased lateral drag and yawing moments should be carefully considered.

A pre-optimization study emphasizes the critical importance of side skirts, precisely the design issues contributing to flow separation and increased rotational moments. Proposed modifications involve repositioning and redesigning side skirts to mitigate these effects while maintaining compliance with safety regulations and standards. Simulations indicate significant reductions in rotational moments and axial drag coefficients under crosswind conditions at 15 and 30 degrees, significantly enhancing stability and predictability.

The research offers valuable insights into optimizing aerodynamic devices to enhance vehicle stability and safety in crosswind conditions. The choice between the original and modified aerodynamic tanker configurations should align with specific operational requirements and lateral and yawing stability considerations.

## Table of Contents

LIMITATION OF USE .....	ii
CERTIFICATION OF DISSERTATION .....	iii
ACKNOWLEDGEMENTS .....	iv
ABSTRACT .....	v
List of Figures .....	x
List of Tables .....	xiv
CHAPTER 1 – INTRODUCTION .....	1
1.1 Background .....	1
1.2 Overview of current research in the aerodynamic performance of road tankers .....	2
1.2.1 Introduction .....	2
1.2.2 The research conducted by McCallen et al. (2005-2013) – “DOE’s Effort to Improve Heavy Vehicle Aerodynamics through Joint Experiments and Computations.” .....	3
1.2.3 The research by Miralbes & Ferrer (2009) – “Analysis of Some Aerodynamic Improvements for Semi-Trailer Tankers Research.” .....	6
1.2.4 Limitation on the Apply of Aerodynamic Devices .....	7
1.3. Research Gaps .....	8
1.3.1 Introduction .....	8
1.3.2 “A Study on Aerodynamic Drag of a Semi-trailer Truck” by Chowdhury et al. (2013) .....	9
1.3.3 “Considerable Drag Reduction and Fuel Saving of a Tractor-trailer Using Additive Aerodynamic Devices” by Kim et al. (2019) .....	11
1.3.4 “DOE’s Effort to Improve Heavy Vehicle Fuel Efficiency Through Improved Aerodynamics” project conducted by Salari (2016) .....	12
1.3.5 Summary of research gaps .....	13
1.4 Research Aims and Objectives .....	14
1.5 Outline of the Study .....	15
1.5.1 Project Limitation .....	16
1.5.2 Project Plan (Project Specifications) .....	17
1.6 Dissertation Outline .....	18
Chapter 1 – Introduction .....	18
Chapter 2 – Literature Review .....	19
Chapter 3 – Research Methodology .....	20
Chapter 4 – CFD Performance .....	20
Chapter 5 – Result and Discussion .....	21
Chapter 6 – Conclusion .....	22
1.7 Risk Assessment .....	22

1.8 Resource Requirements.....	23
1.9 Project Timelines.....	23
CHAPTER 2 – LITERATURE REVIEW .....	24
2.1 Introduction .....	24
2.2 Study of Aerodynamics .....	24
2.3 Headwind and Crosswind Effects on the Aerodynamics of Vehicles.....	25
2.3.1 Drag and lift force and its effects on moving body.....	25
2.3.2 Equation of drag and lift force exerted on a vehicle .....	26
2.3.2 Effects of Headwind on the aerodynamic performance of road tanker.....	27
2.3.3 Effects of Crosswind on the aerodynamic performance of road tankers.....	27
2.4 Various crosswind-induced accidents.....	30
2.4.1 Aerodynamic Forces and Moments of Crosswind .....	30
2.4.2 Critical relative wind speed for Rollover to occur.....	35
2.4.3 Critical relative wind speed for rotation to occur.....	36
2.4.4 Critical relative wind speed for sideslip to occur.....	36
2.5 Current regulations and design rules for road tankers carrying dangerous goods .....	37
2.5.1 Introduction .....	37
2.5.2 Static Roll Threshold (SRT) .....	37
2.5.3 Performance-Based Standards (PBS) .....	40
2.5.4 Australian Design Rules (ADRs).....	42
2.5.5 Australian Standards for Road Tank Vehicles Carrying Dangerous Goods .....	43
2.6. CFD Modelling of Flow Over a Tractor-Semitrailer Tanker.....	48
2.6.1 Introduction .....	48
2.6.2 CFD Pre-Processing Stage .....	49
2.6.3 CFD Solving Stage.....	60
2.6.4 CFD Post-Processing Stage.....	63
CHAPTER 3 – RESEARCH METHODOLOGY.....	67
3.1 Research Methodology Introduction.....	67
3.2 Static Loaded Radius of Tyres .....	69
3.3 Tractor Selection and Modelling.....	69
3.4 Semitrailer Tanker Selection and Modelling.....	71
3.5 Rollover Threshold Determining Process.....	73
a) Data collection process:.....	73
b) SRT value Calculation Process.....	75
c) Calculating the side force causing the trailer to roll over .....	77
3.6 Critical Lateral Force to cause semi-trailer to slip sideways and rotate .....	78

3.7 Tractor-trailer combination details.....	79
CHAPTER 4 – CFD SETUP AND PERFORMANCE.....	81
4.1 CFD Pre-Processing Stage .....	81
4.1.1 Introduction .....	81
4.1.2 Geometry Creation and Simplification.....	81
4.1.3 Computational Domain.....	81
4.1.4 Mesh Generation and Mesh Quality Checking .....	82
4.2 CFD Solving Stage.....	86
4.2.1 Set-up steps.....	86
4.2.2 Solution control.....	90
4.3 CFD Post-Processing Stage.....	91
4.4 Solution Initialisation and Calculation .....	91
CHAPTER 5 – RESULT AND DISCUSSION.....	92
5.1 Introduction .....	92
5.2 Validating Headwind Simulation Results .....	92
5.3 Studying crosswind simulation results.....	94
5.3.1 Calculation of force and moment coefficient .....	94
5.3.2 Studying the simulation results.....	96
5.4: Determination of the likelihood of sideslip, rotation, or rollover accidents .....	113
5.5 Pre-Optimisation Study.....	113
5.5.1 Investigation of Aerodynamic Devices.....	113
5.5.2 Optimisation of Aerodynamic Devices.....	115
CHAPTER 6 – CONCLUSION .....	135
6.1 Overview .....	135
6.2 Conclusion.....	135
6.3 Limitation and Future Work.....	136
REFERENCES .....	138
APPENDICES .....	141
Appendix A – Original Project Specification .....	141
Appendix B – Resource Requirements.....	142
Appendix C – Project Timelines .....	143
Appendix D – Risk Management.....	144
Appendix E – Semi-Trailer Tanker Specification .....	145
E.1 Geometry of the Baseline Kenworth 6x4 T610 .....	145
E.2 Geometry of the Kenworth 6x4 T610 tractor with tractor side skirts and tractor-trailer gap fairing .....	145

E.3 The geometry of a baseline semi-trailer tanker.....	146
E.4 The geometry of a semi-trailer tanker with side skirts.....	146
E.5 Geometry of baseline tractor-semitrailer .....	147
E.6 Geometry of tractor-semitrailer tanker equipped with aerodynamic devices.....	148
Appendix F – SRT calculators .....	149
F.1 SRT calculator published by Western Australia Government .....	149
F.2 SRT calculator published by New Zealand Government (Link: <a href="https://www.ternz.co.nz/SRT_Calculator/main.html">https://www.ternz.co.nz/SRT_Calculator/main.html</a> ) .....	152
Appendix G – Semi-trailer general safety requirements .....	153
Appendix H – Baseline and Aerodynamic Tankers Simulation Results Graphs and Contours.....	154
H.1 X-Y Chart of Headwind Simulation: .....	154
H.2 X-Y Chart of 15-Degree Crosswind Simulation: .....	155
H.3 Pressure Contours and Flow Pathlines of Baseline and Aerodynamic Tankers at 0-Degree Crosswind Angle.....	156
H.4 Pressure Contours and Flow Pathlines of Baseline and Aerodynamic Tankers at 30-Degree Crosswind Angle.....	159
H.5 Pressure Contours and Flow Pathlines of Baseline and Aerodynamic Tankers at 45-Degree Crosswind Angle.....	161
H.6 Pressure Contours and Flow Pathlines of Baseline and Aerodynamic Tankers at 60-Degree Crosswind Angle.....	163
H.7 Pressure Contours and Flow Pathlines of Baseline and Aerodynamic Tankers at 75-Degree Crosswind Angle.....	166
H.8 Pressure Contours and Flow Pathlines of Baseline and Aerodynamic Tankers at 90-Degree Crosswind Angle.....	168
Appendix I –Modified Aerodynamic and Aerodynamic Tankers Simulation Contours and Pathlines .....	171
I.1 Pressure Contours and Flow Pathlines of Modified Aerodynamic and Aerodynamic Tankers at 0-Degree Crosswind Angle.....	171
I.2 Pressure Contours and Flow Pathlines of Modified Aerodynamic and Aerodynamic Tankers at 30-Degree Crosswind Angle.....	173
I.3 Pressure Contours and Flow Pathlines of Modified Aerodynamic and Aerodynamic Tankers at 45-Degree Crosswind Angle.....	176
I.4 Pressure Contours and Flow Pathlines of Modified Aerodynamic and Aerodynamic Tankers at 60-Degree Crosswind Angle.....	178
I.5 Pressure Contours and Flow Pathlines of Modified Aerodynamic and Aerodynamic Tankers at 75-Degree Crosswind Angle.....	180
I.6 Pressure Contours and Flow Pathlines of Modified Aerodynamic and Aerodynamic Tankers at 90-Degree Crosswind Angle.....	183

## List of Figures

Figure 1.2-1: Flux around the tanker trailer. Source (R.Miralbes 2012) .....	3
Figure 1.2-2: Major drag sources on a trailer tanker. Source (Salari 2013).....	5
Figure 1.2-3: The effect of the tractor-tanker gap on the drag coefficient. Source (Salari 2013) .....	5
Figure 1.2-4: The impact of tanker underbody treatment on the drag coefficient. Source (Salari 2013) .....	6
Figure 1.2-5: Aerodynamic skirt for the configuration with boxes in the lower zone. Source (R.Miralbes 2012).....	7
Figure 1.2-6: Vehicle tanker with the aerodynamic forehead. Source (R.Miralbes 2012) .....	7
Figure 1.2-7: Aerodynamic adapter for the rear box. Source (R.Miralbes 2012) .....	7
Figure 1.3-8: Experimental arrangement in the test section of RMIT Wind Tunnel (Chowdhury et al. 2013) .....	10
Figure 1.3-9: Different combinations of fairing on the baseline semi-trailer truck model (Chowdhury et al. 2013) .....	10
Figure 1.3-10: Drag reduction over the base vehicle in percentage as a function of yaw angle (Chowdhury et al. 2013) .....	10
Figure 1.3-11: Schematics of the side, top and isometric views of (a) gap fairing, (b) flap-type side skirt, and (c) LIAD boat tail attached to a tractor-trailer model (Kim et al. 2019).....	11
Figure 1.3-12: Variations in (a) drag coefficient (CD) and (b) CD reduction rate of the reference vehicle model with attached additive aerodynamic devices according to yaw angle. Variations in (c) drag coefficient (CD) and (d) CD reduction rate of gap fairing-based vehicle model with attached additive aerodynamic devices according to yaw angle. (Kim et al. 2019) .....	12
Figure 1.3-13: Tanker 1 Geometry (Salari 2016) .....	13
Figure 1.3-14: Tanker 2 Geometry (Salari 2016) .....	13
Figure 1.3-15: Test Results (Salari 2016).....	13
Figure 1.5-16: Semi-trailer Tanker (Salari 2013) .....	16
Figure 2.3-17: Drag and Lift Forces on an aerofoil. Souce: (Çengel et al. 2017).....	25
Figure 2.3-18: Vehicle accidents in crosswind. Source (Batista & Perkovič 2014) .....	29
Figure 2.3-19: Rollover accident of road tankers in Oct-2014. Source: Metropolitan Engineering .....	29
Figure 2.3-20: Road tanker rollover.Source: Metropolitan Engineering .....	30
Figure 2.4-21: Forces and Moments acting on the vehicle. Source (Batista & Perkovič 2014) .....	31
Figure 2.4-22: Aerodynamic force and moment caused by crosswind. Source (Batista & Perkovič 2014) .....	33
Figure 2.5-23: Relationship between rollover crash risk and SRT. Source (De Pont et al. 2002) .....	38
Figure 2.5-24: Vehicle Roll Notation. Source (De Pont et al. 2002) .....	38
Figure 2.5-25: Minimum Force that causes Rollover to occur. Source (De Pont 2017).....	40
Figure 2.5-26: The PBS approval process. Source (NHVR 2022) .....	41
Figure 2.5-27: Frontal Swing Requirement. Source (NHVR 2022) .....	41
Figure 2.5-28: Envelope of Semi-Trailer. Source (ADRs 2006c) .....	43
Figure 2.5-29: Stability Angle of road tank vehicle. Source Tigerspider .....	45
Figure 2.6-30: Computational domain for a CFD simulation of a heavy-goods vehicle. (Idealsimulations 2020a).....	50
Figure 2.6-31: Triangular mesh example (Versteeg & Malalasekera 2011).....	52
Figure 2.6-32: Hexahedral (A-D) and tetrahedral (E-H) meshes. (Sharma et al. 2017) .....	52
Figure 2.6-33: A grid consisting of polyhedral cells of the 90° bend geometry. (Tu et al. 2018) .....	53
Figure 2.6-34: Turbulence models in CFD (Idealsimulations 2020b) .....	55
Figure 2.6-35: An overview of the solution procedure (Tu et al. 2018). .....	61

Figure 2.6-36: Typical ANSYS CFX GUIs for monitoring convergence (Tu et al. 2018).....	62
Figure 2.6-37: Typical FLUENT GUIs for monitoring convergence (Tu et al. 2018).....	63
Figure 2.6-38: X–Y plot of the normalized horizontal velocity along the length (Tu et al. 2018). ....	64
Figure 2.6-39: Velocity vectors showing the flow development along the parallel-plate channel (Tu et al. 2018) .....	65
Figure 2.6-40: Velocity vectors accentuating the localized wake recirculation zones (Tu et al. 2018).65	
Figure 2.6-41: Example of Flooded Contours on rainbow-scale colour map (Tu et al. 2018). ....	66
Figure 2.6-42: Example of Line contours on a rainbow-scale colour map (Tu et al. 2018). ....	66
Figure 3.2-43: Tyre's Static Loaded Radius and Free Radius (Pacejka 2012) .....	69
Figure 3.3-44: Real Kenworth T610 Night Cab and its simplified model (Kenworth_AU 2023) .....	71
Figure 3.3-45: Simplified Kenworth T610 with side skirts and tractor-trailer gap fairing .....	71
Figure 3.4-46: Tri-axle, 5-compartment semitrailer tanker (ATE_Tankers 2023).....	72
Figure 3.4-47: Isometric views of simplified semitrailer tankers without side skirts. ....	73
Figure 3.4-48: Isometric views of simplified semitrailer tankers with side skirts.....	73
Figure 3.4-49: Details of side skirts installed on semi-trailer tanker .....	73
Figure 3.5-50: Semitrailer details.....	74
Figure 3.5-51: Load data of semitrailer tanker .....	75
Figure 3.5-52: Step 1 - Selecting the Type of Vehicle .....	75
Figure 3.5-53: Step 2 - Inputing Tyre and Axle Data .....	76
Figure 3.5-54: Step 3 - Inputing Unsprung mass, Sprung mass, and load type and geometry.....	76
Figure 3.5-55: Step 4 - Inputing suspension data .....	77
Figure 3.5-56: Result of the estimated SRT value .....	77
Figure 3.7-57: Baseline and Aerodynamic Tractor-Semitrailer Tankers .....	80
Figure 4.1-58: Simplified Baseline Tractor-Trailer .....	81
Figure 4.1-59: Simplified Aerodynamic Tractor-Trailer .....	81
Figure 4.1-60: Computational Domain of a tractor-semitrailer tanker. ....	82
Figure 4.1-61: Adding Local Sizes.....	83
Figure 4.1-62: Surface Mesh Quality.....	84
Figure 4.1-63: Baseline Model Final Volume Mesh. ....	84
Figure 4.1-64: Aerodynamic Model Final Volume Mesh. ....	85
Figure 65: Domain Description .....	86
Figure 66: Cell Zone Conditions .....	87
Figure 4.2-67: Boundary Definition for Headwind Simulation .....	88
Figure 4.2-68: Boundary Definition for Crosswind Simulation .....	89
Figure 4.2-69: Residual Monitors.....	90
Figure 4.4-70: Solution Initialisation .....	91
Figure 4.4-71: Calculation Running .....	91
Figure 5.2-72: Reference Values for both Baseline and Aerodynamic Models .....	93
Figure 5.2-73: Drag Coefficient of Baseline Model .....	93
Figure 5.2-74: Drag Coefficient of Aerodynamic Model .....	94
Figure 5.3-75: Impact of Crosswind on Forces and Moments Coefficient of Aerodynamic Tankers at Various Wind Angles .....	98
Figure 5.3-76: Impact of Aerodynamic Devices on Axial Drag Coefficient ( $C_z$ ) .....	99
Figure 5.3-77: Impact of Aerodynamic Devices on Lateral Drag Coefficient ( $C_x$ ).....	99
Figure 5.3-78: Impact of Aerodynamic Devices on Lift Coefficient ( $C_y$ ) .....	100
Figure 5.3-79: Impact of Aerodynamic Devices on Pitching Moment Coefficient ( $C_{PM}$ ).....	100
Figure 5.3-80: Impact of Aerodynamic Devices on Rotational Moment Coefficient ( $C_{RM}$ ) .....	101
Figure 5.3-81: Impact of Aerodynamic Devices on Rollover Moment Coefficient ( $C_{ROM}$ ).....	101



Figure 5.3-82: Static Pressure on the Winward Side of Baseline Tanker 15-degree crosswind angle	102
Figure 5.3-83: Static Pressure on the Winward Side of Aerodynamic Tanker 15-degree crosswind angle.....	102
Figure 5.3-84: Static Pressure on the Leeward Side of Baseline Tanker 15-degree crosswind angle	103
Figure 5.3-85: Static Pressure on the Leeward Side of Aerodynamic Tanker 15-degree crosswind angle.....	103
Figure 5.3-86: Total Pressure on the Windward Side of Baseline Tanker 15-degree crosswind angle .....	104
Figure 5.3-87: Total Pressure on the Windward Side of Aerodynamic Tanker 15-degree crosswind angle.....	104
Figure 5.3-88: Total Pressure on the Leeward Side of Baseline Tanker 15-degree crosswind angle .	105
Figure 5.3-89: Total Pressure on the Leeward Side of Aerodynamic Tanker 15-degree crosswind angle .....	105
Figure 5.3-90: Flow Around Baseline Tanker at 15-degree crosswind angle.....	106
Figure 5.3-91: Flow Around Aerodynamic Tanker at 15-degree crosswind angle.....	106
Figure 5.3-92: Flow Around Baseline Tanker at 15-degree crosswind angle – Top View .....	107
Figure 5.3-93: Flow Around Aerodynamic Tanker at 15-degree crosswind angle – Top View.....	107
Figure 5.3-94: Flow Around Baseline Tanker at 15-degree crosswind angle – Underside View .....	108
Figure 5.3-95: Flow Around Aerodynamic Tanker at 15-degree crosswind angle – Underside View	108
Figure 5.3-96: Elevation View of Flow Around Baseline Tanker at 15-degree crosswind angle - Winward Side.....	109
Figure 5.3-97: Elevation View of Flow Around Aerodynamic Tanker at 15-degree crosswind angle - Winward Side.....	109
Figure 5.3-98: Elevation View of Flow Around Baseline Tanker at 15-degree crosswind angle - Leeward Side.....	110
Figure 5.3-99: Elevation View of Flow Around Aerodynamic Tanker at 15-degree crosswind angle - Leeward Side.....	110
Figure 5.3-100: Isometric View of Flow Around Baseline Tanker at 15-degree crosswind angle - Windward Side.....	111
Figure 5.3-101: Isometric View of Flow Around Aerodynamic Tanker at 15-degree crosswind angle - Windward Side.....	111
Figure 5.3-102: Isometric View of Flow Around Baseline Tanker at 15-degree crosswind angle - Leeward Side.....	112
Figure 5.3-103: Isometric View of Flow Around Aerodynamic Tanker at 15-degree crosswind angle - Leeward Side.....	112
Figure 5.5.1-104: Flow at Leeward Side of Aerodynamic Tanker .....	114
Figure 5.5.1-105: Flow at Windward Side of Aerodynamic Tanker .....	114
Figure 5.5.1-106: Aerodynamic Tanker.....	115
Figure 5.5.2-107: Detail of Side Skirt Improvement .....	116
Figure 5.5.2-108: Comparison of Axial Drag Coefficient.....	120
Figure 5.5.2-109: Comparison of Lateral Drag Coefficient.....	120
Figure 5.5.2-110: Comparison of Lift Coefficient .....	121
Figure 5.5.2-111: Comparison of Pitch Moment Coefficient .....	121
Figure 5.5.2-112: Comparison of Yawing Moment Coefficient.....	122
Figure 5.5.2-113: Comparison of Rollover Moment Coefficient.....	122
Figure 5.5.2-114: Static Pressure on the Winward Side of Modified Aerodynamic Tanker 15-degree crosswind angle.....	123

Figure 5.5.2-115: Static Pressure on the Winward Side of Aerodynamic Tanker 15-degree crosswind angle.....	123
Figure 5.5.2-116: Static Pressure on the Leeward Side of the Modified Aerodynamic Tanker 15-degree crosswind angle .....	124
Figure 5.5.2-117: Static Pressure on the Leeward Side of Aerodynamic Tanker 15-degree crosswind angle.....	124
Figure 5.5.2-118: Total Pressure on the Windward Side of Modified Aerodynamic Tanker 15-degree crosswind angle.....	125
Figure 5.5.2-119: Total Pressure on the Windward Side of Aerodynamic Tanker 15-degree crosswind angle.....	125
Figure 5.5.2-120: Total Pressure on the Leeward Side of Modified Aerodynamic Tanker 15-degree crosswind angle.....	126
Figure 5.5.2-121: Total Pressure on the Leeward Side of Aerodynamic Tanker 15-degree crosswind angle.....	126
Figure 5.5.2-122: Flow Around Modified Aerodynamic Tanker at a 15-degree crosswind angle. ....	127
Figure 5.5.2-123: Flow Around Aerodynamic Tanker at 15-degree crosswind angle.....	127
Figure 5.5.2-124: Flow Around Modified Aerodynamic Tanker at 15-degree crosswind angle – Top View. ....	128
Figure 5.5.2-125: Flow Around Aerodynamic Tanker at 15-degree crosswind angle – Top View.....	128
Figure 5.5.2-126: Flow Around Modified Aerodynamic Tanker at 15-degree crosswind angle – Underside View.....	129
Figure 5.5.2-127: Flow Around Aerodynamic Tanker at 15-degree crosswind angle – Underside View. ....	129
Figure 5.5.2-128: Elevation View of Flow Around Modified Aerodynamic Tanker at 15-degree crosswind angle - Winward Side. ....	130
Figure 5.5.2-129: Elevation View of Flow Around Aerodynamic Tanker at 15-degree crosswind angle - Winward Side.....	130
Figure 5.5.2-130: Elevation View of Flow Around Modified Aerodynamic Tanker at 15-degree crosswind angle - Leeward Side. ....	131
Figure 5.5.2-131: Elevation View of Flow Around Aerodynamic Tanker at 15-degree crosswind angle - Leeward Side.....	131
Figure 5.5.2-132: Isometric View of Flow Around Modified Aerodynamic Tanker at 15-degree crosswind angle - Windward Side. ....	132
Figure 5.5.2-133: Isometric View of Flow Around Aerodynamic Tanker at 15-degree crosswind angle - Windward Side.....	132
Figure 5.5.2-134: Isometric View of Flow Around Modified Aerodynamic Tanker at 15-degree crosswind angle - Leeward Side. ....	133
Figure 5.5.2-135: Isometric View of Flow Around Aerodynamic Tanker at 15-degree crosswind angle - Leeward Side.....	133

## List of Tables

Table 1.3-1: Percentage reduction of drag (D) on yaw angle variation from 0° to 15° over the baseline (Chowdhury et al. 2013) .....	10
Table 2.5-2: Maximum weight and weight distribution of Level 1 semi-trailer. Source (NHVR 2022). 42	
Table 2.5-3: Minimum material grades and mechanical properties (Standards_Australia 2020a).....	46
Table 2.5-4: Thickness of material for U-coamings and valances. Source (Standards_Australia 2020a) .....	46
Table 2.5-5: Example of heights for rollover protection. Source (Standards_Australia 2020a).....	47
Table 3.5-6: Summary of data required for the SRT calculator .....	74
Table 3.6-7: Average Values of Coefficient of Road Adhesion (Wong 2001).....	79
Table 3.6-8: Critical lateral force at different road surface conditions .....	79
Table 4.1-9: Comparison between meshing time and mesh quality .....	83
Table 4.1-10: Geometry's meshing details .....	85
Table 4.2-11: Headwind and Crosswind at Difference Wind Angle.....	88
Table 4.2-12: Boundary Condition for Headwind Simulation .....	89
Table 4.2-13: Boundary Condition for Crosswind Simulation at Difference Wind Angles From 0 to 90 degrees.....	89
Table 4.2-14: Definition of Forces and Moments .....	91
Table 5.2-15: Headwind Simulation Results .....	93
Table 5.3-16: Simulation Results of Crosswind for Baseline and Aerodynamic Tankers.....	95
Table 5.5.2-17: Simulation Results of Crosswind for Baseline and Improved Aerodynamic Tankers	116
Table 5.5.2-18: Comparison of Original Aerodynamic and Improved Aerodynamic Tankers .....	119

## CHAPTER 1 – INTRODUCTION

### 1.1 [Background](#)

The liquid transportation industry is an indispensable pillar of the global economy, facilitating the cost-effective, efficient, and secure movement of vast liquid volumes worldwide. This vital sector encompasses the transportation of diverse liquids, including petroleum, chemicals, and food-grade products, utilizing an array of vessels such as tankers, ships, and specialized containers.

Road tankers, comprising both rigid and articulated variants, play a pivotal role in the terrestrial segment of this industry. These vehicles primarily transport hazardous and nonhazardous liquids, gases, chemicals, and dry bulk cargo from refineries to distribution centres, retailers, and industrial sites nationally.

Providing the precise number of road tankers registered in Australia and worldwide proves challenging. As of June 30, 2020, the Australian Bureau of Statistics (ABS) reported 19,768,518 registered vehicles in Australia. Among these, 512,255 were rigid trucks, and approximately 104,442 were articulated trucks, accounting for 2.6% and 0.5% of the total registered vehicles. Within these categories, it's estimated that there are about 15,632 rigid tankers and 19,229 tanker trailers. Notably, these rigid and articulated trucks collectively consume approximately 7,480 megalitres of fuel annually, constituting 23.2% of the total fuel consumption by all vehicles in Australia each year. Remarkably, articulated trucks exhibit the highest fuel consumption rate per vehicle at 53.1 litres per 100 kilometres, in stark contrast to the average fuel consumption rate of passenger vehicles, which stands at 11.1 litres per 100 kilometres, as reported by ABS (2020).

A significant contributing factor to rigid and articulated trucks' high fuel consumption rate is the formidable aerodynamic resistance, commonly called drag force, encountered as these vehicles traverse through the atmosphere. The relationship between drag force and vehicle speed is non-linear—when speed doubles, drag force increases by four times; when speed triples, drag force increases ninefold, and so on (Hejdesten & Tenstam 2022). Consequently, It is estimated that about 50% of the truck engine power is used to overcome this drag force at the typical high speed of 90-100 km/h (Salati et al. 2017). As Hejdesten and Tenstam (2022) underscored, a truck's aerodynamics wield a profound and direct influence on fuel efficiency and, by extension, environmental impact.

The emergence and progress of virtual simulation methods have ushered in the potential for cost-effective analysis and visualization of a truck's airflow characteristics and aerodynamics. It has elevated the significance of research to reduce drag forces when designing heavy vehicles for enhanced fuel efficiency and stability. This focus has become paramount in recent years, as it contributes to reduced fuel consumption and enhances

energy efficiency. Moreover, it is noteworthy that this approach benefits the environment by lowering the overall environmental impact, irrespective of the fuel type employed by the truck. (Hejdesten & Tenstam 2022).

## 1.2 [Overview of current research in the aerodynamic performance of road tankers](#)

### 1.2.1 [Introduction](#)

Although many research and development efforts have been made to minimise the adverse effects of drag force on heavy trucks' aerodynamic performance, only a few have been conducted on road tankers. The reason for this study's efforts is that box container trucks and trailers are more commonly used for long-haul transportation than road tankers, especially for consumer goods and e-commerce deliveries. Besides, box container trucks have standard shapes and sizes compared to custom-built road tankers various shapes and sizes, making it easier to conduct aerodynamic research and designs. Therefore, greater demand exists to improve fuel efficiency and economy and reduce environmental impacts. Moreover, the transport industry is more willing to invest in improving the aerodynamics of box container trucks due to their widespread usage and the potential for cost savings. In contrast, the number of road tankers used in transportation is relatively small, and the design of road tankers carrying dangerous goods must adhere to lots of regulations and rules, making it difficult and less economically viable to invest in aerodynamic research and development for this vehicle type (Cooper 2003).

Fortunately, there has also been a few studies on the aerodynamic performance of road tankers in the last two decades. Most of the improvement inherits from the previous research for the box container heavy trucks. For example, considerable efforts focused on adding aerodynamic drag reduction devices such as tractor-trailer gap fairing and tractor and trailer side skirts, flow deflectors, and rear boat-tailing to manage airflow around the tanker (Cooper 2003).

The earliest method of improving road tanker aerodynamic performance was reducing the vehicle's overall weight, which reduced the power required to move it through the air by using aluminium material to construct the tank barrels. Another approach is to optimise the aerodynamic shape of the tanker's barrel by changing its shape from round or rectangular tanks to the more common cylindrical tanks with an oval cross-section to reduce its frontal area and create smoother surfaces to reduce turbulence (Service 2018).

In recent years, road tankers have continuously been developed with a greater focus on efficiency, safety and environmental sustainability. The principle of all the studies was to identify the diversion zones where the detachment of flow occurs and where the turbulence flow exists, as demonstrated in Figure 1.2-1. Through them, improvement would be developed to overcome the adverse drag effects (R.Miralbes 2012).

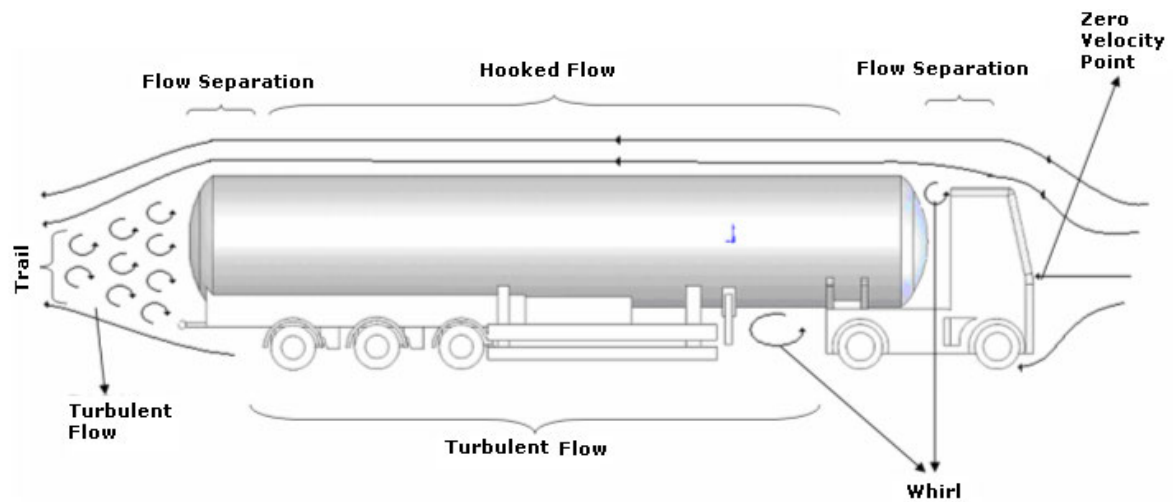


Figure 1.2-1: Flux around the tanker trailer. Source (R.Miralbes 2012)

Details of two research studies on the road tanker aerodynamic performance are listed below.

#### 1.2.2 The research conducted by McCallen et al. (2005-2013) – “DOE’s Effort to Improve Heavy Vehicle Aerodynamics through Joint Experiments and Computations.”

Research supported by the US Department of Energy was to establish a clear understanding of the drag-producing flow phenomena through joint experiments and computations, thus leading to the intelligent design of drag-reducing devices. This research aimed to include the development and demonstration of the ability to simulate and analyse aerodynamic flow around heavy truck vehicles using existing and advanced computational fluid dynamics (CFD) tools. Another effort was to set up an experiment method involving a full-scale wind tunnel and modern instrumentation, measurement techniques and diagnostics at Reynold numbers representative of highway conditions to validate the simulation results (McCallen et al. 2005).

In 2007, the research continued with further in-depth simulation to analyse aerodynamic flow around heavy truck vehicles and road tankers to establish key drag production flow characteristics. Besides, this research also investigated aerodynamic devices such as base flaps, tractor-trailer gap stabilisers, underbody skirts and wedges, and blowing and acoustic instruments, thus, providing the industry with conceptual designs of drag-reducing devices and demonstrating the full-scale fuel economy potential of these devices (McCallen et al. 2007).

In 2012, this research continued with the fuel economy track testing of selected aerodynamic devices at the Transportation Research Center (TRC) facility. It also continued to collect the road performance data for the selected aero devices in collaboration with Frito-Lay and Spirit fleets, designing and improving aerodynamic devices for tractor-trailers and road tankers (Salari 2013).

A year later (2013), the research completed the improvement of selected aero devices based on the knowledge gained from collected on-the-road performance data, conducting scaled experiments to validate the improved performance of aero devices for both tractor-trailers and road tankers as well as continuing with the development of the aerodynamic fairing for tanker trailers (Salari 2013).

As a result, this research experiment has found that, for class 8 tractor-trailer box container trucks, apart from tractor aerodynamic device adds-on such as top, sides and underbody fairing (drag coefficient value reduces by 0.018), tractor-trailer gap fairing (drag coefficient value reduces by 0.021), tanker trailer side skirts are still the most promising drag reduction device as it reduces the drag coefficient value by 0.073 (75% and 71% more than underbody and tractor-trailer gap fairings respectively) (McCallen et al. 2007).

Figure 1.2-2, Figure 1.2-3 and Figure 1.2-4 show several primary drag sources found on a trailer tanker, the impact of tractor-tanker gap and the effect of trailer tanker underbody treatment on the drag coefficient, respectively. Figure 2 shows that the drag coefficient jumps sharply at the tractor front axle, the hood, the tractor-trailer gap and the trailer rear axle group (bogie). In contrast, the wheelbase area (area between the tractor rear axle group and trailer axle group) has a high coefficient due to turbulent flow.

The DOE's research has found that the drag coefficient decreases sharply when the tractor-trailer gap becomes smaller, from  $C_d = 1.06$  when there is no tractor-trailer gap fairing to  $C_d = 0.79$  when the tractor-trailer gap is installed. When the area between the tractor's front and rear axle group is fully covered with the tractor side skirts, the drag coefficient  $C_d$  can be further reduced to 0.74 (about 30%), as shown in Figure 1.2-3.

Moreover, as shown in Figure 1.2-4, the maximum drag coefficient reduction of 39%, from  $C_d = 1.06$  to  $C_d = 0.65$ , occurs when a trailer tanker is equipped with tractor-trailer gap fairing, tractor sides skirts and trailer side skirts.

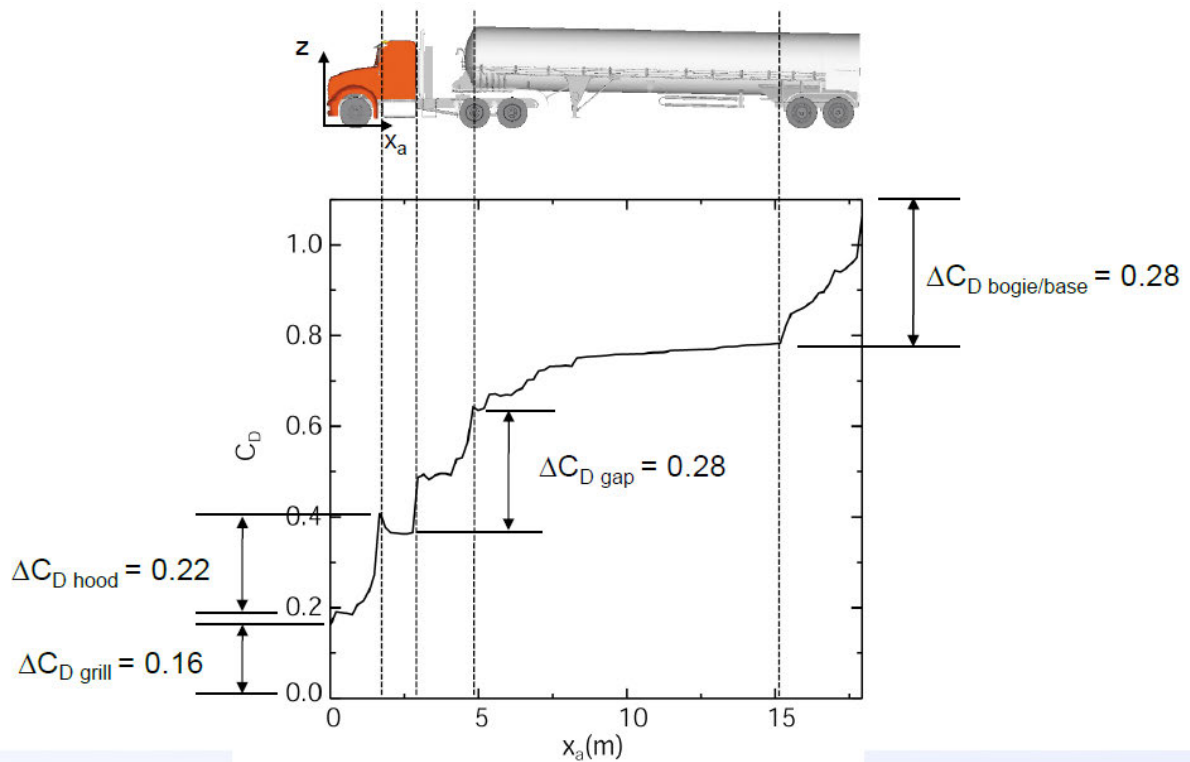


Figure 1.2-2: Major drag sources on a trailer tanker. Source (Salari 2013).

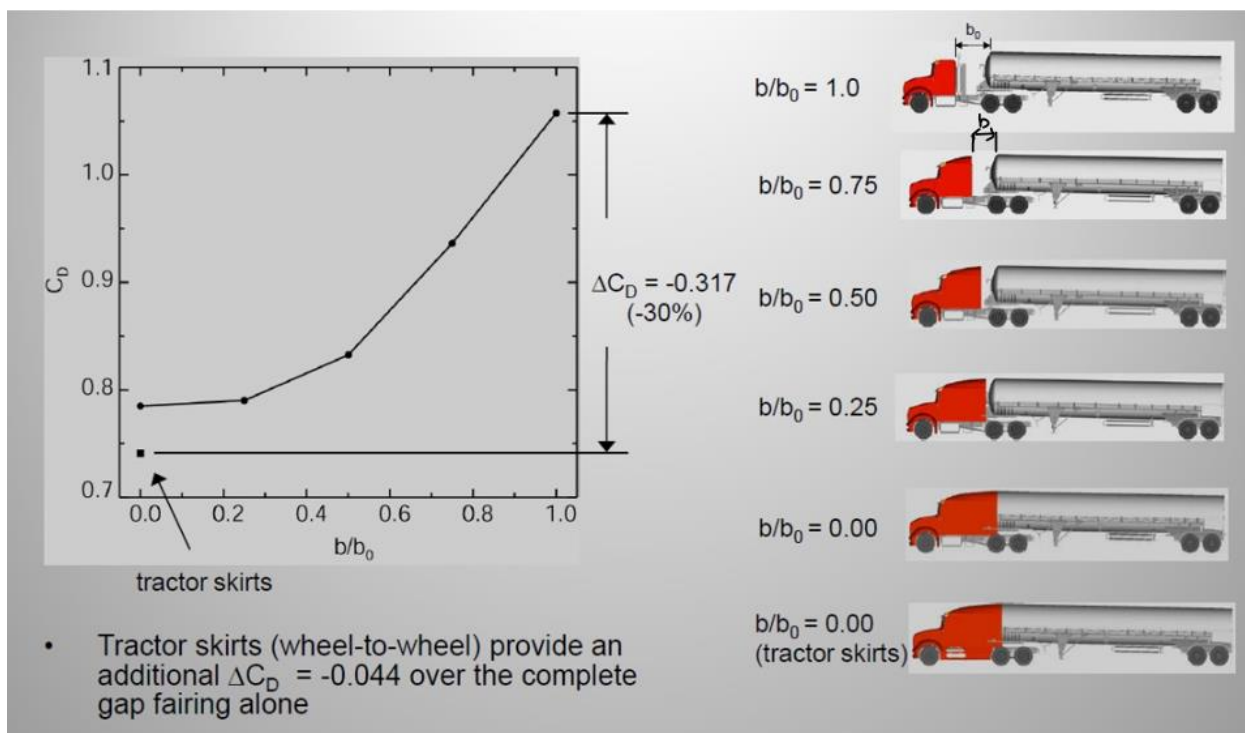


Figure 1.2-3: The effect of the tractor-tanker gap on the drag coefficient. Source (Salari 2013)



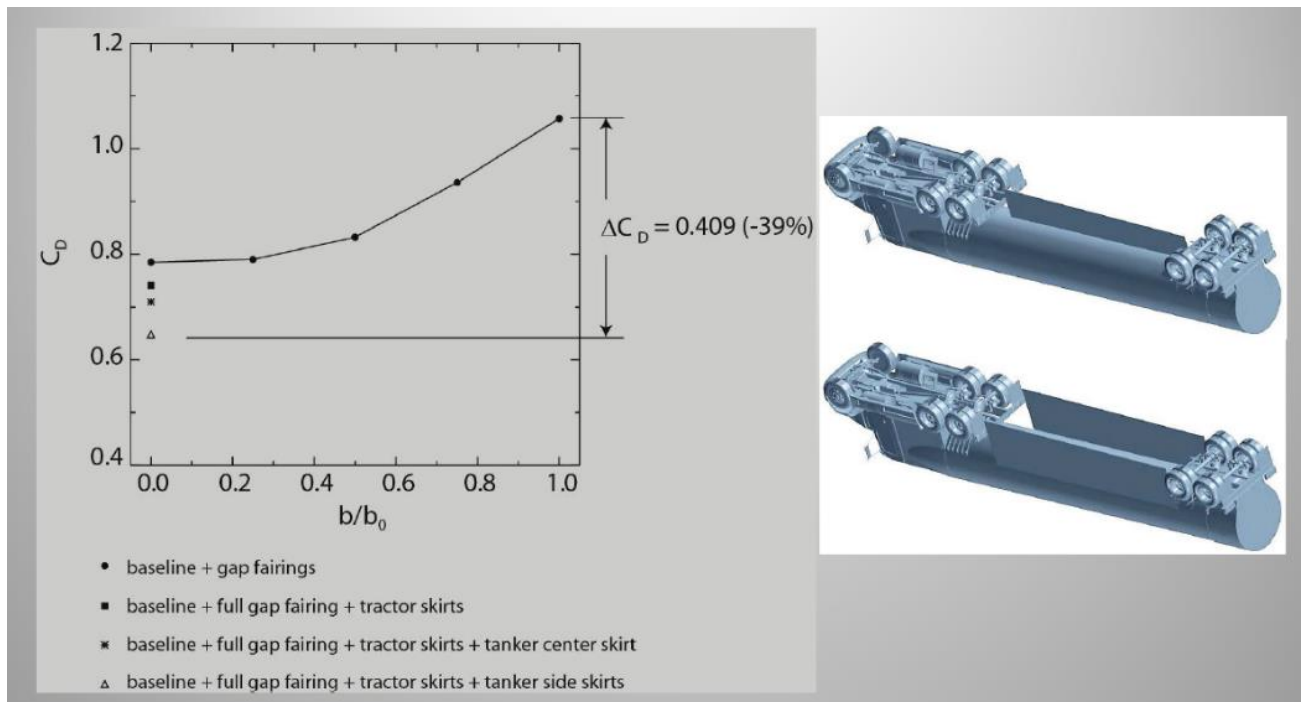


Figure 1.2-4: The impact of tanker underbody treatment on the drag coefficient. Source (Salari 2013)

### 1.2.3 The research by Miralbes & Ferrer (2009) – “Analysis of Some Aerodynamic Improvements for Semi-Trailer Tankers Research.”

A study conducted by Ramon Miralbes & Luis Castellon Ferrer on the aerodynamic analysis of a vehicle tanker resulted in a reduction of 9.6 % in drag coefficient by introducing a continuous aerodynamic underskirt with box from the front zone of the semi-trailer to the end zone of the trailer (Miralbes & Ferrer 2009), as shown in Figure 1.2-5.

Additionally, Introducing the aerodynamic forehead, which reduced the kingpin gap and allowed the air's re-direction, resulted in a reduction of 6.13% in the drag coefficient (Figure 1.2-6). Besides, introducing the aerodynamics adapter for the rear box (as seen in Figure 1.2-7) enabled the transition between flow zones, leading to a drag coefficient reduction of 7.6 % (Miralbes & Ferrer 2009).

The total reduction of all the above improvements, which applied to semi-trailer tankers, jumped to 23%. It was a significant achievement in the fuel efficiency problem that the current liquid transportation industry faces.

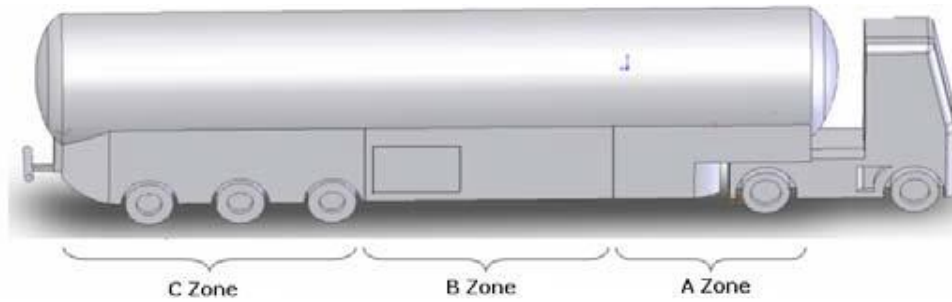


Figure 1.2-5: Aerodynamic skirt for the configuration with boxes in the lower zone. Source (R.Miralbes 2012)

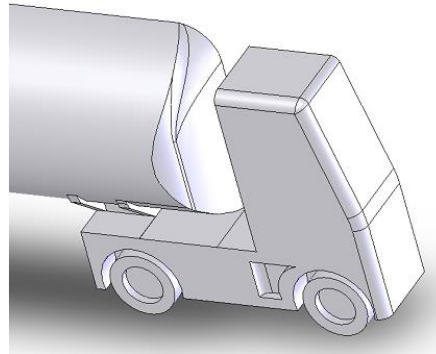


Figure 1.2-6: Vehicle tanker with the aerodynamic forehead. Source (R.Miralbes 2012)

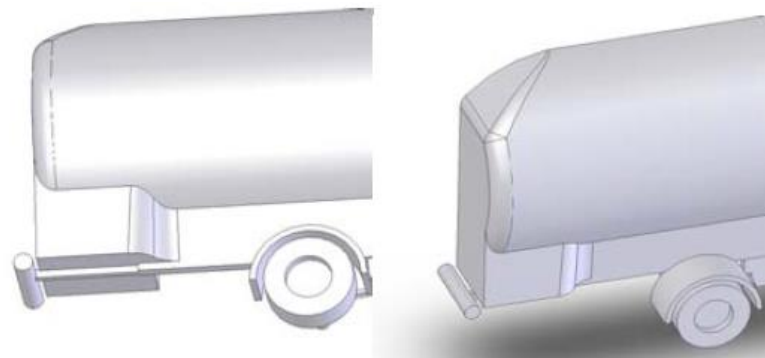


Figure 1.2-7: Aerodynamic adapter for the rear box. Source (R.Miralbes 2012)

#### 1.2.4 Limitation on the Apply of Aerodynamic Devices

Despite the significant advancements in reducing drag forces discussed earlier, the widespread adoption of these aerodynamic improvements in semi-trailer tankers, particularly tractor and tanker side skirts, faces several significant challenges. These limitations can be categorised into three primary areas:

- **Cost and Resource Constraints:** Implementing aerodynamic enhancements demands substantial investments in time, finances, and resources. Fleet operators commonly acquire multiple trailers for each tractor, which come in various shapes

and sizes. Consequently, the economic benefits of add-on devices may diminish significantly, often by a factor of two or more (Cooper 2003).

- **Trade-offs and Maintenance:** Aerodynamic improvements, such as the installation of skirts with boxes, can introduce complexities and additional costs related to maintenance. For instance, the attachment of side skirts may pose challenges for truck drivers in keeping mud flaps secure, adding an element of inconvenience. Moreover, many trailer tankers are designed for both top and side-loading, necessitating unobstructed access to the tanker top and outlet area during loading and unloading. Consequently, side skirts and tractor-trailer gap fairings can limit access to critical areas. Additionally, devices like the adapter for the rear box may reduce the turning angle of the follower trailer, while the aerodynamic forehead may impact the tank's capacity. Companies may hesitate to embrace these trade-offs if they perceive that the benefits of aerodynamic improvements do not outweigh the associated costs (McCallen et al. 2005).
- **Regulatory Barriers:** Complex certification requirements and safety regulations can present a formidable barrier to the widespread adoption of these improvements. Navigating these regulations can be time-consuming and intricate, potentially deterring companies from pursuing aerodynamic enhancements (McCallen et al. 2007).

In summary, the application of aerodynamic devices in semi-trailer tankers is impeded by the significant challenges related to cost, trade-offs in performance and maintenance, and the complexities of regulatory compliance. These limitations underscore the need for a comprehensive approach to address these barriers and encourage the adoption of more fuel-efficient and environmentally friendly technologies in the transportation industry.

### 1.3. [Research Gaps](#)

#### 1.3.1 [Introduction](#)

Crosswinds present a significant and dangerous challenge for heavy vehicles, particularly those with large structures and a high centre of gravity, such as tractor-trailer vehicles. Studies like the one conducted by Batista and Perkovic (2014) highlight the dangers associated with crosswinds, which can lead to accidents like rollovers, sideslips, or spinning, with potentially catastrophic consequences. These risks are particularly elevated for road tankers due to their unfixed hazardous loads and the challenging control resulting from the load sloshing effect. These accidents encompass scenarios where the vehicle overturns, gets pushed sideways over a substantial distance, or rotates significantly around its vertical axis (Batista & Perkovič 2014).

While previous research (as mentioned in Section 1.1.2) has demonstrated that the installation of aerodynamic devices like tractor and trailer side skirts and tractor-trailer gap

fairings can significantly reduce drag coefficients under headwind conditions, concerns have arisen regarding their impact under crosswind conditions, mainly when crosswinds exhibit large yaw angles. There is apprehension that these aero devices may increase drag forces during crosswinds, potentially compromising safety. This concern arises from the enlargement of the vehicle's side areas, rendering it more susceptible to accidents like rollovers, sideslips, and rotations—circumstances particularly hazardous for vehicles transporting dangerous substances such as gas and fuel.

While recent studies have analysed the effect of aerodynamic devices on stability performance during crosswinds, most of these investigations have focused on box semi-trailer trucks. These studies consistently establish that as the yaw angle increases, the crosswind-induced drag force on the vehicle escalates proportionally to the yaw angle. Examples of such research include "A Study on the Aerodynamic Drag of a Semi-Trailer Truck" by Chowdhury et al. (2013) and "Considerable Drag Reduction and Fuel Savings of a Tractor-Trailer Using Additive Aerodynamic Devices" by Kim et al. (2019).

In the context of tractor-semitrailer tankers, the most recent research concerning aerodynamic performance under crosswind conditions was the "DOE's Effort to Improve Heavy Vehicle Fuel Efficiency through Improved Aerodynamics" project led by Kambiz Salari (2016), funded by the US Department of Transportation. However, this project exclusively examined the baseline tractor-trailer model without aerodynamic devices and focused on yaw angles ranging from  $-10^{\circ}$  to  $10^{\circ}$ .

The summaries of these mentioned studies are detailed as follows:

#### 1.3.2 "A Study on Aerodynamic Drag of a Semi-trailer Truck" by Chowdhury et al. (2013)

This study aimed to assess the aerodynamic effects of fuel-saving devices, including front fairings, side skirts, and gap fillers, employed in a commercial vehicle, specifically a semi-trailer truck, under crosswind conditions. The RMIT Wind Tunnel experiments were conducted, encompassing wind speeds ranging from 40 km/h to 120 km/h at four yaw angles ( $0^{\circ}$ ,  $5^{\circ}$ ,  $10^{\circ}$ , and  $15^{\circ}$ ) to replicate crosswind conditions (Chowdhury et al. 2013). Figure 1.3-8, Figure 1.3-9, and Figure 1.3-10 depict the experimental setup, various fairing combinations on the baseline semi-trailer truck model, and the percentage reduction in drag compared to the base vehicle concerning yaw angles, respectively.

Figure 1.3-10 illustrates that as yaw angles increase from  $0^{\circ}$  to  $15^{\circ}$ , the percentage drag reduction over the baseline model diminishes, implying an increase in drag coefficient with higher yaw angles.

Table 1.3-1 presents a detailed breakdown of the average percentage reduction in drag over the baseline model across the  $0^{\circ}$  to  $15^{\circ}$  yaw angle range for each combination. Notably, combination f, featuring a full-size tractor-trailer gap fairing and trailer side skirts, demonstrates the most substantial reduction (26.1%) in average drag reduction. This combination achieves a 27% drag coefficient reduction at a  $0^{\circ}$  yaw angle, decreasing slightly to 26.1% at a  $15^{\circ}$  yaw angle (Figure 1.3-10). This trend suggests that the crosswind effect

(drag coefficient) amplifies as yaw angles increase due to the increased truck side area attributable to side skirts and gap fairings.

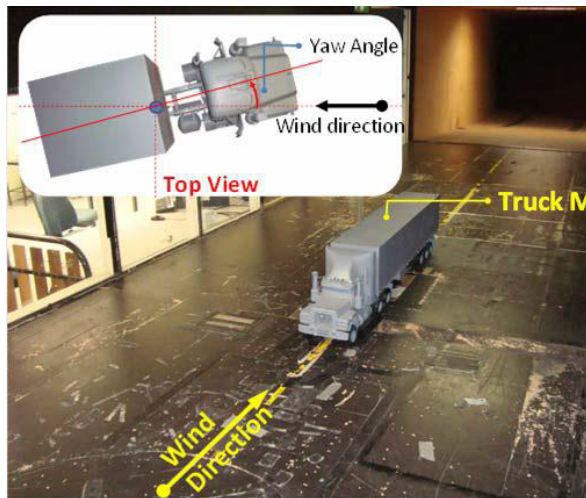


Figure 1.3-8: Experimental arrangement in the test section of RMIT Wind Tunnel (Chowdhury et al. 2013)

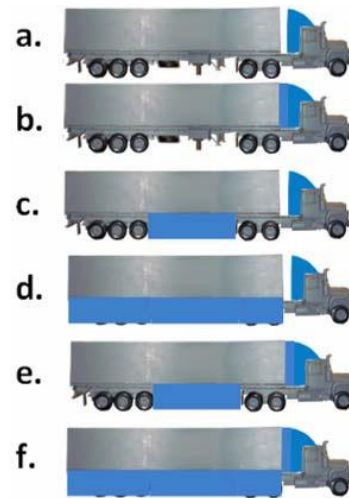


Figure 1.3-9: Different combinations of fairing on the baseline semi-trailer truck model (Chowdhury et al. 2013)

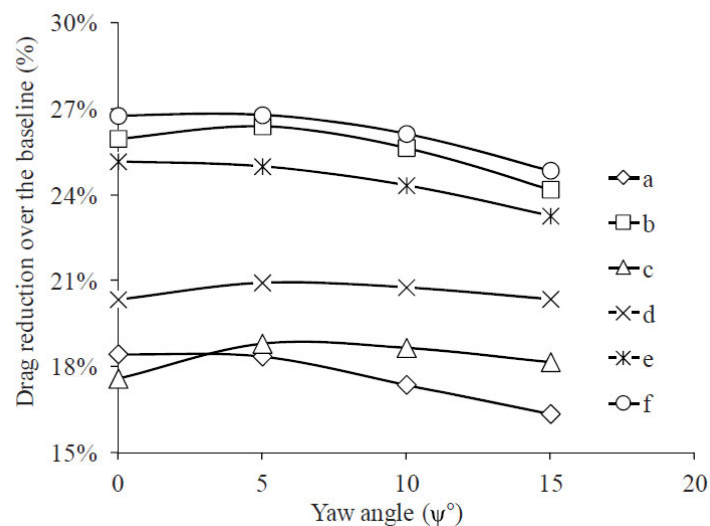


Figure 1.3-10: Drag reduction over the base vehicle in percentage as a function of yaw angle (Chowdhury et al. 2013)

Table 1.3-1: Percentage reduction of drag (D) on yaw angle variation from 0° to 15° over the baseline (Chowdhury et al. 2013)

Configuration	Average drag reduction
a	17.6%
b	25.5%
c	18.3%
d	20.6%
e	24.4%
f	26.1%

### 1.3.3 “Considerable Drag Reduction and Fuel Saving of a Tractor-trailer Using Additive Aerodynamic Devices” by Kim et al. (2019)

This study assessed the aerodynamic impact of devices like tractor-trailer gap fairings, flap-type side skirts, and LIAD boat tails applied to a 1/8 scale truck model under crosswind conditions (Figure 1.3-11). Experiments were conducted in the POSTECH subsonic wind tunnel, with dimensions of 1.8m (W) x 1.5m (H) x 4.3 m (L). The experiments utilised a free stream velocity of  $U_{\infty} = 25$  m/s and a corresponding Reynolds number of  $Re = 8.6 \times 10^5$ . The turbulence intensity of the free stream remained below 0.2%, and four yaw angles ( $0^\circ$ ,  $5^\circ$ ,  $10^\circ$ , and  $15^\circ$ ) were employed to simulate crosswind effects (Kim et al. 2019).

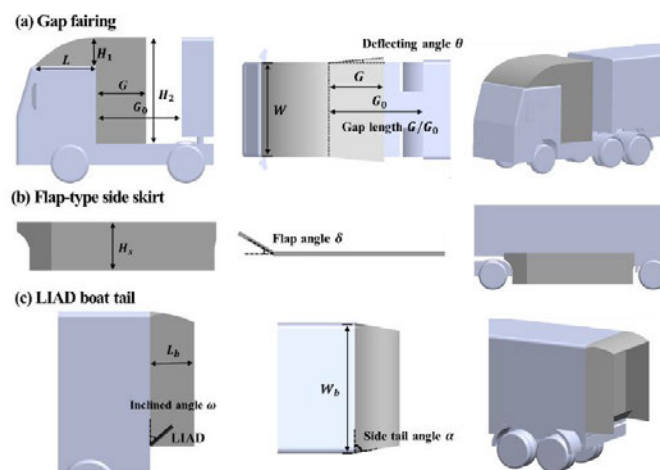


Figure 1.3-11: Schematics of the side, top and isometric views of (a) gap fairing, (b) flap-type side skirt, and (c) LIAD boat tail attached to a tractor-trailer model (Kim et al. 2019)

The results of this study in Figure 1.3-12 (d) reveal that the percentage drag coefficient reductions over the baseline model for different combinations of aerodynamic devices, such as vehicles equipped with gap fairings, vehicles with gap fairings and flap-type side skirts, vehicles with gap fairings and LIAD boat tails, and vehicles with the Aero Full Package (AFP), exhibit a sharp increase within yaw angles ranging from  $0^\circ$  to  $5^\circ$ . These reductions peak at a  $5^\circ$  yaw angle and decrease as yaw angles increase further. This pattern indicates that as yaw angles increase, the side drag force acting on the vehicle intensifies due to the increased truck side area resulting from the installation of these aerodynamic devices.



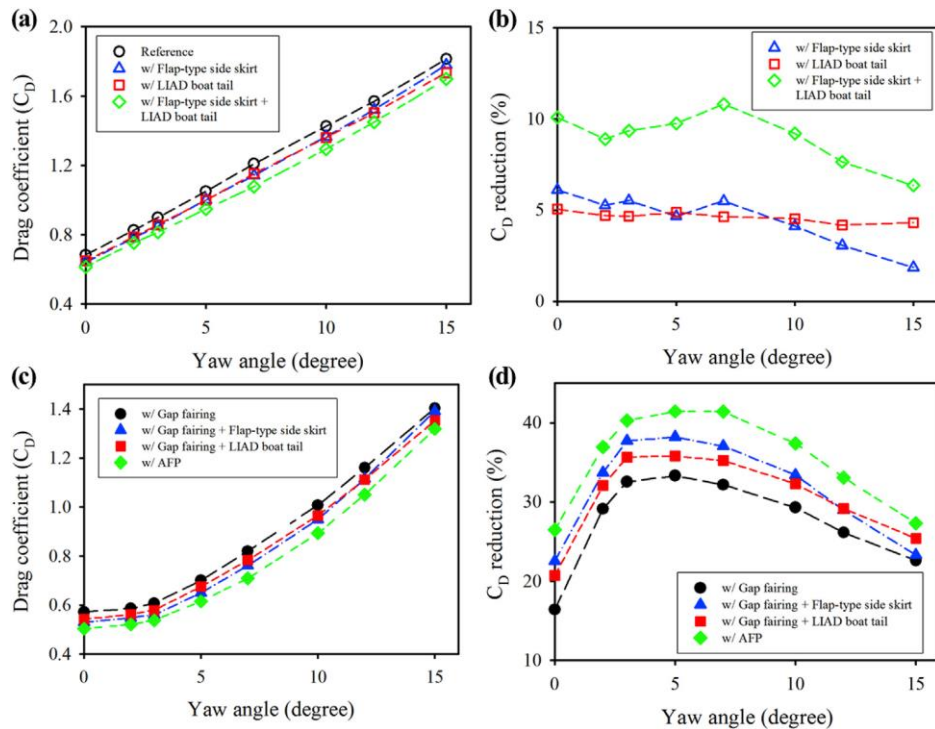


Figure 1.3-12: Variations in (a) drag coefficient ( $C_D$ ) and (b)  $C_D$  reduction rate of the reference vehicle model with attached additive aerodynamic devices according to yaw angle. Variations in (c) drag coefficient ( $C_D$ ) and (d)  $C_D$  reduction rate of gap fairing-based vehicle model with attached additive aerodynamic devices according to yaw angle. (Kim et al. 2019)

#### 1.3.4 “DOE’s Effort to Improve Heavy Vehicle Fuel Efficiency Through Improved Aerodynamics” project conducted by Salari (2016)

Salari's project involved the analysis of crosswind effects on the aerodynamic performance of two distinct baseline tractor-semitrailer tankers in a wind tunnel, with yaw angles ranging from  $-10^\circ$  to  $10^\circ$  (Salari 2016). The two combinations were as follows:

- Tanker 1 featured a 60” tractor-trailer gap and an elliptical tank cross-section.
- Tanker 2 had a 72” tractor-trailer gap and circular tank cross-section.

Figure 1.3-13, Figure 1.3-14 and Figure 1.3-15 present the vehicle geometrics and wind tunnel test results. The results indicate that as yaw angles increase, the drag coefficient for both tankers increases exponentially, with Tanker 1, equipped with an elliptical cross-section, experiencing a more pronounced effect. This research underscores the substantial impact of crosswinds on tractor-semitrailer tankers, particularly at large yaw angles, necessitating further work to enhance vehicle stability by mitigating the adverse effects of drag forces.



Figure 1.3-13: Tanker 1 Geometry (Salari 2016)



Figure 1.3-14: Tanker 2 Geometry (Salari 2016)

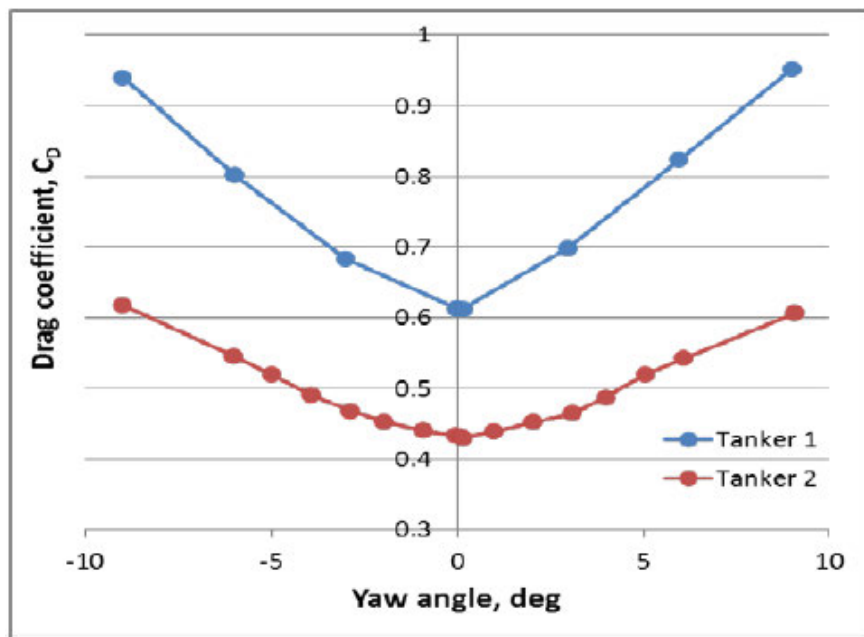


Figure 1.3-15: Test Results (Salari 2016)

### 1.3.5 Summary of research gaps

While existing research has explored the impact of crosswinds on the aerodynamic performance of heavy tractor-trailer vehicles, several critical research gaps have emerged, necessitating further investigation, particularly concerning the potential dangers posed to the stability and safety of road tankers carrying hazardous materials. The severity of accidents these vehicles can trigger underscores the urgency of addressing these gaps. The identified research gaps include:

- **Limited Yaw Angle Range:** As discussed above, previous studies primarily examined the effects of crosswinds within yaw angles ranging from  $0^\circ$  to  $15^\circ$ . However, crosswinds can assault vehicles at larger yaw angles, exponentially increasing the side forces and elevating the risk of rollovers, side slips, and rotations. Consequently, research beyond the  $15^\circ$  yaw angle threshold is essential to assess these potential hazards comprehensively.



- **Focus on Drag Force Reduction:** Earlier research primarily concentrated on quantifying drag force reduction percentages over baseline vehicle models, neglecting a thorough examination of the side forces generated by crosswinds and their implications for tractor-trailer vehicle stability. Under crosswind conditions, there is a need to investigate the risk of accidents, such as rollovers, rotations, and side slips.
- **Consideration of Regulations and Design Rules:** Many studies investigating the effects of headwinds on road tankers and the impact of aerodynamic devices on drag force reduction did not adequately consider specific regulations, standards, or design rules governing dangerous goods trucks. Factors like skidplate height, which can affect stability, and full-length side skirts, which can impact loading and unloading processes, must be accounted for in these simulations.
- **Limited Studies on Road Tankers:** Few studies have explored the impact of crosswinds on road tankers' stability, and there is a significant lack of research on the effects of aerodynamic devices, such as trailer side skirts and tractor-trailer gap fairings, on road tankers under crosswind conditions. This gap persists due to resistance to adopting these devices on road tankers, as discussed in Section 1.2.4.

Given these research gaps, this study aims to investigate the effects of aerodynamic devices on semi-trailer tankers' stability performance while transporting hazardous materials. The study considers various angles ( $\theta$ ) between the vehicle's direction of travel and the crosswind, ranging from  $0^\circ$  to  $90^\circ$  with  $30^\circ$  increments. Two tractor-semitrailer tanker combinations adhere to Australian design rules and regulations. One is a baseline model, while the other is equipped with aerodynamic devices such as tractor-trailer gap fairings and tractor and trailer side skirts. The study seeks to determine the impact of these aerodynamic devices on the lateral forces induced by crosswinds and assess whether their application increases the risk of instability, including the potential for rollovers, rotations, and side slips. The ultimate goal is to optimize existing aerodynamic devices or barrel shapes to reduce drag forces while enhancing safety and compliance with regulations.

#### 1.4 [Research Aims and Objectives](#)

This research project aims to investigate the behaviour of tractor-semitrailer tankers equipped with aerodynamic enhancements, such as tractor-trailer gap fairings and tractor and trailer side skirts, when exposed to crosswind conditions. The primary objective is to enhance stability and safety performance while providing practical recommendations for optimization.

These research objectives can be categorized as follows:

1. **Evaluate the Impact of Crosswinds on Tanker Aerodynamics:**
  - Compare the lateral drag and lift forces, pitch moment, rotational moment, and rollover moment between two categories: Baseline (non-aerodynamic) tankers and

Aerodynamic (equipped with aerodynamic devices) tankers under crosswind conditions.

- Investigate how these aerodynamic devices influence the tanker's response to crosswinds, specifically regarding aerodynamic forces and moments.

## 2. Assess Rollover and Accident Risk:

- Analyze the crosswind impact on the stability and safety of semi-trailer tankers, focusing on identifying the risk of rollovers, rotations, and sideslip accidents.
- Quantify the likelihood and severity of these accidents in both Baseline and Aerodynamic tankers across various crosswind scenarios.

## 3. Identify High-Drag Areas on Aerodynamic Devices:

- Determine the locations on aerodynamic devices that contribute the most to aerodynamic drag under crosswind conditions.
- Evaluate the effect of aerodynamic devices on reducing drag in these critical areas.

## 4. Propose Modifications or Enhancements to Existing Aerodynamic Devices:

- Develop recommendations for adjustments or improvements to the current aerodynamic devices to enhance performance.

By pursuing these objectives, this research aims to provide valuable insights into the safety and performance of tractor-semitrailer tankers in crosswind conditions. Ultimately, it offers practical recommendations to improve their stability and efficiency.

## 1.5 [Outline of the Study](#)

This study aims to analyze the impact of aerodynamic devices on the stability and safety of tractor-semitrailer tankers under crosswind conditions. It seeks to provide valuable insights into the aerodynamic performance of these tankers, along with recommendations for modifying existing aerodynamic devices to reduce drag forces and establishing optimal operating conditions to prevent accidents caused by adverse weather conditions and crosswinds.

### **Methodology**

In order to accomplish these objectives, this study will leverage the capabilities of virtual Computational Fluid Dynamics (CFD) simulations, offering a cost-effective means of analysing and visualizing the airflow behaviour and aerodynamics of a tractor-semitrailer tanker. Specifically, the ANSYS CFD simulation tool is used to estimate the side drag forces generated by crosswinds at various wind angles, ranging from 0 to 90 degrees, applied to tractor-semitrailer tankers with and without aerodynamic devices.

## Tanker Prototype

The study will utilise a widely used semi-trailer tanker prototype commonly employed by petroleum distributors like Ampol, Strike Fuel Australia, Liberty Oil, Lidocole, etc. The geometric model for simulation consists of a tractor-semitrailer tanker configuration comprising a Kenworth 6x4 T610 tractor and a tri-axle five-compartment semi-trailer tanker. The overall length of the tractor-trailer combination is 17.1 meters. Refer to Figure 1.5-16 for an illustrative example of this tractor-trailer tanker.

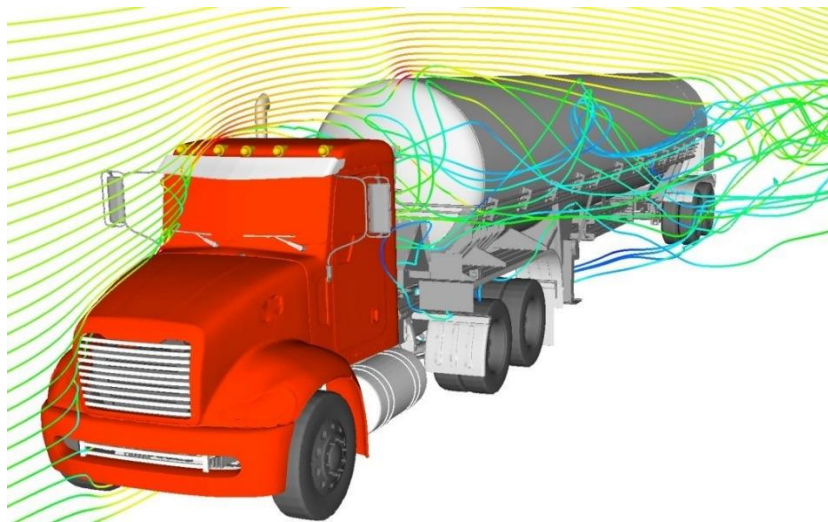


Figure 1.5-16: Semi-trailer Tanker (Salari 2013)

### 1.5.1 Project Limitation

Numerous challenges arose during this project, necessitating adjustments to the initial plan. The primary challenge encountered was the computational complexities of meshing the tractor-semitrailer tanker's full-scale, three-dimensional, realistic model. Initially, this project aimed to achieve the desired orthogonal mesh quality of 0.5 through a volume meshing process. However, this task proved highly time-consuming, taking a staggering 20 hours to complete the meshing and nearly four days to run a single simulation. Consequently, I had no choice but to significantly simplify the tractor-semitrailer tanker's geometry. Ultimately, I opted for an acceptable orthogonal mesh quality of 0.22, reducing the meshing time to 6 hours. Nevertheless, this adjustment may have introduced potential inaccuracies in the simulation results. Given the constraints of resources and time within the project, I considered this compromise acceptable, even though it might result in slightly less precise outcomes when using this simplified model.

Additionally, I initially selected the Kenworth T600A tractor as a crucial component of the project, intending to validate the accuracy of the pre-processing and solving stages in the ANSYS simulation process. This validation was designed to be accomplished by comparing the results to the drag coefficient obtained from a study conducted by McCallen et al.

(2007). However, a significant obstacle arose as the tractor used in that research was created using a publicly available stereolithography model. It rendered the geometry unsuitable for the project purposes due to the absence of an official geometry for the Kenworth T600A, as indicated in McCallen et al.'s study. Furthermore, there was a notable lack of available data or information from truck manufacturers regarding the drag coefficient, and no prior research had been conducted on the aerodynamic performance of this specific tractor. This lack of validating data shifted the validation method from comparing the tractor's drag coefficient to evaluating the tractor-semitrailer's percentage change in drag coefficient between the two models.

In summary, the original project specifications outlined in Appendix A underwent modifications during Phase 2, as detailed in Section 1.5.2 of the Project Plan below. These modifications included excluding the Kenworth T600A tractor simulation under headwind conditions and changing the approach to validating simulation results, aligning them with the scope of the project's revised objectives.

#### 1.5.2 Project Plan (Project Specifications)

This project comprises three distinct phases, with the possibility of an additional step if resources and time allow:

##### **A. Phase 1 – Literature Review**

1. Conduct an exhaustive review of prior research on the impact of aerodynamic drag on trailer tanker performance, identifying existing research gaps.
2. Explore relevant literature concerning the influence of crosswind aerodynamic loading on various accident types (e.g., rollovers, sideslips, rotations). Computational Fluid Dynamics (CFD) simulations are also examined for solving external flow problems.
3. Investigate current regulations related to semi-trailer tanker modifications, including standards such as the Australian Design Rules (ADRs) for heavy vehicles, Road tank vehicles for dangerous goods (AS2809.X), the National Heavy Vehicle Regulation (NHVR), Static Roll Threshold (SRT), and Performance Based Standards (PBS).
4. Develop a research methodology for studying the effects of crosswind drag forces on semi-trailer tanker aerodynamic performance. Create techniques for conducting CFD analyses on the tractor-semitrailer model.

##### **B. Phase 2 – Simulation Performance**

5. Generate two models of tractor-semitrailer tanker combinations: one baseline model devoid of aerodynamic devices and another equipped with tractor-trailer gap fairings and tractor-trailer side skirts. These models will be employed for conducting aerodynamic analyses under crosswind conditions.

6. Utilize Ansys CFD to simulate both Baseline and Aerodynamic models under headwind conditions, utilizing the obtained drag coefficient results to validate the simulation setup and solving process against previous studies.
7. Employ CFD analyses to scrutinize the dynamic stability of the models under steady crosswind conditions, varying the wind angle from 15 to 90 degrees in 15-degree increments.
8. Analyze the results of the two models to pinpoint areas where crosswinds substantially impact vehicle safety and stability performance.
9. Formulate recommendations for mitigating the effects of crosswinds, including potential modifications to aerodynamic devices.
10. Explore future research possibilities within this domain, focusing on conducting in-depth investigations into the impact of strong crosswinds on semi-trailer tanker stability, including the influence of gusty crosswinds on nonlinear tractor-trailer tankers.

**C. Phase 3 – If time and resources permit**

11. Refine trailer tanker aerodynamic devices and the tractor-trailer gap fairing to minimize side drag forces on the semi-trailer and rerun CFD simulations to compare the results.
12. Conduct a transient simulation on the modified semi-trailer tanker under crosswind conditions.

## 1.6 [Dissertation Outline](#)

This section provides an outline of this dissertation. It is a general overview of the seven main chapters presented in this study.

### [Chapter 1 – Introduction](#)

Chapter 1 serves as the introduction to the project, providing the necessary background for the research. It consists of the following key components:

- Background: Overview of road tankers in Australia and the existing fuel consumption issues in the industry.
- Current research review: Summary of recent studies on road tanker aerodynamics, including McCallen et al. (2005-2013) and Miralbes & Ferrer (2009), focusing on the impact of aerodynamic device add-ons and their limitations.
- Research gap: Identification of the research gap regarding the effects of aerodynamic devices on road tankers' stability performance under crosswinds.

- Research aims and objectives: Establishment of the study's goals and objectives based on the identified research gap.
- Study outline: Overview of the study's focus, methodology, and project breakdown.
- Risk assessment: Identification of potential risks associated with the research.
- Resource requirements: Listing the necessary resources for the dissertation.
- Project timelines: Establishment of the project schedule and milestones.

## Chapter 2 – Literature Review

This chapter presents comprehensive literature reviews to understand the project's scope and methodology thoroughly. It includes key points as follows:

### 1. Introduction to Aerodynamics Study

- Purpose of the aerodynamics study.
- Theory of drag and lift forces and their effects on moving bodies.

### 2. Aerodynamic Forces and Moments of Crosswind

- Explanation of how crosswinds can cause a vehicle to slip sideways, rotate, or rollover.
- Methods for estimating critical relative wind speeds leading to crosswind-induced accidents (e.g., rollover, sideslip, rotation).

### 3. Regulations and Design Rules for Road Tankers

- Overview of current regulations and design rules applicable to road tankers carrying dangerous goods.
- Discussion of specific regulations, including the minimum Static Roll Threshold (SRT) values and their relationship to vehicle geometry.
- Performance-Based Standard (PBS) criteria for safe and efficient vehicle operation.
- Australian Design Rules (ADRs) as national standards for vehicle safety.

### 4. Computational Fluid Dynamics (CFD)

- Overview of CFD technology, including its three main stages: pre-processing, solving, and post-processing.
- Emphasis on deep research to facilitate a comprehensive understanding of ANSYS CFD application.
- Prepare model geometry and mesh, configure the solver, and achieve desired results in CFD Pre-Processing.

### Chapter 3 – Research Methodology

This chapter describes the methodology employed to investigate the impact of crosswind drag forces on the aerodynamic performance of semi-trailer tankers. The primary objectives of this chapter are as follows:

#### Model Tractor and Trailer Combinations

- Develop detailed models of T610 tractors paired with 5-compartment trailer tankers, considering configurations with and without aerodynamic devices.

#### Determination of Minimum Static Rollover Threshold (SRT)

- Employ the SRT online calculator in Appendix F to ascertain the minimum SRT value pertinent to the semi-trailer tanker model.
- Emphasize the significance of this step in predetermining the lateral force threshold required for potential rollovers.

#### Computation of Critical Lateral Forces

- Apply calculation techniques and equations introduced in Chapter 2 – Literature Review to pre-determine the critical lateral forces that may induce sideslips or rotations about the kingpin axis.

#### Geometric Modeling Techniques

- Describe the modelling techniques utilized to accurately represent the geometrical aspects of tractor-semitrailer combinations, facilitating their readiness for the ensuing CFD analysis (Chapter 4).

#### Establishing Safety Benchmarks with Minimum SRT Value

- Elaborate on the pivotal role of the determined minimum SRT value as a safety benchmark for the semi-trailer tanker model.
- Clarify how this information contributes to describing safe operational limits and assuring vehicle stability across diverse driving conditions.

### Chapter 4 – CFD Performance

This chapter provides an overview of the Computational Fluid Dynamics (CFD) simulation processes, organized into several sections, each addressing specific aspects of the CFD analysis:

#### ❖ Pre-processing Stage

- Explanation of the geometry creation and simplification process.
- Definition of the computational domain and presentation of the details and results of the geometry meshing process.

- Emphasis on the importance of these preparations for ensuring accurate and reliable simulation results.
- ❖ Solving Stage
  - Detailed description of the simulation domain.
  - Determination of the appropriate viscous model and definition of the fluid material properties.
  - Setup of cell zones, boundary conditions, and solution control parameters for optimal simulation performance.
- ❖ Post-Processing Stage
  - Explanation of the post-processing stage, which focuses on capturing simulation results for subsequent analysis and discussion in Chapter 5.
  - Overview of the predefined post-processing tasks, including:
    - Calculation of forces and generation of reports.
    - Grid display.
    - Vector plots.
    - Line and shaded contour plots.
    - 2D and 3D surface plots.
    - Particle tracking.
    - View manipulation techniques (translation, rotation, scaling).
    - Colour postscript output

## Chapter 5 – Result and Discussion

This chapter analyses the simulation results obtained from Chapter 4, focusing on determining the areas where crosswinds significantly impact vehicle stability performance. The tasks in this chapter are classified into the following main points:

- ❖ Studying Simulation Results
  - Visual presentation of parameters such as drag, lift, lateral forces, pitch moment, rotational moment, and rollover moment coefficients obtained from simulations.
  - Preparation for the result discussion in Chapter 6.
- ❖ Analysis of Simulation Results



- In-depth evaluation of the CFD results, including parameters such as drag force, lift force, lateral force acting on the vehicle, flow streamlines, turbulence kinetic energy, and pressure distribution.
  - Primary objective: Determination of the semi-trailer tanker's aerodynamic performance and safety.
- ❖ Determining Accident Likelihood
- Assessment of the likelihood of sideslip, rotation, or rollover accidents occurring under various crosswind conditions based on simulation results.
  - Understanding critical scenarios to establish optimal operating conditions for accident prevention.
- ❖ Further Work and Issues Encountered
- Discussion of areas for further research and potential re-evaluation.
  - Description of challenges and issues encountered during the study.
  - Suggestions for improvement in future research.

## Chapter 6 – Conclusion

This chapter summarises the study's outcome and evaluates its success in meeting the project specifications and original objectives. It includes the following key elements:

- ❖ Summary of Study Outcome
- Recap of the study's main findings and results.
  - Assessment of the study's overall success in achieving its objectives.
- ❖ Optimal Configuration for Aerodynamic Efficiency and Safety
- Identification of the configuration that demonstrates the most excellent aerodynamic efficiency and safety improvement based on the analysis of simulation results.
- ❖ Future Research Areas
- Discussion of research areas currently beyond the scope of this study.
  - Suggestions for potential future research endeavours in the field.

### 1.7 Risk Assessment

This research does not include any lab work or fieldwork, so there will be no physical risks except for some ergonomic and health issues, such as fatigue due to long working hours on the

computer. The ergonomics and health risks are accessed and shown in Appendix D: Risk Management.

## 1.8 [Resource Requirements](#)

The following resources have been identified as required to complete this research.

- 3D model of Kenworth T610 tractor.
- A 3D modelling software such as Autodesk Inventor student version to build semi-trailers for simulation processing.
- The Australian Design Rules (ADRs) for heavy vehicle
- Australian Standards (AS2809.1, AS2809.2, AS2809.3, AS2809.4) - Road tank vehicles for dangerous goods
- The National Heavy Vehicle Regulation (NHVR)
- The Static Roll Threshold (SRT) definition, formula and calculation
- The Performance Based Standards (PBS)
- ANSYS CFD software

## 1.9 [Project Timelines](#)

Appendix C serves as a reference for outlining the project timelines and schedule. Its primary objective is to offer guidance in specifying critical milestones and establishing accountability to ensure that deadlines are consistently met. The project timeline is visually depicted using a Gantt chart included in this particular appendix.

## CHAPTER 2 – LITERATURE REVIEW

### 2.1 [Introduction](#)

Before researching the aerodynamic performance of semi-trailer tankers under headwind crosswind conditions, it is essential to review the existing literature critically. Besides, to modify the semi-trailer tanker, all current regulations and design rules must be taken into account to ensure that any change of the vehicle has to adhere to all the current laws and design rules in Australia.

This section introduces the study of aerodynamics, reviews the effects of headwinds and crosswinds on the aerodynamic performance of road tankers, and the theoretical estimation of drag forces exerted on a body.

Moreover, It also reviews the current regulations and design rules for road tankers carrying dangerous goods, such as the Static Roll Threshold (SRT), The Performance-Based Standards (PBS) Schemes, the Australian Design Rules (ADR) and the specific Australian Standard AS2809 for road tank vehicles carrying dangerous good.

This section aims to provide a thorough understanding of the problem, together with highlighting current regulations and design rules for which any designs and modifications of the semi-trailer tanker must follow.

### 2.2 [Study of Aerodynamics](#)

Aerodynamics studies gases interacting with solid objects in motion, especially air interacting with solid objects such as cars, trucks, aeroplanes, and buildings. This fluid mechanic study focuses on air and gas properties. The study of aerodynamics involves areas such as fluid dynamics, which studies fluids' motion and the forces that affect their movement. Thermal dynamics explores the relationship between heat, energy and work. Mechanics studies how objects move, and the power that causes them to move, and material science looks at the physical properties of materials and how they react to external forces.

In the automotive industry, the most concerning aerodynamic performance is the stability and fuel efficiency of vehicles under drag forces caused by air while vehicles are in motion. As stated by (Cummins 2013), "The largest single power requirement for a truck is the power needed to overcome air resistance". Therefore, the study of aerodynamics can make considerable economic gains by reducing drag and contributing to a better environment by reducing carbon dioxide emissions through fuel consumption.

## 2.3 Headwind and Crosswind Effects on the Aerodynamics of Vehicles

### 2.3.1 Drag and lift force and its effects on moving body

The external flow of fluid (air) over a body in motion generates drag and lift forces. A motion body always meets some resistance when it moves through a fluid. This fluid exerts forces and moments on the body in and about various directions, and the exerted force in the flow direction is called drag force (Çengel et al. 2017). This force is undesirable from the aerodynamic performance point of view because it requires extra power to overcome its adverse effects, such as the moving body's instability and high fuel consumption. Therefore, the automotive industry always does its best to minimise the force associated with reducing fuel consumption, improving the safety and durability of structures subjected to high wind, and reducing noise and vibration caused by them. In some cases, drag force is a lifesaver that produces beneficial effects where we do want to maximise it, such as in automotive braking.

A moving fluid also generates a force in the direction normal to the flow direction. This force is called lift force, which allows an object to stay aloft. The difference in air pressure above and below an object, which is the lower pressure on the upper surface, creates the lift force. This pressure difference is caused by the object's shape, known as the airfoil, which causes the air to move faster over the upper surface, reducing the pressure under Bernoulli's principle (Çengel et al. 2017).

Figure 2.3-17 shows a demonstration of drag and lift forces exerted on an aerofoil where  $F_L$  is the lift force,  $F_D$  is the drag force,  $F_R$  is the resultant force and  $\phi$  is the angle of the surface made with the flow direction.

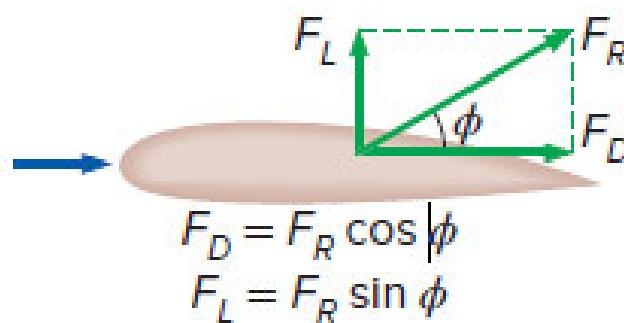


Figure 2.3-17: Drag and Lift Forces on an aerofoil. Source: (Çengel et al. 2017)

### 2.3.2 Equation of drag and lift force exerted on a vehicle

Drag and lift forces exerted on a vehicle can be estimated using equations. These forces depend on the density  $\rho$  of the fluid, the upstream velocity  $V$  and the vehicle's size, shape and orientation, as expressed in (Çengel et al. 2017).

Equations to estimate the dynamic pressure drag and lift forces are as follows (Çengel et al. 2017):

$$\text{drag force: } F_D = C_D A (\rho V^2 / 2)$$

$$\text{lift force: } F_L = C_L A (\rho V^2 / 2)$$

Where:

- $F_D$  and  $F_L$  are drag and lift forces in Newton
- $C_D$  and  $C_L$  are drag and lift coefficients.
- $A$  is the frontal area in  $\text{m}^2$  ( area projected on a plane normal to the direction of flow)
- $\rho$  is the fluid density (air) in  $\text{kg}/\text{m}^3$ .
- $V$  is the ambient upstream velocity in  $\text{m}/\text{s}$

The drag and lift coefficients are functions of the shape of the body. They also depend on the Reynolds number and the surface roughness.

The two equations above present the pressure part of drag force, which is due directly to pressure, as it is strongly dependent on the form or shape of the body. Another aspect of drag force related to wall shear stress is called skin friction drag force since it is caused by frictional effects. The friction and pressure drag coefficients are defined as (Çengel et al. 2017):

$$C_{D,\text{friction}} = \frac{F_{D,\text{friction}}}{0.5 \rho V^2 A} \text{ and } C_{D,\text{pressure}} = \frac{F_{D,\text{pressure}}}{0.5 \rho V^2 A}$$

When the friction and pressure drag coefficients (based on the same area  $A$ ) or forces are available, the total drag coefficient or drag force is determined by simply adding them, according to (Çengel et al. 2017)

$$\begin{cases} C_D = C_{D,\text{friction}} + C_{D,\text{pressure}} \\ F_D = F_{D,\text{friction}} + F_{D,\text{pressure}} \end{cases}$$

Although these equations above simplify the estimation of drag and lift forces exerted on a body, it is too complicated to solve the flow fields and geometries analytically for most external flow problems, as stated by (Çengel et al. 2017). Therefore, the availability of high-speed computers and CFD simulation applications have made it possible to conduct a series of numerical experiments by solving the governing equations numerically and resort to expensive and time-consuming testing and experimentation only in the final design stages.

### 2.3.2 Effects of Headwind on the aerodynamic performance of road tanker

A headwind is a wind that flows directly opposite to the forwarding motion. Research has found that, as in the report published by (OSTI.GOV 2020), "Under the effect of headwind, 85 per cent of the useful energy produced by the truck engine is used to overcome aerodynamic drag and rolling resistance. Additionally, 85% of the engine's useful energy is used to overcome aerodynamic losses and rolling resistance.". This report also states that the effect of skin drag force on tractor-trailers is minimal. Only the pressure drag, which results from air particles compressed in the front of the truck and spread out in the rear, significantly affects the vehicle's performance. It is because the layers of air swirl away from the surface and create a phenomenon called turbulent flow. Since there is more pressure on the front than the back, drag occurs (OSTI.GOV 2020).

Drag force caused by headwinds has adverse effects on the heavy vehicle such as:

- Increase aerodynamic drag: headwind creates higher pressure zones in the front area of vehicles, which increases the pressure on the vehicle's frontal surface. This increased pressure builds more resistance to the vehicle's motion, significantly causing the vehicle to slow down, reduce fuel efficiency, and increase wear on the engine.
- Increase lift: headwinds can also create an upward force on the vehicle, known as lift. This aerodynamic lift is particularly problematic for heavy vehicles as it can cause them to lose control.
- Reduced stability: A strong headwind can also reduce the stability of a vehicle, particularly at high speeds. The wind can create turbulence and buffeting, making it harder for the driver to maintain control of the truck. In extreme cases, the wind can cause the vehicle to flip over or spin out of control. Moreover, strong headwinds can cause heavy vehicles to tip or roll over when carrying heavy loads, which is extremely dangerous in high-speed situations.
- Increased braking distance: If a headwind is strong enough, it can push a heavy vehicle off course and require the driver to use the brakes to correct their course.

### 2.3.3 Effects of Crosswind on the aerodynamic performance of road tankers

Crosswind is the most dangerous and unexpected wind condition for heavy vehicles. It can significantly affect road tankers, which are large, heavy vehicles that transport liquids or gases in bulk. According to Batista & Perkovic (2014), crosswind accidents can be rollover, sideslip, or rotating (as shown in Figure 2.3-18). In the first type of accident, a trailer tanker is blown over; in the second type, the vehicle is blown sideways for a considerable distance. Finally, in the

third type of accident, a trailer tanker rotates around its vertical axis to a significant degree (Batista & Perkovič 2014).

The primary effects of crosswinds on road tankers can be classified as follows:

- a) Reduce stability: Crosswinds can cause the tanker to sway, reducing stability and making it more difficult for the driver to control the vehicle. It can increase the risk of accidents, especially on highways or other high-speed roads (Batista & Perkovič 2014).
- b) Increased risk of Rollover: Tankers have a high centre of gravity due to the weight of their cargo, and crosswinds can increase the risk of Rollover, especially if the driver is travelling at high speeds.

The Rollover is very dangerous for road tankers as they carry unfixed loads, and the sloshing effect of these loads makes the vehicle difficult to control. In the impact of crosswind, road tankers are more subjected to sideways tipping than other trucks. It can be very disastrous as it causes an explosion or fire if the petrol or gasoline comes into contact with a heat source, and the flame can destroy the neighbourhood when gasoline or gas leaks out of the tanker (Winkler & Ervin 1999).

Compared with passenger vehicles, roll instability is more applicable to high-sided commercial vehicles like tractor-trailer units (Baker 1987). For example, in January 2008, more than thirteen tractor-trailers were reported to have overturned due to the prevalence of sudden high crosswinds on a single day (Malviya 2011). Moreover, in a crosswind environment, the side force generated by the crosswind may change the driving direction and reduce the handling stability of the vehicle. Then, the drivers have to adjust the direction frequently. It may cause the drivers to get tired and increase the risk of a rollover accident (Winkler & Ervin 1999).

Figure 2.3-19 and Figure 2.3-20 show an accident in October 2014 when a road tanker rollover under the impact of crosswinds. In Figure 2.3-19, It took 157 firefighters to extinguish the flame in 80 minutes. It also took 4 hours to clean up hazardous materials spilled from the tank. The fire damaged one home and one vehicle, according to (Services 2014). There were nearly 9,000 gallons of fuel spilled on the road in Figure 2.3-20, causing massive traffic delays.

- c) Reduced speed: Crosswinds can also reduce the speed at which road tankers can safely travel. When faced with strong crosswinds, tanker drivers may need to slow down to maintain control of their vehicles, which can cause delays and impact delivery schedules (Brandt et al. 2022).
- d) Increased fuel consumption: Driving in crosswinds can also increase the fuel consumption of road tankers. It is because the driver may need more fuel to maintain a consistent speed and counteract the effects of the wind (Brandt et al. 2022).
- e) Tire wear: Crosswinds can also cause uneven wear on the tires of road tankers. As the vehicle is pushed sideways, the tires on one side may wear more quickly than those on the



other. It can lead to imbalances in the vehicle's handling and stability, increasing the risk of accidents (Kirkham 2016).

The following section (Section 2.4) discusses the various crosswind-induced accidents, which will provide an overview of the effect of lateral side drag forces on the stability of the tractor-trailer vehicle under crosswind.

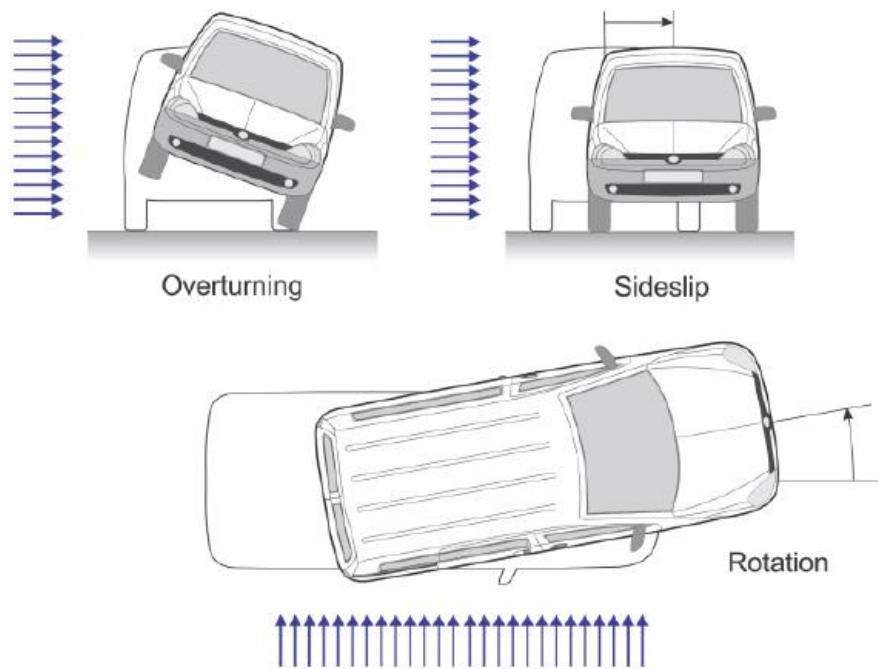


Figure 2.3-18: Vehicle accidents in crosswind. Source (Batista & Perkovič 2014)



Figure 2.3-19: Rollover accident of road tankers in Oct-2014. Source: [Metropolitan Engineering](#)





Figure 2.3-20: Road tanker rollover. Source: [Metropolitan Engineering](#)

## 2.4 Various crosswind-induced accidents.

### 2.4.1 Aerodynamic Forces and Moments of Crosswind

#### a) Forces and moments acting on a vehicle.

From Figure 2.4-21, the forces and moments acting on a vehicle can be determined as stated in (Batista & Perkovič 2014):

- $F_D$  = drag force
- $F_S$  = lateral force (side force)
- $F_L$  = lift force
- $M_R$  = rolling moment
- $M_P$  = pitching moment
- $M_Y$  = yawing moment
- $T_1, T_2, T_3, T_4$  = wheel traction forces
- $\mu$  = static friction coefficient of tyre
- $q$  = unknown traction parameter
- $f_R$  = rolling resistance coefficient = constant

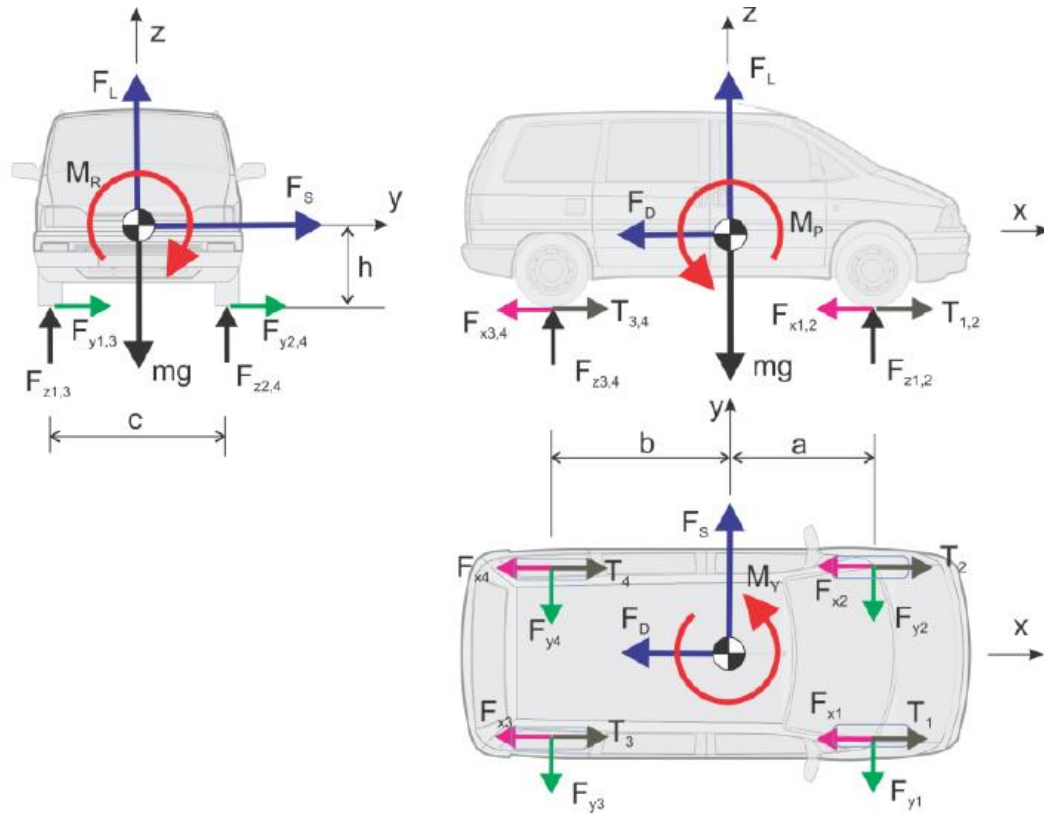


Figure 2.4-21: Forces and Moments acting on the vehicle. Source (Batista & Perkovič 2014)

b) The equilibrium equations

If the vehicle is treated as a rigid body, then the equilibrium conditions of forces and moment with respect to the vehicle's centre of gravity yield six equilibrium equations. These are the equilibrium of forces (Batista & Perkovič 2014).

$$-F_D - F_{x1} - F_{x2} - F_{x3} - F_{x4} + i_1(T_1 + T_2) + i_2(T_3 + T_4) \quad (\text{Eq.1})$$

$$F_S - F_{y1} - F_{y2} - F_{y3} - F_{y4} = 0 \quad (\text{Eq.2})$$

$$-mg + F_L + F_{z1} + F_{z2} + F_{z3} + F_{z4} = 0 \quad (\text{Eq.3})$$

$$-M_R + \frac{c}{2}(F_{z2} - F_{z1} + F_{z4} - F_{z3}) - h(F_{y1} + F_{y2} + F_{y3} + F_{y4}) = 0 \quad (\text{Eq.4})$$

$$-M_P - a(F_{z1} + F_{z2}) + b(F_{z3} + F_{z4}) + h(F_{x1} + F_{x2} + F_{x3} + F_{x4}) = 0 \quad (\text{Eq.5})$$

$$M_Y - a(F_{y1} + F_{y2}) + b(F_{y3} + F_{y4}) + \frac{c}{2}(F_{x2} - F_{x1} + F_{x4} - F_{x3}) + i_1 \frac{c}{2}(T_1 - T_2) + i_2 \frac{c}{2}(T_3 - T_4) = 0 \quad (\text{Eq.6})$$

Where:  $i_1, i_2 = 1$  or  $0$  depends if axle is driven or not

### c) Constraint Equations

As demonstrated in Figure 2.4-21, let  $(x_i, y_i, z_i)$  are the coordinates of the centre of  $i$ th wheels where  $z_i$  is the displacement of wheel centres from their equilibrium position in the vertical direction (Batista & Perkovič 2014).

As seen in Figure 2.4-21:

$$\begin{cases} x_1 = x_2 = a; x_3 = x_4 = -b \\ y_1 = y_3 = -\frac{c}{2}; y_2 = y_4 = \frac{c}{2} \\ z_1 - z_2 + z_4 - z_3 = 0 \end{cases} \quad (Eq. 7)$$

If we assume that each vertical force is proportional to the displacement and all the wheels suspension has the same stiffness, then the vertical force constraint equation is:

$$F_{z1} - F_{z2} + F_{z4} - F_{z3} = 0 \quad (Eq. 8)$$

The unilateral contact between wheels and road demands that:

$$F_{zj} \geq 0 \quad (j = 1, 2, 3, 4) \quad (Eq. 9)$$

If  $F_{zj} = 0$ , then the  $j$ th wheel loose contact.

The well-known Coulomb friction law restricts the reaction side force on a vehicle wheel for static consideration.

$$\sqrt{(T_j - F_{xj})^2 + F_{yj}^2} \leq \mu F_{zj} \quad (Eq. 10)$$

Equation 10 shows that when the inequality holds, then a wheel is stuck with the road. When equality holds, then wheels sliding begins. The unilateral contact between the wheel and the road implies that if  $F_{zj} = 0$  then also  $F_{yj} = 0$

### The Constitutive Equations

The rolling resistances are given by (Batista & Perkovič 2014):

$$F_{xj} = f_R F_{zj} \quad (j = 1, 2, 3, 4) \quad (Eq. 11)$$

The traction forces have a form (Batista & Perkovič 2014):

$$T_j = q F_{zj} \quad (j = 1, 2, 3, 4) \quad (Eq. 12)$$

### d) Aerodynamic forces and moments

Crosswind aerodynamics deals with airflow that does not move in the plane of vehicle travel but at an angle relative to the direction of travel (Mansor & Passmore 2013). Figure 2.4-22 shows the definition of the aerodynamic force and moment caused by crosswind.

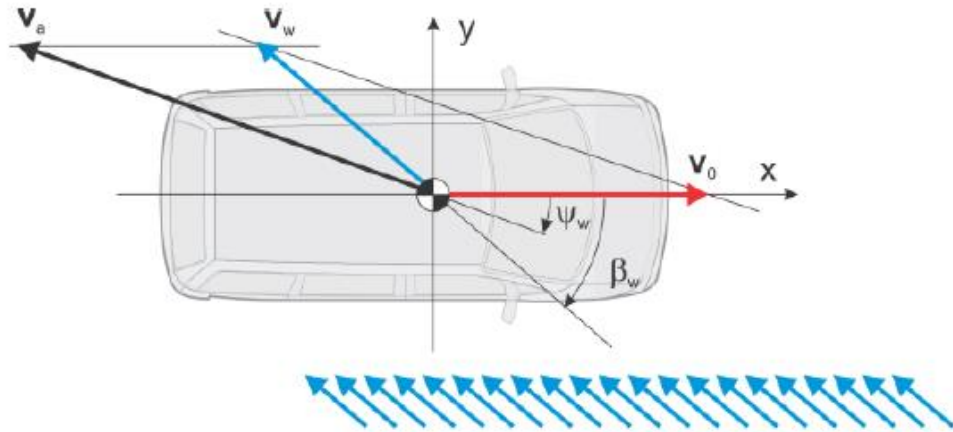


Figure 2.4-22: Aerodynamic force and moment caused by crosswind. Source (Batista & Perkovič 2014)

In Figure 2.4-22:

- $V_0$  = speed of vehicle moving in  $x$  – direction (m/s)
- $V_w$  = absolute crosswind velocity (m/s)
- $\beta_w$  = angle between vehicle travelling direction and crosswind direction
- $V_a$  = relative crosswind velocity that acts on the vehicle (m/s)
- $\psi_w$  = yaw angle between relative velocity  $V_a$  and direction of travel
- $\beta_w$  and  $\psi_w$  positive in a clockwise direction

So, with the help of Figure 2.4-22, we can obtain equations for the relative velocity  $V$  and the yaw angle  $\psi$  as follows (Batista & Perkovič 2014):

- Vector equation:  $V_0 + V_a = V_w$
- So, the relative velocity can be calculated as:

$$V_a^2 = (V_0 + V_w \cos \beta_w)^2 + (V_w \sin \beta_w)^2 \quad (\text{Eq.13})$$

- And yaw angle:

$$\psi_w = \tan^{-1} \left( \frac{V_w \sin \beta_w}{V_0 + V_w \cos \beta_w} \right) \quad (\text{Eq. 14})$$

- The dynamic pressure:  $p = \frac{\rho V_a^2}{2}$
- The aerodynamic forces and moments:

$$\left\{ \begin{array}{l} F_D = \text{drag force} = C_D A \frac{\rho V_a^2}{2} \\ F_L = \text{lift force} = C_L A \frac{\rho V_a^2}{2} \\ M_R = \text{rolling moment} = C_R A h \frac{\rho V_a^2}{2} \\ M_P = \text{pitching moment} = C_P A h \frac{\rho V_a^2}{2} \\ M_Y = \text{yawing moment} = C_Y A h \frac{\rho V_a^2}{2} \end{array} \right. \quad (\text{Eq.15})$$

In these forces and moments equations,  $C_D$ ,  $C_S$ ,  $C_L$ ,  $C_R$ ,  $C_P$  and  $C_Y$  are the non-dimensional drag force, side force, lift force, rolling moment, pitching moment and yawing moment aerodynamic coefficients, respectively (see Figure 2.4-21).  $A$  is the characteristic area of the vehicle, which is usually taken as the projection of the total vehicle's front & side areas in relation to the yaw angle of the relative crosswind  $V_a$  (Batista & Perkovič 2014).

For large flow angles, the frontal area 'A' is no longer the area on which the flow impacts and does not fully characterise the aerodynamic forces. (Malviya et al. 2009). This frontal area 'A' is the front and side face projected normally to the flow direction plane.

$A = \text{projected area of the side face} + \text{projected area of the front face}$

$$A = (L \sin \psi_w + W \cos \psi_w)H$$

$$\text{Where: } \left\{ \begin{array}{l} L = \text{length of vehicle} \\ W = \text{width of vehicle} \\ H = \text{height of vehicle} \\ \psi_w = \text{yaw angle between relative velocity } V_a \text{ and direction of travel} \end{array} \right.$$

As stated in Batista and Perkovic (2014), "The fifteen equations, namely six equilibrium equations Eq.1 to Eq.6, constraint equation (Eq.8) and eight constitutive equations (Eq.11) and (Eq.12), include seventeen unknowns, namely twelve reaction forces, four traction forces and traction parameter  $q$ . The system is clearly indeterminate, and if Coulomb conditions (Eq.10) for each wheel are included, it becomes overdetermined. Consequently, from the system, one cannot determine all the unknowns. However, by inspecting the system, one may see that it is complete if only the resultant side force for each vehicle axis is included as unknowns. In this case, the solution of the system is the following expressions for vertical reaction forces":

$$F_{z1} = \frac{1}{2} \frac{b(mg - F_L)}{a + b} - \frac{1}{2} \frac{hF_S + M_R}{c} - \frac{1}{2} \frac{hF_D + M_P}{a + b} \quad (\text{Eq. 16})$$

$$F_{z2} = \frac{1}{2} \frac{b(mg - F_L)}{a + b} - \frac{1}{2} \frac{hF_S + M_R}{c} - \frac{1}{2} \frac{hF_D + M_P}{a + b} \quad (\text{Eq. 17})$$

$$F_{z3} = \frac{1}{2} \frac{a(mg - F_L)}{a + b} - \frac{1}{2} \frac{hF_S + M_R}{c} - \frac{1}{2} \frac{hF_D + M_P}{a + b} \quad (\text{Eq. 18})$$

$$F_{z4} = \frac{1}{2} \frac{a(mg - F_L)}{a + b} - \frac{1}{2} \frac{hF_S + M_R}{c} - \frac{1}{2} \frac{hF_D + M_P}{a + b} \quad (Eq. 19)$$

The following expressions for the resultant lateral force on each vehicle axis

$$F_{y1} + F_{y2} = \frac{bF_S + M_y}{a + b} - q' \frac{hF_S + M_R}{a + b} \quad (Eq. 20)$$

$$F_{y3} + F_{y4} = \frac{aF_S - M_y}{a + b} - q' \frac{hF_S + M_R}{a + b} \quad (Eq. 21)$$

$$\text{where: } q' = \frac{i_1 + i_2}{2} q - f_R \quad (Eq. 22)$$

The traction parameter is:

$$q = \frac{(a + b)[F_D + f_R(mg - F_L)]}{(i_1 b + i_2 a)(mg - F_L) + (i_2 - i_1)(hF_D + M_P)} \quad (Eq. 23)$$

By using expressions for aerodynamic forces and moments (Eq.15), the traction parameter may also be written as:

$$q = \frac{(a + b) \left[ f_R g m + (C_D - f_R C_L) \frac{\rho A V_a^2}{2} \right]}{(i_1 b + i_2 a) m g - [(i_2 - i_1) h (C_P + C_D) + (i_1 b + i_2 a) C_L] \frac{\rho A V_a^2}{2}} \quad (Eq. 24)$$

In a dynamic case, the wheels' side forces are proportional to the sideslip angle, which is assumed to be zero at the overturning condition.

$$F_{z1} + F_{z4} = F_{z2} + F_{z3} = \frac{1}{2} (mg - F_L) \quad (Eq. 25)$$

#### 2.4.2 Critical relative wind speed for Rollover to occur

The condition for rollover demands that the resultant vertical force on the wheels on the windward side results in the wheels simultaneously losing contact with the road (Batista & Perkovič 2014).

As seen in Figure 2.4-21, the condition occurs when:

$$F_{z1} + F_{z3} = \frac{1}{2} (mg - F_L) - \frac{hF_S + M_R}{c} = 0 \quad (Eq. 28)$$

It indicates that the vehicle rolls over around the leeward wheels (Figure 2.4-21). Therefore, the critical relative wind speed for Rollover can be determined by substituting the expression for aerodynamic in Eq.15 into Eq.28:

$$V_{\text{rollover}} = \sqrt{\frac{2mg}{\rho A} \frac{c}{[2h(C_S + C_R) + cC_L]}} \quad (\text{Eq. 29})$$

In conclusion, a rollover accident will occur when one side wheel's vertical reaction force falls to zero (Batista & Perkovič 2014).

#### 2.4.3 Critical relative wind speed for rotation to occur

According to Batista & Perkovič (2014), “The vehicle reaches the rotation condition if the side forces on one of its axles reach the friction limit”.

Therefore, as stated in (Batista & Perkovič 2014), since wheels on each vehicle axis are assumed to be rigidly connected, the sliding of wheels on the axis will be reached when both wheels satisfy equality Eq.10. From Eq.20, Eq.21, Eq.16 and Eq.19, the condition for wheels on the axle to slip is therefore:

$$\begin{cases} bF_S + M_y - q'(hF_S + M_R) = \mu_1[b(mg - F_L) - (hF_D + M_P)] \\ aF_S - M_y + q'(hF_S + M_R) = \mu_2[a(mg - F_L) + (hF_D + M_P)] \end{cases} \quad (\text{Eq. 30})$$

$$\text{Where: } \begin{cases} \mu_1 = \text{tyre's friction coefficient} \equiv \sqrt{\mu^2 - (i_1 q - f_R)^2} \\ \mu_2 = \text{tyre's friction coefficient} \equiv \sqrt{\mu^2 - (i_2 q - f_R)^2} \end{cases}$$

By substituting expressions for aerodynamic loads, Eq.15 yields critical apparent wind speed

Front Axle Slip:

$$V_{a,slip1} = \sqrt{\frac{2mg}{\rho A} \frac{\mu_1 b}{bC_S + h[C_Y - q'(C_S + C_R)] + \mu_1[bC_L + h(C_D + C_P)]}} \quad (\text{Eq. 31})$$

Rear Axle Slip:

$$V_{a,slip2} = \sqrt{\frac{2mg}{\rho A} \frac{\mu_2 a}{aC_S + h[C_Y - q'(C_S + C_R)] + \mu_2[aC_L + h(C_D + C_P)]}} \quad (\text{Eq. 32})$$

#### 2.4.4 Critical relative wind speed for sideslip to occur

When all the vehicle's wheels' reaction side forces simultaneously reach their maximal values permitted by friction, the vehicle is just beginning to slide (Batista & Perkovič 2014). In this case:

$$F_{y1} + F_{y2} + F_{y3} + F_{y4} = \mu_1(F_{z1} + F_{z2}) + \mu_2(F_{z3} + F_{z4}) \quad (\text{Eq. 34})$$

The critical relative wind speed for the sideslip is:

$$V_{a,sideslip} = \sqrt{\frac{2mg}{\rho A} \frac{\mu_2 a + \mu_1 b}{(a + b)C_S + (\mu_2 a + \mu_1 b)C_L + (\mu_2 - \mu_1)h(C_D + C_P)}}$$

## 2.5 [Current regulations and design rules for road tankers carrying dangerous goods](#)

### 2.5.1 [Introduction](#)

Because this study aims to modify the semi-trailer tanker carrying dangerous goods to optimise its aerodynamic performance under crosswind conditions, current regulations and design rules need to be examined thoroughly to ensure that any modifications will not breach any of these regulations, such as the Static Roll Threshold (SRT), the safety requirements of the Performance-Based Standards, the Australian Design Rules and the Australian Standards AS2809 - road tank vehicles for dangerous goods.

Section 2.5.2 to section 2.5.5 present an overview of these regulations mentioned above, in which all clauses and sections in these regulations and rules not related to the scope of this study will not be considered.

### 2.5.2 [Static Roll Threshold \(SRT\)](#)

Each year in Australia, hundreds of trucks roll over, causing significant loss of life, injuries, and damage to vehicles, properties and goods. Rollover occurs more commonly with trucks carrying unfixed loads such as bulk liquids and livestock. According to (VicRoads 2010), weather conditions, the type of loads, the condition of brakes, inappropriate speed when changing direction, and driver distraction are the leading causes of Rollover.

As defined in (WA\_Government 2022), "Static Roll Threshold (SRT) is a measure of vehicle's resistance to roll over sideways during a steady speed concerning manoeuvre". This threshold is mainly used in designing heavy vehicles such as trucks, dog trailers, semi-trailers, and pig trailers to measure the vehicle's potential to roll over sideways, especially determining the maximum height of the load's centre of gravity from the ground. Vehicles with lower SRT value are more likely to roll over than those with higher SRT value, especially when going around sharp bends, subject to severe weather and sudden emergency manoeuvres.

According to the Australian National Heavy Vehicle Regulator (NHVR), SRT is one of the mandatory safety criteria assessment rules. SRT compliance certificate is required for all heavy vehicles that carry dangerous or non-dangerous goods. The minimum SRT value for road tankers carrying hazardous goods is 0.4g, as stated in (NHVR 2022): "Road tankers hauling dangerous goods in bulk and buses and coaches not less than 0.40g, and other vehicles not less



than 0.35g". In this expression, SRT is the lateral acceleration measured in g-force ( $g = 9.81 \text{ m/s}^2$ ).

Figure 2.5-23 shows the relationship between rollover crash risk and the SRT, in which the high SRT value results in a lower crash risk rate. In this Figure, the relative crash rate is calculated by the total number of crashes / million vehicles in a specific study period.

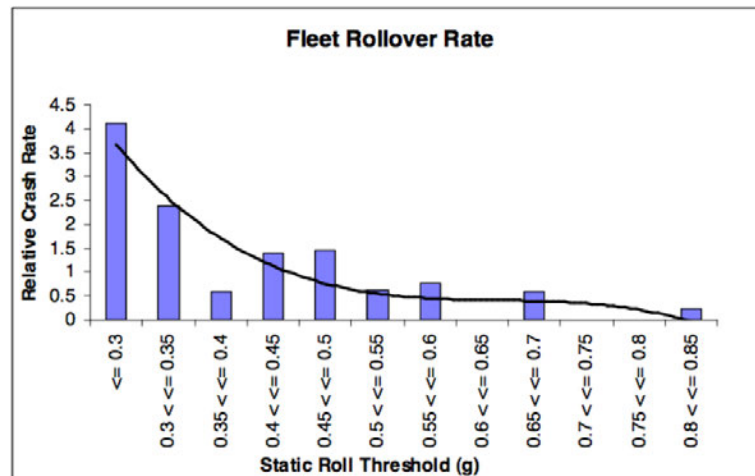


Figure 2.5-23: Relationship between rollover crash risk and SRT. Source (De Pont et al. 2002)

In 2017, a simple method of estimating the SRT value of a vehicle was developed by John De Pont (2017) and was approved for use by the New Zealand Transport Agency. The SRT value is estimated from the centre of gravity (CoG) position. The governing Equation for calculating this value is (De Pont 2017):

#### Equations of the Static Rollover Threshold

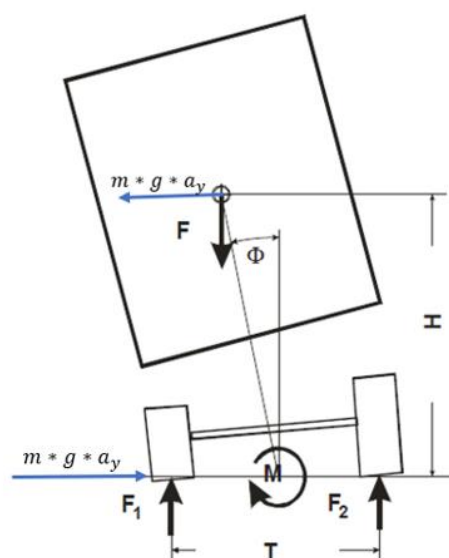


Figure 2.5-24: Vehicle Roll Notation. Source (De Pont et al. 2002)

Where:

$$\left\{ \begin{array}{l} a_y = \text{lateral acceleration } \left( \frac{m}{s^2} \right) \\ F_i = \text{vertical tire loads } (N) \\ g = \text{gravitational constant } \left( \frac{m}{s^2} \right) \\ H = \text{the height of the Centre of Gravity (CoG) } (m) \\ m = \text{mass of the vehicle } (kg) \\ T = \text{track width } (m) \\ \phi = \text{total roll angle due to the compliances in tyres, suspension and other parts of vehicle} \\ F(N) = m * g = \text{Weight of the vehicle} \end{array} \right.$$

Figure 2.5-24 shows a simple roll-plane model of a vehicle. The equilibrium for roll moments acting on the vehicle is (Ervin et al. 2002):

$$m * g * a_y * H = (F_1 - F_2) * \frac{T}{2} - F * \phi = (F_1 - F_2) * \frac{T}{2} - m * g * \phi$$

According to Ervin et al. (2002), the definition of the Static Rollover Threshold (SRT) is the lateral acceleration (measured in  $m/s^2$ ) that causes the tires on one side of the vehicle to lift from the road surface. That is the lateral acceleration at which  $F_2 = 0$ , and by the summation of vertical loads,  $F_1 = m * g$ .

Therefore, the SRT is derived as (Ervin et al. 2002):

$$SRT \left( \text{in } \frac{m}{s^2} \right) = a_y = \frac{T}{2H} - \phi$$

From this equation, it can be seen that the SRT is measured by the two quantities of the vehicle, which are (Ervin et al. 2002):

- The ratio of half-track to the height of the CoG
- The total roll angle due to compliance of the tyre, suspension and other parts of the vehicle.

The Static Rollover Threshold (SRT) can also be measured in g-force because this is the term used in most regulations and rules. The SRT, which is measured in g-force, can be derived as:

$$SRT \text{ (in g force)} = SRT \text{ (in } m/s^2) / g$$

Moreover, the lateral (side) force that causes the vehicle to rollover is:

$$F_s = m * SRT \text{ (in g force)}$$

Although there is a simplified equation, determining the Static Roll Threshold (SRT) value is not a straightforward process, especially the total roll angle  $\phi$ . It involves multiple equations and input data. However, helpful resources, such as the SRT calculators established by the New Zealand and Western Australian governments, simplify the calculation process to help designers determine the vehicle's SRT value. (

Appendix F – SRT calculators) shows the available SRT calculators mentioned above with step-by-step instructions and drawings.

In this study, the SRT calculator will be utilised to determine the SRT value of the investigated semi-tanker. This value will then be used to assess whether the side force resulting from the simulation process could potentially lead to a rollover accident. Based on these findings, recommendations can be provided regarding the optimal operating conditions for the tanker, including setting a maximum speed to avoid adverse weather conditions.

An example of side force that causes a rollover accident to occur can be calculated as follows:

Figure 2.5-25 shows a 3-axle trailer with a total mass of  $m = 25 \times 10^3 (kg)$  and a rollover threshold  $SRT = 0.3g$ . A minimum side force that will cause the vehicle to roll over is calculated (De Pont 2017):

$$F_{S,min} = m \times SRT = 25 \times 10^3 \times 0.3g = 73,575(N) = 7.5 \times 10^3 (kg)$$

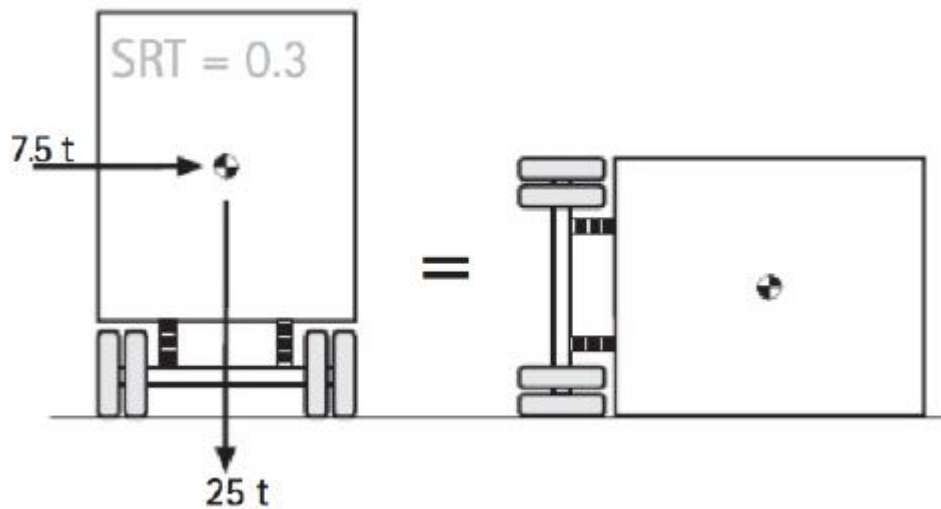


Figure 2.5-25: Minimum Force that causes Rollover to occur. Source (De Pont 2017)

### 2.5.3 Performance-Based Standards (PBS)

As stated in (NHVR 2022), “The PBS scheme is a world-leading program that allows Australia's heavy vehicle industry to match the right vehicles to the right tasks. It gives industry the opportunity to innovate with vehicle design to improve productivity and achieve safer performance while minimising impacts on the environment and road infrastructure and improving overall safety.”

Besides, the PBS Approval process is a strict procedure to ensure PBS vehicles are designed and built to operate as productively, safely and sustainably as possible on networks appropriate for their level of performance. The PBS approval is required for all vehicles carrying dangerous goods, and the approval process is shown in Figure 2.5-26 (NHVR 2022).

In addition to the minimum SRT value (0.4g) requirement for semi-trailer tankers mentioned in section 2.5.1, Other PBS's safety standard criteria must be satisfied when designing a semi-trailer tanker. They are (NHVR 2022):

- The length limit of a semi-trailer is 20m, including the prime mover.
- This project does not consider startability, gradeability, low-speed swept path, and acceleration capacity.
- The frontal swing, which is the maximum projection of the front overhang of the hauling unit outside the path of the front steering wheel in a prescribed 90 degrees low-speed turn, is less than 0.85m, as shown in Figure 2.5-27.
- The General Mass Limit (GML), Concessional Mass Limits (CML), Higher Mass Limits (HML) and weight distribution must adhere to PBS regulations, as shown in Table 2.5-2.

In conclusion, the summary of PBS safety criteria, such as the maximum length and maximum permit mass, required for designing a semi-trailer tanker shape is shown in Appendix G.

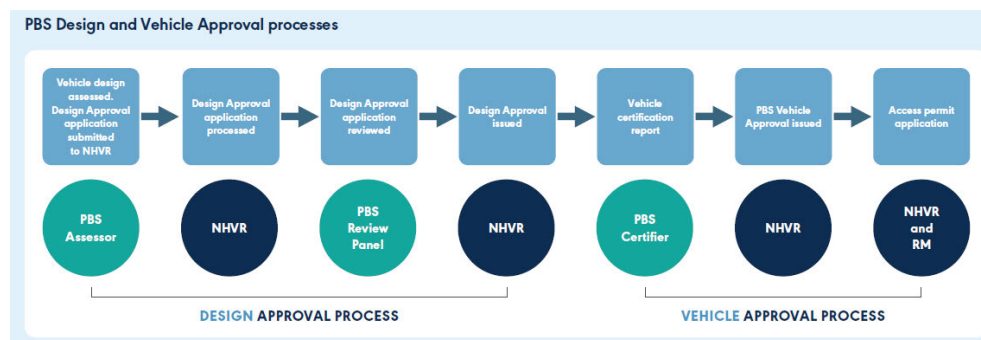


Figure 2.5-26: The PBS approval process. Source (NHVR 2022)

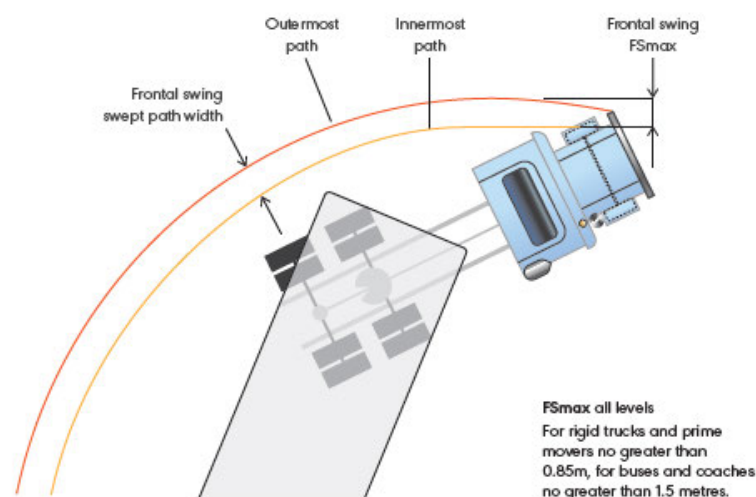


Figure 2.5-27: Frontal Swing Requirement. Source (NHVR 2022)

Table 2.5-2: Maximum weight and weight distribution of Level 1 semi-trailer. Source (NHVR 2022)



A PBS 20m prime mover and tri-axle semitrailer is approved at Level 1, with the masses in Table 7:

	Steer <sup>1</sup> (t)	Drive (t)	Trailer (t)	Total (t)	Length (m)
PBS Level 1 GML	6.5	16.5	20.0	43.0	≤ 20.0
PBS Level 1 CML	6.5	17.0	21.0	44.0	≤ 20.0
PBS Level 1 HML	6.5	17.0	22.5	46.0	≤ 20.0
Prescriptive tri-axle semitrailer GML	6.5	16.5	20.0	43.0	≤ 19.0
Prescriptive tri-axle semitrailer HML	6.5	17.0	22.5	46.0	≤ 19.0

#### 2.5.4 [Australian Design Rules \(ADRs\)](#)

The Australian Government defines that “The Australian Design Rules (ADRs) are national standards for vehicle safety, anti-theft and emissions. The ADRs are generally performance-based and cover issues such as occupant protection, structures, lighting, noise, engine exhaust emissions, braking and a range of miscellaneous items”. The third edition of ADRs became effective on 1 July 1988, and since then, it has become the National Standards for The Vehicle Standard Act 1989. Therefore, the design of any vehicle must adhere strictly to the ADRs specification (Government 2023).

These ADRs criteria will serve as a guide for modifying the tractor-trailer tanker, ensuring that all changes made to the tanker's barrel or chassis comply with the regulations.

The Australian Design Rules (ADRs) define general criteria for the structure of a semi-trailer tanker as follows:

- Every semi-trailer must have a continuous rear bumper bar with the lowest edges, not exceeding 600mm from the ground when unladen. Moreover, the bumper contact surface is not more than 600mm from the vehicle's rear (ADRs 2006a).
- The maximum length of the trailer (not including the prime mover) must not exceed 12.5m, and the distance from the 'Point of Articulation' (kingpin) to the line from which the 'Rear Overhang' is measured shall not exceed 9 m (ADRs 2006c). Besides, the forward projection from the 'Point of Articulation' of the 'Semi-trailer' portion of an 'Articulated Vehicle' shall be contained within a radius of 1.9 m (ADRs 2006c). It can be

understood that the swing radius from the kingpin to the tank barrel's furthest point must be within a 1.9m radius.

- Every 'Semi-trailer' shall be contained wholly within the envelope shown in Figure 2.5-28 when viewed in the plan (ADRs 2006c).
- The maximum overall width (including any equipment) of the semi-trailer must not exceed 2.5m (ADRs 2006c).
- Although the maximum road speed limit for road trains is 90km/h (ADRs 2006b), semi-trailers' speed limit shall be no greater than that determined by the appropriate State or Territory authority.

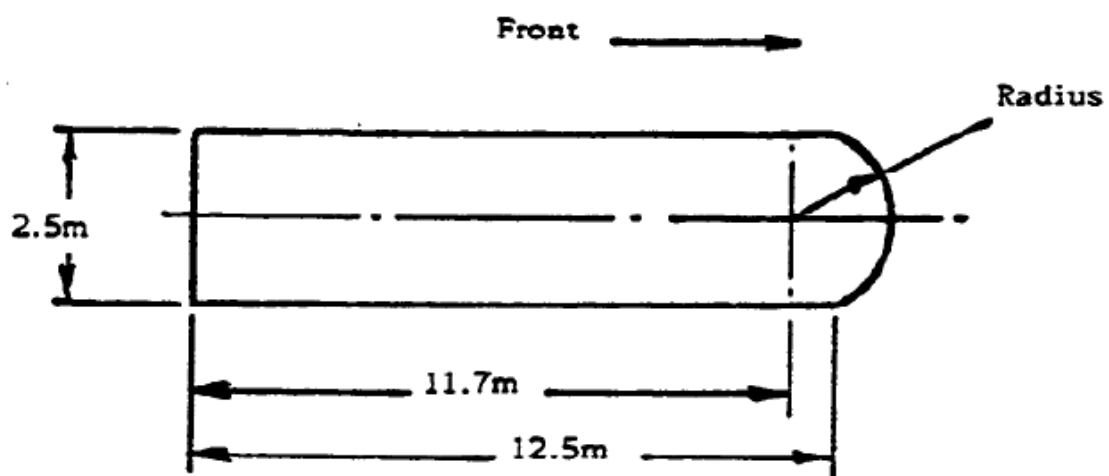


Figure 2.5-28: Envelope of Semi-Trailer. Source (ADRs 2006c)

#### 2.5.5 Australian Standards for Road Tank Vehicles Carrying Dangerous Goods

The Australian standard AS2809 is specifically designed for road tank vehicles in addition to Australian Design Rules. The objective of this standard is to provide designers, planners, operators and regulators with technical requirements for road tanker vehicles transporting dangerous goods, as stated in (Standards\_Australia 2020b).

The Australian Standards AS2809 has six parts, they are:

- AS2809.1 - Road tank vehicles for dangerous goods - Part 1 (General requirement for all road tank vehicles)
- AS2809.2 - Road tank vehicles for dangerous goods - Part 2 (Road tank vehicles for flammable liquids)
- AS2809.3 - Road tank vehicles for dangerous goods - Part 3 (Road tank vehicles for compressed liquified gas)

- AS2809.4 - Road tank vehicles for dangerous goods Part 4 (Tankers for toxic and corrosive cargoes)
- AS2809.5 - Road tank vehicles for dangerous goods Part 5 (Tankers for bitumen-based products)
- AS2809.6. - Road tank vehicles for dangerous goods Part 6 (Tankers for cryogenic liquids)

Because this project only considers the trailer tanker carrying fuel/diesel, only AS2809.1 and AS2809.2 are considered. The criteria addressed in the two parts define the requirements that the design or modification of road tankers must satisfy.

In AS2809.1 Part 1 - General requirements for all road tankers, section 2 – vehicle design and construction states that: (Standards\_Australia 2020b)

- For all road tank vehicles, portable tanks and demountable tanks except rigid road tanks, the maximum allowable stability angle shall be 62 degrees. Figure 2.5-29 demonstrates this criterion. This angle will determine each tanker's maximum kingpin height from the ground.
- The Static Roll Threshold (SRT) value shall equal or exceed 0.4g.
- Clause 2.1.4 in (Standards\_Australia 2020b) states that the ground clearance for tank components and protection devices directly attached to the tank shall be not less than 250mm within 1m of any axle or 350mm for any other location when the vehicle is unladen.
- The length of the rear underrun protection device (RUPD) shall extend to within 300mm of the width of the widest rear axle measured at the outermost points of the wheels, excluding the bulging of the tyres close to the ground.
- The distance from the ground plane to the underside of the RUPD shall not exceed 550mm over its entire length when the road tank vehicle is unladen.
- A ladder and handrail must be provided for the top-loading tanker and adhere to the Australian Standard AS 1657.

AS2809.2 Part 2 – Road tank vehicle for flammable liquids, Section 2 – Design, construction, inspection and testing states that: (Standards\_Australia 2020a)

- The material used in the construction of tanks shall not be of a lesser quality than the grades specified in Table 2.5-3. Therefore, any attempt to change the tank's material to reduce weight needs to ensure that this material requirement is met.
- Clause 2.2.2 – Design criteria require the design load for the tank shall not less than 2g applied along each axis (vertical, longitudinal and lateral). This design load includes the total tank mass, accessories, and cargo when filled to the safe fill level. The mass of the cargo shall be calculated from its actual density or 1000 kg/m<sup>3</sup>, whichever is greater.
- The design pressure shall be the summation of the following:
  - Pressure due to the liquid head (calculated from its actual density or 1000 kg/m<sup>3</sup>, whichever is greater)

- Vapour pressure (minimum of 20 kPa for the small-compartment tanks and large-compartment R-type tanks, or a minimum of 30 kPa for large-compartment U-type tanks).
- Hatches and fittings on top of the tank shall be protected with rollover protection which conforms with the following requirements, as appropriate:
  - For small-compartment tanks and large-compartment R-type tanks, the rollover protection shall comprise a guard in the form of inverted U-coaming (Rollover coaming) and valances.
  - The thickness of the valance shall not be less than the value given in Table 2.5-4. The space between the U-coamings shall be closed by valances level with the top of the coaming at the front and at least 50mm high at the rear.
  - The front valance shall have a rearward-facing return of a minimum of 25mm.
  - Table 2.5-5 shows an example of heights for rollover protection.

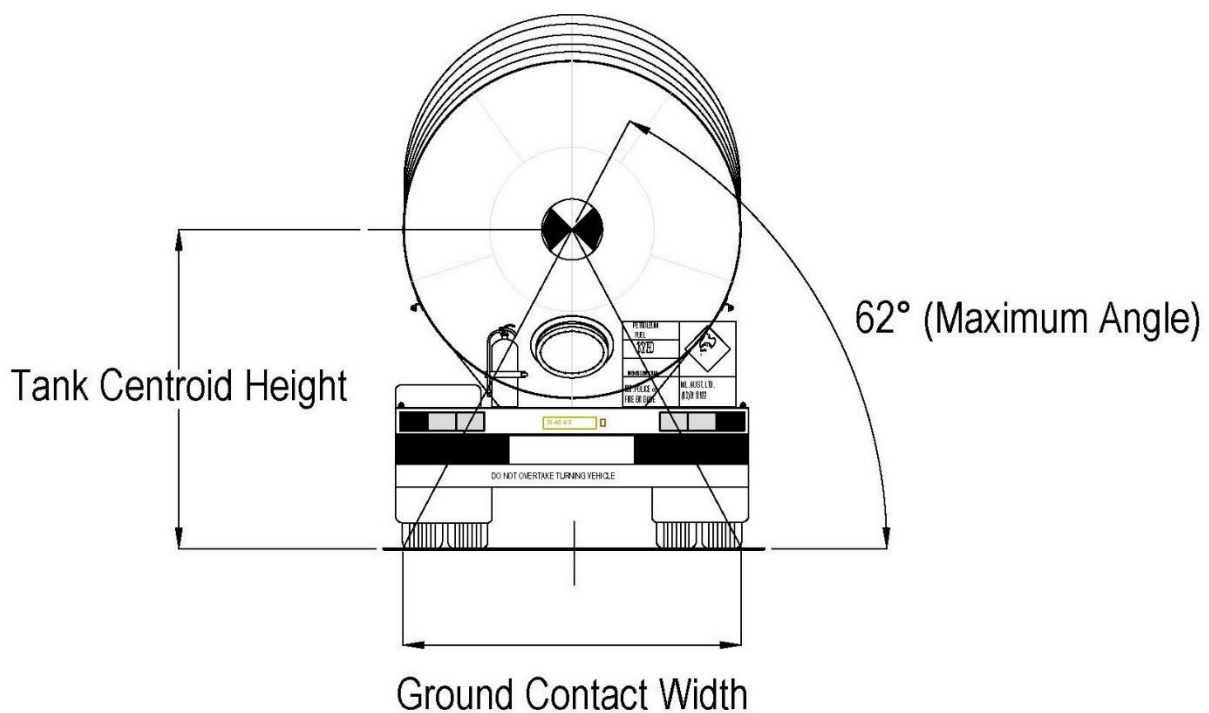


Figure 2.5-29: Stability Angle of road tank vehicle. Source [Tigerspider](#)



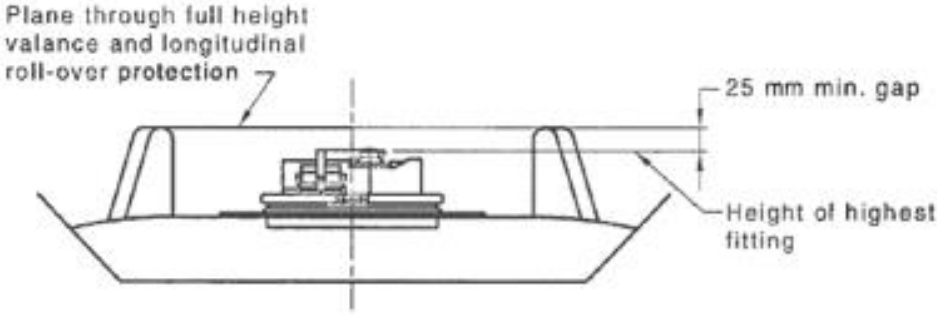
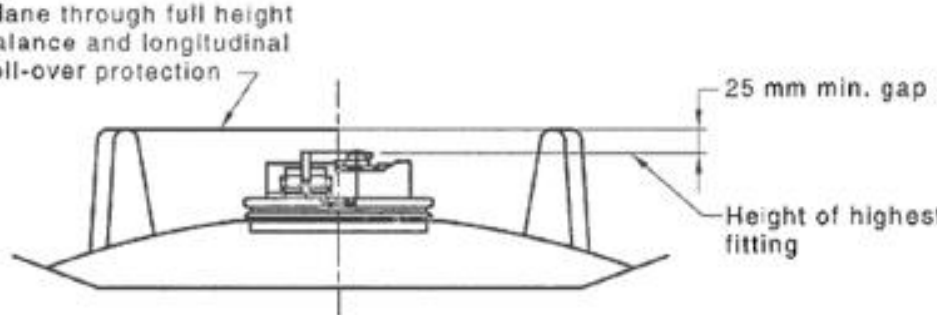
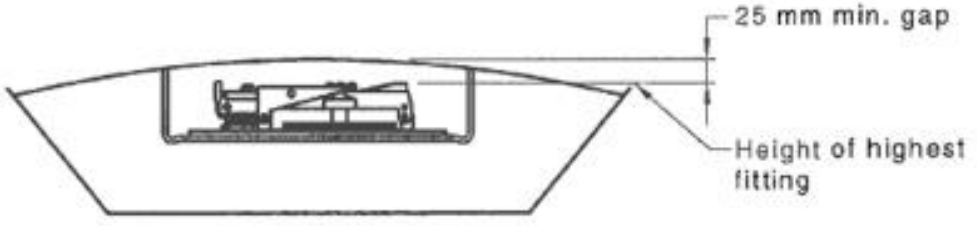
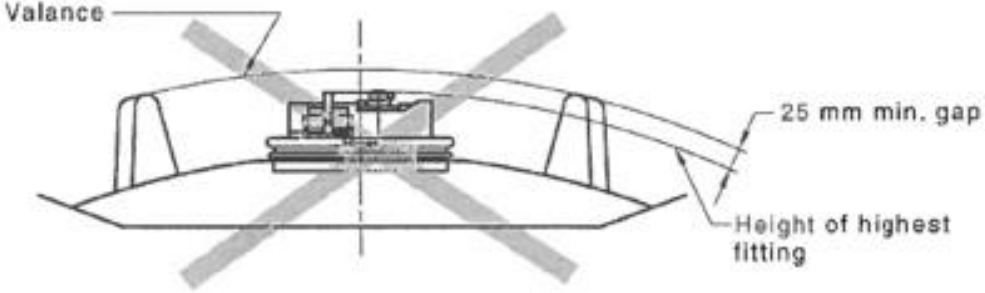
Table 2.5-3: Minimum material grades and mechanical properties (Standards\_Australia 2020a)

	Material			
	Aluminium	Low carbon steel	High strength low alloy steel	Stainless steel
Material grade	AS/NZS 1734 Grade 5454 H32 <sup>a</sup>	AS/NZS 3678 Grade 250	AS 3597 Grade 500	ASTM A240 Grade 304
Yield strength (MPa)	180	280	500	205
Ultimate tensile strength (MPa)	250	410	590	515
Elongation (%)	10	22	20	40
<sup>a</sup> Due to the level of deformation required to form heads, bulkheads and baffles, the use of O temper aluminium in the same grade may be used.				

Table 2.5-4: Thickness of material for U-coamings and valances. Source (Standards\_Australia 2020a)

Type of tank	Thickness mm		
	Aluminium	Low carbon steel	High strength low alloy or stainless steel
Large compartment U type tank	6	5	5
Small compartment and large compartment R type tank	5	3	2.5

Table 2.5-5: Example of heights for rollover protection. Source (Standards\_Australia 2020a)

 <p>Plane through full height valance and longitudinal roll-over protection</p> <p>25 mm min. gap</p> <p>Height of highest fitting</p> <p>(a) Conforming roll over coaming</p>
 <p>Plane through full height valance and longitudinal roll-over protection</p> <p>25 mm min. gap</p> <p>Height of highest fitting</p> <p>(b) Conforming roll over coaming</p>
 <p>25 mm min. gap</p> <p>Height of highest fitting</p> <p>(c) Conforming integrated manway</p>
 <p>Valance</p> <p>25 mm min. gap</p> <p>Height of highest fitting</p> <p>(d) Non-conforming roll over coaming</p>

## 2.6. CFD Modelling of Flow Over a Tractor-Semitrailer Tanker

### 2.6.1 Introduction

Traditionally, the only way for engineers to optimise their design is to conduct physical tests on product prototypes. However, the availability and advancement of virtual Computational Fluid Dynamics (CFD) simulation technology have opened up a low-cost analysis and visualisation of airflow behaviour and aerodynamics. It significantly reduces the cost and lead times for new designs, enabling the ability to study systems where controlled experiments are extremely difficult or impossible to perform, such as analysing the system under hazardous conditions or beyond their normal [performance limits. Therefore, CFD has become a commonly applied tool for predicting real-world physics (SIMSCALE 2023a).

Versteeg and Malalasekera (2011) state that “CFD analysis is the discipline of science devoted to predicting fluid flow, heat transfer, mass transfer and chemical reactions by solving the governing equations using computational power ”. Since the 1960s, the aerospace sector has incorporated Computational Fluid Dynamics (CFD) techniques into various aspects of aircraft and jet engine design, research and development, and manufacturing processes. Recently, these methods have found application in designing internal combustion engines, combustion chambers for gas turbines, and furnaces. Additionally, automotive manufacturers now regularly employ CFD to anticipate drag forces, analyse under-bonnet air flows, and optimise in-car environments. As a result, CFD is progressively emerging as an indispensable element in the design of industrial products and processes. However, the tremendous complexity of CFD analysis requires an excellent understanding of the CFD analysis’s theories and the modelling skills of users to provide easy access to its solving power and problem parameters sophisticated data input user interfaces, as well as to examine the results (Versteeg & Malalasekera 2011).

Versteeg and Malalasekera (2011) state that “CFD technology consists of three main stages: pre-processing, solving and post-processing stages”.

The pre-processing stage involves activities (Versteeg & Malalasekera 2011) such as:

- Defining the geometry’s region of interest (the computational domain)
- Grid generating: sub-dividing the domain into a number of smaller, non-overlapping sub-domains ( a grid or mesh of cells or control volumes or elements).
- Selection of the physical and chemical phenomena that need to be modelled.
- Defining fluid properties.
- Specifying the appropriate boundary conditions at cells that coincide with or touch the domain boundary.

Although there are three distinct streams of numerical solution techniques such as finite difference, finite elements and spectral methods, the solving stage considered in this project is the finite volume method. It is central to most well-established CDF codes, such as CFX and FLUENT. The solving stage consists of the following steps (Versteeg & Malalasekera 2011):

- Integration of governing equations of fluid flow over all the control volumes of the domain.

- Discretisation – conversion of the resulting integral equations into a system of algebraic equations.
- Solution of the algebraic equations by an iterative method.

The post-processing stage is where all the development work takes place. This stage is supported by the many outstanding graphics capabilities listed below (Versteeg & Malalasekera 2011):

- Domain geometry and grid display
- Vector plots
- Line and shaded contour plots
- 2D and 3D surface plots
- Particle tracking
- View manipulation (translation, rotation, scaling)
- Colour PostScript output
- Animation display for dynamic results.

In solving fluid flow problems, the operator must have skills in several areas to set up and run the CFD simulation correctly to give a result as good as the physics embedded in it and, at worst, as good as its operator (Versteeg & Malalasekera 2011). Therefore, the mentioned main stages must be carefully investigated before performing CFD simulations.

### 2.6.2 CFD Pre-Processing Stage

#### *a) Geometry Creation and Simplification.*

The very first step in the Pre-Processing stage is geometric creation and simplification. This step requires a geometric that is accurate and simple enough for the simulation to run without consuming too much time and computer resources. It means that the geometric should capture the precise shape, dimensions and any specific features like mirrors, spoilers or air vents, which may cause inaccurate results if they do not exist in the geometry. Besides, for external flow analysis, unnecessary components and features such as internal parts and fasteners can be omitted in the geometry to reduce time-consuming and errors in the meshing step. Moreover, any features such as slivers (extremely thin, high-aspect-ratio geometry faces), small gaps and overlaps that cause problems in the meshing operation should be avoided (Smith 2015).

The next important step of the pre-processing stage is the definition and creation of the geometry of the flow region, which is the computational domain for the CFD calculation. For external flow analysis, Tu et al. (2018) discuss the importance of the size of the geometry “One important aspect that should always be noted in the creation of the geometry for CFD calculations is to allow for flow dynamics to be sufficiently developed across the length of the computational domain.”

As suggested by Idelsimulations (2020), “When deciding on the size of the computational domain for external aerodynamics problem, it would be beneficial to know in advance the

effect of the body on the surrounding flow field”. It can be done by considering the previous CFD simulation of similar geometries. If the previous studies are not available or when carrying out a simulation with a large domain is not feasible due to the computational cost, it is possible to use experience and best practices to estimate the domain dimensions (Idealsimulations 2020a). The author also recommends the best practices for dimensioning a domain at the starting point:

- Roughly two times the body length at the upstream region, enough to allow the flow to adjust due to the presence of the geometry.
- Approximately a minimum of five times the body length at the downstream region to allow enough space for the boundary condition imposed at the domain outlet. The best practice is between 5 and 20 times the body length.
- Minimum two times the body width on each side to allow for local flow deviation.

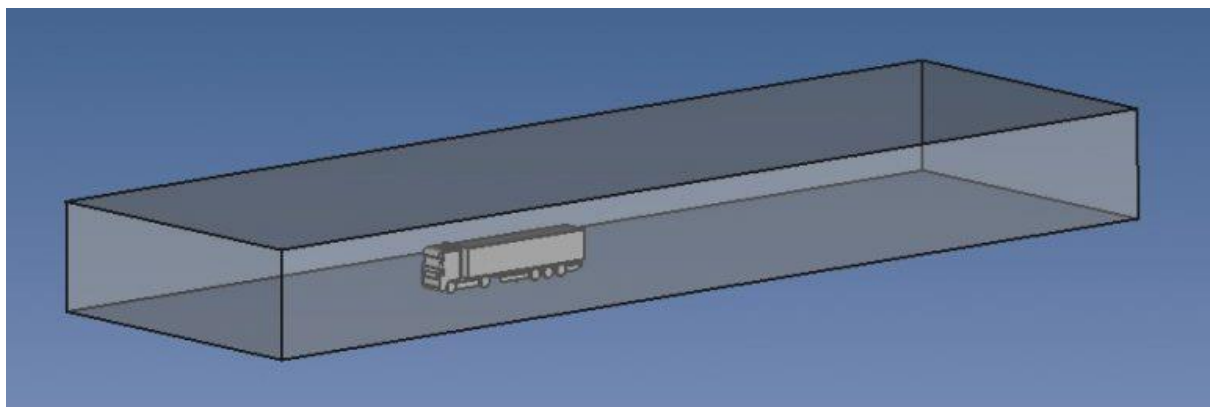


Figure 2.6-30: Computational domain for a CFD simulation of a heavy-goods vehicle. (Idealsimulations 2020a)

Besides, for the height of the domain, “It needs to be a distance that sufficiently removes any of these boundary effects on the fluid flow surrounding the body but still manageable for CFD calculations”, as stated by (Tu et al. 2018), best practice for the domain height is about two times the length of the body itself.

The domain geometry in this project is built based on the recommended dimensions. Then it is adjusted during the simulation process to allow the flow to be fully developed.

#### b) Mesh Generation, Mesh Type and Mesh Quality

##### Mesh Generation:

Mesh generation is essential for CFD simulation because it requires the domain to be subdivided into several smaller, nonoverlapping subdomains to solve the flow physics within the domain geometry. Tu et al. (2018) state, “The accuracy of a CFD solution is strongly influenced by the number of cells in the mesh within the computational domain”. The accuracy of the solution generally improves with an increase in the number of cells. However, this improvement is also affected by various other factors. These factors include the type of mesh used, the accuracy order of the numerical

method employed, and the appropriateness of the chosen techniques for the specific physics of the problem. Nonetheless, it ultimately remains the responsibility of the CFD user to skillfully design a mesh that strikes a balance between design accuracy and solution cost (Tu et al. 2018).

#### Mesh Types:

The structured mesh type, also known as Cartesian mesh, is the simplest mesh type for grid generation. It divides the domain into cubes using the Cartesian coordinate system. However, when dealing with complex geometries that do not align with the structured grid's coordinate lines, such as flow around cylindrical or elliptical shapes, using a fine Cartesian mesh can result in simulation errors or excessive computer resource usage. Therefore, two mesh types are introduced: structured curvilinear grids and unstructured grids (Versteeg & Malalasekera 2011).

Structured curvilinear or body-fitted grids involve mapping the flow domain onto a computational domain with a simpler shape. These grids are effective in handling flows like the half-cylinder problem. However, finding viable mappings proves to be difficult when the geometry becomes very complex. In such cases, dividing the flow domain into multiple sub-regions or blocks is often beneficial, each meshed separately and properly connected to neighbouring blocks. This approach leads to block-structured grids offering greater flexibility than Cartesian or body-fitted meshes (Versteeg & Malalasekera 2011).

For the complex geometries such as the tractor-semitrailer tanker geometry in this project, “the ideal mesh type is the unstructured grid, where each mesh cell is a block. It gives unlimited geometric flexibility and allows the most efficient use of computing resources for complex flows, so this technique is now widely used in industrial CFD”, as stated in Versteeg and Malalasekera (2011).

One of the main advantages of an unstructured grid is that it does not impose any implicit structure of coordinate lines. This allows for greater flexibility in concentrating the mesh without wasting computer storage. Additionally, unstructured grids enable control volumes to have arbitrary shapes, and there are no limitations on the number of adjacent cells that can meet at a point or along a line (Versteeg & Malalasekera 2011).

In practical Computational Fluid Dynamics (CFD), triangles or quadrilaterals are frequently employed for 2D problems due to their simplicity and computational efficiency. On the other hand, for 3D problems, a more comprehensive range of element shapes is commonly used in CFD simulations. These include tetrahedral, hexahedral, and polyhedral elements. Tetrahedral elements consist of four-sided pyramids and are suitable for representing complex geometries with irregular shapes. Hexahedral elements are six-sided polyhedra resembling boxes or cubes and are well-suited for representing regular and symmetric geometries. Polyhedral elements are created by combining tetrahedral cells into more complex polyhedral shapes. They compromise tetrahedral elements' flexibility and hexahedral elements' efficiency. These different element shapes efficiently represent the geometry of the problem and enable

accurate calculations in the respective dimensions, contributing to the overall effectiveness of CFD simulations (Versteeg & Malalasekera 2011). Therefore, this project's geometry meshed with the Polyhedral mesh type.

Figure 2.6-31, Figure 2.6-32 and Figure 2.6-33 show examples of triangular mesh, tetrahedral and hexahedral meshes and polyhedral mesh, respectively.

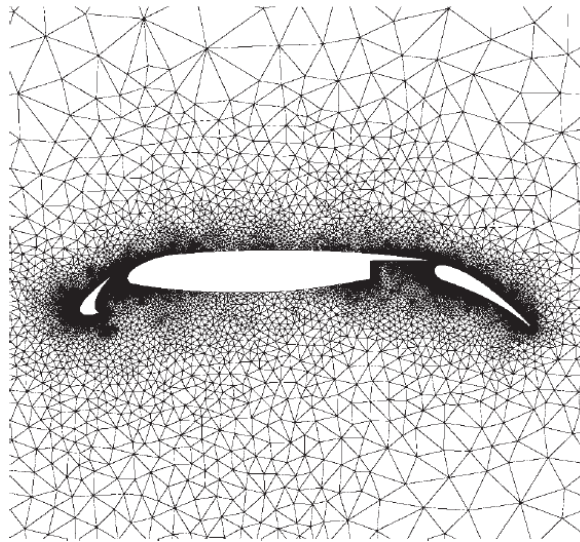


Figure 2.6-31: Triangular mesh example (Versteeg & Malalasekera 2011)

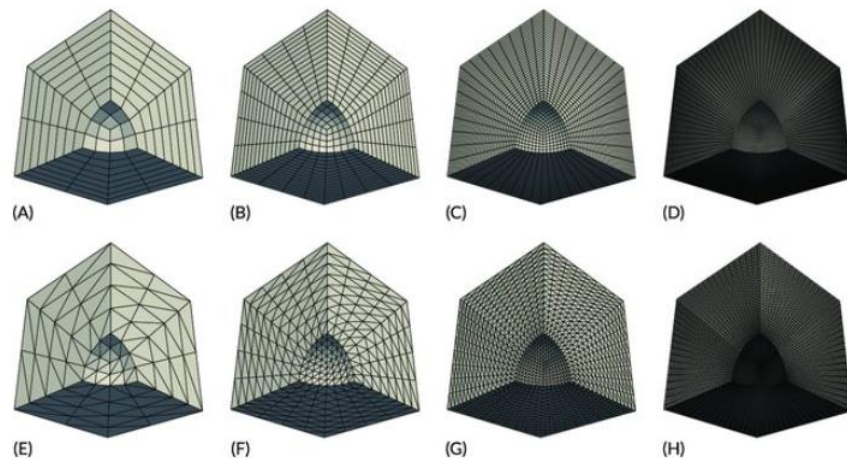


Figure 2.6-32: Hexahedral (A-D) and tetrahedral (E-H) meshes. (Sharma et al. 2017)



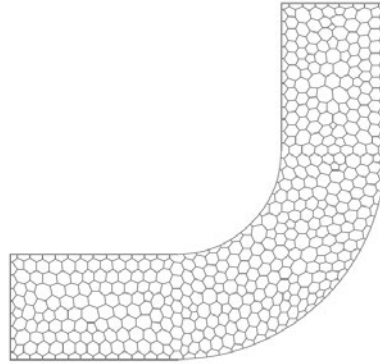


Figure 2.6-33: A grid consisting of polyhedral cells of the 90° bend geometry. (Tu et al. 2018)

### Mesh Quality

Ensuring the accuracy and stability of simulation results relies heavily on the generated mesh's quality. Thus, assessing the mesh quality before commencing the simulation process is crucial, as meshing often poses a bottleneck. Guaranteeing a high-quality mesh is vital for achieving fast and accurate analysis. As a practical approach, starting with a coarse mesh during the initial steps is advisable, allowing for an evaluation of computer storage and running time. Once the solution is observed to be converging, further mesh refinement can be performed in the flow domain, ultimately leading to the desired Computational Fluid Dynamics (CFD) solution (Tu et al. 2018).

According to Wandel (2021), mesh quality can be assessed using three criteria: element quality, skewness, and orthogonal quality. If the mesh fails to meet these criteria, modifications to the mesh are necessary. Here is a breakdown of each measure:

- **Element quality:** This criterion determines how close the element is to a cube or a tetrahedron. It is calculated by dividing the volume of the cell by the sum of the square of the edge length and multiplied by a scaling factor based on the cell's volume type. A value of 1 indicates a perfect match to the ideal shape, while zero signifies the cell has zero or negative volume.
- **Skewness:** Skewness measures the deviation of a shape from an equilateral triangle or a rectangle. A skewed form can be visualized as a triangle or rectangle, with the top being pushed sideways. A value of zero represents an exact shape, while a value of 1 indicates that two sides are in contact. Generally, values above 0.75 are considered poor, and values above 0.9 indicate that the shape is a sliver (two sides are so close). For valid mesh, the maximum skewness should be below 0.95, with the average skewness significantly lower. In this project, the target maximum skewness was set to 0.7, with the average skewness significantly below this value to generate a good volume mesh for the project's computational domain.
- **Orthogonal quality:** Orthogonal quality determines the alignment between the normal vector from the cell centre to the cell face and the vector from the cell centre to the neighbouring cell centre through that face. A zero value signifies that the normal vector is orthogonal to the cell centre direction vectors, while a value of



1 means that all vectors are parallel. For a valid mesh, the smallest orthogonal quality should be 0.01, with the average being much higher. The "Inverse Orthogonal Quality" is calculated as 1.

By evaluating the mesh based on these criteria, one can identify the need for mesh modifications to ensure better quality and accuracy in the simulation process (Wandel 2021).

c) *Specification of Boundary Conditions and Turbulence Models*

Boundary condition:

The complex nature of many fluid flow behaviours has essential implications in which boundary conditions are prescribed for the flow problem. Suitable fluid flow boundary conditions must be defined to represent the actual physical of the fluid flow into a solvable CFD problem (Tu et al. 2018).

Two boundary conditions are typically used in CFD (Versteeg & Malalasekera 2011):

- The Dirichlet boundary condition specifies the value the unknown function needs to take along the domain's boundary (SIMSCALE 2023b).
- The Neumann boundary condition specifies the values that the derivative of a solution is going to take on the domain's boundary (SIMSCALE 2023b).

Because all differential equations require boundary conditions for each independent dimension, CFD's most common boundary conditions, such as inlet, outlet, wall, prescribed pressure, symmetry and periodicity or cyclic boundary conditions, must be correctly specified to solve boundary-value problems (Versteeg & Malalasekera 2011).

Turbulence Modelling:

Regarding CFD simulations in engineering, turbulent flows are often encountered due to the inherent nature of engineering flows. Consequently, accurate turbulence modelling is vital in achieving correct and reliable CFD results. Turbulence modelling is considered one of the critical aspects of CFD modelling, given its significance in accurately capturing turbulent flow behaviour (Idealsimulations 2020b).

Three broad frameworks are used to solve the Navier–Stokes equations for complex industrial problems (Wandel 2021). They are:

- Large Eddy Simulation (LES) modelling
- Reynolds-Averaged Navier-Stokes (RANS) modelling for the steady flow
- URANS modellings for the unsteady flow
- Hybris RANS-LES modelling

Figure 2.6-34 compares these approaches based on computational cost, degrees of freedom, geometry complexity and modelling importance.

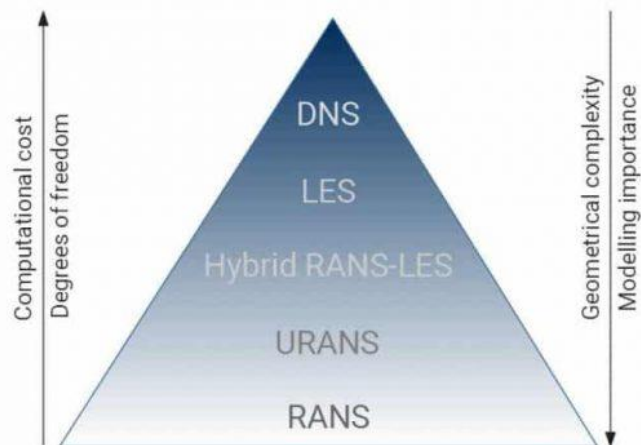


Figure 2.6-34: Turbulence models in CFD (Idealsimulations 2020b)

According to Tu et al. (2018), "It is possible to directly solve the governing equations of fluid flows, known as the Navier-Stokes equations, without relying on any modelling assumptions. This approach is referred to as Direct Numerical Simulation (DNS), and it involves solving the wide range of temporal and spatial scales present in turbulent flows, spanning from very large to very small scales, down to the Kolmogorov length scale". However, solving the Navier-Stokes equations without modelling assumptions increases the complexity of the problem, as it introduces a higher degree of freedom. In practice, this makes it practically impossible to apply DNS to engineering problems. Therefore, the DNS approach is primarily used in academic and research institutions to model simple flows in laminar regions or to enhance the understanding of turbulence without resorting to any turbulent model." (Idealsimulations 2020b)

Figure 2.6-34 illustrates the relationship between computational cost and modelling capabilities in CFD simulations. On the one hand, the computational cost of CFD simulations increases from RANS to DNS modelling due to the higher degrees of freedom required to solve the flow accurately. On the other hand, the ability to handle complex geometries and capture important flow features decreases from DNS to RANS. Consequently, RANS modelling is the most suitable choice for engineering projects involving complex steady-flow problems, such as the one at hand. RANS can handle intricate geometries while keeping the computational cost lower than other models (Idealsimulations 2020b).

### Reynolds-Averaged Navier-Stokes (RANS) modelling

According to (Versteeg & Malalasekera 2011), "An averaging operation can be applied to the Navier-Stokes equations to obtain the mean equations of fluid flows called

Reynolds Averaged Navier-Stokes (RANS) equations. These are similar to the original equations but contain some additional terms in the momentum equations called Reynolds stress terms that are unknown and need to be modelled.”

In CFD simulation, there are five most commonly used RANS turbulence models in CFD practices. They are the Spalart-Allmaras model, the k-epsilon ( $k-\epsilon$ ) model, the k-omega ( $k-\omega$ ) model, the Transition model and the Reynolds-Stress equation model (Wandel 2021).

Below is the summary of each model's advantages and disadvantages and the recommended choice for particular applications.

❖ The Spalart–Allmaras turbulence model:

Spalart–Allmaras turbulence model is a one-equation model that solves a modelled transport equation for the kinematic eddy turbulent viscosity. It was designed for the aerospace industry to predict flow around aerofoils with minimal additional computational expense accurately and can predict flows with adverse pressure gradients and separations (Wandel 2021).

Advantages (Menter et al. 2018):

- Provide improved performance relative to the k-epsilon model for flow with adverse pressure gradients and separations.
- The model only requires the solution of one transport equation instead of two. Therefore it reduces the use of computational resources significantly.

Disadvantages (Menter et al. 2018):

- The accuracy in predicting separation is lower than for optimal two-equation models like SST and GEKO.
- It is not well calibrated for free shear flows.
- The model does not predict the decay of freestream turbulence, which is essential for some laminar-turbulent transition predictions.

❖ The k-epsilon ( $k-\epsilon$ ) model

The k-epsilon turbulence model is commonly used in computational fluid dynamics (CFD) to simulate mean flow characteristics under turbulent flow conditions. It is a two-equation model that comprehensively describes turbulence through two transport equations. This model utilizes the turbulence kinetic energy ( $k$ ) and the turbulence kinetic energy dissipation rate ( $\epsilon$ ) to determine the turbulence viscosity (Wandel 2021).

Advantages:

- The k-epsilon model is ideal for predicting flow behaviour in regions away from the wall (Menter 2009).

- Predicts confined flows reasonably well, particularly if the flow is axisymmetric, even if there are recirculation zones (Wandel 2021).
- Low mesh density is required and can work with limited computational facilities (Wandel 2021).
- It uses wall functions with good convergence and low memory requirements (Solmaz 2023).
- Convenient: Can be used for external flow interactions with complex geometry and to deal with compressible and incompressible flows (Solmaz 2023).
- It is the simplest turbulence model where only initial or boundary conditions need to be supplied. Besides, it has excellent performance for many industrial relevant flows, is well established, and is the most widely validated turbulence model (Versteeg & Malalasekera 2011).

Disadvantages:

- Not accurate for non-slip walls, adverse pressure gradients, strong curvature into the flow and jet flows (Solmaz 2023).
- It has poor performance in a variety of important cases, such as some unconfined flows (such as flows not through pipes or ducts), flows with large strain rates, rotating flows, and flows driven by anisotropy of regular Reynolds stresses (Versteeg & Malalasekera 2011).

#### ❖ The k-omega (k- $\omega$ ) model

The k- $\omega$  model serves as an alternative to the k- $\epsilon$  model, primarily due to the challenges in accurately calculating the transport of  $\epsilon$ , which represents turbulence dissipation rate. To address this, the k- $\omega$  model introduces the concept of using turbulence frequency  $\omega = \epsilon/k$  as the second variable. In this model, the first transported variable is turbulence kinetic energy, denoted as k, which quantifies the energy within the turbulence. The second variable,  $\omega$ , represents the specific turbulence dissipation rate and determines the rate of dissipation per unit of turbulence kinetic energy (Wandel 2021).

Advantages:

- The k-omega model is well suited for simulating flow in the viscous sub-layer (Menter 2009).
- The k- $\omega$  model is good at resolving internal flows, separated flows and jets and flows with high-pressure gradients and internal flows through curved geometries (Menter et al. 2018).
- The k- $\omega$  model does not require wall functions. The wall boundary of k=0 is satisfactory (Wandel 2021).
- In external aerodynamics applications, The SST k- $\omega$  model is the most general, and tests suggest that it performs better for zero pressure gradient,

adverse pressure gradient boundary layers, and free shear layers (Versteeg & Malalasekera 2011).

Disadvantages:

- The major challenge for the model is that in a stationary freestream far away from any source of turbulence, both  $k$  and  $\omega$  must be zero, which causes the turbulent viscosity to be mathematically undefined.
- This model is severely restricted in flows where the transport assumptions for convective and diffusive effects do not apply – validation is necessary to define performance limits (Versteeg & Malalasekera 2011).
- Can suffer from stability problems attributed to the appearance of singularities in the factor  $\alpha_{ASM} = \alpha_{ASM}(P/\epsilon)$ , which becomes indeterminate in turbulence-free flow regions (Versteeg & Malalasekera 2011).
- The standard  $k$ - $\omega$  model has a strong dependency of the solution on the freestream value of  $\omega$  outside of shear layers. (Menter et al. 2018)

#### ❖ The Transition model

According to (Wandel 2021), “The transition of boundary layers from the laminar to turbulence is a complex process that requires additional attention.” In Ansys, the transition model consists of the Transition  $k$ - $k_L$ - $\omega$  model and the Transition SST model (Wandel 2021).

The Transition  $k$ - $k_L$ - $\omega$  model separates the total kinetic energy into turbulent kinetic energy ( $k$ ) and laminar kinetic energy ( $k_L$ ) to model the transition from the laminar boundary layer to the turbulent boundary layer. The Transition  $k$ - $k_L$ - $\omega$  model has also been shown to accurately predict boundary layer development and determine the transition point, making it particularly useful in flows with significant laminar regions (Wandel 2021).

According to Menter (2009), the Transition SST (Shear Stress Transport) models were developed to combine the best elements of the  $k$ - $\epsilon$ ,  $k$ - $\omega$ , and JK models, blending their different elements into a single formulation.

Advantages:

- The  $k$ - $\omega$  SST model provides a better prediction of flow separation than most RANS models and accounts for its good behaviour in adverse pressure gradients. It can account for the transport of the principal shear stress in adverse pressure gradient boundary layers. It is the most commonly used model in the industry, given its high accuracy to the expense ratio (Menter 2009).

Disadvantages (Wandel 2021):

- It should not be used for fully-enclosed flows (i.e. pipes and ducts): it requires at least one domain boundary to be a freestream (and this should not be in the direction of potential symmetry).
- It should only be used when there is at least one wall (i.e. there is a boundary layer): it cannot predict transition in free shear flows.
- It should not be used when there is a moving wall relative to the flow field, e.g. a car, where the ground moves relative to the car, or in turbomachinery, where rotor blades move relative to stator blades.
- It has not been calibrated for buoyancy or multi-phase flows.

#### ❖ The Reynolds-Stress Equation Model (RSM)

Due to its high complexity, the Reynolds-Stress Equation Model (RSM) represents the pinnacle of classical turbulence models. Referred to as a second-order or second-moment closure model, it stands apart from others in handling turbulence. Unlike models based on the eddy-viscosity hypothesis, RSM directly computes the individual components of the Reynolds stress tensor, bypassing the need for such assumptions. Using the precise Reynolds stress transport equation, these models account for the directional effects of Reynolds stresses and the intricate interactions within turbulent flows. Regarding accuracy, Reynolds stress models offer a significant advantage over eddy-viscosity-based models, providing superior results. Additionally, they are computationally more efficient than costlier methods like Direct Numerical Simulations (DNS) and Large Eddy Simulations (LES) (Versteeg & Malalasekera 2011).

Advantages (Versteeg & Malalasekera 2011):

- It is potentially the most general of all classical turbulence models.
- Only initial and (or) boundary conditions need to be supplied.
- Very accurate calculation of mean flow properties and all Reynolds stresses for many simple and complex flows, including wall jets, asymmetric channels, non-circular ducts, and curved flows.

Disadvantages (Versteeg & Malalasekera 2011):

- It is not widely used in industrial flow calculations because of the high computing cost due to the addition of seven extra PDE equations.
- This model can suffer from convergence problems.
- It is not as widely validated as the mixing length and  $k-\epsilon$  models.
- It performs just as poorly as the  $k-\epsilon$  model in some flows due to identical problems with the  $\epsilon$ -equation modelling (e.g. axisymmetric jets and unconfined recirculating flows).

❖ Conclusion: The recommended choice of turbulence models

As summarized in Wandel (2021), “For most flows, the Shear-Stress Transport (SST)  $k-\omega$  model is the best choice, but some other model may produce superior results for a particular case, so it is advisable to check the performance of several models and validate them”. The recommended steps to select the turbulence models are listed below, according to (Wandel 2021):

- The Shear-Stress Transport (SST)  $k-\omega$  model should be the first choice.
- If the effects of turbulence are less important than other effects, then the standard  $k-\epsilon$  model is suitable.
- If there are convergence issues with the SST  $k-\omega$  model, then the BSL  $k-\omega$  model or Realisable  $k-\epsilon$  model with Enhanced Wall Treatment should be tried.
- For aerofoils, the Spalart–Allmaras model is the best choice.
- The Reynolds-Stress model is best for flows with powerful swirls (e.g., cyclones, some combustors) and high anisotropy.
- For flows with a sizeable laminar region in a boundary layer where the opposite boundary is the freestream and there is crossflow instability, the intermittency transition model is the best option.
- The transition SST model is the best option for all other flows with a large laminar region in a boundary layer where the opposite boundary is the freestream. However, the other transition models are also likely to produce good results.

### 2.6.3 CFD Solving Stage

The second stage of CFD simulation is the solving stage. In this stage, a core understanding of the CFD solver's numerical aspects must be achieved before conducting any simulations. The prerequisite processes in the solution procedure that have implications on the computational solution are initialization, solution control, monitoring solution, CFD calculation, and checking for convergence, as shown in Figure 2.6-35 (Tu et al. 2018).

These CFD analysis prerequisite processes can be grouped into two steps. The first step is the initialisation and solution control, and the second is the convergence monitoring (Tu et al. 2018).

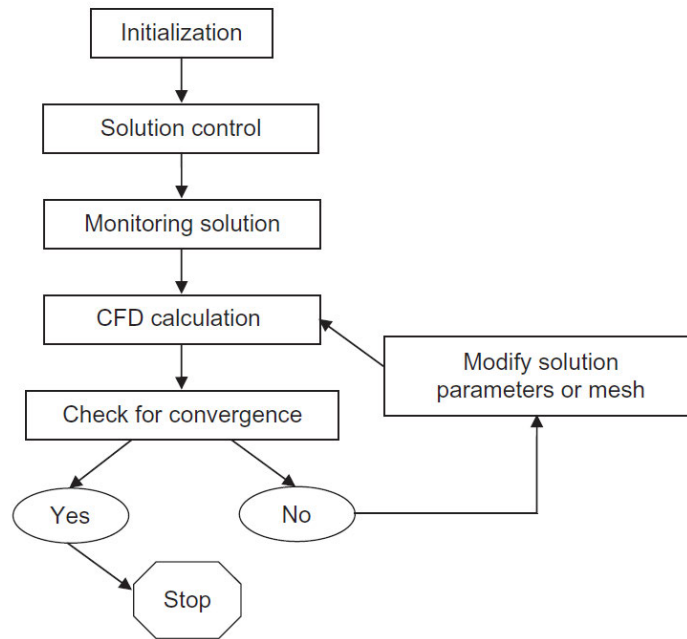


Figure 2.6-35: An overview of the solution procedure (Tu et al. 2018).

#### a) Initialisation and Solution Control Step

In this step, the values of the flow properties, such as the velocity, pressure, temperature and other transport parameters of interest, need to be initialised before calculating a solution (Tu et al. 2018).

According to Tu et al. (2018), It is important to note that good initial conditions are crucial to the iterative procedure. Three reasons for this are:

- If the initial conditions are close to the final steady-state solution, the quicker the iterative procedure will converge, resulting in a shorter computational time.
- If the initial conditions are far from reality, the computations will result in more extended computational efforts to reach the desired convergence.
- Improper initial conditions may lead to the iterative procedure misbehaving and possibly 'blowing up' or diverging.

Besides, the setting up of appropriate parameters in the solution control usually entails the specification of proper discretisation schemes and the selection of suitable iterative solvers. Therefore, It is imperative that background knowledge on the appropriate choice of these parameters must be acquired before any CFD calculation is performed (Tu et al. 2018).

#### b) Monitoring Convergence Step

The subsequent stage of the CFD solver encompasses the interconnected operations of three essential processes: solution monitoring, CFD calculation, and convergence



verification. Two crucial factors contribute to the success of a CFD computation, namely the convergence of the iterative process and grid independence, as detailed below:

### Convergence:

Convergence can be evaluated by monitoring the more pronounced imbalances as the numerical calculations progress through each iteration. These imbalances are indicators of the overall conservation of flow properties and are commonly referred to as residuals. Typically, they are visualized and analyzed through commercial CFD software's graphical user interfaces (GUIs), according to (Tu et al. 2018).

Figure 2.6-36 and Figure 2.6-37 show typical ANSYS CFX and FLUENT GUIs for monitoring convergence corresponding to the prescribed convergence criteria, respectively.

As depicted in the figures, the downward trends indicate a consistent reduction rather than a potential accumulation of undesirable imbalances. This reduction signifies the convergence of the iterative process rather than divergence. A converged solution is attained when the residuals decrease below predetermined convergence criteria or tolerance set within the solver's control parameters for the iterative solvers (Tu et al. 2018).

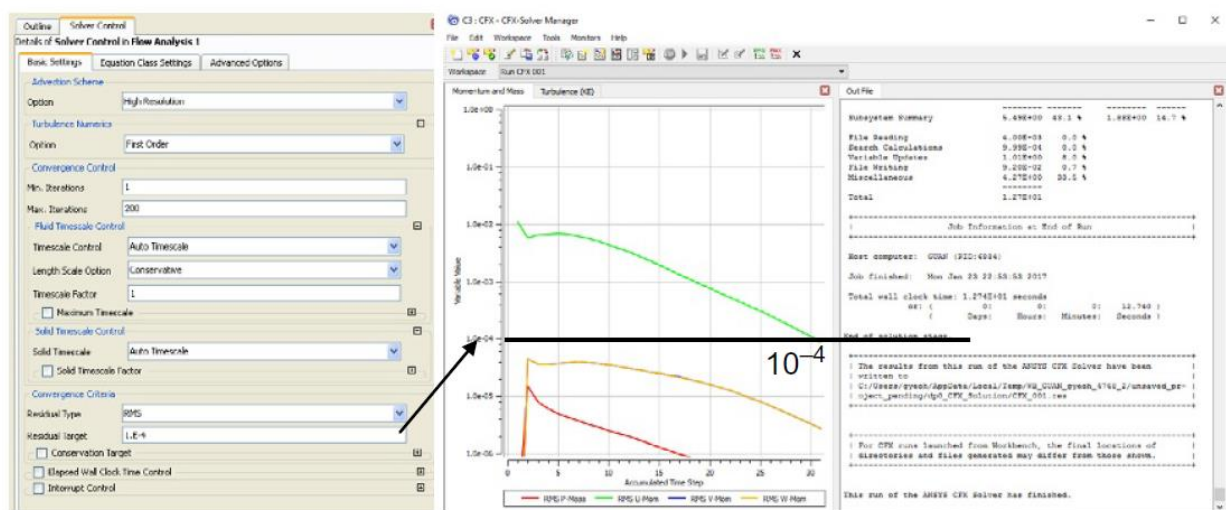


Figure 2.6-36: Typical ANSYS CFX GUIs for monitoring convergence (Tu et al. 2018).

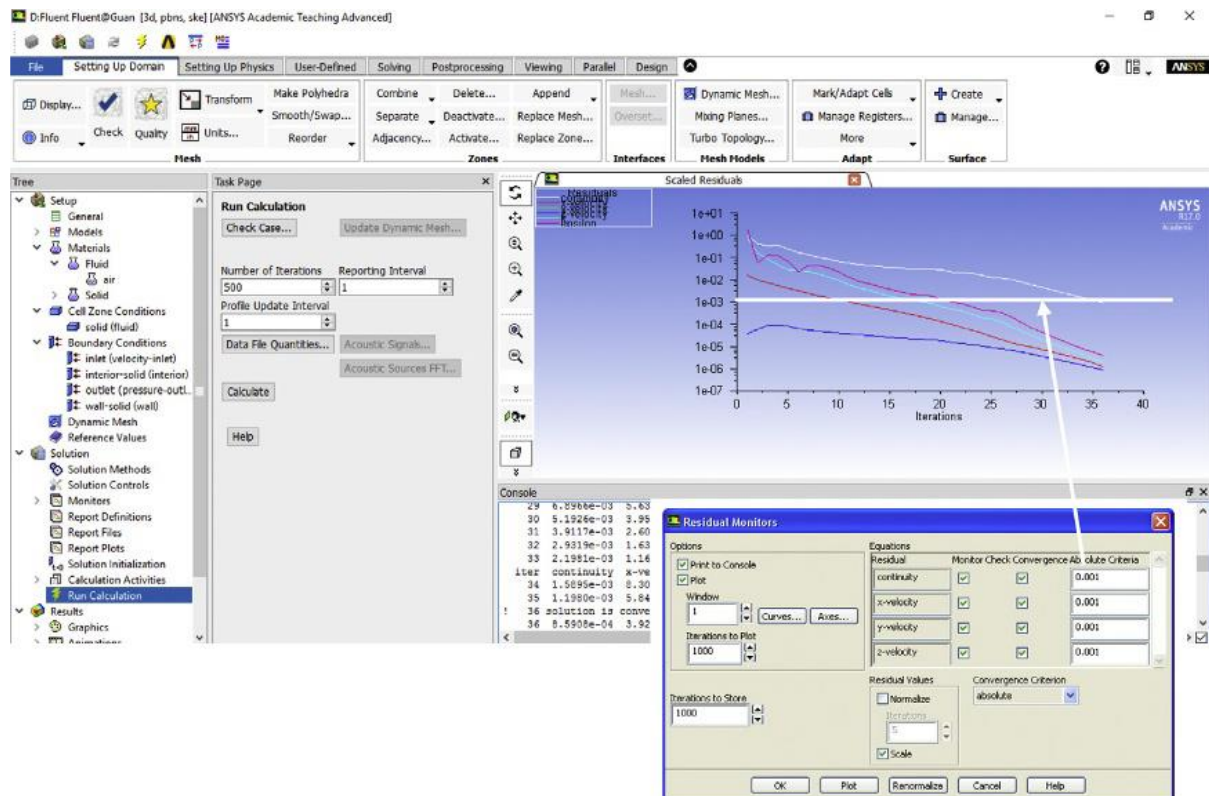


Figure 2.6-37: Typical FLUENT GUIs for monitoring convergence (Tu et al. 2018).

### Grid Independence:

According to Tu et al. (2018), achieving a well-prepared initial mesh design relies on prior knowledge or understanding of the expected flow properties. When dealing with the coarseness of a mesh, the only way to eliminate errors is to employ a process of iterative refinement, gradually refining an initially coarse mesh until specific crucial results show no significant changes. This iterative refinement serves as an integral part of the solution procedure. By systematically searching for grid-independent results, it is possible to achieve high-quality CFD solutions.

In conclusion, various aspects are critical in the numerical considerations for simulating a CFD problem. These include convergence, convergence criteria or tolerance values, residuals, stability, errors, under-relaxation factors, and grid independence. These factors significantly influence the accuracy, reliability, and efficiency of the CFD simulation process. Proper management and understanding of these aspects are essential for obtaining accurate and meaningful results in computational fluid dynamics (Tu et al. 2018).

### 2.6.4 CFD Post-Processing Stage

Versteeg and Malalasekera (2011) stated, "As in pre-processing, a vast amount of development work has recently taken place in the post-processing field. Due to the increased popularity of engineering workstations, many of which have outstanding graphics capabilities, the leading

CFD packages are now equipped with versatile data visualisation tools.” These include Domain geometry and grid display, Vector plots, Line and shaded contour plots, 2D and 3D surface plots, Particle tracking, View manipulation (translation, rotation, scaling), and Colour PostScript output (Versteeg & Malalasekera 2011). These tools serve an essential role in the results validation and verification processes, as well as assisting the CFD user to better analyse and visualize the many relevant physical characteristics within the fluid flow problem, thus optimising the design by revising the input parameters such as fluid flow properties and boundary conditions (Tu et al. 2018).

Below are examples of some graphic tools that CFD applications provide:

a) X-Y Plots

These plots are two-dimensional graphs that represent the variation of one dependent transport variable against another independent variable, as shown in Figure 2.6-38. They are the popular way of directly comparing the numerical data with the experimentally measured values and the most precise and quantitative way to present the numerical data (Tu et al. 2018).

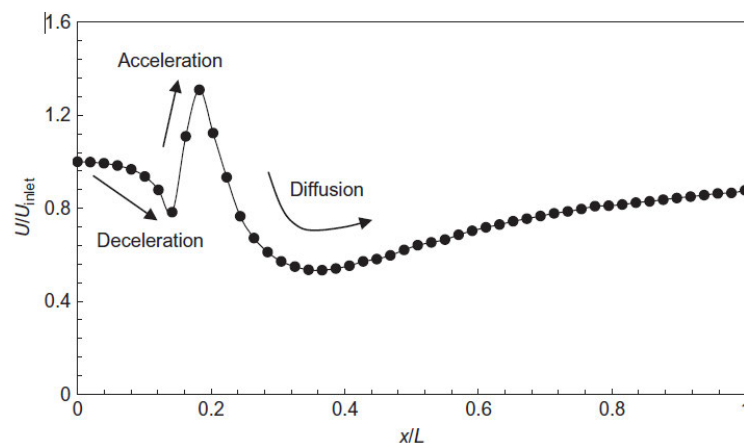


Figure 2.6-38: X–Y plot of the normalized horizontal velocity along the length (Tu et al. 2018).

b) Vector Plots

A vector plot visualisation tool displays vector quantities, typically velocity, at discrete points. It utilises arrows to indicate the vectors' direction and the arrows' size to represent their magnitude, as shown in Figure 2.6-39 and Figure 2.6-40. This plot offers a perspective view of the flow field in two dimensions. In the case of a three-dimensional flow field, it is possible to generate different slices of two-dimensional planes that contain the vector quantities. Examining these planes from different orientations can provide a more comprehensive understanding of the global flow phenomena (Tu et al. 2018).

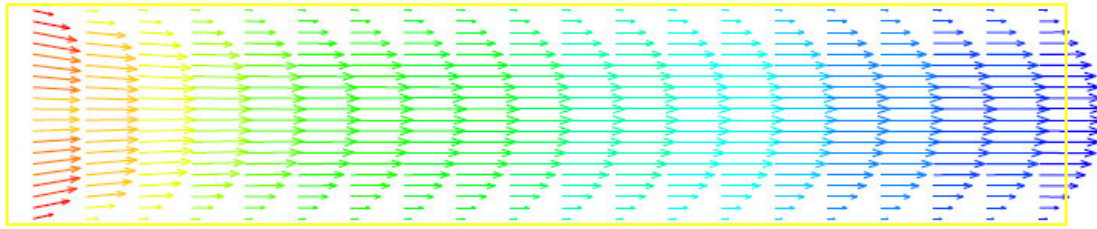


Figure 2.6-39: Velocity vectors showing the flow development along the parallel-plate channel (Tu et al. 2018)

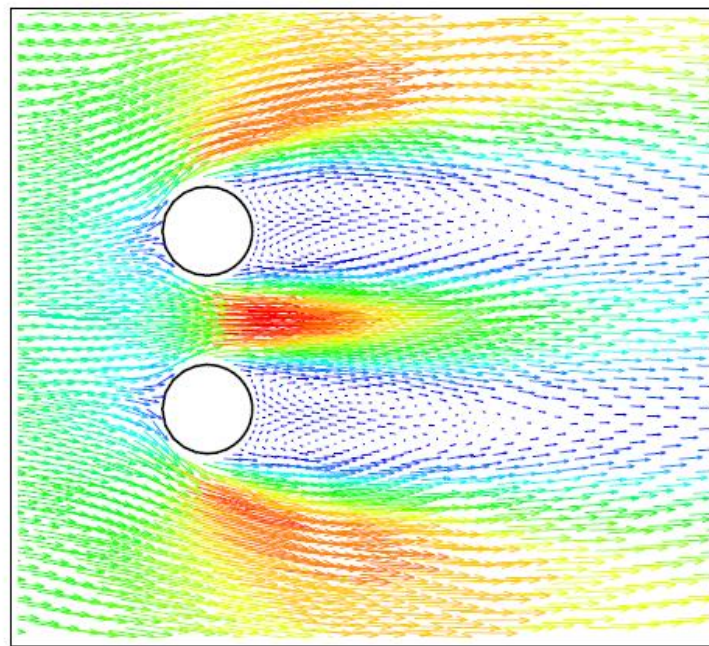


Figure 2.6-40: Velocity vectors accentuating the localized wake recirculation zones (Tu et al. 2018).

### c) Contour Plots

Contour plotting is an effective graphical technique for visualising CFD results. It offers a valuable way to represent data visually. Contour plots are commonly used in CFD to display information in a graphic form. A contour line, also known as an isoline, represents a constant value of a specific property in space. In three dimensions, the equivalent representation is an isosurface.

Unlike X-Y plots, contour plots, similar to vector plots, provide a comprehensive overview of the fluid flow in a single view. They offer a global description of the flow field. However, it is essential to note that contour plots are not intended for precisely evaluating numerical values between contour lines. While some mental or numerical interpolation between the contour lines can be performed, it is an inherently imprecise process.

Nevertheless, contour plots are an invaluable tool for gaining insights into the spatial distribution and patterns of properties within a flow field. They allow engineers and



researchers to quickly grasp the overall behaviour and characteristics of the fluid flow without requiring a detailed examination of individual numerical values (Tu et al. 2018).

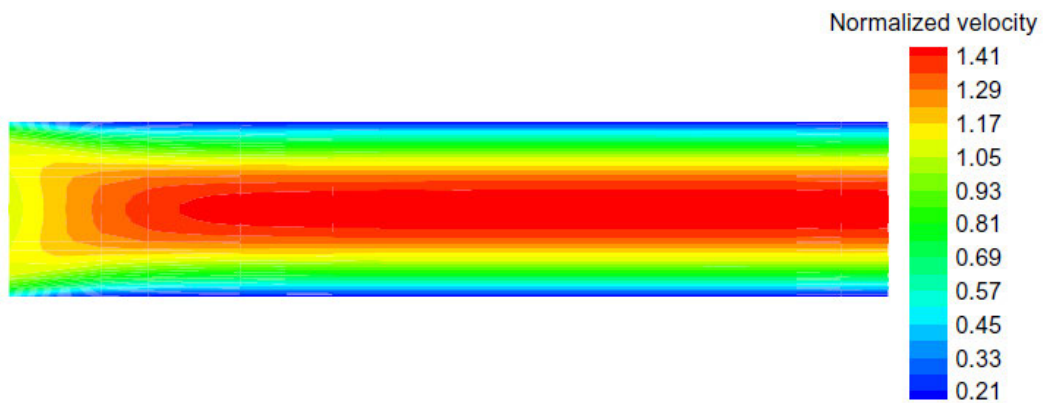


Figure 2.6-41: Example of Flooded Contours on rainbow-scale colour map (Tu et al. 2018).

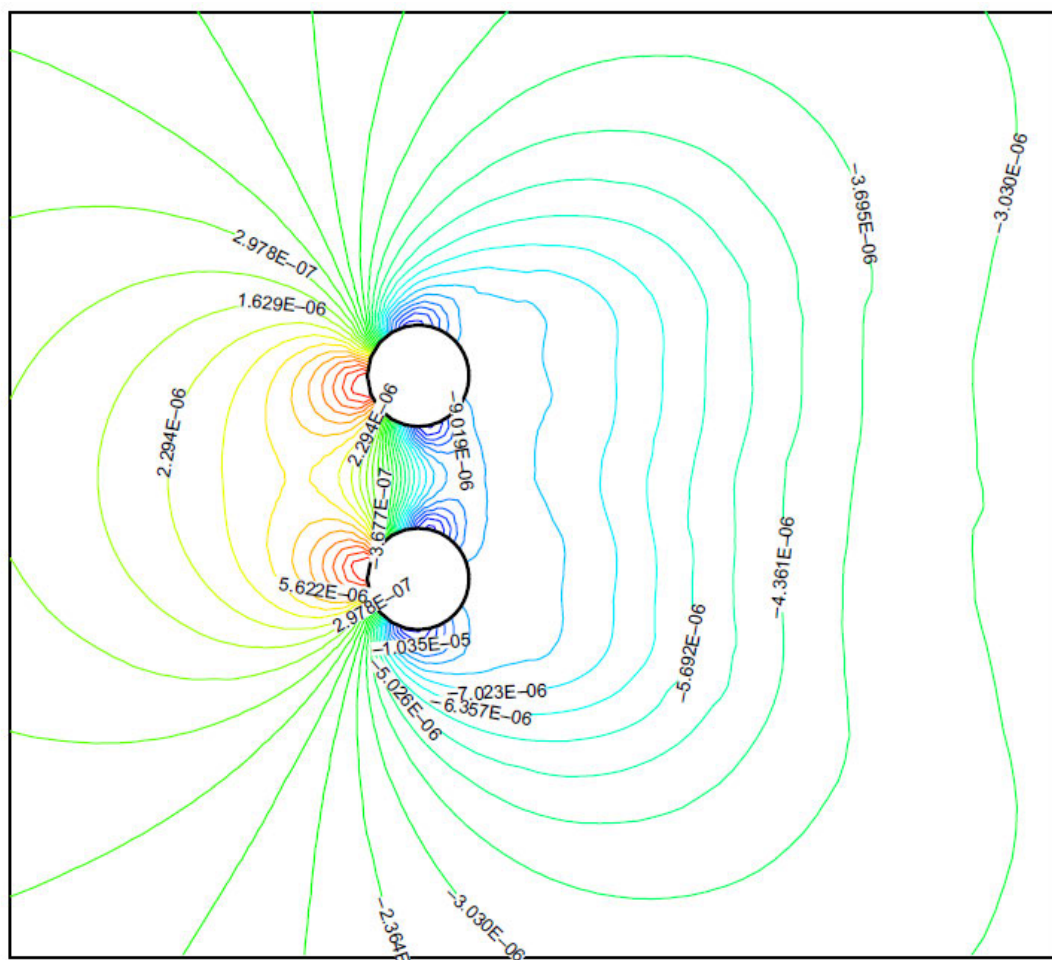


Figure 2.6-42: Example of Line contours on a rainbow-scale colour map (Tu et al. 2018).

## CHAPTER 3 – RESEARCH METHODOLOGY

### 3.1 [Research Methodology Introduction](#)

This chapter outlines the methodology for studying the effects of crosswind drag forces on the aerodynamic performance of a semi-trailer tanker. The proposed research methodology for the study can be broken down and listed below:

#### Chapter 3: Geometric Modeling and Analysis

1. Selection and Modeling of Vehicle Geometries:
  - Describe the process of selecting and modelling the geometric configurations of the tractor and the trailer, considering various combinations.
  - Specify the software or methodology employed for this purpose.
2. Geometric Specifications:
  - Provide detailed specifications for the selected geometric configurations, ensuring a comprehensive understanding of the vehicle's physical attributes.
3. Static Rollover Threshold (SRT) Determination:
  - As discussed in Section 2.5.2 and Appendix F, utilise the SRT calculator tool to calculate the minimum side force required to induce rollover in the semi-trailer tanker.
4. Critical Lateral Force Analysis:
  - Investigate the critical lateral force necessary to trigger the vehicle's lateral slip or rotational motion about its axis.

#### Chapter 4: Computational Fluid Dynamics (CFD) Analysis

1. Geometry Creation and Simplification:
  - Detail the procedure for creating and simplifying the vehicle geometries, emphasizing their relevance to the CFD analysis.
2. Simulation Process in ANSYS CFD:
  - Present a comprehensive overview of the Pre-Processing, Solving, and Post-Processing stages within ANSYS CFD.
3. Meshing for Geometries:
  - Elaborate on the meshing process for the vehicle geometries to ensure precise CFD simulations.
4. Wind Simulation:

- Simulate the selected geometries under both headwind and crosswind conditions.
- Investigate crosswind conditions at wind angles ranging from 15 to 90 degrees in 15-degree increments.

## Chapter 5: Analysis and Results

### 1. Validation of Headwind Simulation:

- Validate the results of headwind simulations by comparing them with previous studies, as outlined in Section 1.2 and Section 1.3.

### 2. Simulation Result Examination:

- Analyse various parameters, including the simulations' drag, lift, pitch, rotational, and rollover moment coefficients.

### 3. Safety Assessment:

- Evaluate the safety of the tractor-trailer configurations equipped with aerodynamic devices.
- Determine optimal operating conditions to mitigate the risk of sideslip, rotation, or rollover accidents.

### 4. Pre-Optimization Study:

- Investigate areas on the aerodynamic devices where crosswinds exert the most significant influence.
- Propose modifications to lessen the adverse effects of crosswinds.

## Chapter 6: Conclusion and Future Research

### 1. Summary of Findings:

- Summarize the study's outcomes and assess its success in achieving the project objectives.

### 2. Aerodynamic Efficiency and Safety Enhancement:

- Highlight the configuration that exhibits the greatest aerodynamic efficiency and safety improvements.

### 3. Optimal Highway Speed:

- Identify the optimal highway speed to maximize both performance and safety of the semi-trailer tanker.

### 4. Future Research Directions:

- Address areas of research that are currently beyond the scope of this study, suggesting potential avenues for future investigations.

### 3.2 Static Loaded Radius of Tyres

To avoid errors in the CFD mesh-generating process when the fluid domain is set at ground level where there is no gap between the tyres and the ground, point contact between the tyres and the ground should be considered when modelling the tractor and trailer by applying the tyre's static loaded radius.

The tyre's static loaded radius is specified by the tyre manufacturer, and according to Yokohama (2023), "The tyre's static loaded radius, specified by the tyre manufacturer, is the distance from the wheel axle centreline to the tread contact surface. It is measured after the tyre has been mounted on its measuring rim, inflated to the test pressure and placed under a prescribed load" (Yokohama 2023).

This static loaded radius " $R$ " is the difference between the free (undeformed) radius  $R_F$  and the tyre deflection  $\rho$ , as defined in (Pacejka 2012) and shown in Figure 3.2-43.

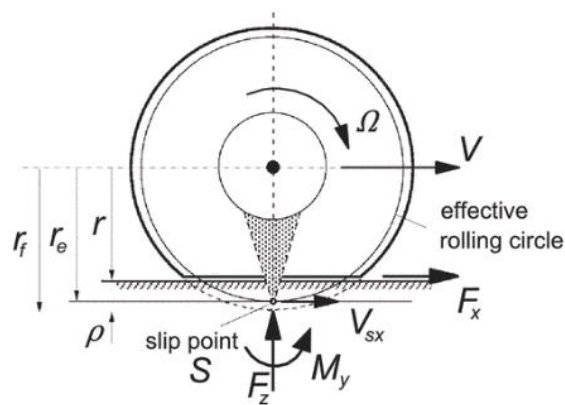


Figure 3.2-43: Tyre's Static Loaded Radius and Free Radius (Pacejka 2012)

This static loaded radius depends on the type of tyres used and is specified by the tyre manufacturer based on the applications. Therefore, this radius was considered when modelling the tractor and trailer for CFD simulation to ensure no point contact between the tires and the ground.

### 3.3 Tractor Selection and Modelling

The tractor selected for this project, the 6x4 Kenworth T610 Night Cab, was chosen for its suitability in meeting the project requirements. The general dimensions and specifications of this tractor, according to Kenworth\_AU (2023), are as follows:

- Wheelbase length: 4860mm
- Axle Spread: 1320mm.
- Cabin length: 3830mm
- Aero roof height from top of chassis: 2843mm
- Fifth-wheel height: 1250mm



- And the laden tyre radius (the static load radius): 485mm
- Gross Combination Mass: 97,000 kg (for vehicle and trailer combined weight)
- Tare Weight: 8,980 kg

The suspension details are as follows:

- Front suspension: DANA E-1462I - 6.6T GAWR
- Rear suspension: KENWORTH AIRGLIDE 400 - 18.1T GAWR

The tires and springs used are:

- Front axle: 11R22.5/R251 tyres
- Rear axles: 11R22.5/M766 tyres

As discussed in the project limitations (Section 1.5.1), to minimize computational resources required for simulation meshing and solving, the tractor was simplified by omitting all internal components and complex geometries, including the engine, seats, lights, and ventilation devices, as shown in Figure 3.3-44.

Additionally, a simplified tractor model was created to examine the impact of crosswinds on specific aero devices, such as tractor and trailer side skirts and a tractor-trailer gap fairing (Figure 3.3-45), as follows:

- The side skirts were added on both sides of the vehicle, from the steering wheel to the front of the driving axle. The gap between the side skirts and the ground is 250mm, as required by ADRs (Section 2.5.4).
- The tractor-trailer gap fairing was added to the aero roof and both sides of the vehicle, as depicted in Figure 3.3-45.

Detailed drawings of these models can be found in Appendices E.1 and E.2. These models and drawings were created using Autodesk Inventor based on the dimensions provided by the Kenworth T610 specification sheets available for download from the Kenworth Australia website. Since the official T610 3-D model was unavailable, these models were built with a close approximation to the supplied dimensions, with minor differences in the aero roof and cabin.

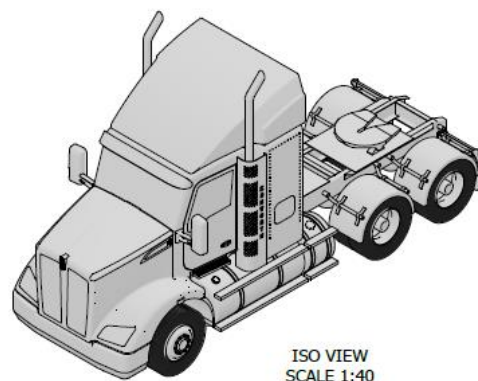


Figure 3.3-44: Real Kenworth T610 Night Cab and its simplified model (Kenworth\_AU 2023)

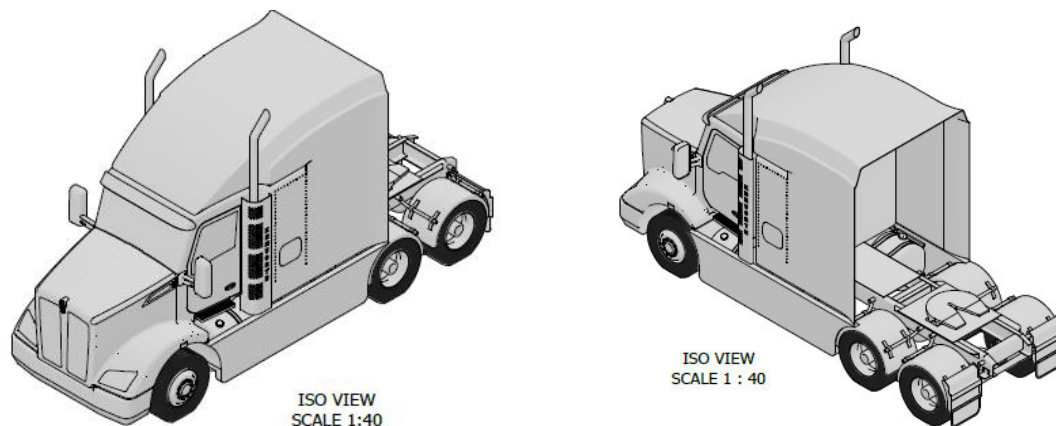


Figure 3.3-45: Simplified Kenworth T610 with side skirts and tractor-trailer gap fairing

### 3.4 Semitrailer Tanker Selection and Modelling

The semi-trailer tanker selected for this project is Australia's most common tri-axle, five-compartment, oval-sectional semi-trailer tanker (Figure 3.4-46). It was chosen for its suitability in meeting the project requirements. This tanker's general dimensions and specifications, with and without aerodynamic devices, are detailed in Appendix E.3 and E.4, according to ATE\_Tankers (2023). The following are the key specifications:

- Wheelbase length: 8648mm
- Axle Spread: 1250mm
- Maximum volume of each compartment: 8,600 Litres
- Safe fill volume of each compartment: 8,300 Litres
- Ride height: 389mm
- Laden tyre radius (the static loaded radius): 490mm
- Skidplate height (kingpin height): 1250mm
- Overall length from kingpin to the rear of tanker: 11,006mm
- Barrel centroid height (at fully loaded): 2257mm
- Centroid distance from the centre of axle group (at fully loaded): 3,710mm
- Ground Contact Width: 2490mm
- Tare Weight: 4,700 kg
- Payload: 17,800 kg (at safe fill level)
- Gross weight: 22,500 kg
- Suspensions: Hendrickson AAT250, drum brake, standard travel
- Tyres: 11R22.5/R251.

The stability angle of  $61.1^\circ$  (calculated based on the centroid height and the ground contact width) and the overall length of 11,793mm (as shown in Appendix E3 and E4) are both within the maximum stability angle ( $62^\circ$ ) and the maximum length (12.5m) required by Australian Standard AS2809.1 - Part 1 (Section 2.5.5) and Australian Design Rules (Section 2.5.4).

Furthermore, the wheelbase length of 8,648mm and the ground contact width of 2,490mm are within the maximum allowed limits of 9m and 2.5m, respectively, according to the Australian Design Rules (Section 2.5.4). These criteria indicate that the chosen semi-trailer tanker's geometry meets the requirements of this project.



Figure 3.4-46: Tri-axle, 5-compartment semitrailer tanker (ATE\_Tankers 2023)

Figure 3.4-47 and Figure 3.4-48 depict the isometric view of the simplified tankers with and without side skirts, respectively. In Figure 3.4-48, the side skirts were added to both sides in compliance with the Australian Standard AS2908.1 - Part 1 discussed in Section 2.5.5. The standard specifies that the ground clearance for tank components and protection devices directly attached to the tank should not exceed 250mm within 1m of any axle or 350mm for any other location when the vehicle is unladen (Standards\_Australia 2020b). The details of these side skirts are illustrated in Figure 3.4-49.

As discussed in the project limitations (Section 1.5.1), certain simplifications were made to minimize the computational resources needed for simulation meshing and solving. These simplifications included omitting various internal components and complex geometries typically found in semi-trailer tankers. These overlooked components consist of suspensions, air and water tanks, outlet fittings, toolboxes, fire extinguishers, Hazchem signs, safety cones, bumperettes, lights, hoses, side underruns, hose trays, and other similar elements. Removing these components makes the simulation process more efficient while still capturing the essential aspects of the semi-trailer tanker system.

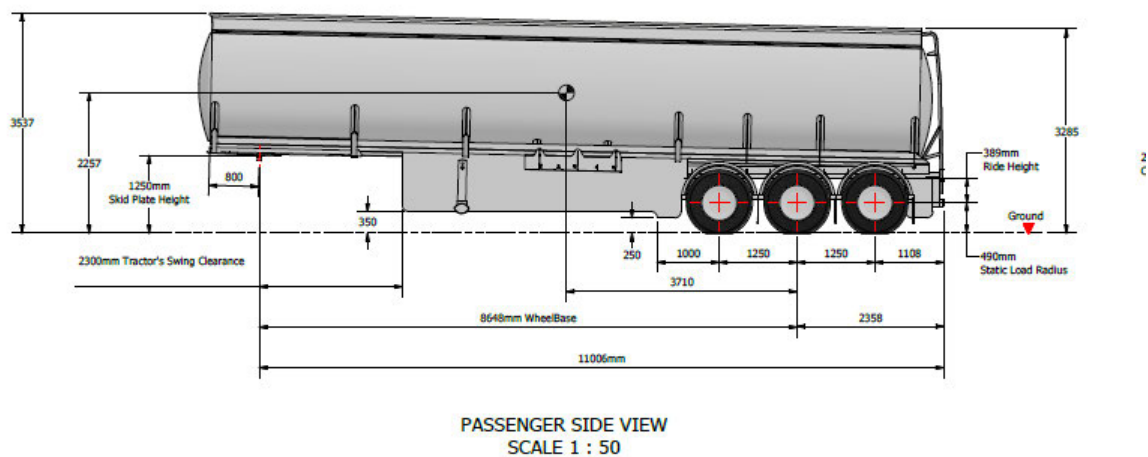
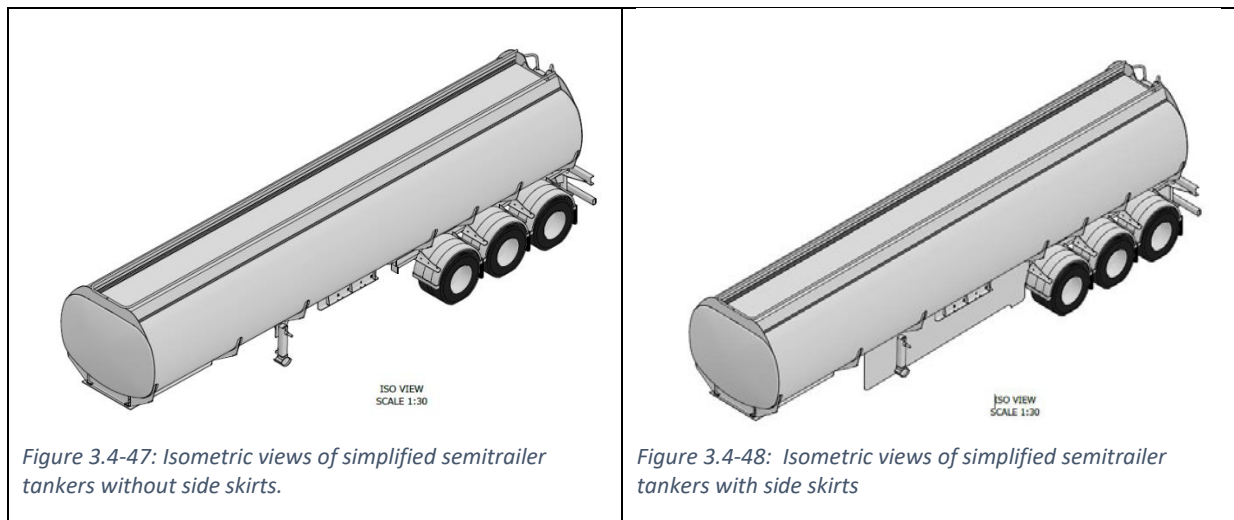


Figure 3.4-49: Details of side skirts installed on semi-trailer tanker

### 3.5 Rollover Threshold Determining Process

The baseline semitrailer tanker's minimum static rollover threshold value was determined using the SRT Calculator established by the Western Australian government, as discussed in Sections 2.5.2 and Appendix F.1.

First, the data required for this calculator was collected from the suspension and tanker manufacturers. Then, these data were input into the calculator to determine the estimated Static Rollover Threshold value. Finally, the estimated side force that caused the semitrailer tanker to roll over was calculated. These processes are detailed as follows:

#### a) Data collection process:

- Axle's data were collected and shown in Table 3.5-6

Table 3.5-6: Summary of data required for the SRT calculator

Tyres' data (Figure 3.5-50). More details are shown in Appendix E.3	<ul style="list-style-type: none"> <li>• Tyre's size: 11R22.5</li> <li>• Maximum ground contact width: 2490mm</li> </ul>
Load on rear axle group data (Figure 3.5-51)	<ul style="list-style-type: none"> <li>• Gross mass: 22,500 kg</li> <li>• Trailer tare mass: 4,700 kg</li> <li>• Payload mass: 17,800 kg</li> </ul>
Unsprung mass data (Figure 3.5-50)	<ul style="list-style-type: none"> <li>• Total unsprung mass (mass of components that are not supported by the axle, such as wheels, tyres, nuts, springs, and brakes): 960kg</li> <li>• Unsprung mass Centre of Gravity (CoG) height from the ground" 490mm</li> </ul>
Sprung mass data (Figure 3.5-50)	<ul style="list-style-type: none"> <li>• Mass: 3740 kg</li> <li>• CoG height from the ground: 827mm</li> </ul>
Load data (Figure 3.5-50)	<ul style="list-style-type: none"> <li>• Load bed height from the ground: 1353 mm</li> <li>• Load height from the ground: 3086mm</li> </ul>
Suspension data (Hendrickson 2023)	<ul style="list-style-type: none"> <li>• Track width: 1854mm (73")</li> <li>• Axle lash: 150mm</li> <li>• Suspension model: AAT250, Drum Brake.</li> <li>• Total roll stiffness/axle: 1,768,208 Nm/radian</li> <li>• Spring stiffness/spring: 1,000,000 N/m</li> <li>• Roll centre height (from axle centre): 100mm</li> </ul>

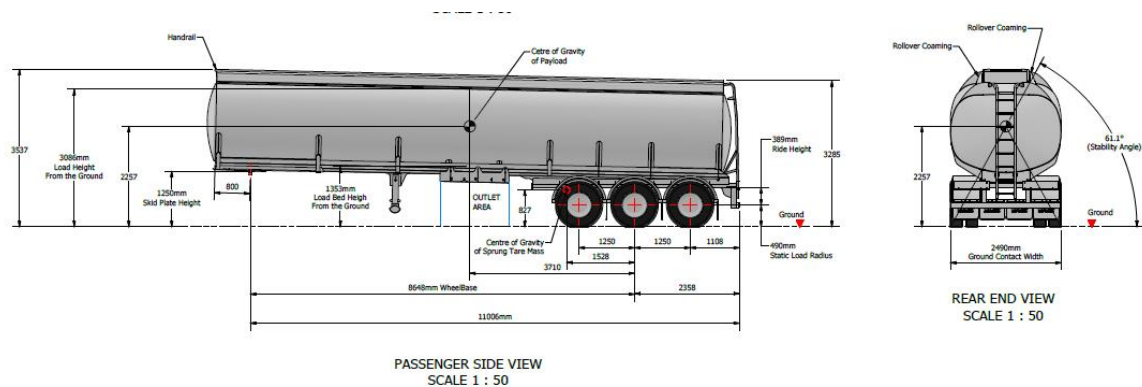


Figure 3.5-50: Semitrailer details



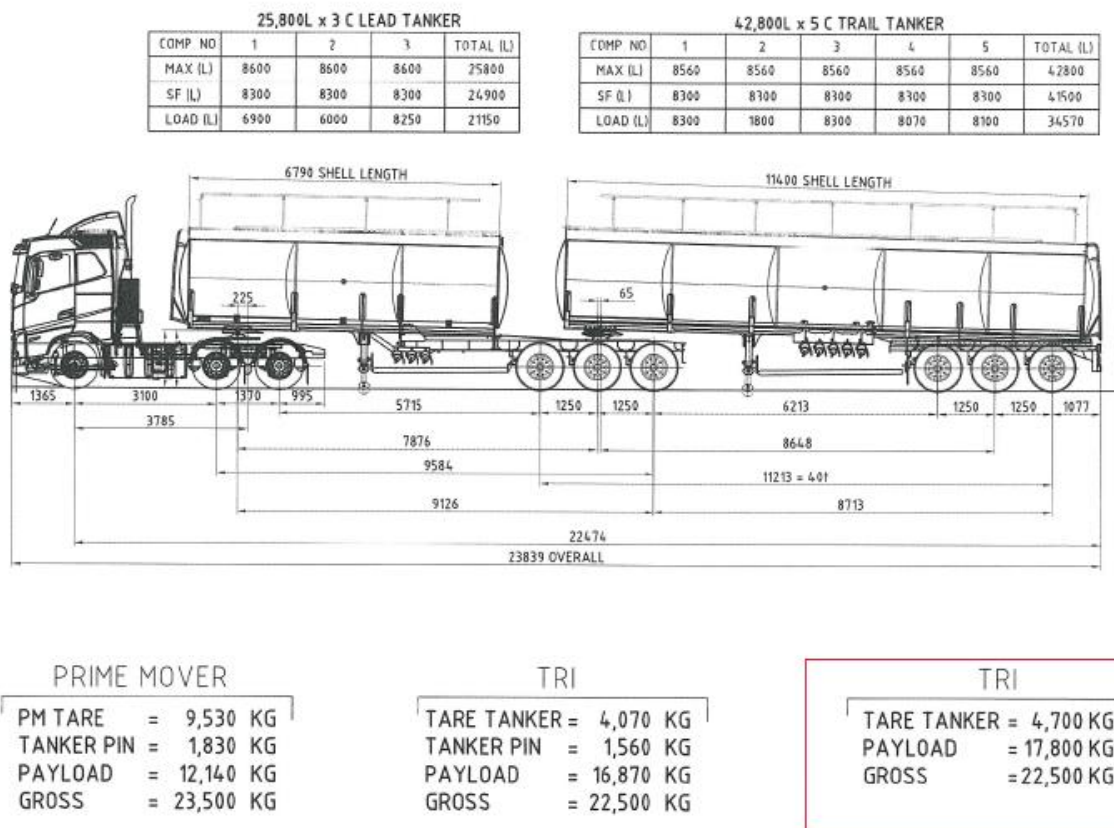


Figure 3.5-51: Load data of semitrailer tanker

## b) SRT value Calculation Process

The data collected above were input into the SRT Calculator established by the Western Australia Government, as depicted in Figure 3.5-52 to Figure 3.5-56 below:

**SRT CALCULATOR**  
Version 3.01wa Issued August 2022

Static Roll Threshold (SRT) is a measure of a vehicle's resistance to roll over during a steady speed cornering maneuver. This software provides a calculator for estimating a vehicle's SRT. New users are encouraged to open the [help](#) page to assist them with the input parameter definitions. A detailed [user guide](#) which is formatted for printing is also available. A validation test using a tilt table has been undertaken and the [result](#) is available on-line.

By using this software the user accepts the terms and conditions of the [licence agreement](#).

Type of Vehicle: Semi-Trailer

No of Front Axles: 0

No of Rear Axles: 3

**SRT requirement**  
☐ Non-dangerous goods  
☒ Dangerous goods  
☐ User Specified

Target Minimum SRT (g): 0.4

Enter

This software has been designed to run on Microsoft Edge version 103.0.1264.62 and Google Chrome version 103.0.5060.114  
 It may well run on other browsers but this has not been tested

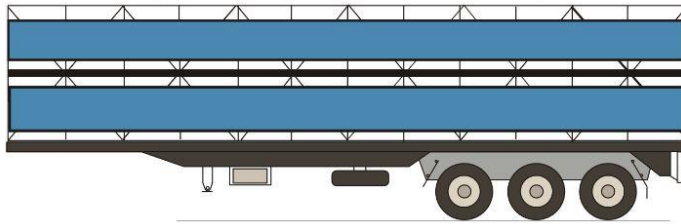
Optimised for 16-bit colour, 800 \* 600 resolution. Cookies and JavaScript must be enabled.

Figure 3.5-52: Step 1 - Selecting the Type of Vehicle

## SRT CALCULATOR

<

New users are encouraged to open the [help](#) page to assist them with the input parameter definitions.



(Diagram as visual aid only :-)

### Tyre Data:

Axle	Tyre Size:	Tyre Configuration:	Maximum Ground Contact Width(m):
1	22.5 ▼	Dual ▼	2.49
2	22.5 ▼	Dual ▼	2.49
3	22.5 ▼	Dual ▼	2.49

### Axle Load Data:

	Rear	Total
Gross Mass:(kg)	22500	22500
Tare Mass:(kg)	4700	4700
Payload Mass:(kg)	17800	17800

Figure 3.5-53: Step 2 - Inputting Tyre and Axle Data

### Unsprung Mass Data:

Axle	Unsprung Mass (kg):	Unsprung Mass Cg Height (m):
1	320	0.49
2	320	0.49
3	320	0.49

### Sprung Tare Mass:

Mass (kg)	3740
Centre of Gravity Height from the ground:(m)	0.827

### Load Categories:

Mixed Freight ▼

### Deck Style:

Standard ▼

### Load Geometry:

Load Bed Height from the ground:(m)	1.353
Load Height from the ground:(m)	3.086
Payload Cg Height from the ground:(m) (only required if load type is other)	

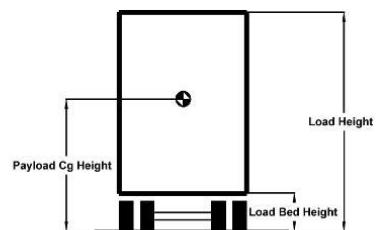


Figure 3.5-54: Step 3 - Inputting Unsprung mass, Sprung mass, and load type and geometry

### Suspension data:

Suspension Type:

#### Rear

- ☐ Generic Air (low roll stiffness type)
- ☐ Generic Air (high roll stiffness type)
- ☐ Generic Steel
- ☒ User Defined:

### Enter data for 'User-Defined', optional for 'Generic':

Suspension Track Width:(m)  
Axle lash:(mm)

1.854  
150

### Please enter the following details for 'User-Defined':

Suspension brand/model:  
Total Roll Stiffness / axle:(Nm/radian)  
Spring Stiffness / spring:(N/m)  
Roll Center Height:(m)  
(from axle center)

Hendrickson AAT250  
1768208  
1000000  
0.1

Calculate SRT Reset Form

Figure 3.5-55: Step 4 - Inputing suspension data

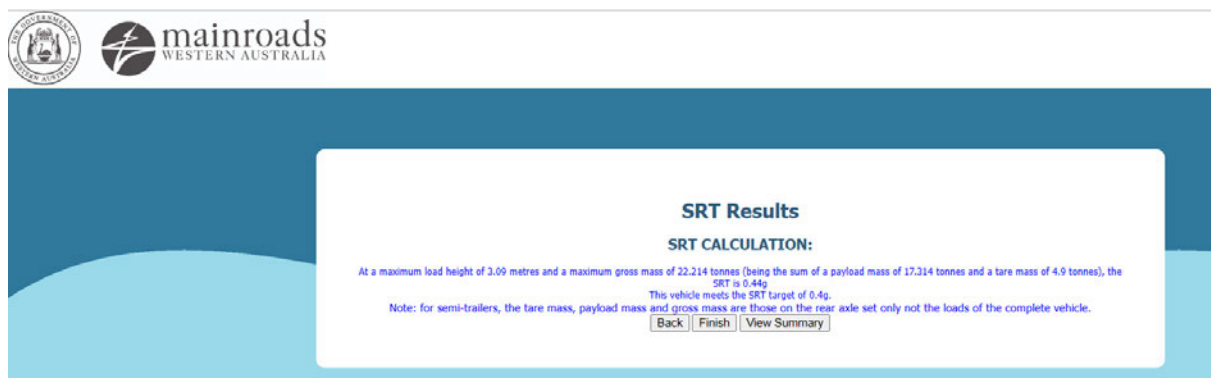


Figure 3.5-56: Result of the estimated SRT value

### c) Calculating the side force causing the trailer to roll over

As seen in Figure 3.5-56, the estimated SRT value of this semitrailer tanker is 0.44g. Therefore, the minimum side force acting on the trailer body, which causes it to roll over, is calculated as follows:

$$F_s = M_{trailer, total} \times SRT = 22,500 \text{ (kg)} \times 0.44 \times 9.81 \text{ (m/s}^2\text{)} = 97,1 \text{ (kN)}$$

Thus, a side force of 97.1 kN applied to the fully loaded semi-trailer body would cause it to roll over. It is important to note that this value represents the estimated minimum lateral force, assuming the vehicle is stationary. The actual side force required for rollover can vary depending on the vehicle's dynamic conditions.



### 3.6 Critical Lateral Force to cause semi-trailer to slip sideways and rotate

As discussed in Literature Review – Section 2.4.4, the critical lateral force that causes the semi-trailer tanker to slip sideways occurs when all the vehicle's wheel reaction side forces reach their maximal values permitted by friction, and the semi-trailer begins to slide (Figure 2.4-21).

Because the semi-trailer unit has three axles with dual tyres, the total number of sliding friction forces is the sum of twelve individual friction forces produced by tyres. Therefore, the critical lateral force can be expressed as:

$$F_{s,critical} = \sum_{i=1}^{12} F_{y,i} = \mu_s \times \sum_{i=1}^{12} F_{z,i} \quad (Eq. 35)$$

Where:  $\begin{cases} \mu_s = \text{Sliding friction coefficient (unitless)} \\ F_{y,i} = \text{wheel's reaction side force (N)} \\ F_{z,i} = \text{wheel's normal force (N)} \end{cases}$

An example of calculating the critical lateral forces that cause the semitrailer to slip sideways is performed as follows:

- As shown in Table 3.5-6, the total gross mass of the trailer is 22,500 kg, so the entire normal force equals 220,725 N or 220.1 kN.
- When the tanker operates on an earth road in wet weather, the sliding friction value  $\mu_s$ , as shown in Table 7, is estimated at 0.4, according to Wong (2001, p.29).
- So, the critical lateral force in Eq.35 can be calculated as :

$$F_{s,critical} = 0.4 \times 220.1 \text{ (kN)} = 88 \text{ (kN)}$$

- Besides, in an empty tanker with a total tare mass of 4,700 kg, the entire normal force equals 46,107 N or 46.1 kN. The critical lateral force in Eq.35 can be calculated as:

$$F_{s,critical} = 0.4 \times 46.1 \text{ (kN)} = 18.44 \text{ (kN)}$$

These critical lateral forces of 88kN and 18.44 kN represent the minimum force produced by crosswinds at which the trailer unit will rotate about the kingpin axis when the tanker is fully loaded and empty, respectively.

For other road conditions, such as snow and icy road conditions, the critical lateral force that causes the semitrailer to slip sideways could be much less. These forces are listed in Table 3.6-8.

This rotation or sliding sideways of the trailer can pose a significant risk, especially during adverse weather conditions like wet weather on earth roads.

It is important to note that this conclusion is based on the assumptions and data presented in the earlier sections of the report. Further research and analysis may be needed to validate and refine these findings, considering other factors that could influence the trailer's stability and lateral forces.

Table 3.6-7: Average Values of Coefficient of Road Adhesion (Wong 2001)

Surface	Peak Value $\mu_p$	Sliding Value $\mu_s$
Asphalt and concrete (dry)	0.8–0.9	0.75
Asphalt (wet)	0.5–0.7	0.45–0.6
Concrete (wet)	0.8	0.7
Gravel	0.6	0.55
Earth road (dry)	0.68	0.65
Earth road (wet)	0.55	0.4–0.5
Snow (hard-packed)	0.2	0.15
Ice	0.1	0.07

Table 3.6-8: Critical lateral force at different road surface conditions

Road Surface	Sliding Value	Critical Lateral Force (kN)	
		Fully Loaded Tanker	Empty Tanker
Asphalt and Concrete (dry)	0.75	165.08	34.58
Asphalt (wet)	0.45	99.05	20.75
Concrete (wet)	0.7	154.07	32.27
Gravel	0.55	121.06	25.36
Earth road (dry)	0.65	143.07	29.97
Earth road (wet)	0.4	88.04	18.44
Snow (hard-packed)	0.15	33.02	6.92
Ice	0.07	15.41	3.23

### 3.7 [Tractor-trailer combination details](#)

Figure 3.7-57 displays the baseline and Aerodynamic tractor-trailer combinations constructed for this project, featuring the following specifications:

- The overall length measures 17.1m, with a total weight of 32.5 tonnes (10 tonnes of tractor tare mass plus 22.5 tonnes of semitrailer tanker gross mass).
- The continuous rear bumper bar is positioned at a height of 425mm above the ground.
- The distance between the kingpin and the centre of the rear axles group (wheelbase) is 8,648mm.
- The swing radius measures 1.47m.
- The minimum gap between the ground and the outlet area is 350mm, whereas the minimum gap is 250mm in a radius of 1 metre from the rear axles group of the semitrailer.
- The ladder and handrail comply with the specifications outlined in the Australian Standard AS1657.
- Additionally, all other components mandated by the Australian Standards AS2809.1 and AS2809.2 for flammable liquid are duly met.

These characteristics of the tractor-trailer combination fulfil the safety criteria outlined in the Performance Based Standards (PBS) and the Australian Design Rules. These criteria are discussed in detail in Section 2.5.3 and Section 2.5.4. For more comprehensive information

regarding the baseline tractor-semitrailer and the tractor-semitrailer equipped with aerodynamic devices, refer to Appendix E.5 and E.6.

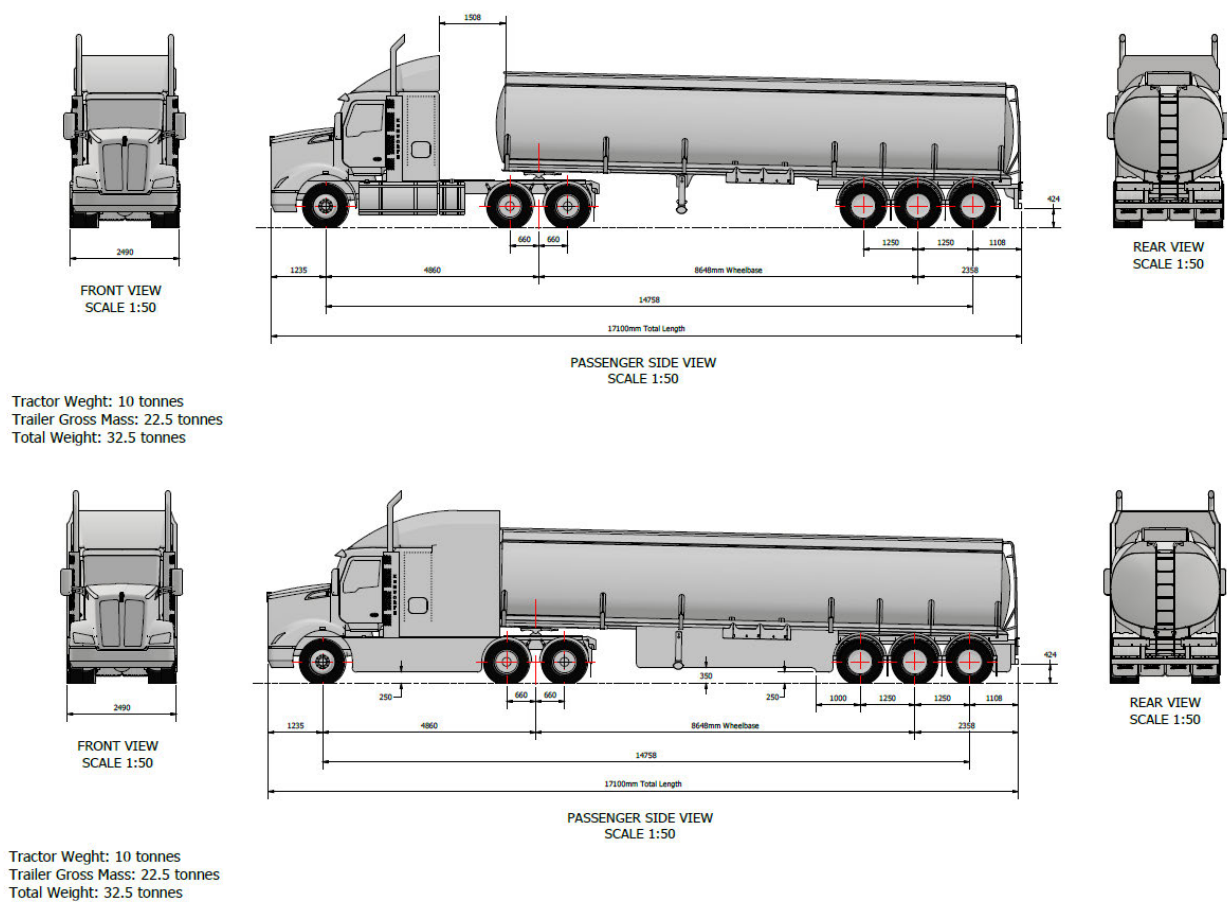


Figure 3.7-57: Baseline and Aerodynamic Tractor-Semitrailer Tankers

## CHAPTER 4 – CFD SETUP AND PERFORMANCE

### 4.1 [CFD Pre-Processing Stage](#)

#### 4.1.1 [Introduction](#)

This chapter provides comprehensive details of the Computational Fluid Dynamics (CFD) simulation processes, organized into several sections, each addressing specific aspects of the CFD analysis.

#### 4.1.2 [Geometry Creation and Simplification](#)

Due to the extensive number of nodes created during the meshing process (108 million for the Baseline model and 112 million for the Aerodynamic model), the tractor-semitrailer tankers geometries created in Sections 3.3 and 3.4 were further simplified, such as removing the tractor's mudflaps and the trailer landing legs, handrails and ladder, to significantly reduce the number of nodes, meshing and calculating time to suit the available computational resource.

Subsequently, in ANSYS SpaceClaim, further simplification steps were taken, including fixing gaps and missing faces, stitching edges, merging faces, and simplifying spline faces. Additionally, any silver gaps and overlapping features and edges were eliminated. As discussed in Section 2.6.2, these repair steps were necessary to ensure accurate and simplified geometries for efficient simulations without excessively consuming time and computer resources.

The final simplification of the tractor-trailer models is shown in Figure 4.1-58 and Figure 4.1-59.

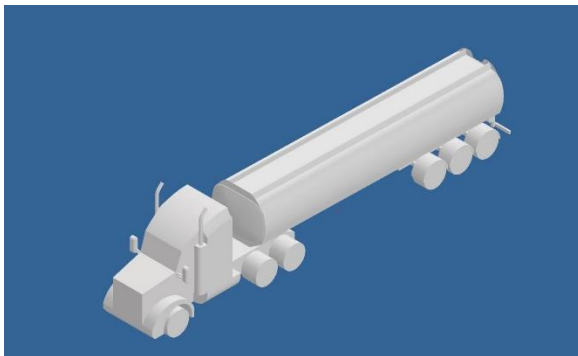


Figure 4.1-58: Simplified Baseline Tractor-Trailer

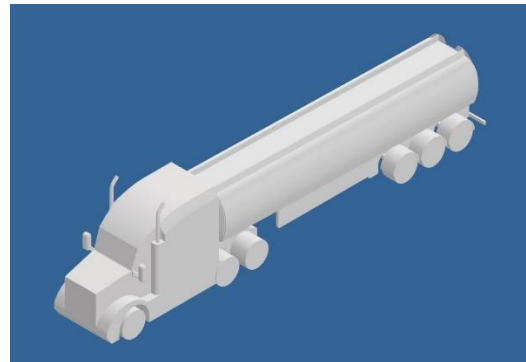


Figure 4.1-59: Simplified Aerodynamic Tractor-Trailer

#### 4.1.3 [Computational Domain](#)

Following the discussion in Section 2.6.2, we created the computational domain for full-scale tractor-semitrailer combinations using ANSYS SpaceClaim. This domain was designed with critical dimensions to investigate the tractor-trailer combination at various wind angles, ranging from 0 to 90 degrees. Initially, the first domain was created with the following measurements:

- Length: 2L upstream and 5L downstream, in addition to the vehicle's total length (17.1 meters), to account for flow adjustment upstream and fully developed flow downstream.

- Width: 2L on each side of the vehicle, along with the vehicle's width (2.5 meters), to allow for local flow deviation.
- Height: 2L from the top of the tanker to minimize boundary effects on fluid flow around the body while remaining manageable for CFD calculations.

Subsequently, the domain size was increased to investigate domain size independence by creating a second domain with a length of 3L upstream and 6L downstream and a width of 3L on each geometry side. As the results were significantly affected, the third domain was created with a length of 4L upstream, 7L downstream and a width of 4L on each geometry side. The simulation results changed insignificantly (around  $\pm 3\%$ ) this time, but the calculating time increased significantly. Therefore, the second domain was chosen for simulation. It measures 171 meters in length, 105.1 meters in width, and 38.2 meters in height (Figure 4.1-60).

After establishing the domain enclosure, the truck body was subtracted from the domain. This approach significantly reduced the time and resources required for meshing, as no meshing was necessary for the solid truck bodies.

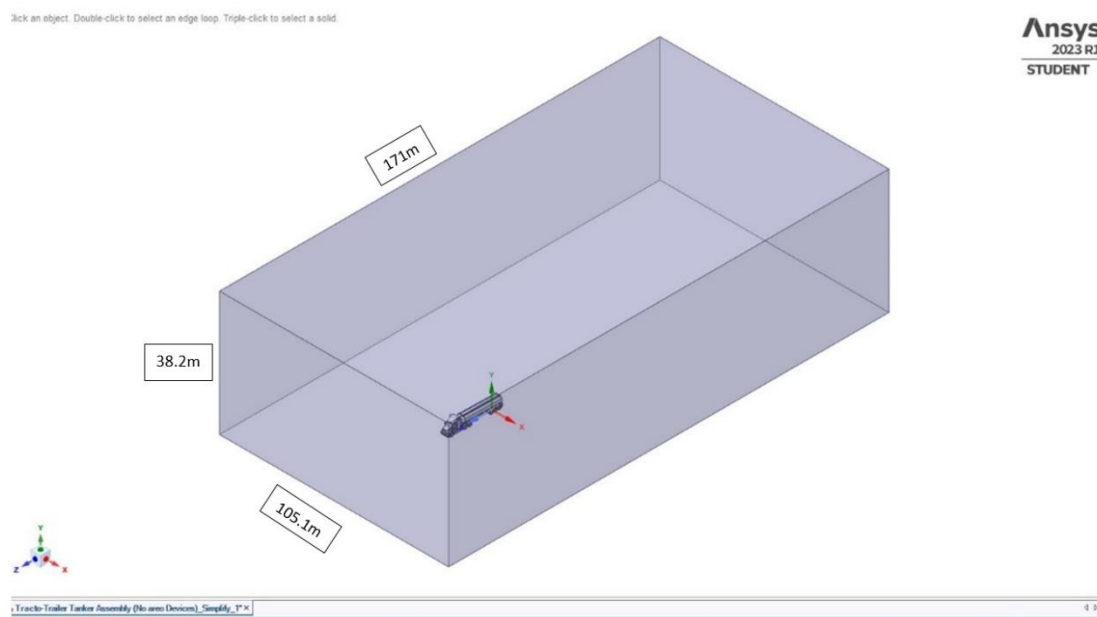


Figure 4.1-60: Computational Domain of a tractor-semitrailer tanker.

#### 4.1.4 [Mesh Generation and Mesh Quality Checking](#)

The computational domains meshed using the Ansys Fluent Meshing Watertight Geometry Workflow. Specifically, the unstructured grid Polyhedral mesh was utilised, notably the poly-hexcore meshing algorithm. This choice was made due to its efficiency in reducing hands-on meshing time, accurately representing the geometry of the problem, and enabling precise calculations in various dimensions. It contributed to the overall effectiveness of the CFD simulations, as discussed in Section 2.6.2.

In the meshing process, local sizing curvature and proximity were incorporated around the tractor-trailer (truck) geometry to capture the complex flow physics around the truck's outer surfaces (Figure 4.1-61). Subsequently, surface and volume meshes were created with the desired skewness below 0.7 and orthogonal quality below 0.01.

Table 4.1-9 presents a comparison between running time and mesh quality. Initially, very coarse mesh sizes were applied, resulting in an invalid mesh (skewness of 0.95 and minimum orthogonal of zero). The element sizes were refined to achieve better mesh quality. After 90 minutes of meshing time, the surface mesh skewness and volume mesh orthogonal quality reached 0.7 and 0.24, respectively. Further attempts were made to increase the volume mesh quality to the desired values above 0.5. However, meshing time significantly increased from 90 to 600 minutes, with the number of nodes rising from 5.6 million to 65 million (see Table 4.1-10)

Therefore, considering both meshing and calculation time efficiency, the final surface mesh skewness value of 0.7 (as shown in Figure 4.1-62) and the volume mesh quality of 0.24 were deemed valid and acceptable for this project, following the discussion in Section 2.6.2b.

For more details on the meshing process and the final domain volume mesh, please refer to Table 4.1-10, Figure 4.1-63 and Figure 4.1-64.

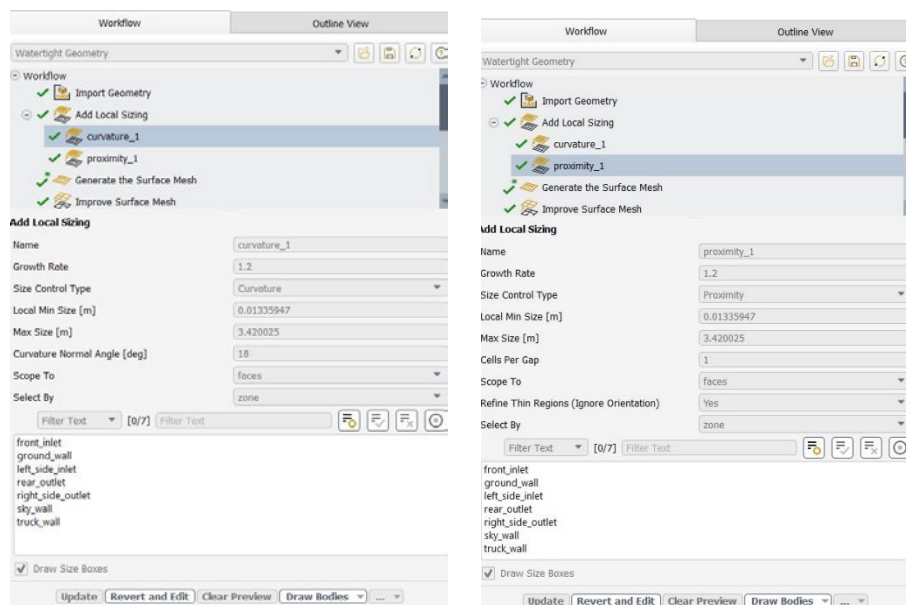


Figure 4.1-61: Adding Local Sizes

Table 4.1-9: Comparison between meshing time and mesh quality

Meshing Time versus Quality								
Surface Mesh		Local Sizing		Maximum Skewness	Meshing Time (minutes)	Minimum Volum Mesh Quality (Orthogonal)	Status	Number of node
Maximum Size (m)	Element Size (m)	Max Size (m)	Min Size (m)					
5	0.5	5	0.5	0.95	15	0	Invalid Mesh	N/A
5	0.25	5	0.25	0.9	30	0	Invalid Mesh	N/A
3.4	0.013	3.4	0.013	0.7	90	0.24	Valid Mesh	5.6 million
0.5	0.01	0.01	0.005	0.65	600	0.34	Valid Mesh	65 million



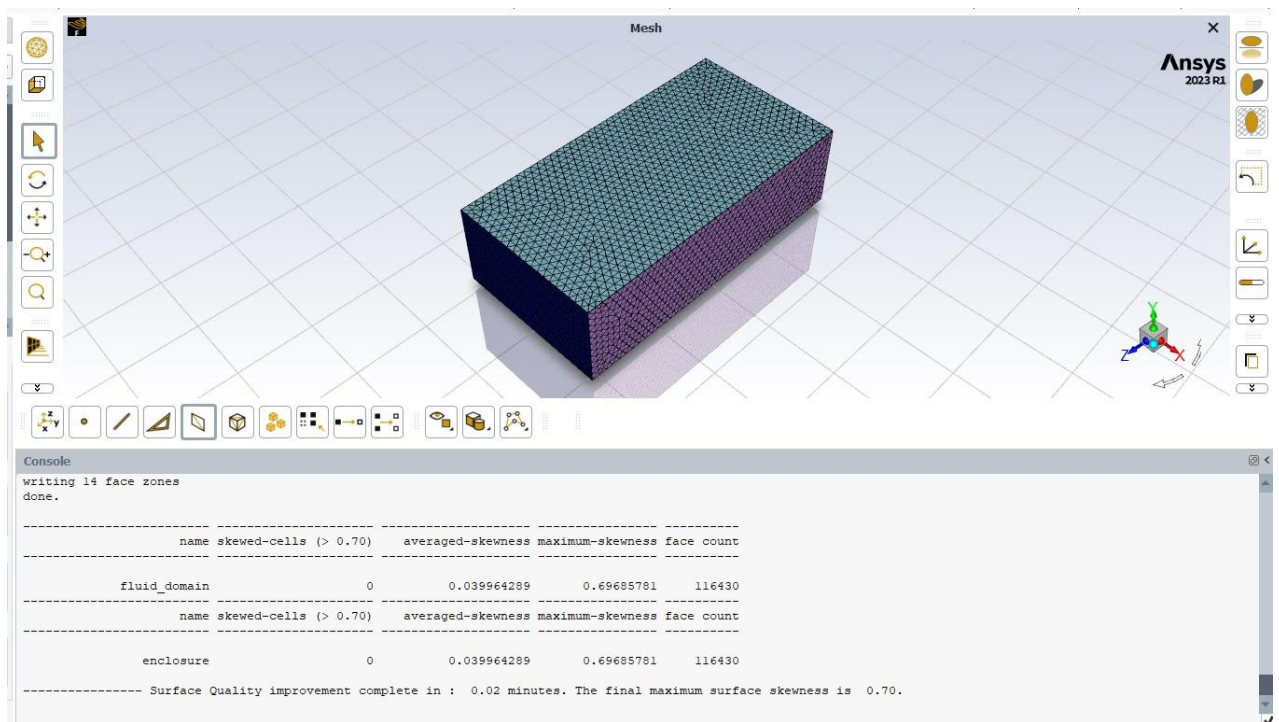


Figure 4.1-62: Surface Mesh Quality

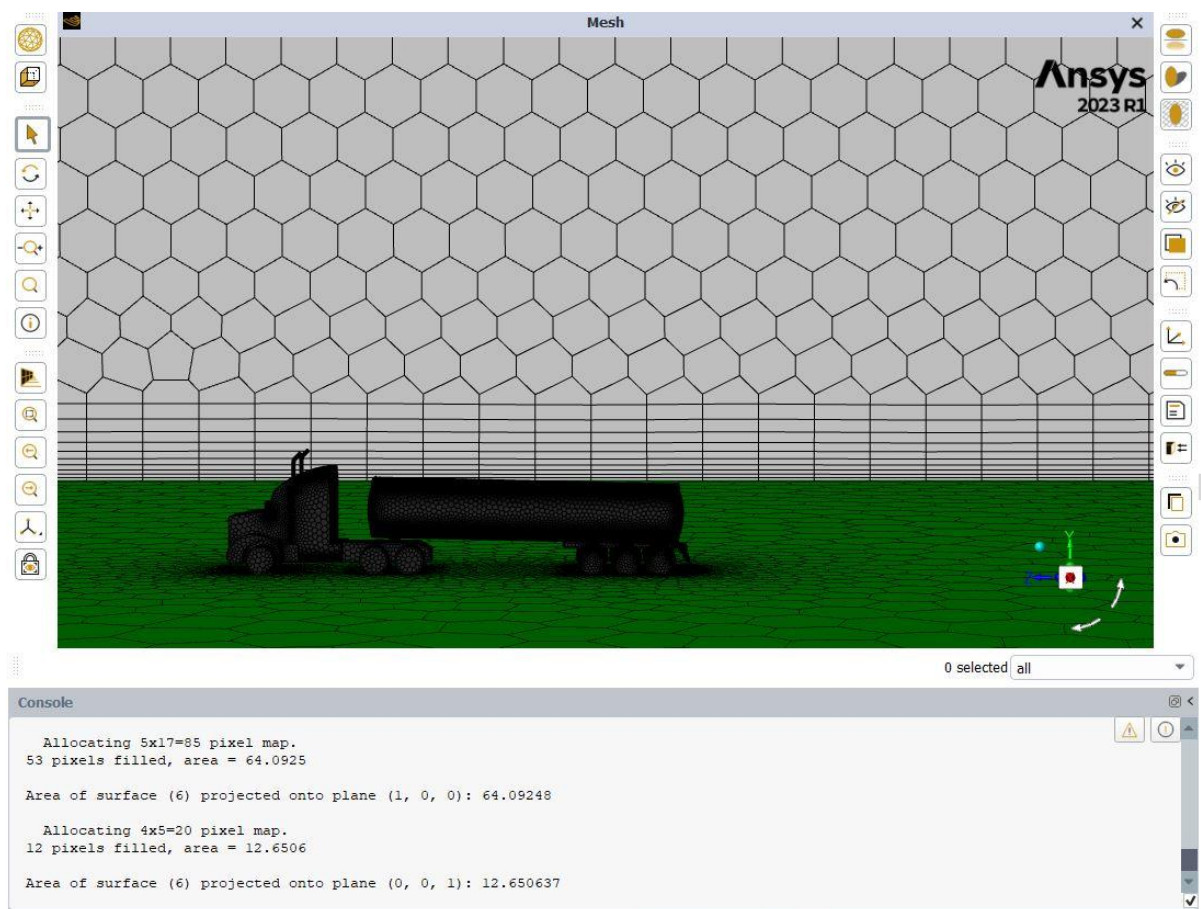


Figure 4.1-63: Baseline Model Final Volume Mesh.



Figure 4.1-64: Aerodynamic Model Final Volume Mesh.

Table 4.1-10: Geometry's meshing details

Meshing Tye	Watertight Geometry	
Local Sizing Control Type: Curvature & Proximity	Mesh size	Max 3.4m, Min 13mm
	Growth rate	1.2
	Scope To	Faces
Surface mesh	Min size	13mm
	Max size	3.4m
	Growth rate	1.2
	Size functions	Curvature & Proximity
	Curvature normal angle	18 deg
	Cells per gap	1
	Scope proximity to	Faces & edges
Boundary Layers	Offset Method Type	Smooth-transition
	Number of Layers	10
	Transition ratio	0.272
	Growth rate	1.2
	Grow on	ground_wall & truck surface
Volume Mesh	Solver	Fluent
	Fill with	Poly hex-core
	Buffer Layers	2
	Peel Layers	1
	Min cell length	13mm
	Max cell length	3.4m



## 4.2 CFD Solving Stage

The solving stage is the second stage of CFD simulation. In this stage, set-up and solution control steps are conducted to prepare for CFD analysis calculation.

In the set-up step, the turbulence viscous model, material, cell zone conditions, boundary conditions and reference values criteria are defined. In contrast, the solution methods, report definitions and residual monitors are also pre-defined in the solution control step.

The details of this solving stage can be broken down as follows:

### 4.2.1 Set-up steps

#### 1. Domain Description

The created computational domain (Figure 65) was used to simulate headwind and crosswind at various angles in which, in headwind simulation, the `lef_side_inlet` and `right_side_outlet` were treated as stationary non\_slip walls. In contrast, they were defined as `velocity_inlet` and `pressure_outlet` in crosswind simulations.

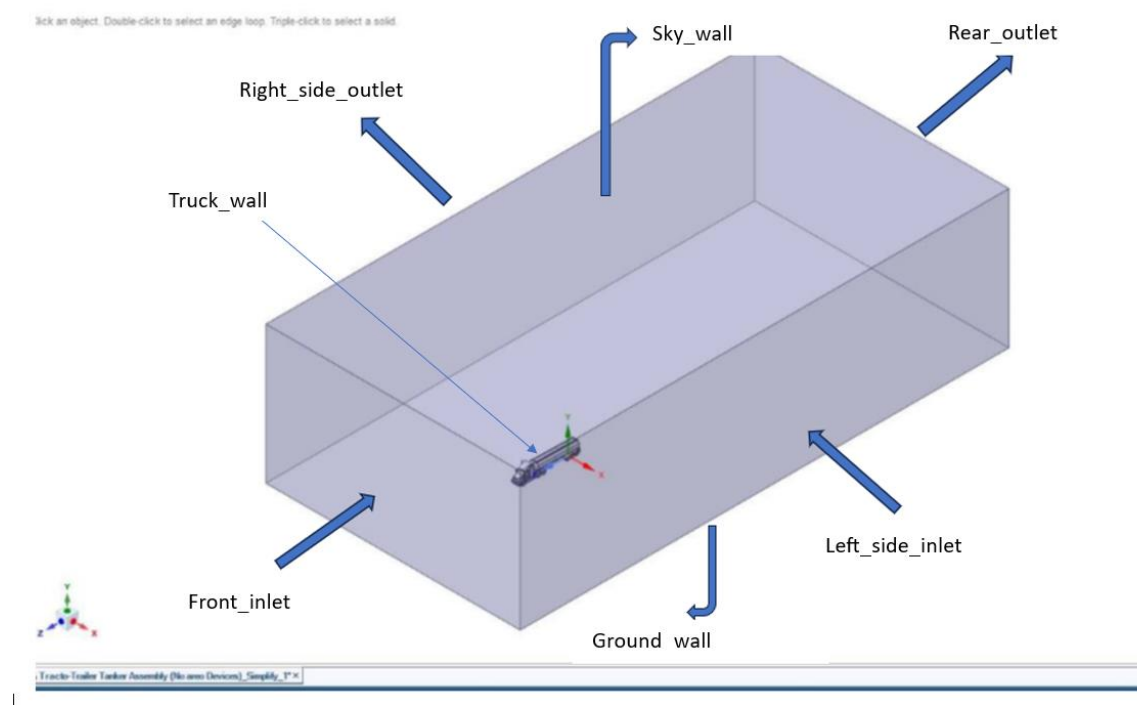


Figure 65: Domain Description

#### 2. Viscous Model

The most accurate viscous model, SST k-omega, was initially selected for the solving stage. However, due to the converging issue (solutions were not converged after 2000 iterations) caused by the quality of mesh discussed in 4.1.2, this viscous model was changed to a Realizable k-epsilon model with Enhanced Wall Treatment, Curvature Correction and Production Limiter options selected. Although the k-epsilon model gave less accurate results than the original k-omega viscous model, this option enabled solutions to converge,

and the results were stabilised in a shorter calculating time. Therefore, this k-epsilon viscous model was considered acceptable for this project due to the limited computational resources.

### 3. Material Definition

The fluid material is defined as air with the properties listed below:

- Density: Constant,  $1.225 \text{ kg/m}^3$
- Viscosity: Constant  $1.7894 \times 10^{-5}$

### 4. Cell Zone Conditions

Cell Zone conditions are defined as shown in Figure 66.

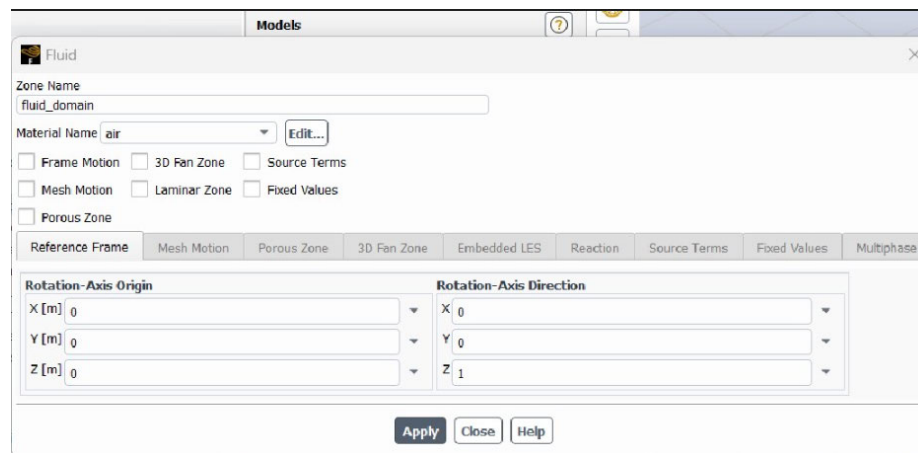


Figure 66: Cell Zone Conditions

### 5. Boundary Conditions

In this project, assumptions were made as follows:

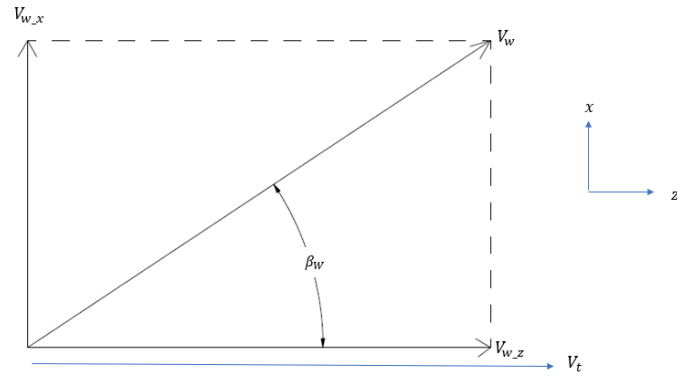
- The tractor-semitrailer tanker is stationary.
- The air flows at the velocity of the vehicle's max travelling speed of 100 km/h:

$$\rightarrow V_t = 100 \left( \frac{\text{km}}{\text{h}} \right) = 27.8 \left( \frac{\text{m}}{\text{s}} \right)$$

- According to Geoscience\_Australia (2023), the average windspeed in Australia is:

$$V_w = 6.5 \left( \frac{\text{m}}{\text{s}} \right) \text{ (Geoscience\_Australia 2023)}$$

Therefore, the magnitude of wind speed flows normal to the front\_inlet ( $V_z$ ) and left\_side inlet ( $V_x$ ) are calculated and shown in Table 4.2-11 as follows:



$$\begin{cases} V_z = V_t + V_{w,z} = V_t + V_w \cos(\beta_w) \\ V_x = V_{w,x} = V_w \sin(\beta_w) \\ \beta_w = \text{direction of crosswind relating to headwind} \end{cases}$$

Table 4.2-11: Headwind and Crosswind at Difference Wind Angle

Crosswind Angles $\beta_w$ (Degree)	Headwind $V_z$ (m/s)	Crosswind $V_x$ (m/s)
0	34.3	0.0
15	34.1	1.7
30	33.4	3.3
45	32.4	4.6
60	31.1	5.6
75	29.5	6.3
90	27.8	6.5

Below are the summarised boundary conditions defined for the domain in headwind simulation (Figure 4.2-67 and Table 4.2-12) and crosswind simulation (Figure 4.2-68 and Table 4.2-13).

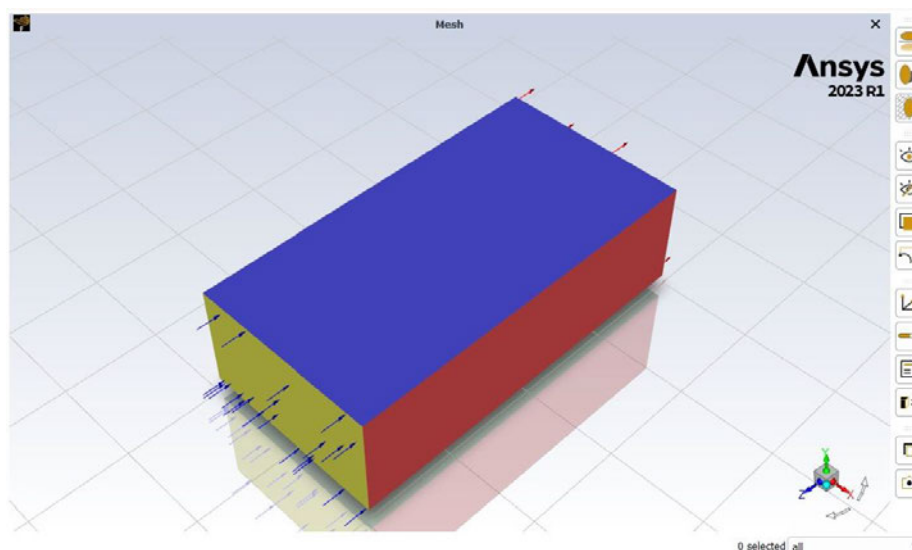


Figure 4.2-67: Boundary Definition for Headwind Simulation

Table 4.2-12: Boundary Condition for Headwind Simulation

Face (Figure 65)	Type	Conditions
Front_inlet	Velocity_Inlet	<ul style="list-style-type: none"> <li>Velocity Specification Method: Magnitude, Normal to Boundary</li> <li>Velocity Magnitude: 34.3 (m/s)</li> <li>Gauge Pressure: 0 (Pa)</li> <li>Turbulence Method: Intensity (5%) and Viscosity Ratio (10)</li> </ul>
Left_side_inlet, Right_side_outlet, Ground_wall, Sky_wall and Truck_wall	Walls	<ul style="list-style-type: none"> <li>Stationary wall</li> <li>Shear Condition: No Slip</li> <li>Roughness: 0 (m)</li> <li>Roughness Constant: 0.5</li> </ul>
Rear_outlet	Pressure Outlet	<ul style="list-style-type: none"> <li>Backflow Reference Frame: Absolute</li> <li>Gauge Pressure: 0 (Pa)</li> <li>Backflow Direction: Normal to Boundary</li> <li>Backflow Pressure: Total Pressure</li> <li>Backflow Turbulence Method: Intensity (5%) and Viscosity Ratio (10)</li> </ul>
Domain	Operating Conditions	<ul style="list-style-type: none"> <li>Operating Pressure: 101,325 (Pa)</li> </ul>

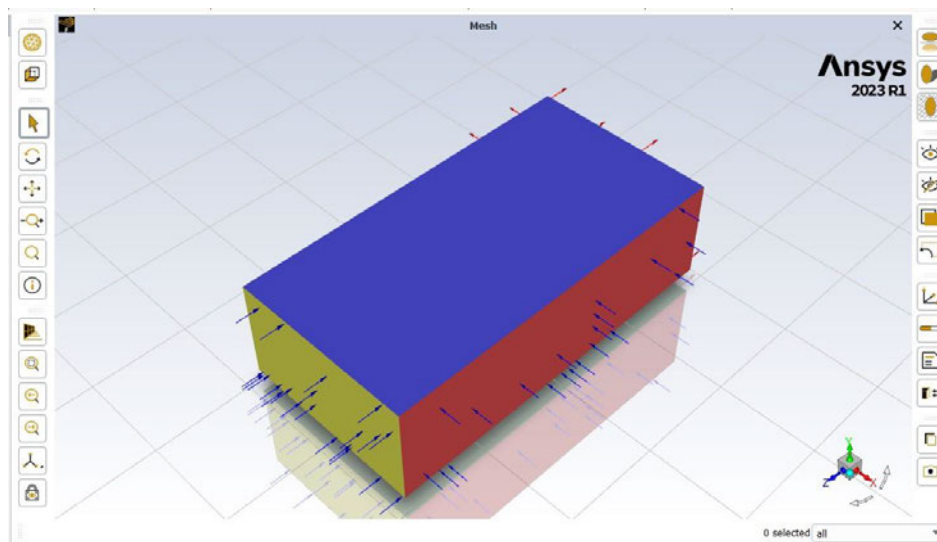


Figure 4.2-68: Boundary Definition for Crosswind Simulation

Table 4.2-13: Boundary Condition for Crosswind Simulation at Difference Wind Angles From 0 to 90 degrees

Face (Figure 65)	Type	Conditions
Front_inlet and Left_side_inlet	Velocity_Inlet	<ul style="list-style-type: none"> <li>Velocity Specification Method: Components</li> <li>Reference Frame: Absolute</li> <li>Gauge Pressure: 0 (Pa)</li> </ul>

		<ul style="list-style-type: none"> <li>• Coordinate System: Cartesian (X,Y,Z)</li> <li>• X-Velocity: <math>-V_x</math> (m/s)</li> <li>• Y-Velocity: 0 (m/s)</li> <li>• Z-Velocity: <math>-V_z</math> (m/s)</li> <li>• Turbulence Method: Intensity (5%) and Viscosity Ratio (10)</li> </ul>
Ground_wall, Sky_wall and Truck_wall	Walls	<ul style="list-style-type: none"> <li>• Stationary wall</li> <li>• Shear Condition: No Slip</li> <li>• Roughness: 0 (m)</li> <li>• Roughness Constant: 0.5</li> </ul>
Rear outlet and Right_side_outlet	Pressure Outlet	<ul style="list-style-type: none"> <li>• Backflow Reference Frame: Absolute</li> <li>• Gauge Pressure: 0 (Pa)</li> <li>• Backflow Direction: Normal to Boundary</li> <li>• Backflow Pressure: Total Pressure</li> <li>• Backflow Turbulence Method: Intensity (5%) and Viscosity Ratio (10)</li> </ul>
Domain	Operating Conditions	<ul style="list-style-type: none"> <li>• Operating Pressure: 101,325 (Pa)</li> </ul>

#### 4.2.2 Solution control

In this step, the required report, plots, and solution control were predefined to control the converging of solution and to capture the interested forces, such as the drag and lift forces in x, y and z directions acting on the truck, as well as the pitch moment, rotational moment and rollover moment that these forces produced on the vehicle.

Figure 4.2-69 shows the residual monitors' converging criteria were set to 0.0001 for continuity, x-velocity, y-velocity, z-velocity, k and epsilon to measure the solution's convergence. In contrast, Table 4.2-14 shows the definition of forces and moments required to obtain from the CFD simulations.

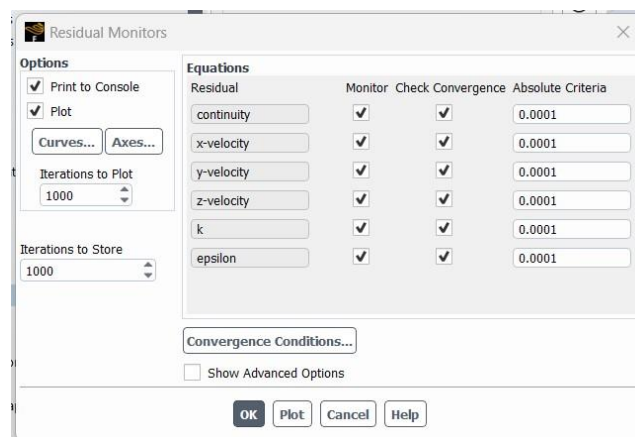


Figure 4.2-69: Residual Monitors

Table 4.2-14: Definition of Forces and Moments

Name	Force Vector (X, Y, Z)	Report Output Type	Zones
x-drag-force	-1,0,0	Drag Force	Truck_wall
y-lift-force	0,1,0	Lift Force	Truck_wall
z-drag-force	0,0,-1	Drag Force	Truck_wall
x-pitch-moment	1,0,0	Moment	Truck_wall
y-rotational-moment	0,1,0	Moment	Truck_wall
z-rollover-moment	0,0,1	Moment	Truck_wall

### 4.3 CFD Post-Processing Stage

The Post-Processing Stage is the stage where the domain geometry and grid display, vector plots, line and shaded contour plots, 2D and 3D surface plots, particle tracking, view manipulation (translation, rotation, scaling), and colour postscript output were predefined (Versteeg & Malalasekera 2011). These tools serve an essential role in the results validation and verification processes, as well as assisting the CFD user to better analyse and visualize the many relevant physical characteristics within the fluid flow problem, thus optimising the design by revising the input parameters such as fluid flow properties and boundary conditions (Tu et al. 2018).

### 4.4 Solution Initialisation and Calculation

The solution of the headwind and crosswind simulations was initialised with a hybrid initialisation method and was run with an initial 200 iterations. These number of iterations increased until the solutions converged, as shown in Figure 4.4-70 and Figure 4.4-71.



Figure 4.4-70: Solution Initialisation

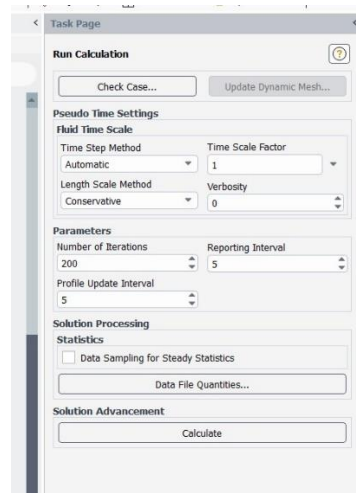


Figure 4.4-71: Calculation Running

## CHAPTER 5 – RESULT AND DISCUSSION

### 5.1 [Introduction](#)

In this chapter, The first step is to analyse the results obtained from the simulations. It compares the simulation results for the baseline and the aerodynamic tractor-semitrailer tanker models under headwind conditions with previous studies to validate the Computational Fluid Dynamics (CFD) simulations. Following this was the analysis of crosswind simulation results, including drag force, lift force, and moments acting on the vehicles, to assess the aerodynamic performance of the aerodynamic tractor-semitrailer tanker.

The next objective is to investigate the safety of tractor-trailers equipped with aero devices, focusing on the likelihood of sideslip, rotation, or rollover accidents. This analysis aims to identify optimal operating conditions to mitigate these accidents effectively.

The final step in this chapter is the Pre-optimization study, which examines areas such as the tractor-trailer gap, tractor and trailer sides, and the tanker barrel, thus proposing modifications aimed at reducing the adverse effects of crosswinds and assessing their compliance with the current regulations discussed in Section 2.5.

### 5.2 [Validating Headwind Simulation Results](#)

The drag coefficients obtained from headwind simulations for the baseline and the aerodynamic tractor-semitrailer tankers are presented in Table 5.2-15 and visualized in Figure 5.2-73 and Figure 5.2-74. These drag coefficients are calculated using consistent reference values, including frontal area, length, and velocity, as depicted in Figure 5.2-72. For a more comprehensive understanding of the forces involved, such as drag and lift forces, pitch moment, rotation moment, and rollover moment, please refer to Appendix H.1.

The results show that the baseline model exhibits a drag coefficient of 0.510. In contrast, the aerodynamic model, equipped with tractor side skirts, tractor-trailer gap fairing, and trailer side skirts, achieves a reduced drag coefficient of 0.419. Implementing these aerodynamic enhancements results in an impressive 18% reduction in the drag coefficient.

These findings align with prior research conducted by McCallen et al. in 2007. Their study, detailed in Table 1 and the conclusion of the research publication, confirms that installing trailer side skirts and tractor-trailer gap fairings can reduce the drag coefficient caused by headwinds by 18% (McCallen et al. 2007). This validation further solidifies the credibility of the simulation domain and setup employed for this project.

Task Page

**Reference Values**

Compute from  
front\_inlet

**Reference Values**

Area [m<sup>2</sup>] 12.65

Density [kg/m<sup>3</sup>] 1.225

Enthalpy [J/kg] 0

Length [m] 17.1

Pressure [Pa] 0

Temperature [K] 288.16

Velocity [m/s] 34.3

Viscosity [kg/(m.s)] 1.7894e-05

Ratio of Specific Heats 1.4

Yplus for Heat Tran. Coef. 300

Reference Zone  
fluid\_domain

Figure 5.2-72: Reference Values for both Baseline and Aerodynamic Models

Table 5.2-15: Headwind Simulation Results

Baseline Frontal Projected Area (m2)	12.65	Aero Frontal Projected Area (m2)	12.65	Air Density (kg/m3)	1.225	Length of Vehicle (m)	17.1	Air Dynamic Viscosity (kg/m.s)
Wind Angle	Velocity <b>V<sub>z</sub></b> (m/s)	Velocity <b>V<sub>x</sub></b> (m/s)	Resulant Velocity <b>V<sub>R</sub></b> (m/s)	Axial Drag Forces: <b>F<sub>z</sub></b> (N)				
				Baseline Model	Aerodynamic Model	Baseline Axial Drag Coefficient <b>C<sub>B,Z</sub></b>	Aero Axial Drag Coefficient <b>C<sub>A,Z</sub></b>	Percentage Change in Drag Coefficient
0	34.3	0	34.3	4,647	3,815	0.510	0.419	-18%

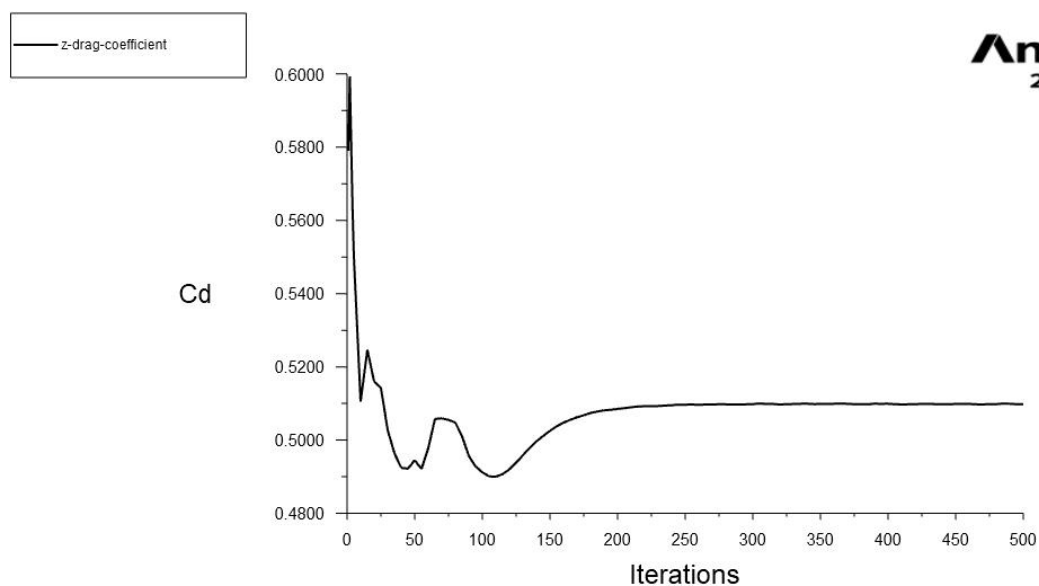


Figure 5.2-73: Drag Coefficient of Baseline Model



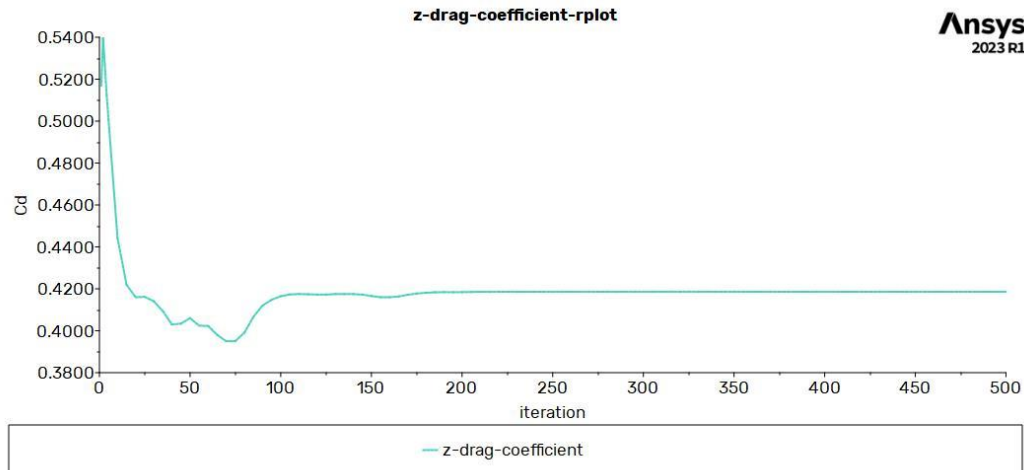


Figure 5.2-74: Drag Coefficient of Aerodynamic Model

### 5.3 Studying crosswind simulation results

The results of CFD simulations for the baseline and the aerodynamic tractor-semitrailer tankers under crosswinds at wind angles ranging from 15 to 90 degrees (with an increment step of 15 degrees) relative to the headwind direction are shown in Table 5.3-16. The X-Y charts showing the convergence of results for Headwind and Crosswind Simulations can be found in Appendix H.1 and H.2.

#### 5.3.1 Calculation of force and moment coefficient

##### a) The selected vehicles

Figure 4.1-58 and Figure 4.1-59 in Section 4.1.2 shows the simplified geometries of the Baseline and Aerodynamic tractor-semitrailer tankers used for this project simulations. These geometries have general dimensions as follows:

- Vehicle length:  $L = 17.1$  m
- Vehicle width :  $W = 2.5$ m
- Vehicle Overall Height: 4m
- Baseline truck's frontal projected area:  $A_B = 12.65$  m<sup>2</sup> (calculated by Ansys Fluent)
- Aerodynamic truck's frontal projected area:  $A_A = 12.65$  m<sup>2</sup> (calculated by Ansys Fluent)
- Air density:  $\rho = 1.225$  (kg/m<sup>3</sup>)
- Baseline truck's side area:  $A_{S(B)} = 64.1$  m<sup>2</sup> (calculated by Ansys Fluent)
- Aerodynamic truck's side area:  $A_{S(A)} = 68.9$  m<sup>2</sup> (calculated by Ansys Fluent)

##### b) Calculating Force and Moment Coefficients

Figure 4.1-60 in Section 4.1.2 demonstrates the computational domain setup for CFD simulation. The force and moment coefficients were calculated based on that domain for Baseline geometry as follows:

$$\begin{cases}
 \text{Resultant Velocity: } V_R = \sqrt{(V_z^2 + V_x^2)} \\
 \text{Baseline axial drag coefficient: } C_{B,Z} = \frac{2 \times F_z}{\rho \times V_R^2 \times A_B} \\
 \text{Baseline lateral drag coefficient: } C_{B,X} = \frac{2 \times F_x}{\rho \times V_R^2 \times A_B} \\
 \text{Baseline lift coefficient: } C_{B,Y} = \frac{2 \times F_L}{\rho \times V_R^2 \times A_B} \\
 \text{Baseline pitch moment coefficient: } C_{B,PM} = \frac{2 \times M_x}{\rho \times V_R^2 \times A_B \times L} \\
 \text{Baseline rotational moment coefficient: } C_{B,RM} = \frac{2 \times M_y}{\rho \times V_R^2 \times A_B \times L} \\
 \text{Baseline rollover moment coefficient: } C_{B,ROM} = \frac{2 \times M_z}{\rho \times V_R^2 \times A_B \times L}
 \end{cases}$$

Similarly, the force and moment coefficients were calculated for the aerodynamic geometry:

$$\begin{cases}
 \text{Aero axial drag coefficient: } C_{A,Z} = \frac{2 \times F_z}{\rho \times V_R^2 \times A_A} \\
 \text{Aero lateral drag coefficient: } C_{A,X} = \frac{2 \times F_x}{\rho \times V_R^2 \times A_A} \\
 \text{Aero lift coefficient: } C_{A,Y} = \frac{2 \times F_L}{\rho \times V_R^2 \times A_A} \\
 \text{Aero pitch moment coefficient: } C_{A,PM} = \frac{2 \times M_x}{\rho \times V_R^2 \times A_A \times L} \\
 \text{Aero rotational moment coefficient: } C_{A,RM} = \frac{2 \times M_y}{\rho \times V_R^2 \times A_A \times L} \\
 \text{Aero rollover moment coefficient: } C_{A,ROM} = \frac{2 \times M_z}{\rho \times V_R^2 \times A_A \times L}
 \end{cases}$$

Table 5.3-16 shows the simulation and calculation results for the project based on the equations above.

Table 5.3-16: Simulation Results of Crosswind for Baseline and Aerodynamic Tankers

Baseline Frontal Projected Area (m2)	12.65	Aero Frontal Projected Area (m2)	12.65	Air Density (kg/m3)	1.225	Length of Vehicle (m)	17.1	Air Dynamic Viscosity (kg/m.s)	1.79E-05	Baseline Side Area (m2)	64.1	Aero Side Area (m2)	68.9
Wind Angle	Velocity $V_z$ (m/s)	Velocity $V_x$ (m/s)	Resultant Velocity $V_R$ (m/s)	Axial Drag Forces: $F_z$ (N)					Lateral Drag Forces: $F_x$ (N)				
				Baseline Model	Aerodynamic Model	Baseline Axial Drag Coefficient $C_{B,Z}$	Aero Axial Drag Coefficient $C_{A,Z}$	Percentage Change in Drag Coefficient	Baseline Model	Aerodynamic Model	Baseline Lateral Drag Coefficient $C_{B,X}$	Aero Lateral Drag Coefficient $C_{A,X}$	Percentage Change in Drag Coefficient
15	34.1	1.7	34.1	5,115	4,085	0.567	0.453	-20.1%	1,273	1,550	0.141	0.172	21.8%
30	33.4	3.3	33.6	5,607	4,169	0.642	0.477	-25.6%	2,529	3,029	0.289	0.347	19.8%
45	32.4	4.6	32.7	5,625	4,264	0.678	0.514	-24.2%	3,507	4,231	0.423	0.510	20.6%
60	31.1	5.6	31.6	5,491	4,343	0.712	0.563	-20.9%	4,059	4,950	0.526	0.642	22.0%
75	29.5	6.3	30.1	5,279	4,113	0.750	0.584	-22.1%	4,353	5,317	0.618	0.755	22.1%
90	27.8	6.5	28.5	4,854	3,795	0.769	0.601	-21.8%	4,290	5,251	0.679	0.831	22.4%
							Average	-22.5%				Average	21.4%

Wind Angle	Velocity $V_z$ (m/s)	Velocity $V_x$ (m/s)	Resulant Velocity $V_R$ (m/s)	Lift Forces: $F_y$ (N)					Pitching Moment: $M_x$ (N.m)				
				Baseline Model	Aerodynamic Model	Baseline Lift Coefficient $C_{B,Y}$	Aero Lift Coefficient $C_{A,Y}$	Percentage Change in Lift Coefficient	Baseline Model	Aerodynamic Model	Baseline Pitch Moment Coefficient $C_{B,PM}$	Aero Pitch Moment Coefficient $C_{A,PM}$	Percentage Change in Pitch Moment Coefficient
15	34.1	1.7	34.1	1,602	661	0.178	0.073	-58.7%	11,518	10,871	0.075	0.070	-5.6%
30	33.4	3.3	33.6	2,179	1,135	0.249	0.130	-47.9%	9,602	9,241	0.064	0.062	-3.8%
45	32.4	4.6	32.7	2,236	1,740	0.270	0.210	-22.2%	7,949	5,546	0.056	0.039	-30.2%
60	31.1	5.6	31.6	2,221	2,400	0.288	0.311	8.1%	5,517	2,342	0.042	0.018	-57.5%
75	29.5	6.3	30.1	2,464	2,778	0.350	0.395	12.7%	2,456	437	0.020	0.004	-82.2%
90	27.8	6.5	28.5	2,500	3,031	0.396	0.480	21.2%	727	247	0.007	0.002	-66.0%
				Average				-14.47%	Average				-40.9%

Wind Angle	Velocity $V_z$ (m/s)	Velocity $V_x$ (m/s)	Resulant Velocity $V_R$ (m/s)	Rotational (Yawning) Moment: $M_y$ (N.m)					Rollover Moment: $M_z$ (N.m)				
				Baseline Model	Aerodynamic Model	Baseline Rotational Moment Coefficient $C_{B,RM}$	Aero Rotational Moment Coefficient $C_{A,RM}$	Percentage Change in Rotational Moment Coefficient	Baseline Model	Aerodynamic Model	Baseline Rollover Moment Coefficient $C_{B,ROM}$	Aero Rollover Moment Coefficient $C_{A,ROM}$	Percentage Change in Rollover Moment Coefficient
15	34.1	1.7	34.1	563	1,370	0.004	0.009	143.3%	2,282	2,672	0.0148	0.017	17.1%
30	33.4	3.3	33.6	3,079	3,776	0.021	0.025	22.6%	4,440	5,121	0.0297	0.034	15.3%
45	32.4	4.6	32.7	4,985	3,577	0.035	0.025	-28.2%	6,117	7,076	0.0431	0.050	15.7%
60	31.1	5.6	31.6	5,491	2,243	0.042	0.017	-59.2%	7,083	8,205	0.0537	0.062	15.8%
75	29.5	6.3	30.1	5,546	3,397	0.046	0.028	-38.7%	7,538	8,800	0.0626	0.073	16.7%
90	27.8	6.5	28.5	5,140	4,781	0.048	0.044	-7.0%	7,395	8,884	0.0685	0.082	20.1%
				Average				5.5%	Average				16.8%

### 5.3.2 Studying the simulation results

#### 5.3.2.1 Studying the percentage difference of force and moment coefficients between the baseline and the aerodynamic model

The comparison between the "Baseline Model" and the "Aerodynamic Model" across various wind angles (as shown in Table 5.3-16 and Figure 5.3-75 to Figure 5.3-81) yields several significant insights:

##### ➤ Drag and Lift Forces

- Axial Drag Coefficient ( $C_z$ ): The Aerodynamic Model consistently reduces the Axial Drag coefficient ( $C_z$ ) compared to the Baseline Model, achieving an average 22.5% decrease in most crosswind angles with the most significant reduction of 25.6% at a 30-degree wind angle (Figure 5.3-76).
- However, it's worth noting that the lateral drag coefficient ( $C_x$ ) generally increases with the Aerodynamic Model, showing an average rise of 22% in drag coefficient across various crosswind angles (Figure 5.3-77). This increase is attributed to the 7.5% larger side area of the Aerodynamic Model (68.9 m<sup>2</sup> vs. 64.1 m<sup>2</sup> for the Baseline Model), indicating increased resistance to lateral air movement.
- Lift Coefficient ( $C_y$ ): The Aerodynamic Model influences the lift coefficient ( $C_y$ ) differently, resulting in reductions ranging from -58.7% to -22.2% across crosswind angles from 15 to 45 degrees. In contrast, there are increases in lift coefficient at angles above 45 degrees (Figure 5.3-78), peaking at a 90-degree wind angle with a rise of 21.2%. These changes can significantly impact the vehicle's vertical stability and control.

➤ Moments: The tendency to cause the vehicle to rotate about its axes.

- Pitch Moment ( $C_{PM}$ ): The Aerodynamic Model consistently results in lower pitch moments ( $M_x$ ) and pitch moment coefficients ( $C_{PM}$ ) compared to the Baseline Model. The percentage change in pitch moment coefficient suggests that the Aerodynamic Model can substantially reduce pitch moments, ranging from approximately 3.8% to 82.2%. (Figure 5.3-79).
- Rotational Moment ( $C_{RM}$ ): The percentage change in rotational moment coefficient varies across different cases, ranging from -59.2% to 143.3%. It indicates that the Aerodynamic Model significantly impacts increasing rotational moments at wind angles ranging from 15 to 30 degrees, with the most significant increase being 143.3% at a 15-degree wind angle (Figure 5.3-80). However, this rotational moment constantly reduces at wind angles above 30 degrees. It indicates crosswinds significantly impact the vehicle's balance and manoeuvrability at wind angles equal to or less than 30 degrees. These moments are crucial for understanding the vehicle's rotational behaviour and stability.
- Rollover Moment ( $C_{ROM}$ ): The presence of aerodynamic devices increases the rollover moment coefficient across cases, ranging from 15.3% to 20.1% (Figure 5.3-81). It suggests that installing aerodynamic devices makes the vehicle more susceptible to rollovers than the baseline model at most wind angles.

In summary, these findings underscore the significant impact of the Aerodynamic Model on various aerodynamic parameters. It emphasises the importance of carefully considering the specific design requirements and intended use of aerodynamic devices, especially tractor and trailer side skirts and the tractor-trailer gap fairing. These enhancements increase lateral drag force, rotation and rollover moments, especially from 15 and 30-degree wind angles where the lateral drag coefficient, rotational, and rollover moments are at peak values, potentially leading to instability and increased fuel consumption for the vehicle. Moreover, the significant increase in the rotational moment at 15 and 30-degree wind angles indicates that the crosswinds significantly impact the vehicle's balance and manoeuvrability.

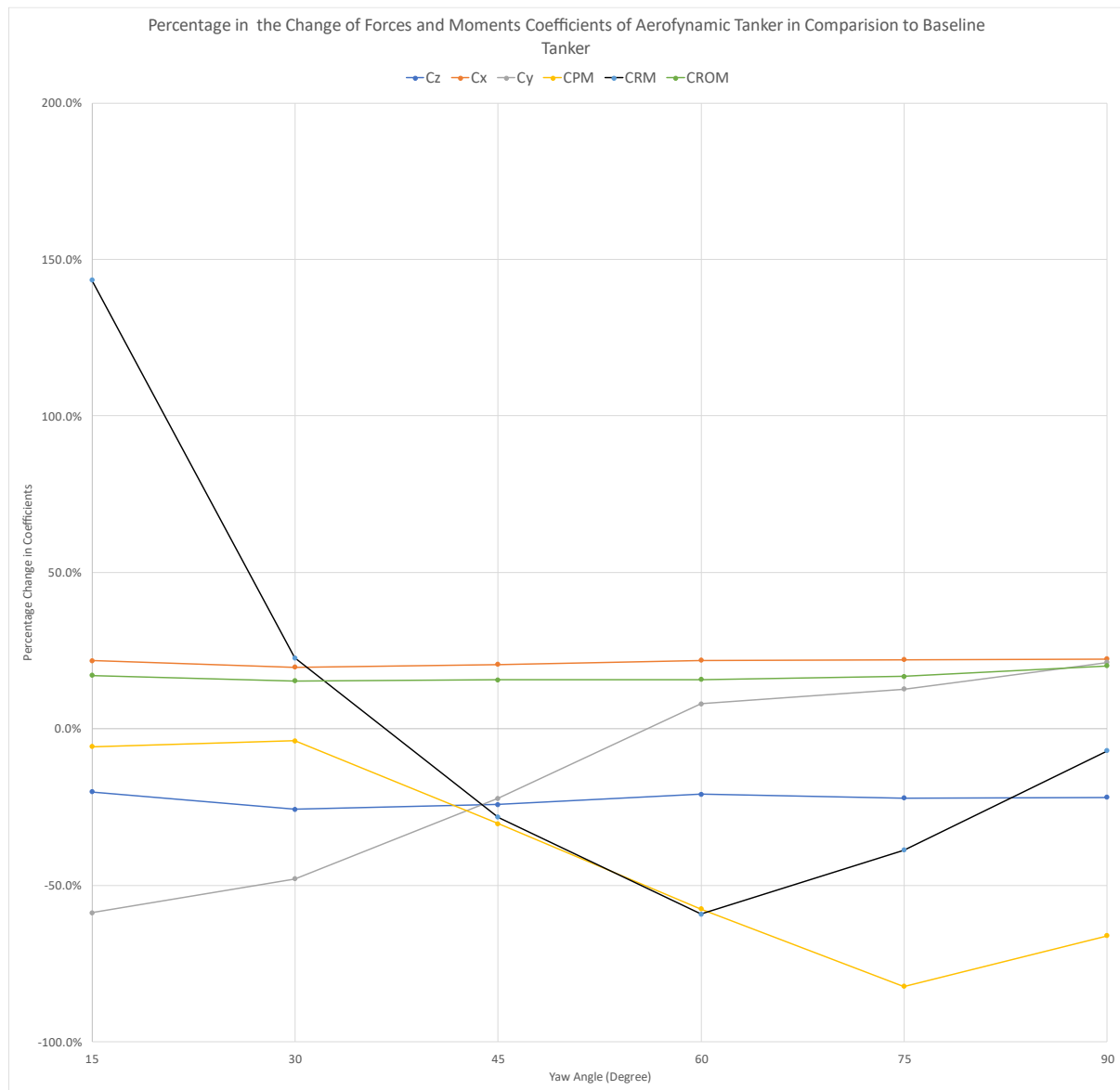


Figure 5.3-75: Impact of Crosswind on Forces and Moments Coefficient of Aerodynamic Tankers at Various Wind Angles

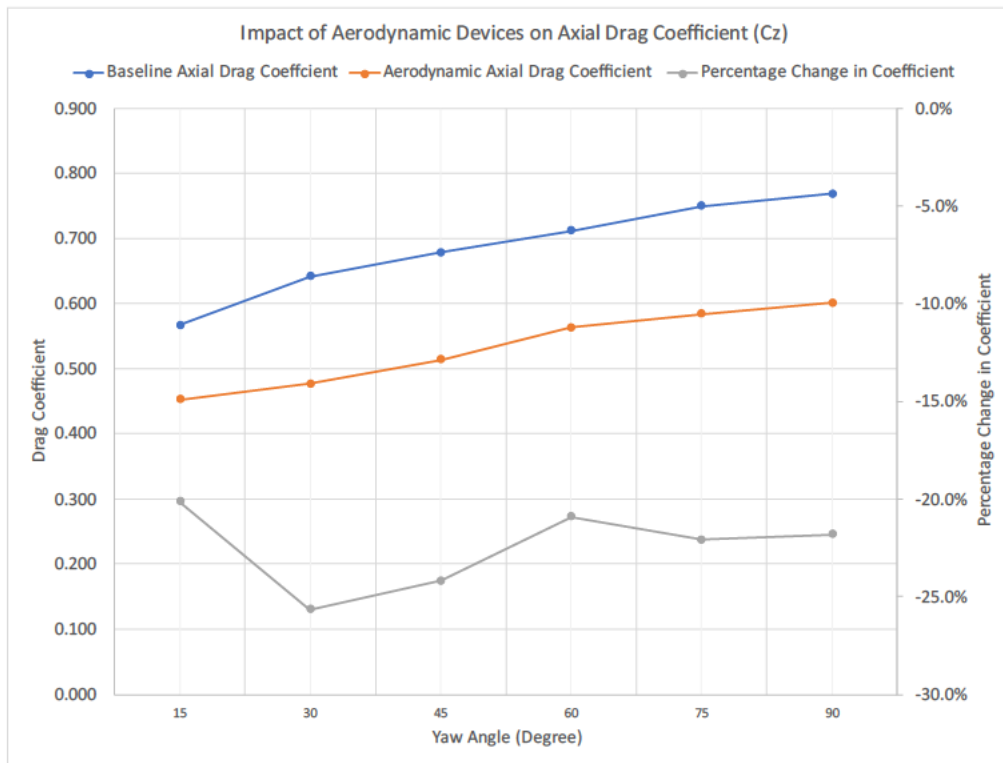


Figure 5.3-76: Impact of Aerodynamic Devices on Axial Drag Coefficient ( $C_z$ )

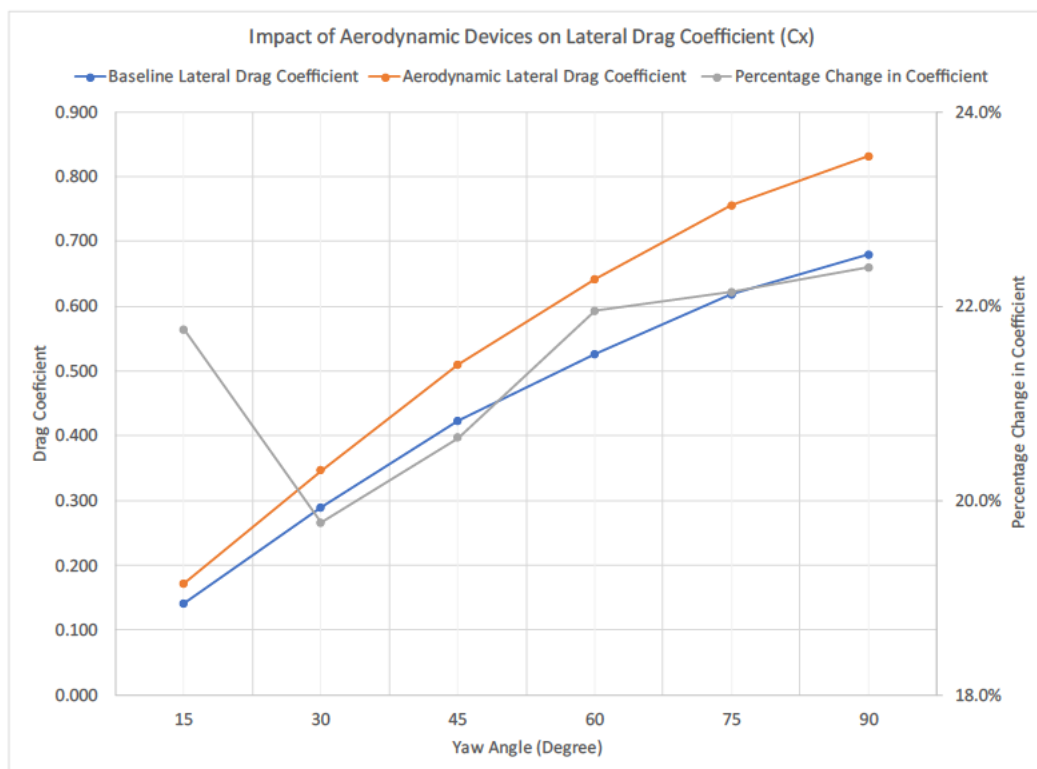


Figure 5.3-77: Impact of Aerodynamic Devices on Lateral Drag Coefficient ( $C_x$ )

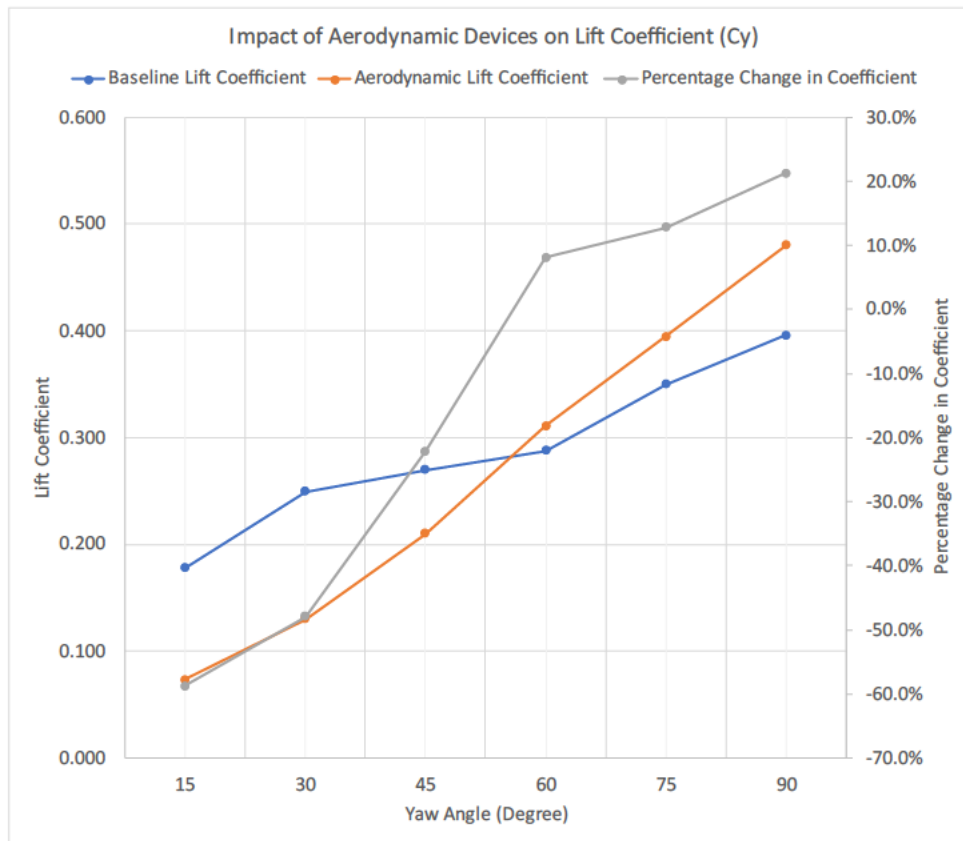


Figure 5.3-78: Impact of Aerodynamic Devices on Lift Coefficient ( $C_y$ )

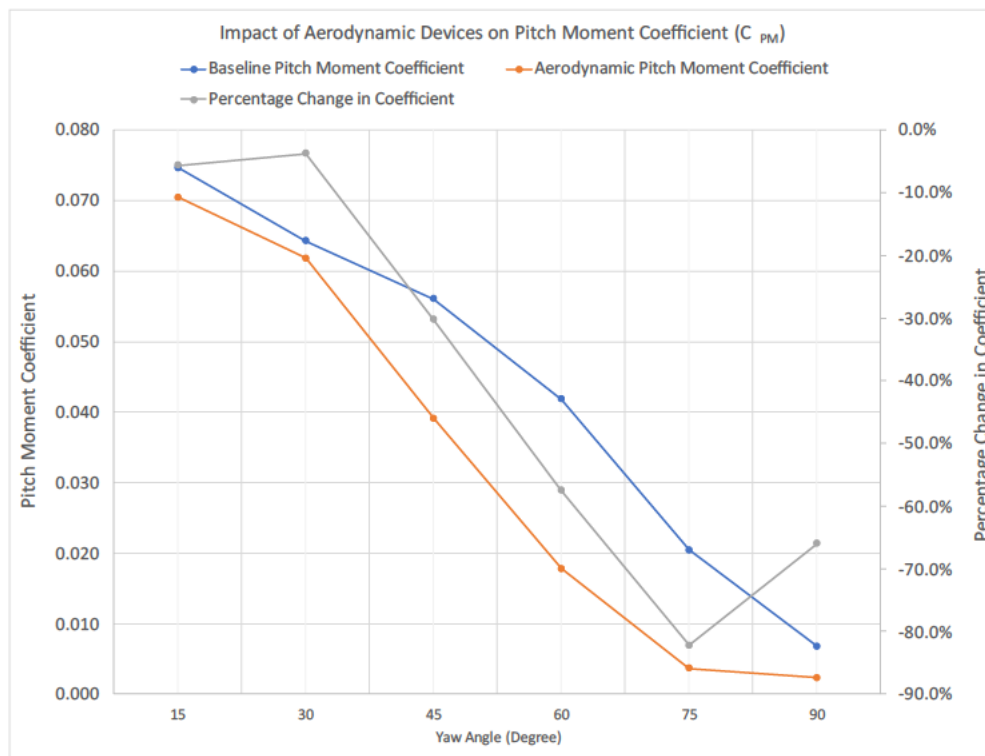


Figure 5.3-79: Impact of Aerodynamic Devices on Pitching Moment Coefficient ( $C_{PM}$ )

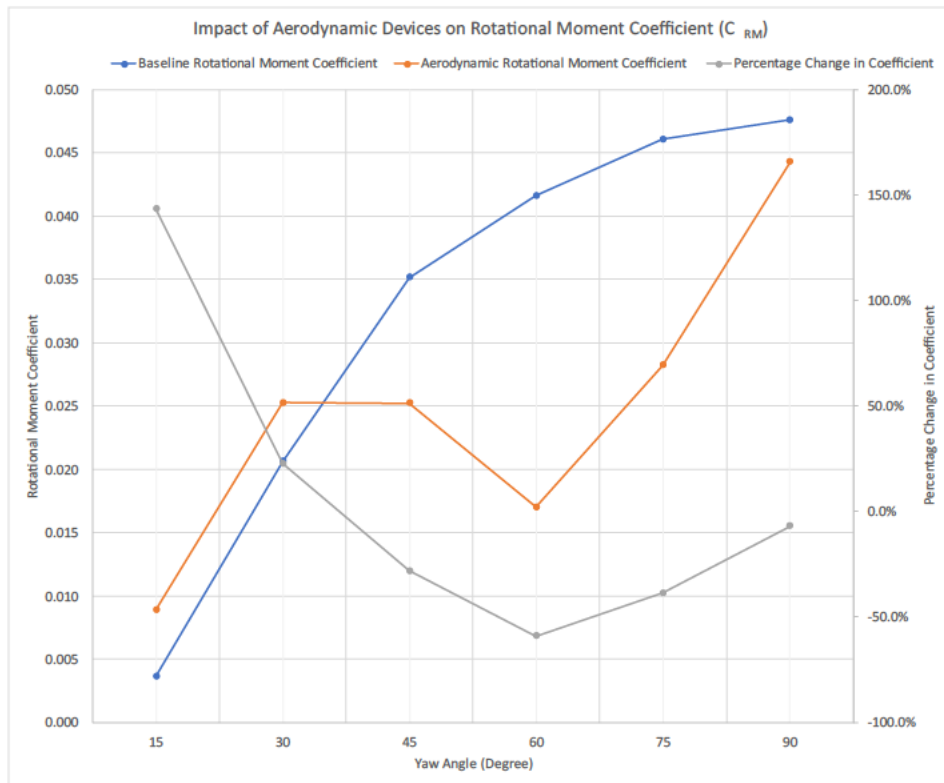


Figure 5.3-80: Impact of Aerodynamic Devices on Rotational Moment Coefficient ( $C_{RM}$ )

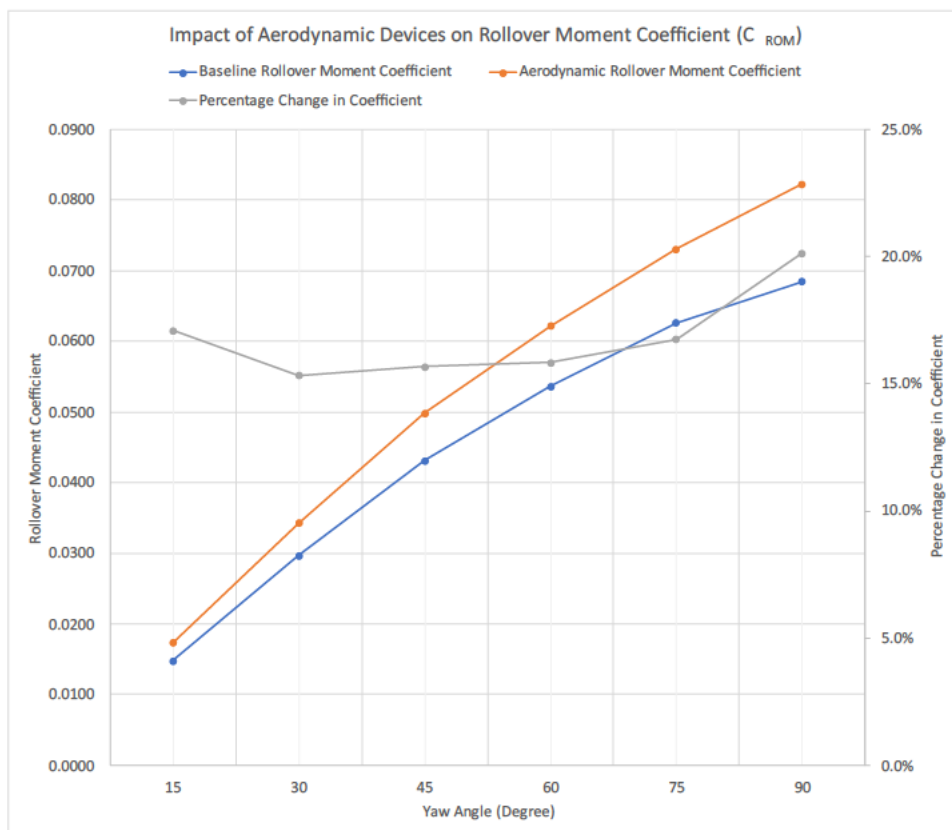


Figure 5.3-81: Impact of Aerodynamic Devices on Rollover Moment Coefficient ( $C_{ROM}$ )



### 5.3.2.2 Studying pressure and flow around road tankers of the baseline and aerodynamic models at 15-degree crosswind

Figure 5.3-82 to Figure 5.3-103 compares the contour plot of static and total pressure and the flow pathlines of the Baseline and the Aerodynamic tankers at 15-degree crosswind angles where crosswind has the most effect on the change in rotational moment coefficient. Other contours and pathlines of both tankers at different crosswind angles are depicted in Appendix H.3 to H.8.

#### a) Static Pressure Distribution in both tankers at 15-degree crosswind angle

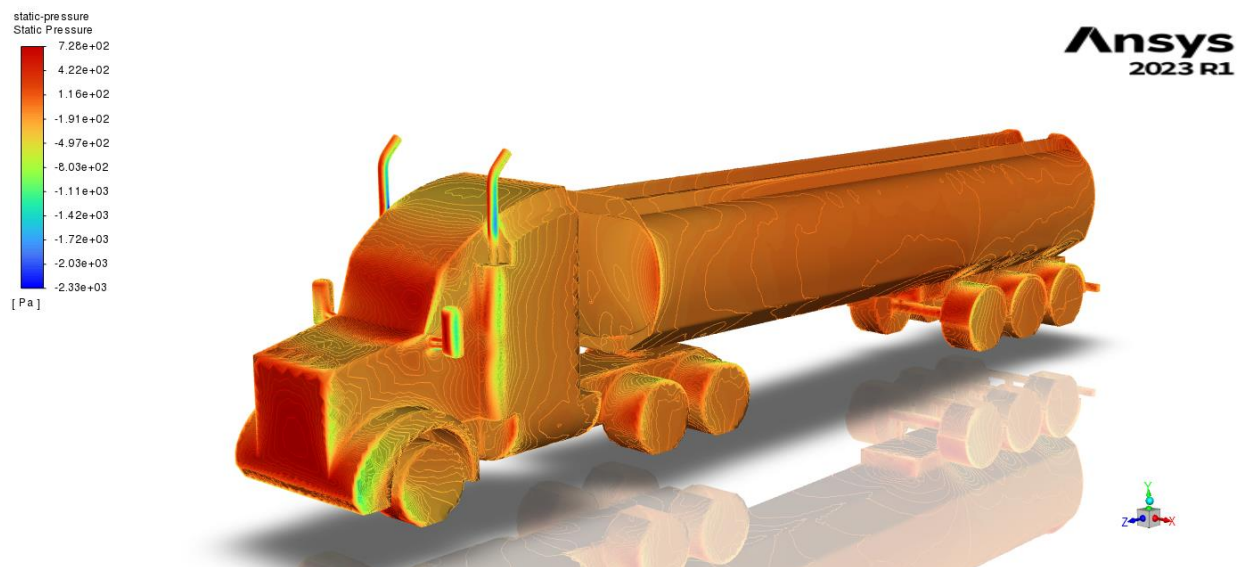


Figure 5.3-82: Static Pressure on the Winward Side of Baseline Tanker 15-degree crosswind angle

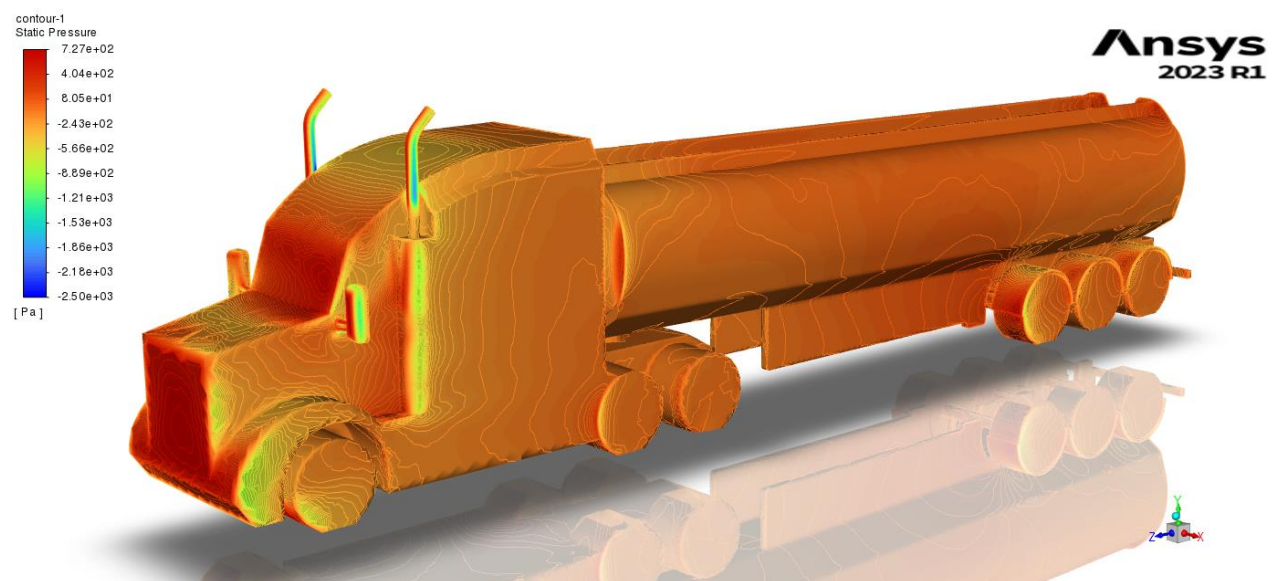


Figure 5.3-83: Static Pressure on the Winward Side of Aerodynamic Tanker 15-degree crosswind angle

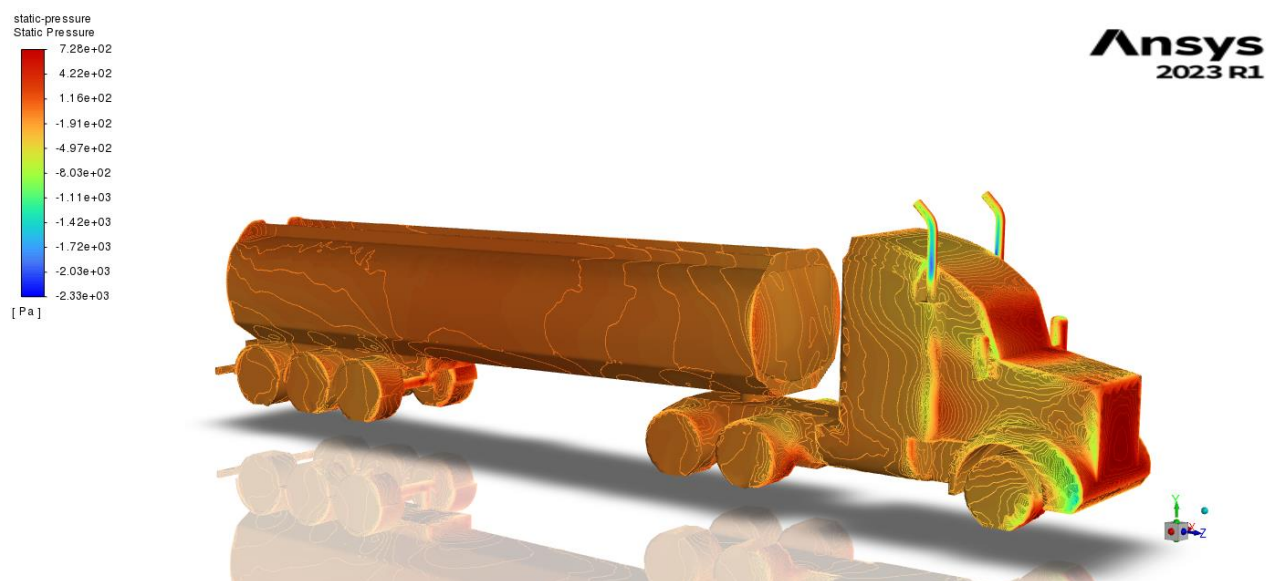


Figure 5.3-84: Static Pressure on the Leeward Side of Baseline Tanker 15-degree crosswind angle

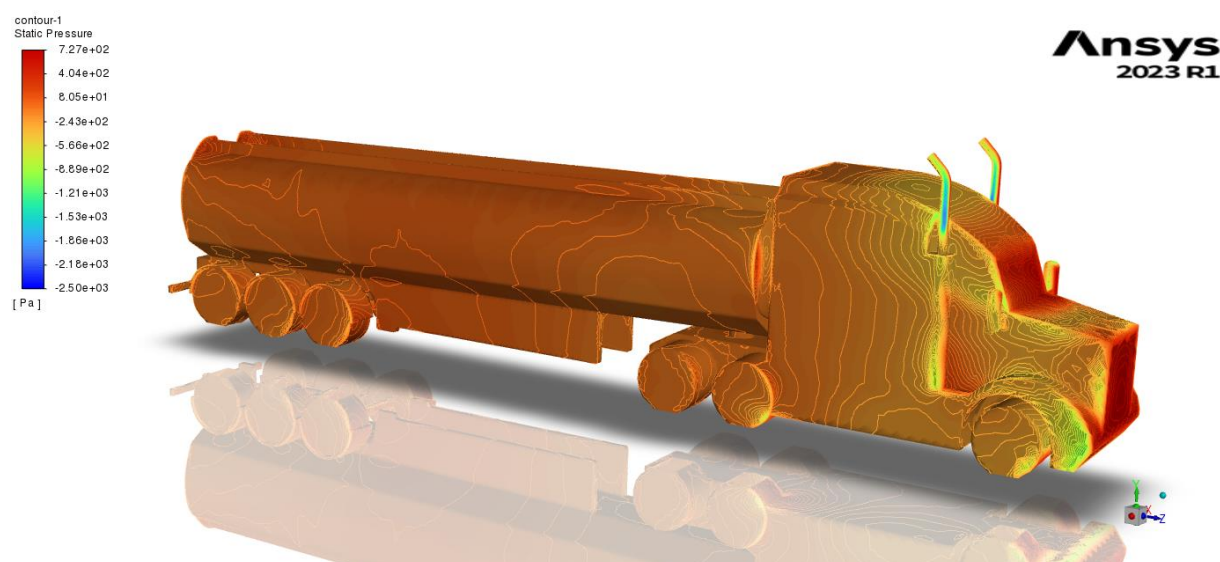


Figure 5.3-85: Static Pressure on the Leeward Side of Aerodynamic Tanker 15-degree crosswind angle

b) Total Pressure Distribution on both tankers 15-degree crosswind angle

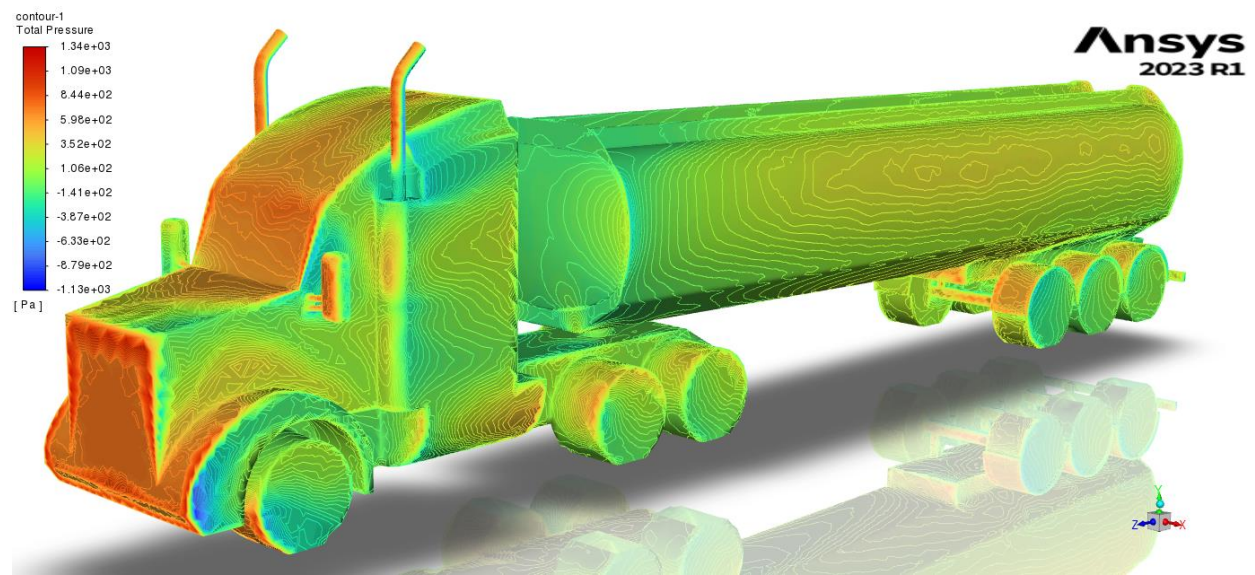


Figure 5.3-86: Total Pressure on the Windward Side of Baseline Tanker 15-degree crosswind angle

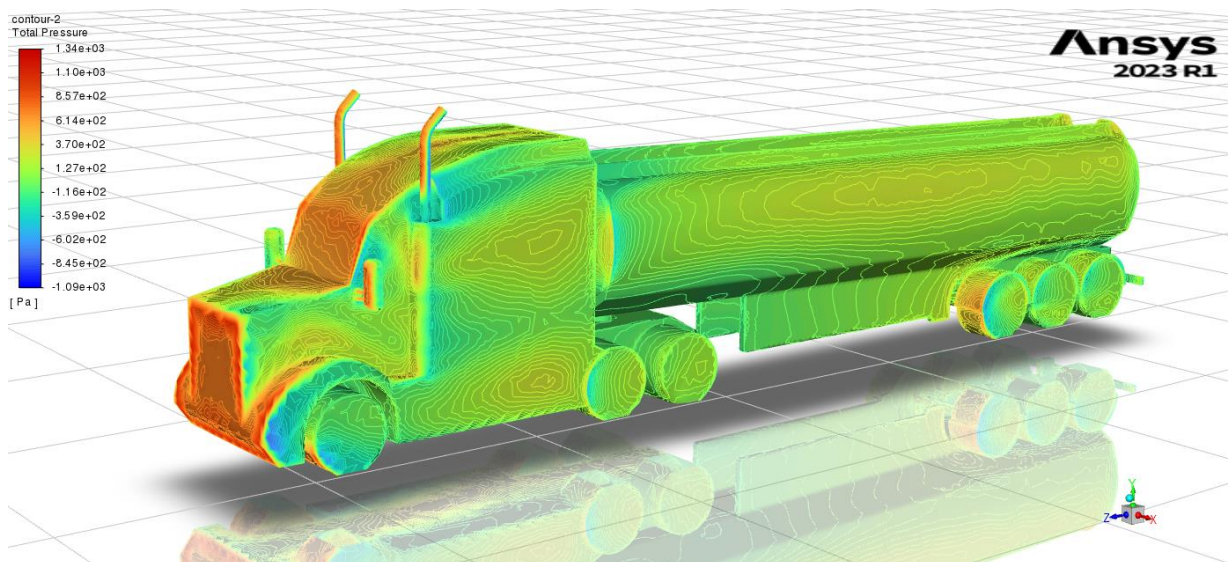


Figure 5.3-87: Total Pressure on the Windward Side of Aerodynamic Tanker 15-degree crosswind angle



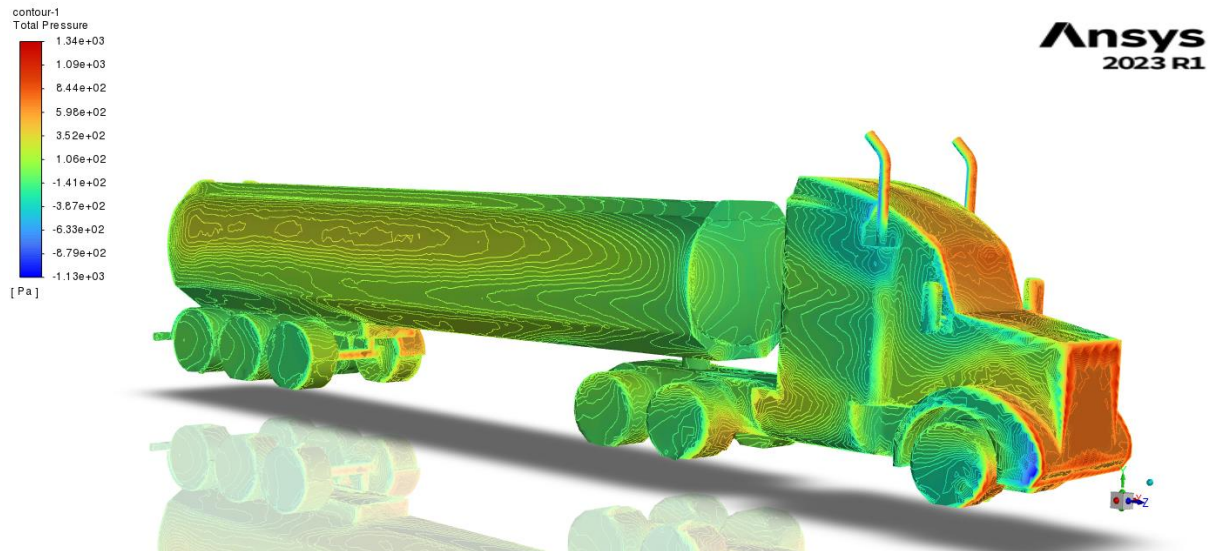


Figure 5.3-88: Total Pressure on the Leeward Side of Baseline Tanker 15-degree crosswind angle

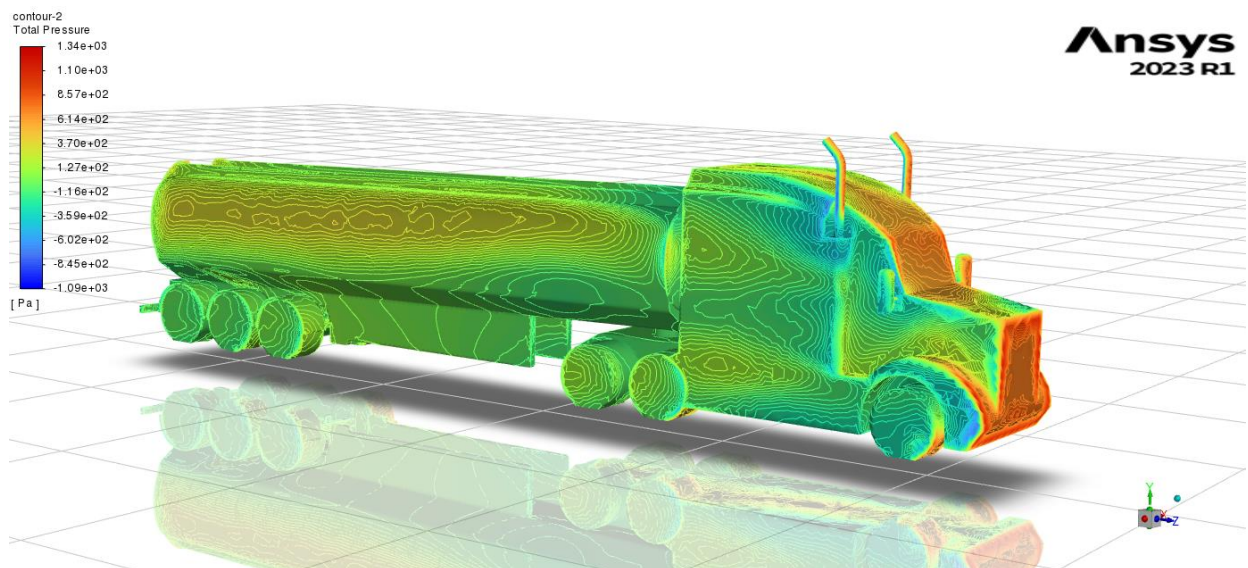


Figure 5.3-89: Total Pressure on the Leeward Side of Aerodynamic Tanker 15-degree crosswind angle

c) Flow Pathlines of both Tankers 15-degree crosswind angle

❖ Overview of Flow Pathlines

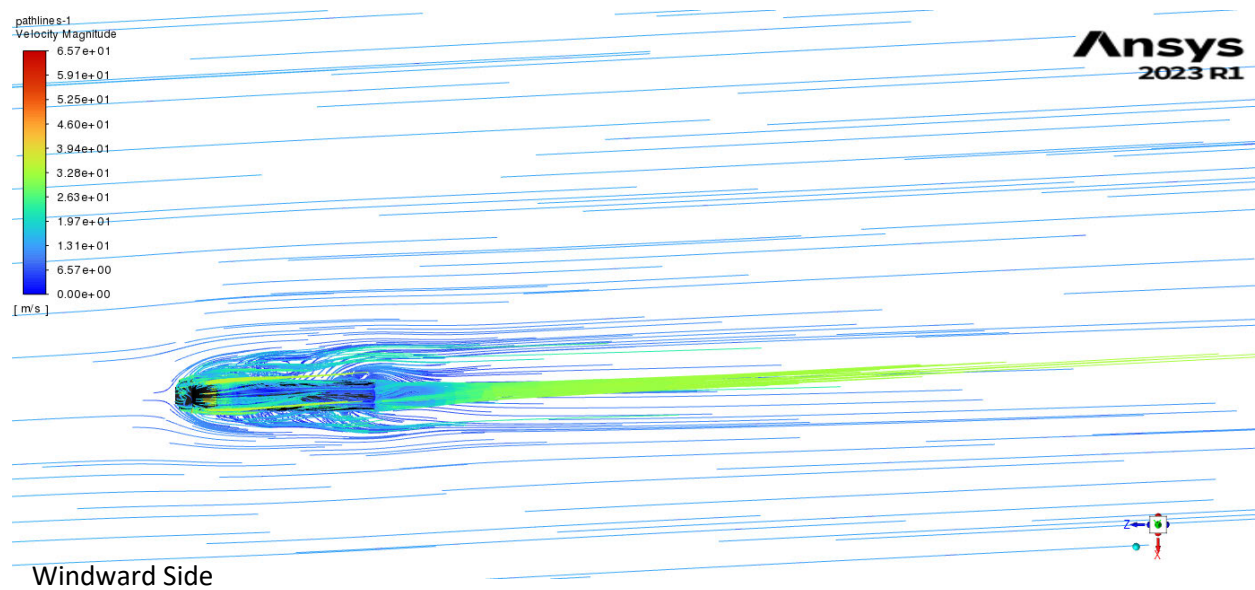


Figure 5.3-90: Flow Around Baseline Tanker at 15-degree crosswind angle

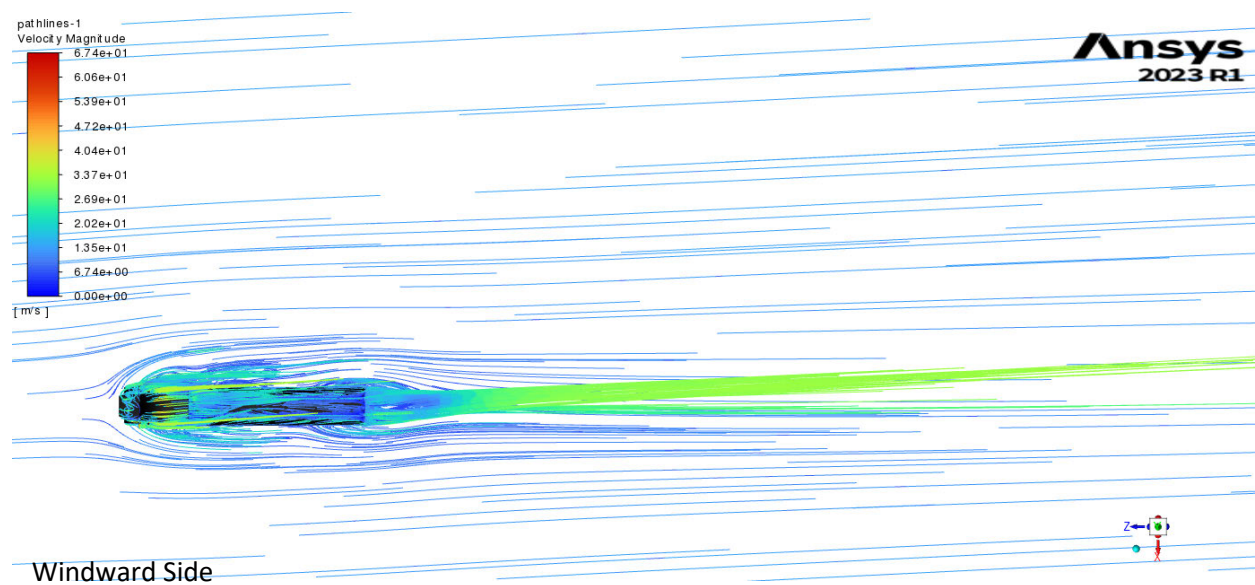


Figure 5.3-91: Flow Around Aerodynamic Tanker at 15-degree crosswind angle



## ❖ Top View of Flow Pathlines

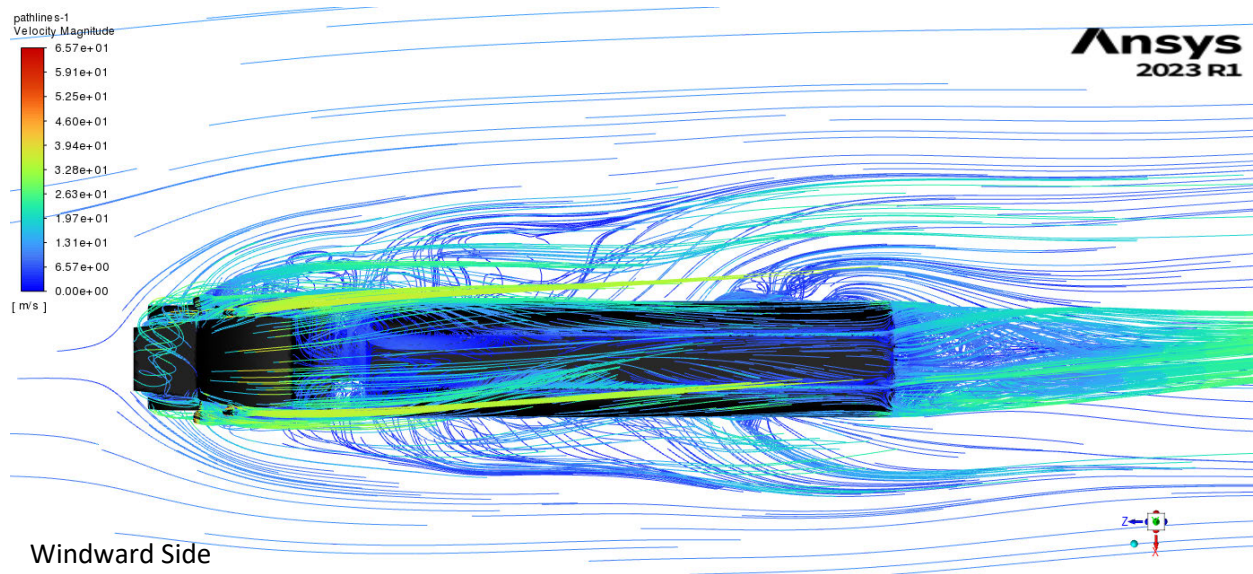


Figure 5.3-92: Flow Around Baseline Tanker at 15-degree crosswind angle – Top View

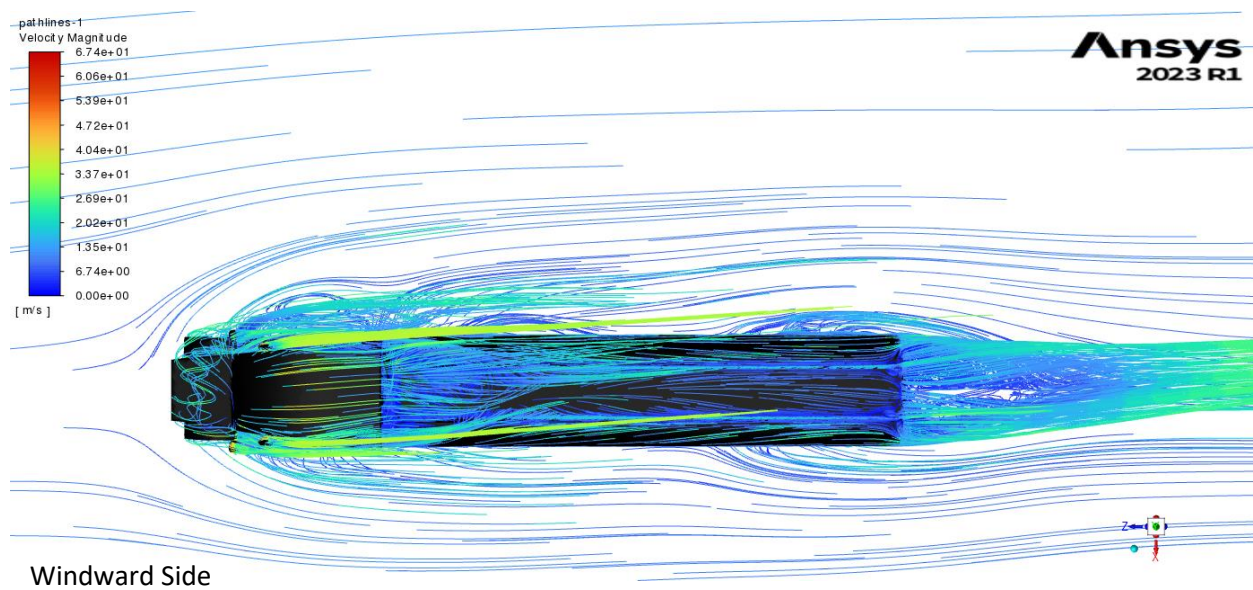


Figure 5.3-93: Flow Around Aerodynamic Tanker at 15-degree crosswind angle – Top View

## ❖ Underside View of Flow Pathlines

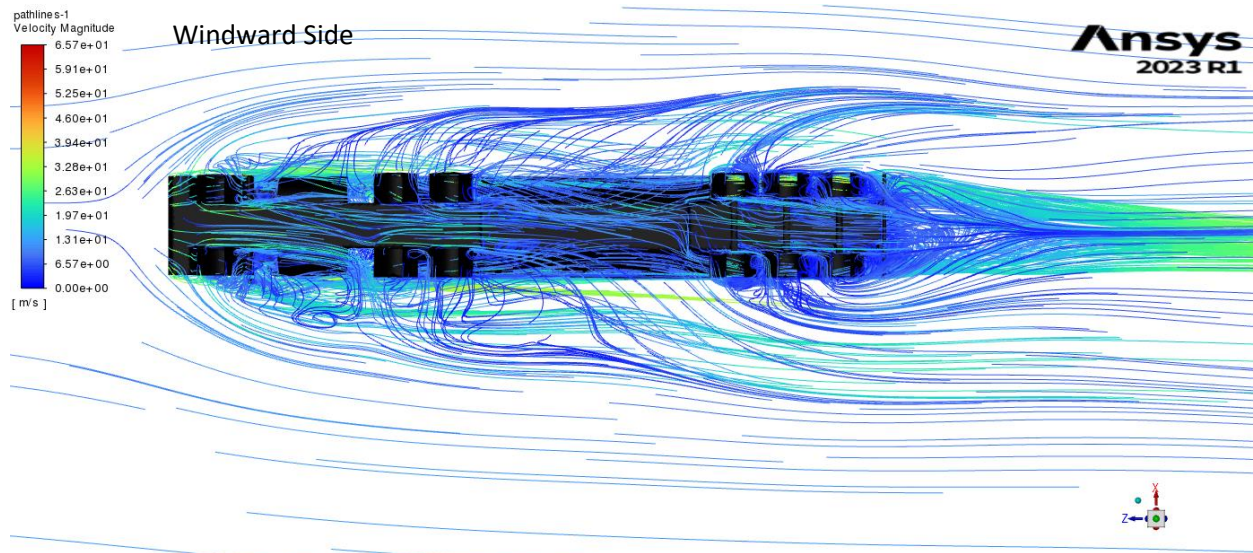


Figure 5.3-94: Flow Around Baseline Tanker at 15-degree crosswind angle – Underside View

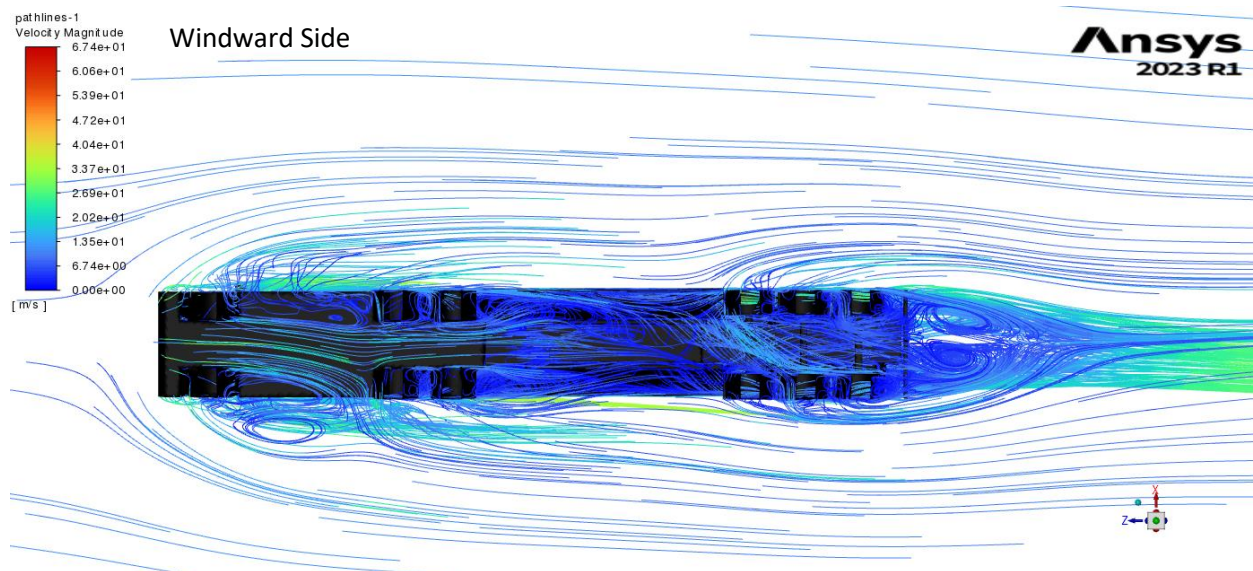


Figure 5.3-95: Flow Around Aerodynamic Tanker at 15-degree crosswind angle – Underside View



## ❖ Elevation View of Flow Pathlines

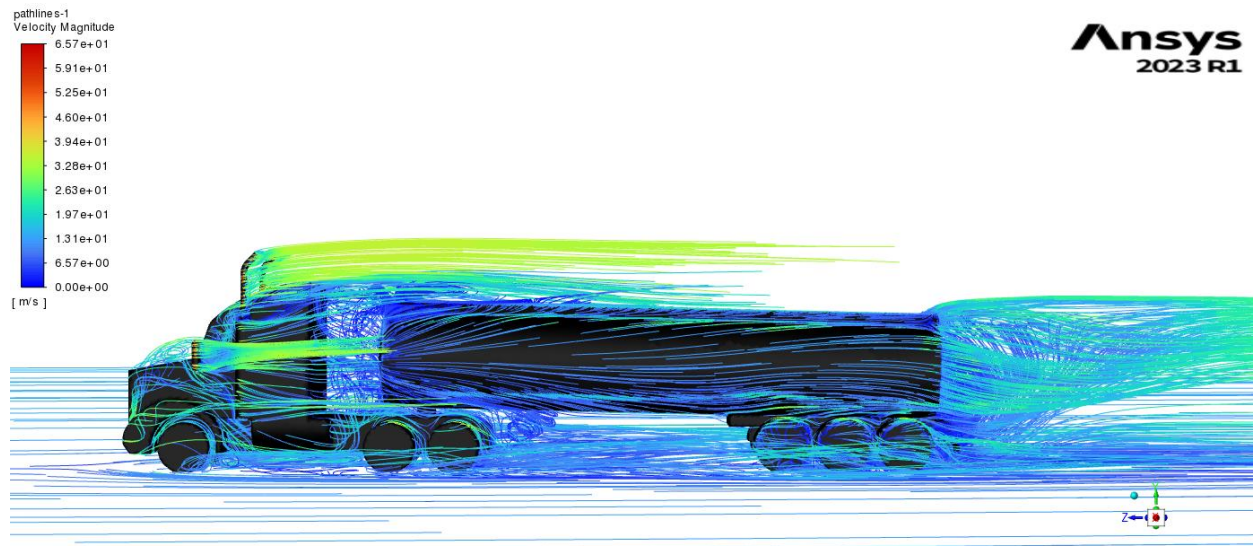


Figure 5.3-96: Elevation View of Flow Around Baseline Tanker at 15-degree crosswind angle - Winward Side

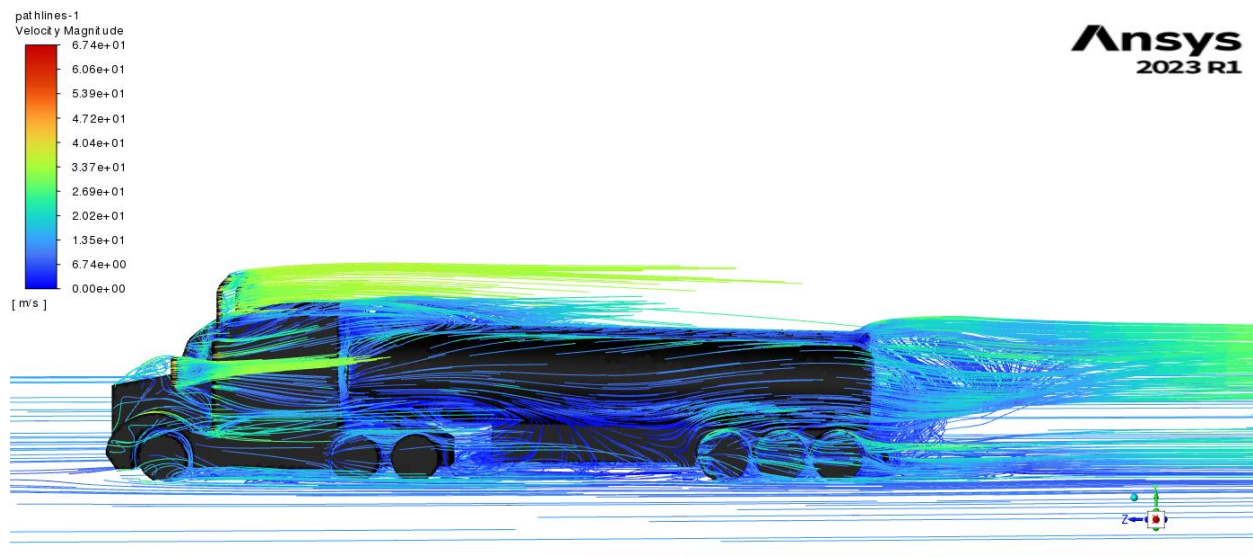


Figure 5.3-97: Elevation View of Flow Around Aerodynamic Tanker at 15-degree crosswind angle - Winward Side

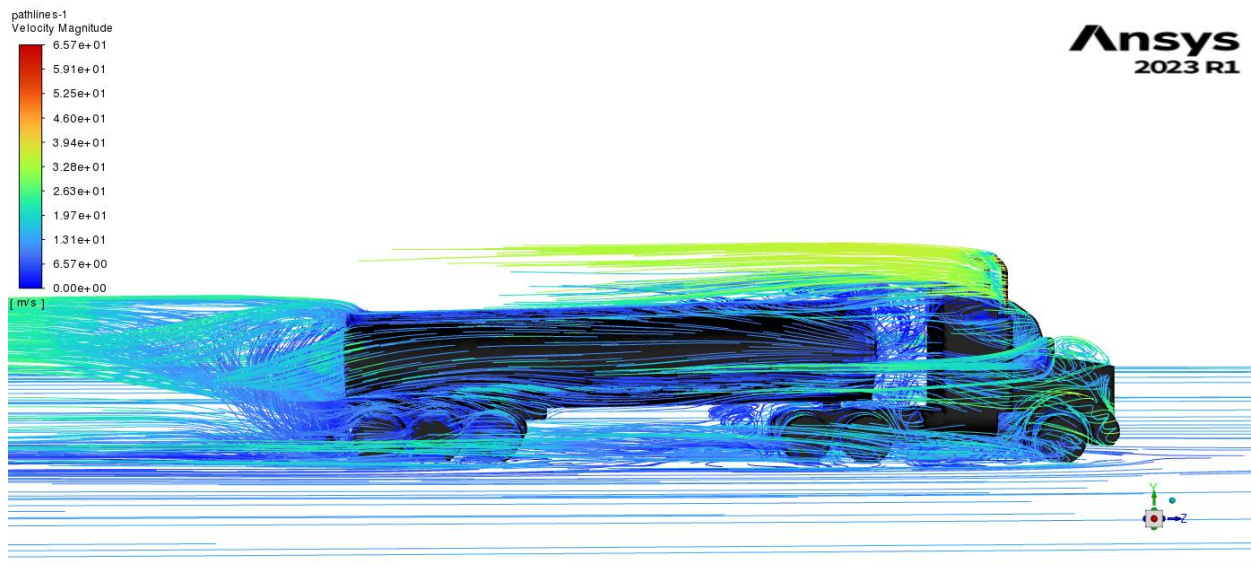


Figure 5.3-98: Elevation View of Flow Around Baseline Tanker at 15-degree crosswind angle - Leeward Side

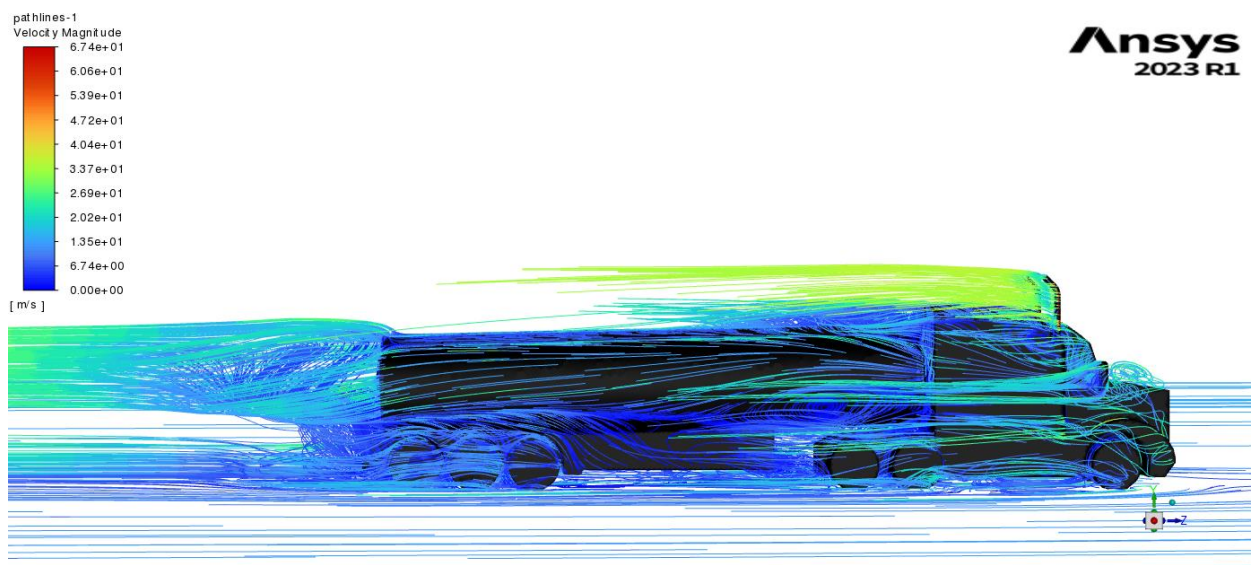


Figure 5.3-99: Elevation View of Flow Around Aerodynamic Tanker at 15-degree crosswind angle - Leeward Side



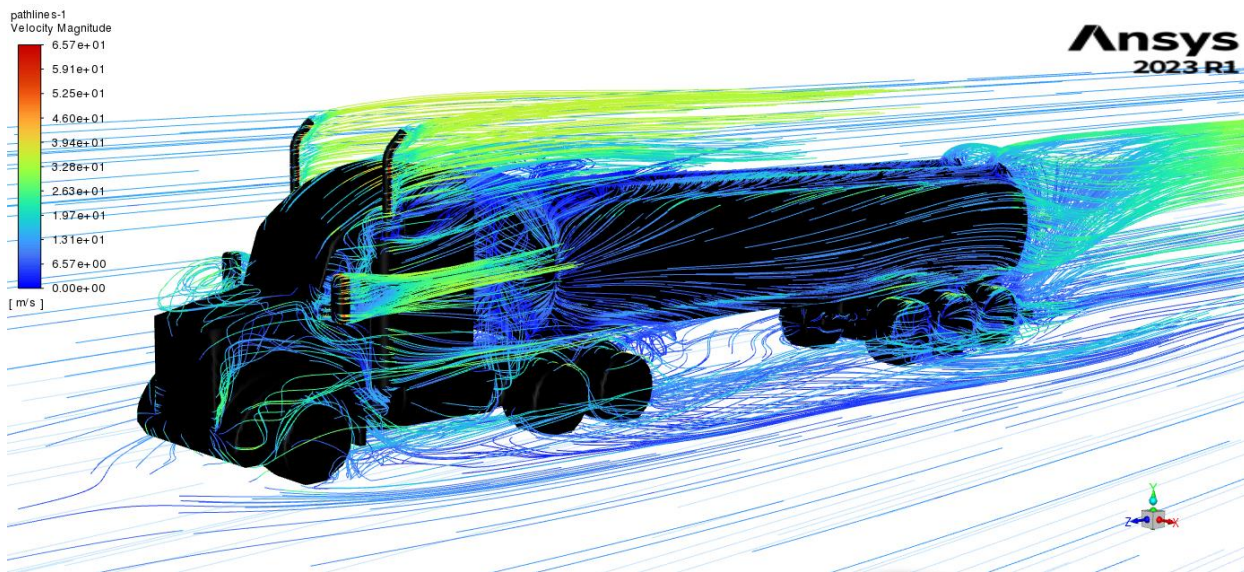
❖ Isometric View of Flow Pathlines

Figure 5.3-100: Isometric View of Flow Around Baseline Tanker at 15-degree crosswind angle - Windward Side

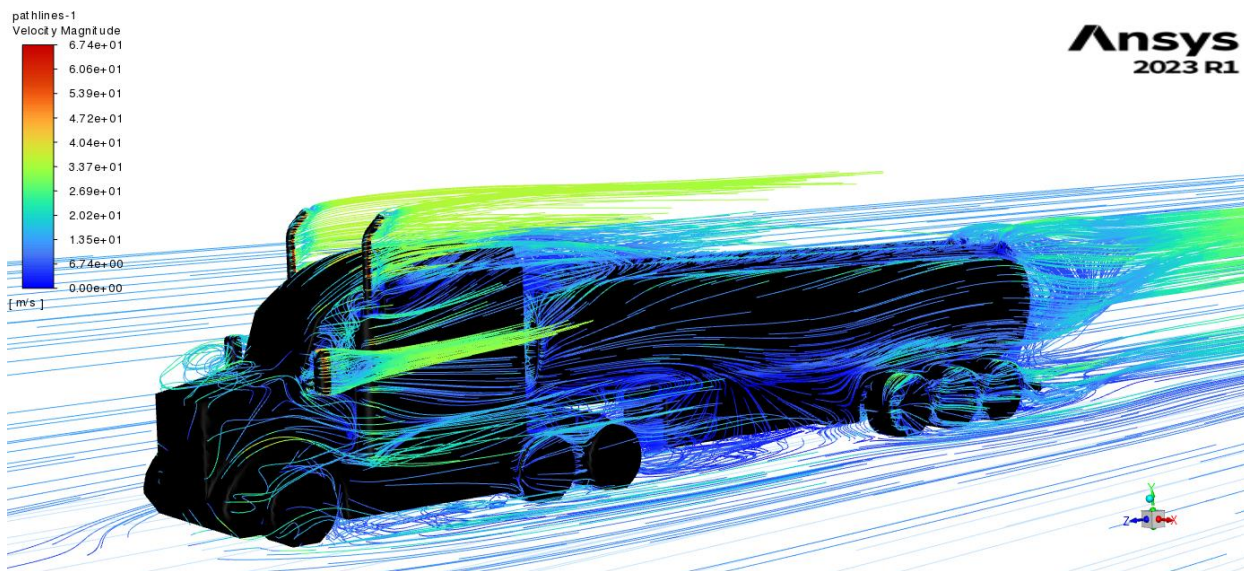


Figure 5.3-101: Isometric View of Flow Around Aerodynamic Tanker at 15-degree crosswind angle - Windward Side

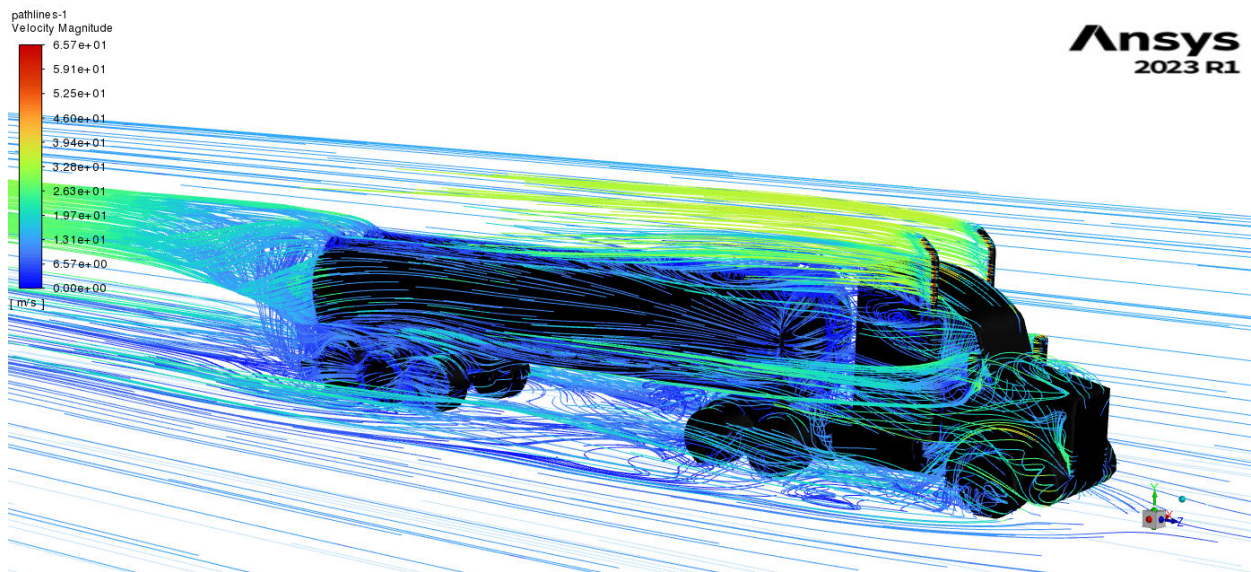


Figure 5.3-102: Isometric View of Flow Around Baseline Tanker at 15-degree crosswind angle - Leeward Side

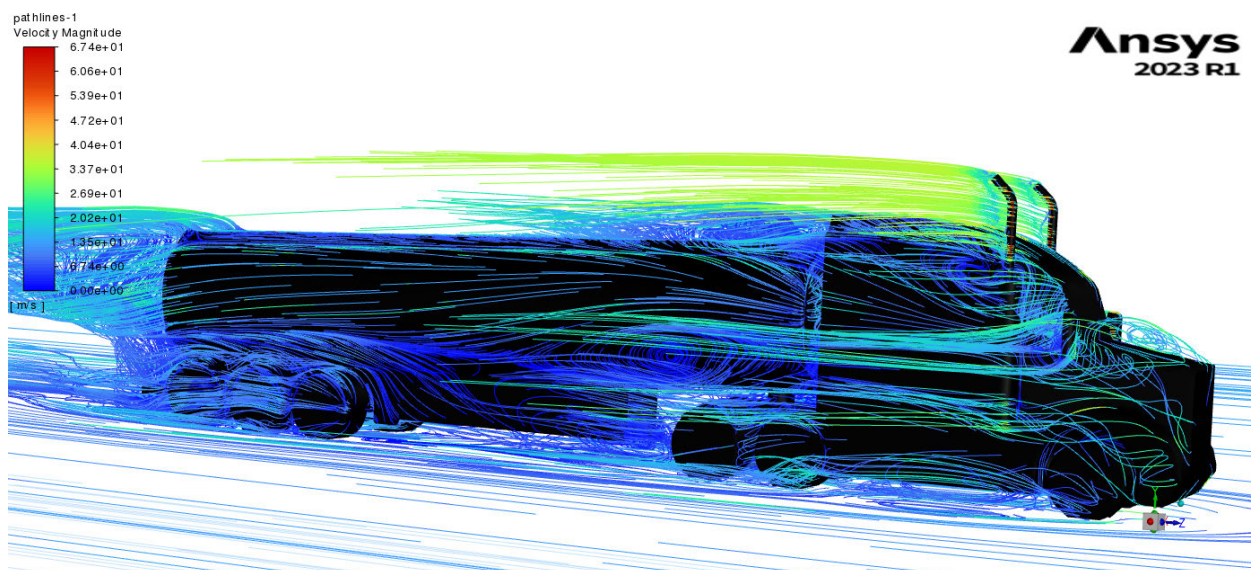


Figure 5.3-103: Isometric View of Flow Around Aerodynamic Tanker at 15-degree crosswind angle - Leeward Side

#### d) Contours and Pathlines Comparison Discussion

As depicted in Figure 5.3-82 to Figure 5.3-89, the installation of side skirts on both the tractor and the semitrailer, along with a gap fairing between the tractor and trailer, results in a reduction of both static and total pressure on the rear wheel group of the tractor and the trailer's wheels. Furthermore, the airflow around the aerodynamic tanker is noticeably less turbulent when compared to the baseline tanker (Figure 5.3-90 to Figure 5.3-103), leading to a decrease in the axial drag coefficient for the aerodynamic model.



Additionally, the airflow around the aerodynamic tanker exhibits less separation than the baseline model, reducing lift force and pitch moment. It contributes to more excellent stability and predictability when controlling the aerodynamic tanker, as opposed to the baseline tanker.

However, it's important to note that the increased side area of the aerodynamic tanker does raise the total pressure on the semitrailer. It, in turn, leads to an increase in lateral drag and rotational and rollover moments about the kingpin axis of the trailer. Moreover, the airflow beneath the aerodynamic trailer, particularly between the trailer side skirts and the rear axle group, displays higher turbulence and distortion along the trailer's length (Figure 5.3-94 and Figure 5.3-95). Additionally, the extensive flow separation at the junctions of the trailer side skirts and the front axle of the trailer and rear axle of the tractor (Figure 5.3-101, Figure 5.3-103 and Appendix H.4) significantly elevates the rotational moment coefficient of the trailer at 15 and 30-degree wind angles, especially at 15-degree by approximately 143%. These increases make vehicles unstable and more challenging to control.

Addressing this flow separation area is crucial to mitigate the impact of crosswinds on the performance of the semitrailer tanker.

#### 5.4: Determination of the likelihood of sideslip, rotation, or rollover accidents

Based on the simulation results presented in Table 5.3-16 and the calculations outlined in Sections 3.5 and 3.6, with an average crosswind speed of 6.5m/s and a vehicle travelling speed of 27.8 m/s (100 km/h), it is improbable that the aerodynamic tanker will experience sideslip, rotation, or rollover accidents. However, it is crucial to note that the increases observed in lateral drag force and rollover moments may warrant further investigation, as these factors could compromise the tanker's stability under crosswind conditions. Additionally, the inconsistent change in lift force and the substantial rise in the rotational moment may significantly impact the vehicle's stability and safety.

#### 5.5 Pre-Optimisation Study

Table 5.3-16 shows that crosswind angles of 15 degrees significantly impact the vehicle's aerodynamic behaviour. Specifically, the lift coefficient experiences a 59% reduction at this wind angle, while the rotational moment coefficient increases by 143%. These findings highlight the need for an in-depth investigation into the performance of aerodynamic devices compared to the baseline model at specific 15-degree crosswind angles. Such an investigation is crucial for identifying the areas most affected by crosswinds, which, in turn, will allow us to optimize these devices effectively, thereby enhancing vehicle stability, safety, and overall efficiency.

##### 5.5.1 Investigation of Aerodynamic Devices

As emphasized in section 5.3.2.2 (d), the area most heavily impacted by crosswinds in terms of aerodynamic devices is the side skirts of the trailer. Here, extensive flow separation at the

junctions of these side skirts results in a significant increase in rotational moment, approximately 143%. This imbalance makes it considerably more challenging to control the vehicle (refer to Figure 5.5.1-104 and Figure 5.5.1-105).

The flow separation occurs due to the step-in design of the side skirts toward the centre of the tanker, which extends beyond the outer edges of the tractor and trailer wheels. This design is primarily implemented for cost-efficiency and to ensure access to the outlet pipes (as shown in Figure 5.5.1-106). The step-in design increases turbulence in this area, thereby contributing to the heightened rotational moment coefficient of the semitrailer around the kingpin axis.

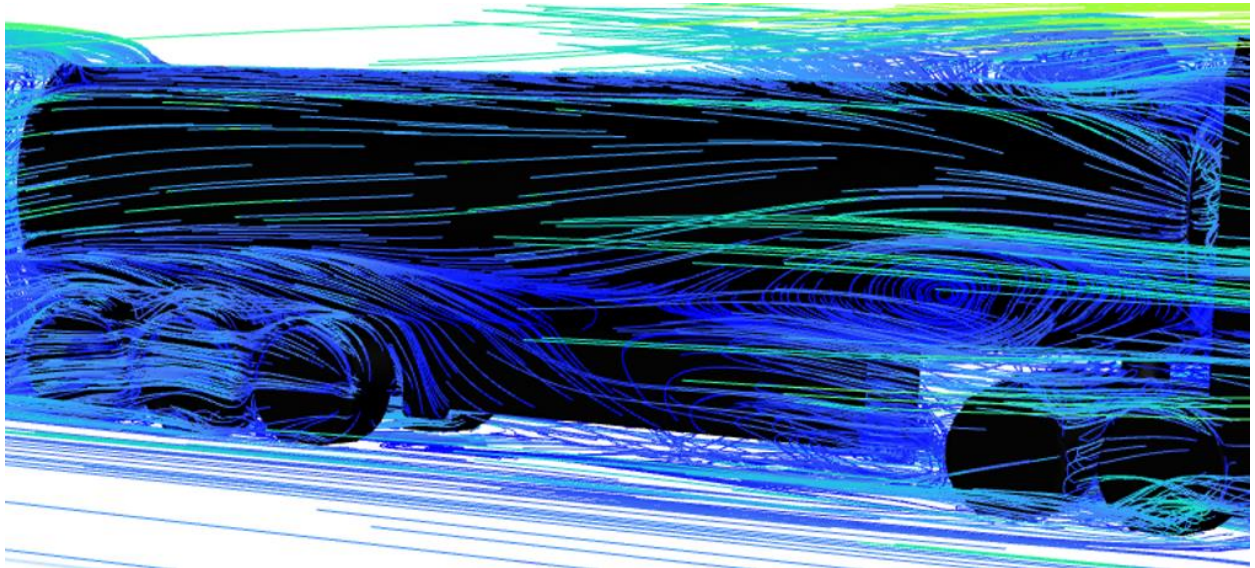


*Figure 5.5.1-104: Flow at Leeward Side of Aerodynamic Tanker*

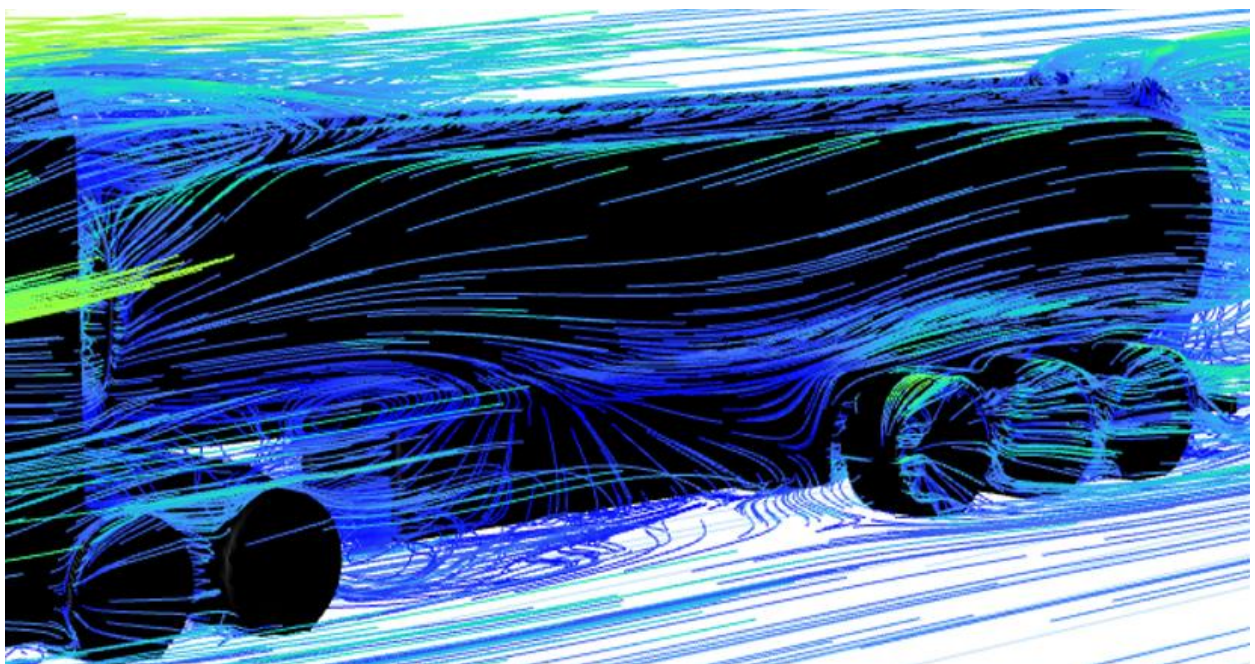


*Figure 5.5.1-105: Flow at Windward Side of Aerodynamic Tanker*

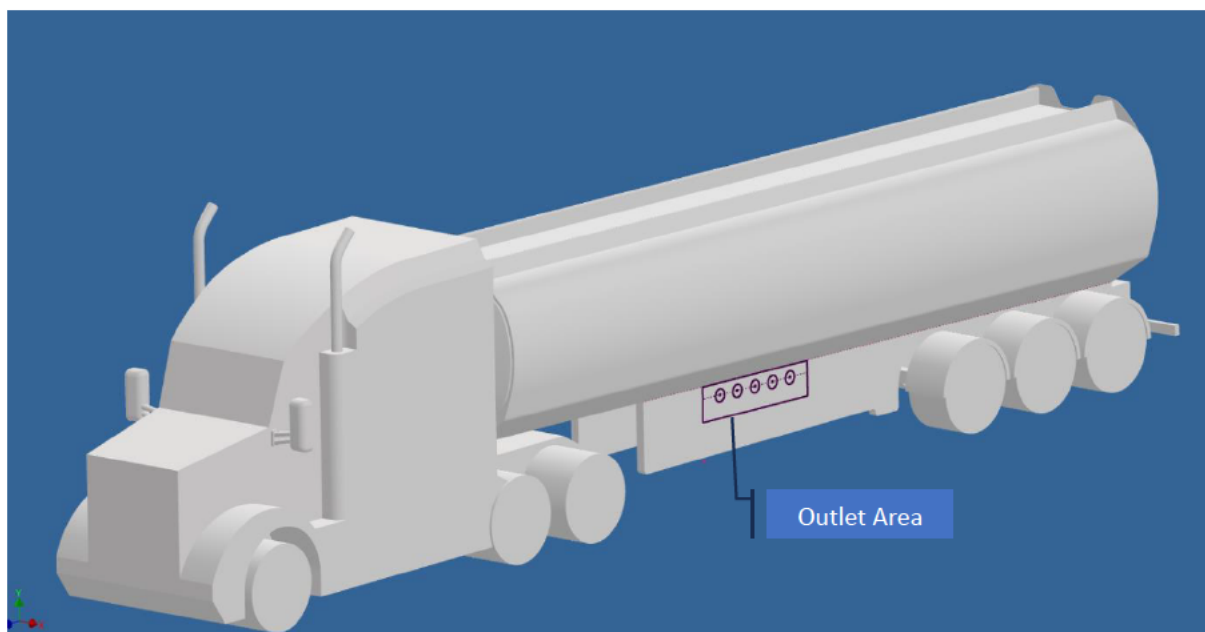


Figure 5.5.1-106: Aerodynamic Tanker

## 5.5.2 Optimisation of Aerodynamic Devices

### a) Proposed Modification to Trailer Side Skirts

To mitigate the rotational moment coefficient of the aerodynamic tanker under crosswind conditions at 15 and 30 degrees, it is imperative to address turbulence and flow separation issues occurring along the side skirts of the trailer. Complying with regulations such as Australian Standards AS2809.1 to AS2809.6, Australian Design Rules (ADRs), and Performance-Based Standards (PBS) place constraints on potential modifications. However, the most effective solution involves implementing box-shaped side skirts and repositioning them to align with the outer edges of the trailer wheels. This adjustment significantly improves flow dynamics along the side skirts, resulting in smoother airflow, reduced flow separation, and decreased turbulence.

These improvements maintain the original dimensions of the aerodynamic tanker, with the sole modification being the extension of the trailer's side skirts outward to match the outer wheel edges while adopting a box shape. These side skirt boxes accommodate various tanker components, including outlet pipes, safety cones, tire carriers, pump systems, and more (as illustrated in Figure 5.5.2-107). Given that the enhanced side skirts retain the original dimensions of the previous aerodynamic tanker but are extended to the trailer's wheel edges, they remain compliant with ADRs and PBS regulations.

Simulation results for the new aerodynamic tanker, tested under various crosswind angles, are presented in Table 5.5.2-17, allowing for a comparison with the baseline and original aerodynamic tankers.



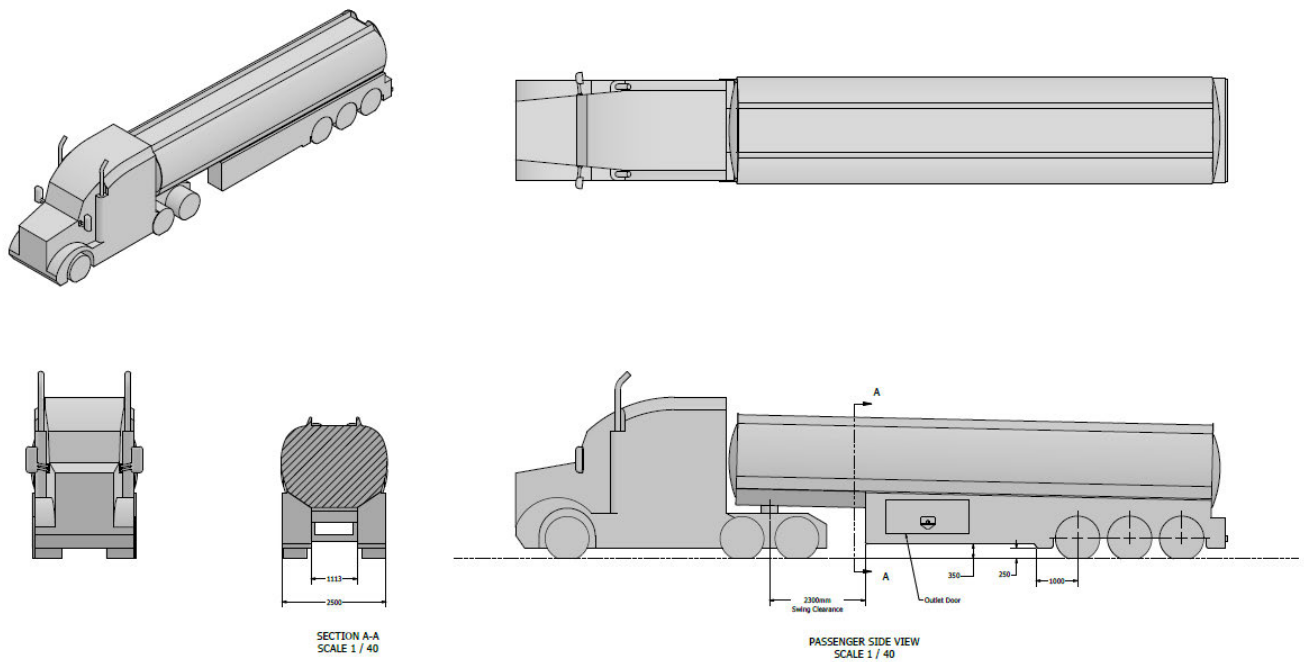


Figure 5.5.2-107: Detail of Side Skirt Improvement

Table 5.5.2-17: Simulation Results of Crosswind for Baseline and Improved Aerodynamic Tankers

Wind Angle	Velocity <b>V<sub>z</sub></b> (m/s)	Velocity <b>V<sub>x</sub></b> (m/s)	Resulant Velocity <b>V<sub>R</sub></b> (m/s)	Axial Drag Forces: <b>F<sub>z</sub></b> (N)									
				Baseline Model	Modified Aerodynamic Model	Baseline Axial Drag Coefficient <b>C<sub>B,Z</sub></b>	Aero Axial Drag Coefficient <b>C<sub>A,Z</sub></b>	Percentage Change in Drag Coefficient					
0	34.3	0	34.3	4,647	3,590	0.510	0.394	-23%					
Baseline Frontal Projected Area (m2)	12.65	Aero Frontal Projected Area (m2)	12.65	Air Density (kg/m3)	1.225	Length of Vehicle (m)	17.1	Air Dynamic Viscosity (kg/m.s)	1.79E-05	Baseline Side Arear (m2)	64.1	Aero Side Arear (m2)	69.2
Wind Angle	Velocity <b>V<sub>z</sub></b> (m/s)	Velocity <b>V<sub>x</sub></b> (m/s)	Resulant Velocity <b>V<sub>R</sub></b> (m/s)	Axial Drag Forces: <b>F<sub>z</sub></b> (N)					Lateral Drag Forces: <b>F<sub>x</sub></b> (N)				
				Baseline Model	Modified Aerodynamic Model	Baseline Axial Drag Coefficient <b>C<sub>B,Z</sub></b>	Aero Axial Drag Coefficient <b>C<sub>A,Z</sub></b>	Percentage Change in Drag Coefficient	Baseline Model	Modified Aerodynamic Model	Baseline Lateral Drag Coefficient <b>C<sub>B,X</sub></b>	Aero Lateral Drag Coefficient <b>C<sub>A,X</sub></b>	Percentage Change in Drag Coefficient
15	34.1	1.7	34.1	5,115	3,955	0.567	0.438	-22.7%	1,273	1,639	0.141	0.182	28.8%
30	33.4	3.3	33.6	5,607	4,072	0.642	0.466	-27.4%	2,529	3,155	0.289	0.361	24.8%
45	32.4	4.6	32.7	5,625	4,280	0.678	0.516	-23.9%	3,507	4,280	0.423	0.516	22.0%
60	31.1	5.6	31.6	5,491	4,325	0.712	0.561	-21.2%	4,059	5,028	0.526	0.652	23.9%
75	29.5	6.3	30.1	5,279	4,151	0.750	0.590	-21.4%	4,353	5,411	0.618	0.769	24.3%
90	27.8	6.5	28.5	4,854	3,816	0.769	0.604	-21.4%	4,290	5,279	0.679	0.836	23.1%
							Average	-23.0%				Average	24.5%

Wind Angle	Velocity <b>V<sub>z</sub></b> (m/s)	Velocity <b>V<sub>x</sub></b> (m/s)	Resulant Velocity <b>V<sub>R</sub></b> (m/s)	Lift Forces: <b>F<sub>y</sub></b> (N)					Pitching Moment: <b>M<sub>x</sub></b> (N.m)						
				Baseline Model	Modified Aerodynamic Model	Baseline Lift Coefficient <b>C<sub>B,Y</sub></b>	Aero Lift Coefficient <b>C<sub>A,Y</sub></b>	Percentage Change in Lift Coefficient	Baseline Model	Modified Aerodynamic Model	Baseline Pitch Moment Coefficient <b>C<sub>B,PM</sub></b>	Aero Pitch Moment Coefficient <b>C<sub>A,PM</sub></b>	Percentage Change in Pitch Moment Coefficient		
15	34.1	1.7	34.1	1,602	301	0.178	0.033	-81.2%	11,518	13,950	0.075	0.090	21.1%		
30	33.4	3.3	33.6	2,179	637	0.249	0.073	-70.8%	9,602	12,506	0.064	0.084	30.2%		
45	32.4	4.6	32.7	2,236	1,482	0.270	0.179	-33.7%	7,949	7,846	0.056	0.055	-1.3%		
60	31.1	5.6	31.6	2,221	2,364	0.288	0.306	6.4%	5,517	4,881	0.042	0.037	-11.5%		
75	29.5	6.3	30.1	2,464	2,866	0.350	0.407	16.3%	2,456	2,258	0.020	0.019	-8.1%		
90	27.8	6.5	28.5	2,500	3,008	0.396	0.476	20.3%	727	571	0.007	0.005	-21.5%		
							Average	-23.77%						Average	1.5%

Wind Angle	Velocity <b>V<sub>z</sub></b> (m/s)	Velocity <b>V<sub>x</sub></b> (m/s)	Resulant Velocity <b>V<sub>R</sub></b> (m/s)	Rotational (Yawning) Moment: <b>M<sub>y</sub></b> (N.m)					Rollover Moment: <b>M<sub>z</sub></b> (N.m)						
				Baseline Model	Modified Aerodynamic Model	Baseline Rotational Moment Coefficient <b>C<sub>B,RM</sub></b>	Aero Rotational Moment Coefficient <b>C<sub>A,RM</sub></b>	Percentage Change in Rotational Moment Coefficient	Baseline Model	Modified Aerodynamic Model	Baseline Rollover Moment Coefficient <b>C<sub>B,ROM</sub></b>	Aero Rollover Moment Coefficient <b>C<sub>A,ROM</sub></b>	Percentage Change in Rollover Moment Coefficient		
15	34.1	1.7	34.1	563	10	0.004	0.000065	-98.2%	2,282	2,692	0.0148	0.017	18.0%		
30	33.4	3.3	33.6	3,079	2,436	0.021	0.016	-20.9%	4,440	5,123	0.0297	0.034	15.4%		
45	32.4	4.6	32.7	4,985	2,772	0.035	0.020	-44.4%	6,117	6,993	0.0431	0.049	14.3%		
60	31.1	5.6	31.6	5,491	3,319	0.042	0.025	-39.6%	7,083	8,267	0.0537	0.063	16.7%		
75	29.5	6.3	30.1	5,546	4,122	0.046	0.034	-25.7%	7,538	8,893	0.0626	0.074	18.0%		
90	27.8	6.5	28.5	5,140	3,958	0.048	0.037	-23.0%	7,395	8,677	0.0685	0.080	17.3%		
							Average	-42.0%						Average	16.6%

As demonstrated in Table 5.5.2-17, the enhancements made to the side skirts not only result in a significant reduction in the rotational moment coefficient across all crosswind angles, with the most notable improvements occurring at 15 and 30 degrees (from +143% and +22.6% to -98.2% and -20.9%, respectively), but also further reduce the axial drag coefficient at 0-degree wind angle (from -18% to -23%). Meanwhile, the axial, lateral, lift, pitch, and rollover moment coefficients experience only minor changes. These findings affirm that the new side skirts effectively reduce airflow separation and turbulence, contributing to enhanced vehicle stability and improved control under crosswind conditions.

#### *b) Analysing of Simulation Results*

To provide a comprehensive comparison between the original and improved aerodynamic tankers, the percentage changes in axial, lateral, lift, pitch moment, rotational moment, and rollover moment are compiled into Table 5.5.2-18 and represented the data in Figure 5.5.2-108 to Figure 5.5.2-113. These figures offer valuable insights into the differences between tanker configurations at various wind angles:

##### ❖ Axial Drag Coefficient:

The Aero Tanker consistently demonstrates a lower axial drag coefficient than the Baseline Tanker, with an average reduction of 22.5%.

In contrast, the Modified Aero Tanker also exhibits a lower axial drag coefficient than the Baseline Tanker, showing an average decrease of 23.0%.

##### ❖ Lateral Drag Coefficient:

The Aero Tanker consistently registers a higher lateral drag coefficient compared to the Baseline Tanker, with an average increase of 21.4%.

Similarly, the Modified Aero Tanker displays a higher lateral drag coefficient than the Baseline Tanker, with an average increase of 24.5%.

#### ❖ Lift Coefficient:

Both the Aero Tanker and Modified Aero Tanker show a reduction in lift coefficients when compared to the Baseline Tanker at wind angles below 45 degrees. However, they exhibit an increase at wind angles above 45 degrees, resulting in an average decrease of 14.5% and 23.8%, respectively.

#### ❖ Pitch Moment Coefficient:

The Aero Tanker demonstrates a significant reduction in the pitch moment coefficient compared to the Baseline Tanker across all wind angles, with an average decrease of 40.9%.

In contrast, the Modified Aero Tanker only exhibits a minor reduction in the pitch moment coefficient at 30, 45, and 90 degrees while showing increases at other wind angles when compared to the Baseline Tanker.

#### ❖ Rotational (Yawing) Moment Coefficient:

The Aero Tanker significantly increases the yawing moment coefficient at 15 and 30-degree wind angles. In contrast, the Modified Aero Tanker shows a steep decrease in the yawing moment coefficient at these angles when compared to the Baseline Tanker. Moreover, the Modified Aero Tanker consistently reduces this yawing moment coefficient compared to the fluctuating performance of the Aero Tanker.

#### ❖ Rollover Moment Coefficient:

The Aero Tanker exhibits a significantly higher rollover moment coefficient than the Baseline Tanker, with an average increase of 16.8%.

Similarly, the Modified Aero Tanker shows a higher rollover moment coefficient than the Baseline Tanker, with an average increase of 16.6%.

Generally, The Modified Aero Tanker produces slightly lower axial drag and rollover moment coefficients while significantly reducing lift and yawing moment coefficients. However, lateral drag and pitch moment coefficients increase from 21.4% and -40.9% to 24.5% and 1.5%, respectively.

Although the Modified Aero Tanker falls somewhere between the Baseline and Original Aero configurations and leans closer to the Original Aero Tanker in terms of performance, it excels in terms of yawing stability. This is attributed to the significant reduction in rotational moment at all crosswind angles, especially at 15 and 30 degrees, where the Original Aero Tanker increases this moment to 143.3% and 22.6%, respectively.

In conclusion, the Baseline Tanker performs better when considering lateral stability under crosswind conditions due to its lower lateral drag coefficients. However, if yawing stability is a critical concern, the Modified Aero Tanker is the superior choice due to its lower yawing moment coefficients. The choice between these models should be made with specific operational requirements and the trade-offs between lateral and yawing stability in mind.

Table 5.5.2-18: Comparison of Original Aerodynamic and Improved Aerodynamic Tankers

Wind Angle	Axial Drag Coefficient					Lateral Drag Coefficient				
	Baseline Tanker Axial Drag Coefficient $C_{B,Z}$	Aero Tanker Axial Drag Coefficient $C_{A,Z}$	Modified Aero Tanker Axial Drag Coefficient $C_{MA,Z}$	Difference Between Aero and Baseline Tankers	Difference Between Modified Aero and Baseline Tankers	Baseline Tanker Axial Drag Coefficient $C_{B,X}$	Aero Tanker Axial Drag Coefficient $C_{A,X}$	Modified Aero Tanker Axial Drag Coefficient $C_{MA,X}$	Difference Between Aero and Baseline Tankers	Difference Between Modified Aero and Baseline Tankers
15	0.567	0.453	0.438	-20.1%	-22.7%	0.141	0.172	0.182	21.8%	28.8%
30	0.642	0.477	0.466	-25.6%	-27.4%	0.289	0.347	0.361	19.8%	24.8%
45	0.678	0.514	0.516	-24.2%	-23.9%	0.423	0.510	0.516	20.6%	22.0%
60	0.712	0.563	0.561	-20.9%	-21.2%	0.526	0.642	0.652	22.0%	23.9%
75	0.750	0.584	0.590	-22.1%	-21.4%	0.618	0.755	0.769	22.1%	24.3%
90	0.769	0.601	0.604	-21.8%	-21.4%	0.679	0.831	0.836	22.4%	23.1%
			Average	-22.5%	-23.0%			Average	21.4%	24.5%
Wind Angle	Lift Coefficient					Pitch Moment Coefficient				
	Baseline Tanker Axial Drag Coefficient $C_{B,Y}$	Aero Tanker Axial Drag Coefficient $C_{A,Y}$	Modified Aero Tanker Axial Drag Coefficient $C_{MA,Y}$	Difference Between Aero and Baseline Tankers	Difference Between Modified Aero and Baseline Tankers	Baseline Tanker Axial Drag Coefficient $C_{B,PM}$	Aero Tanker Axial Drag Coefficient $C_{A,PM}$	Modified Aero Tanker Axial Drag Coefficient $C_{MA,PM}$	Difference Between Aero and Baseline Tankers	Difference Between Modified Aero and Baseline Tankers
15	0.178	0.073	0.033	-58.7%	-81.2%	0.075	0.070	0.090	-5.6%	21.1%
30	0.249	0.130	0.073	-47.9%	-70.8%	0.064	0.062	0.084	-3.8%	30.2%
45	0.270	0.210	0.179	-22.2%	-33.7%	0.056	0.039	0.055	-30.2%	-1.3%
60	0.288	0.311	0.306	8.1%	6.4%	0.042	0.018	0.037	-57.5%	-11.5%
75	0.350	0.395	0.407	12.7%	16.3%	0.020	0.004	0.019	-82.2%	-8.1%
90	0.396	0.480	0.476	21.2%	20.3%	0.007	0.002	0.005	-66.0%	-21.5%
			Average	-14.5%	-23.8%			Average	-40.9%	1.5%
Wind Angle	Rotational (Yawing) Moment Coefficient					Rollover Moment Coefficient				
	Baseline Tanker Axial Drag Coefficient $C_{B,RM}$	Aero Tanker Axial Drag Coefficient $C_{A,RM}$	Modified Aero Tanker Axial Drag Coefficient $C_{MA,RM}$	Difference Between Aero and Baseline Tankers	Difference Between Modified Aero and Baseline Tankers	Baseline Tanker Axial Drag Coefficient $C_{B,ROM}$	Aero Tanker Axial Drag Coefficient $C_{A,ROM}$	Modified Aero Tanker Axial Drag Coefficient $C_{MA,ROM}$	Difference Between Aero and Baseline Tankers	Difference Between Modified Aero and Baseline Tankers
15	0.004	0.009	0.000065	143.3%	-98.2%	0.015	0.017	0.017	17.1%	18.0%
30	0.021	0.025	0.016	22.6%	-20.9%	0.030	0.034	0.034	15.3%	15.4%
45	0.035	0.025	0.020	-28.2%	-44.4%	0.043	0.050	0.049	15.7%	14.3%
60	0.042	0.017	0.025	-59.2%	-39.6%	0.054	0.062	0.063	15.8%	16.7%
75	0.046	0.028	0.034	-38.7%	-25.7%	0.063	0.073	0.074	16.7%	18.0%
90	0.048	0.044	0.037	-7.0%	-23.0%	0.068	0.082	0.080	20.1%	17.3%
			Average	5.5%	-42.0%			Average	16.8%	16.6%

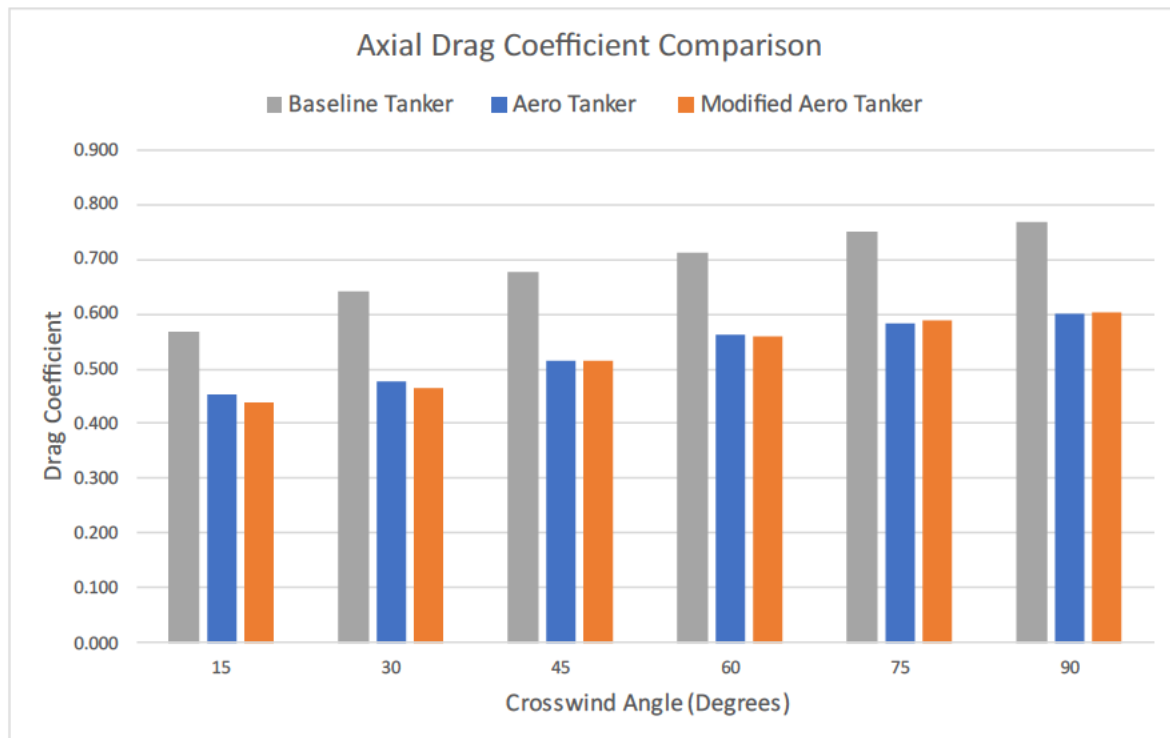


Figure 5.5.2-108: Comparison of Axial Drag Coefficient

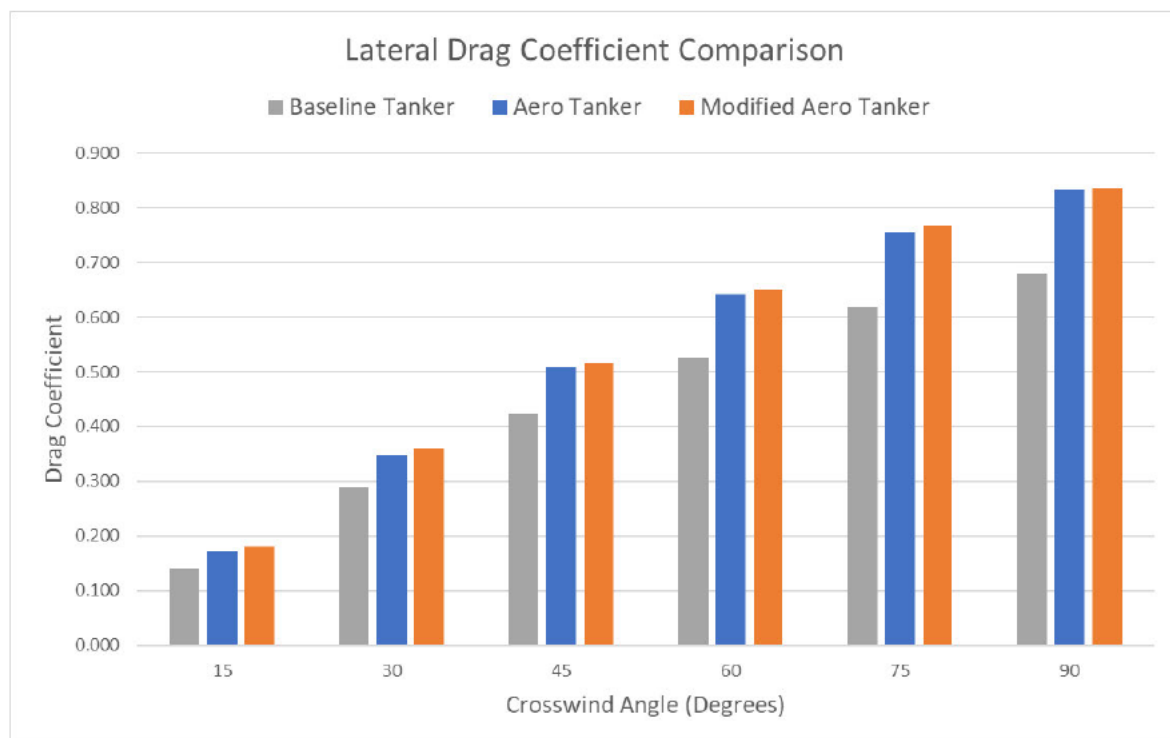


Figure 5.5.2-109: Comparison of Lateral Drag Coefficient



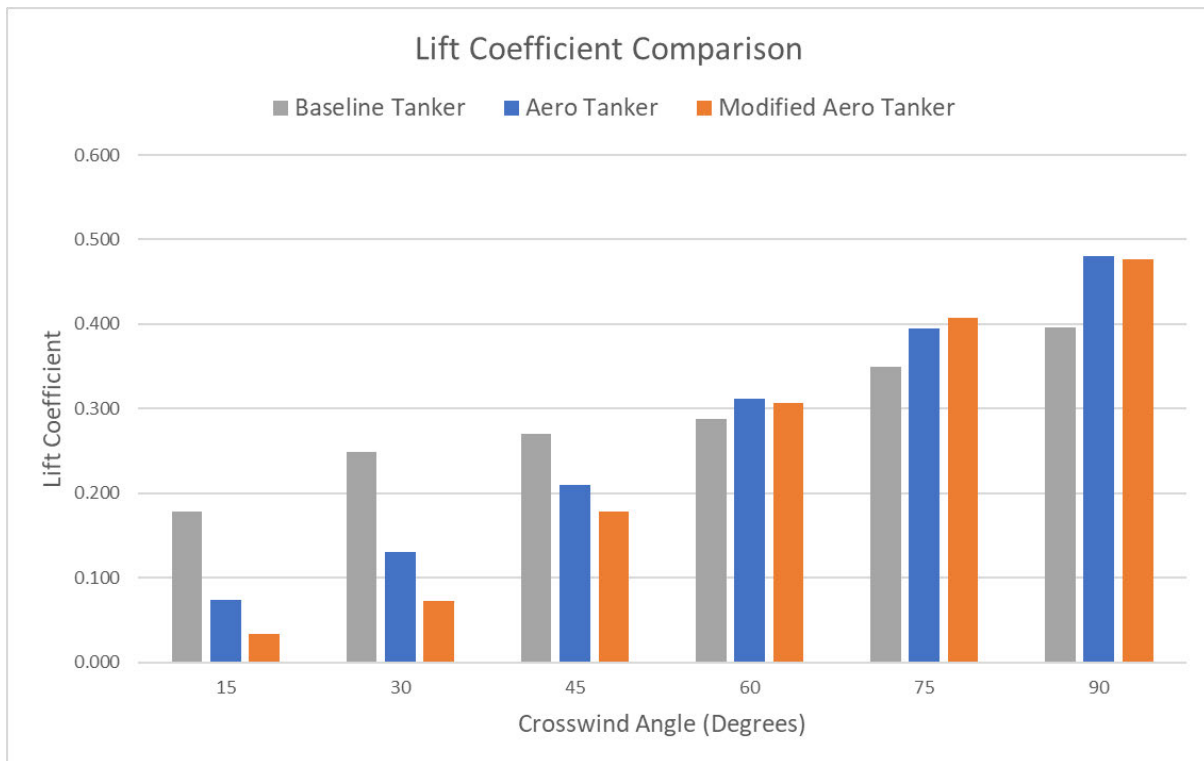


Figure 5.5.2-110: Comparison of Lift Coefficient

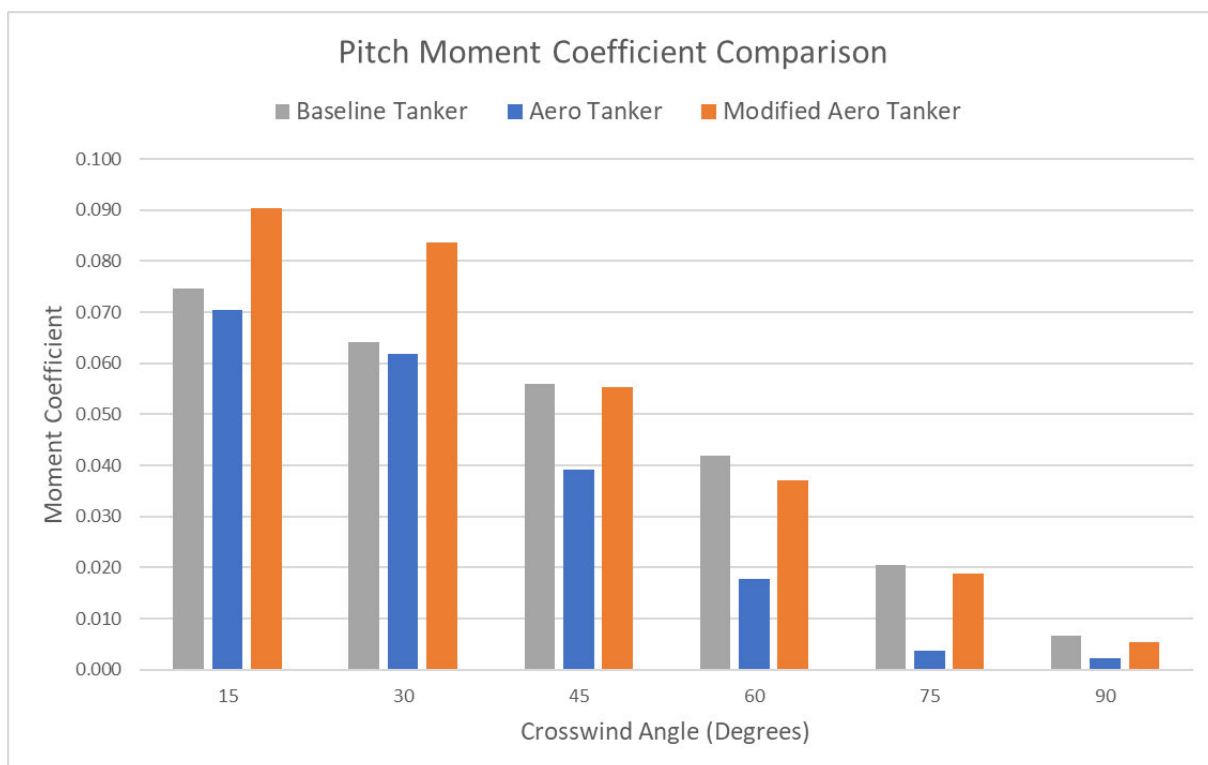


Figure 5.5.2-111: Comparison of Pitch Moment Coefficient



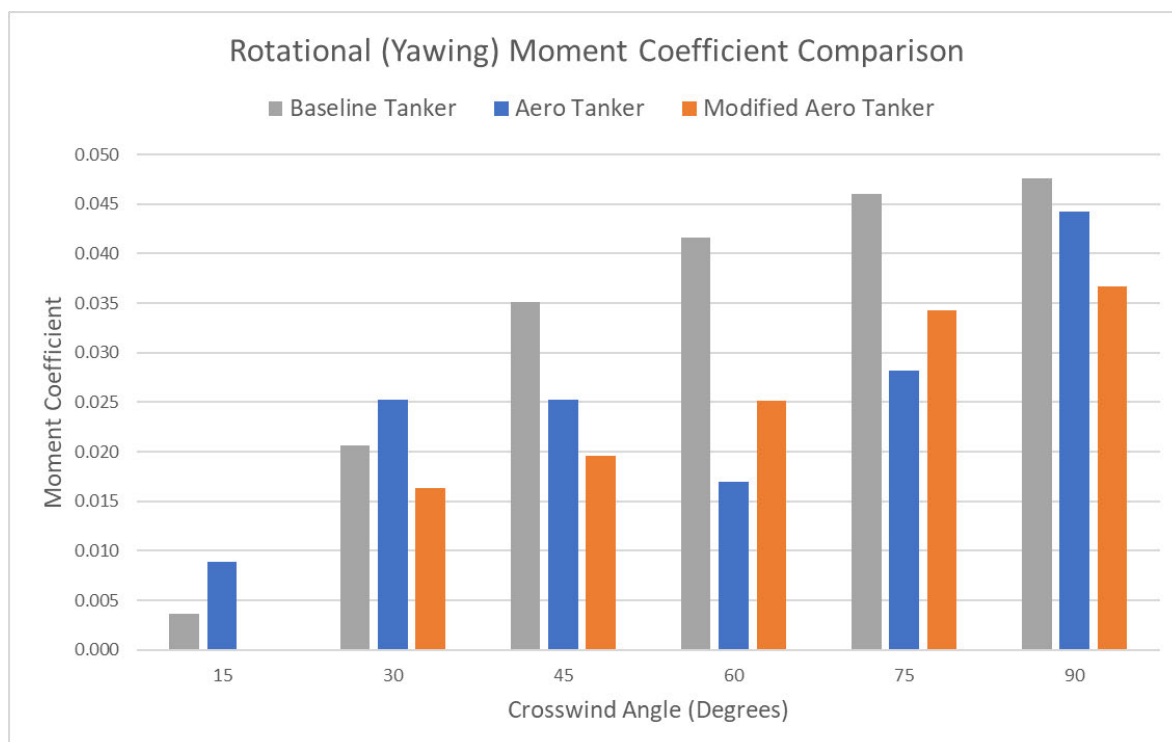


Figure 5.5.2-112: Comparison of Yawing Moment Coefficient

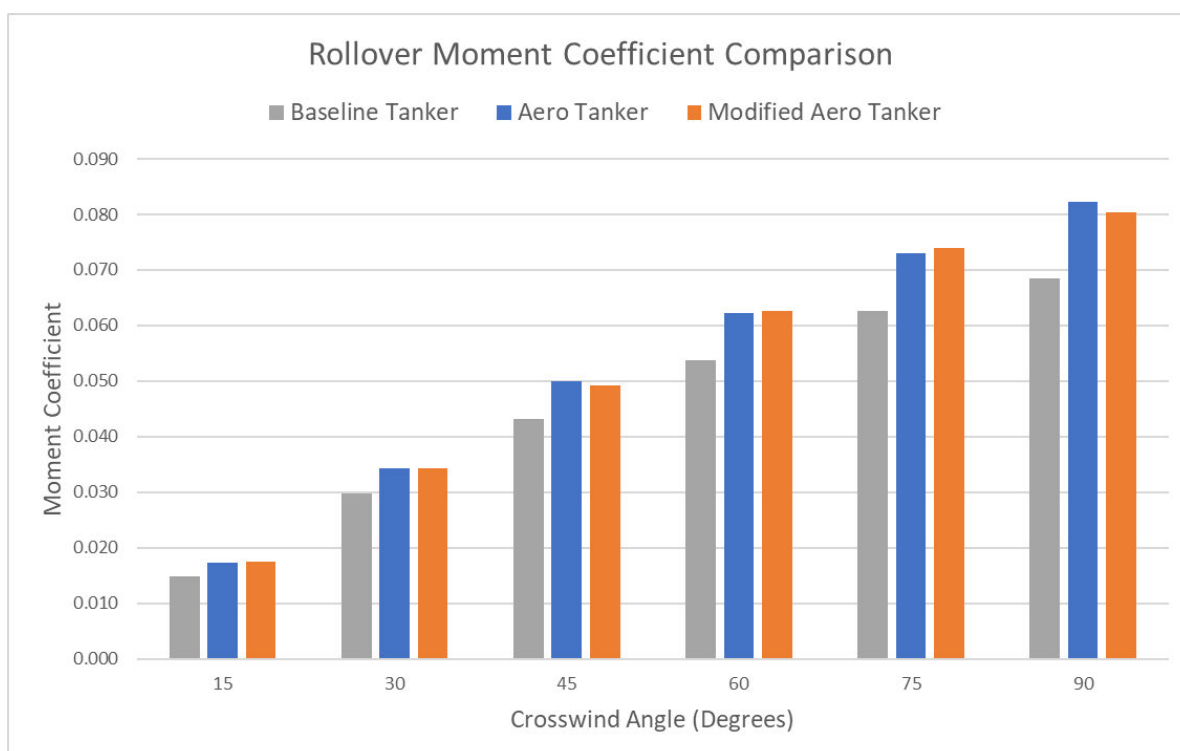
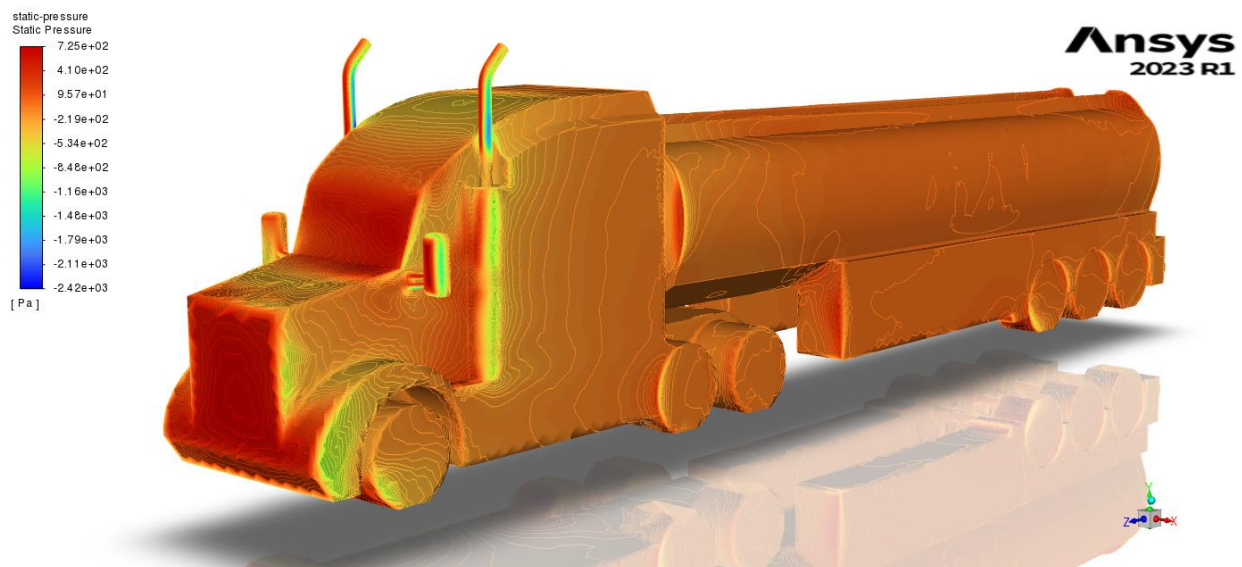


Figure 5.5.2-113: Comparison of Rollover Moment Coefficient

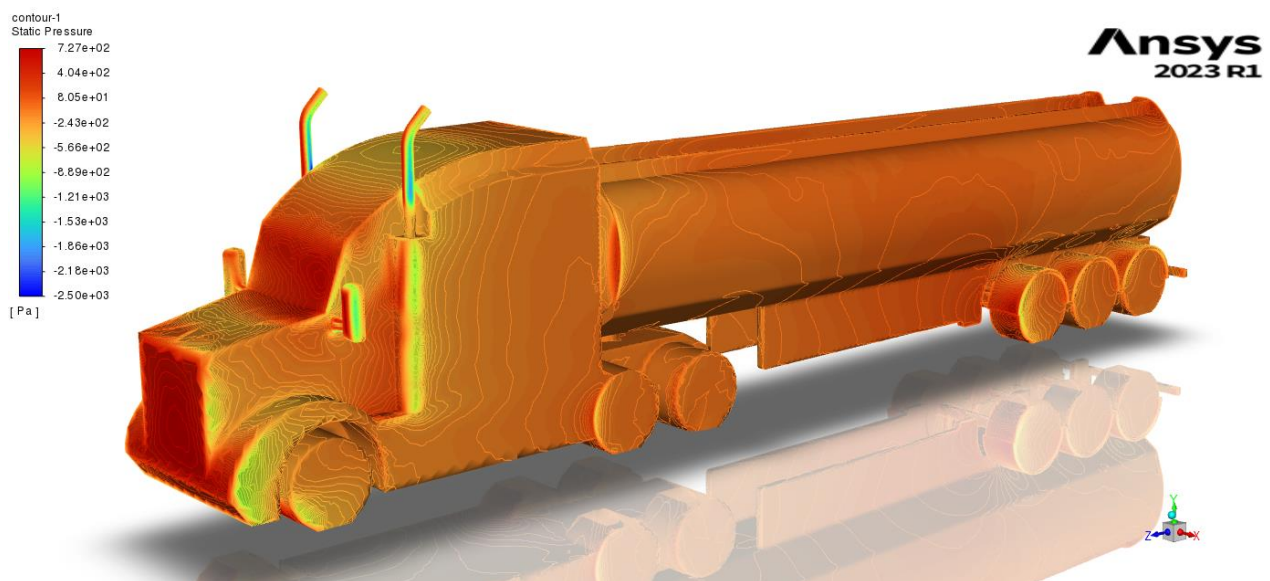
*c) Analysis of Modified Aero Tanker Flow Pathlines*

Figure 5.5.2-114 to Figure 5.5.2-135 present a comparison of contour plots depicting static and total pressure, as well as flow pathlines, for both the Original Aero and the Modified Aero tankers at 15-degree crosswind angles. These figures highlight the most significant improvement observed in reducing the lift and rotational (yawing) moment coefficients. Additional contour plots and pathlines for both tankers at various crosswind angles can be found in Appendix I.9 to I.6.

❖ *Static Pressure Distribution in both tankers at 15-degree crosswind angle*



*Figure 5.5.2-114: Static Pressure on the Winward Side of Modified Aerodynamic Tanker 15-degree crosswind angle*



*Figure 5.5.2-115: Static Pressure on the Winward Side of Aerodynamic Tanker 15-degree crosswind angle*

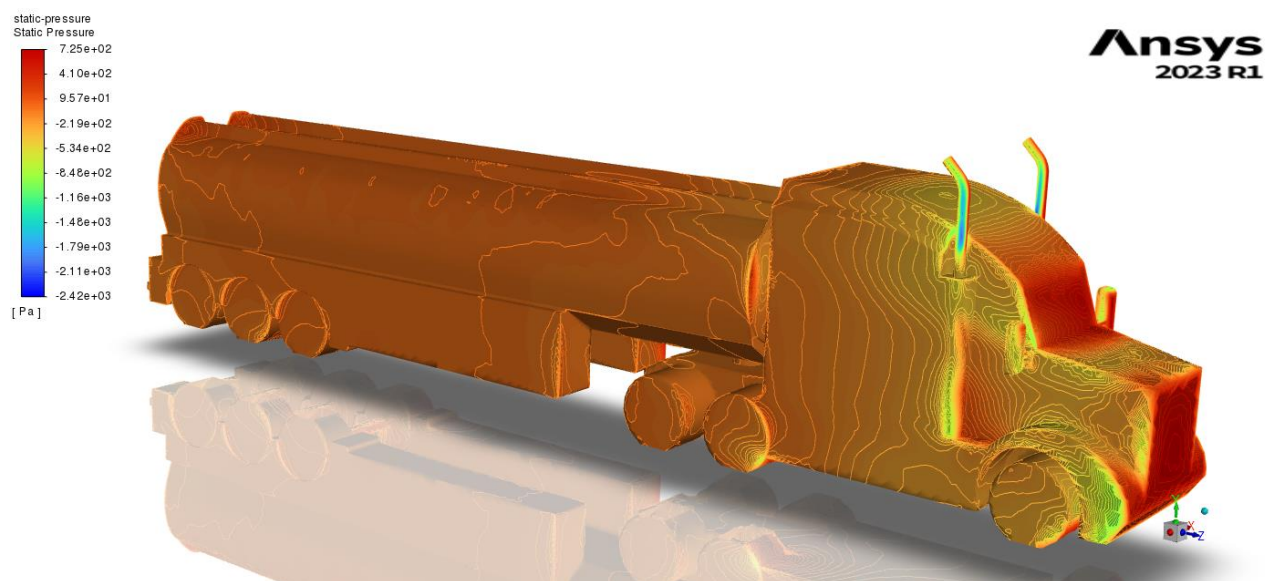


Figure 5.5.2-116: Static Pressure on the Leeward Side of the Modified Aerodynamic Tanker 15-degree crosswind angle

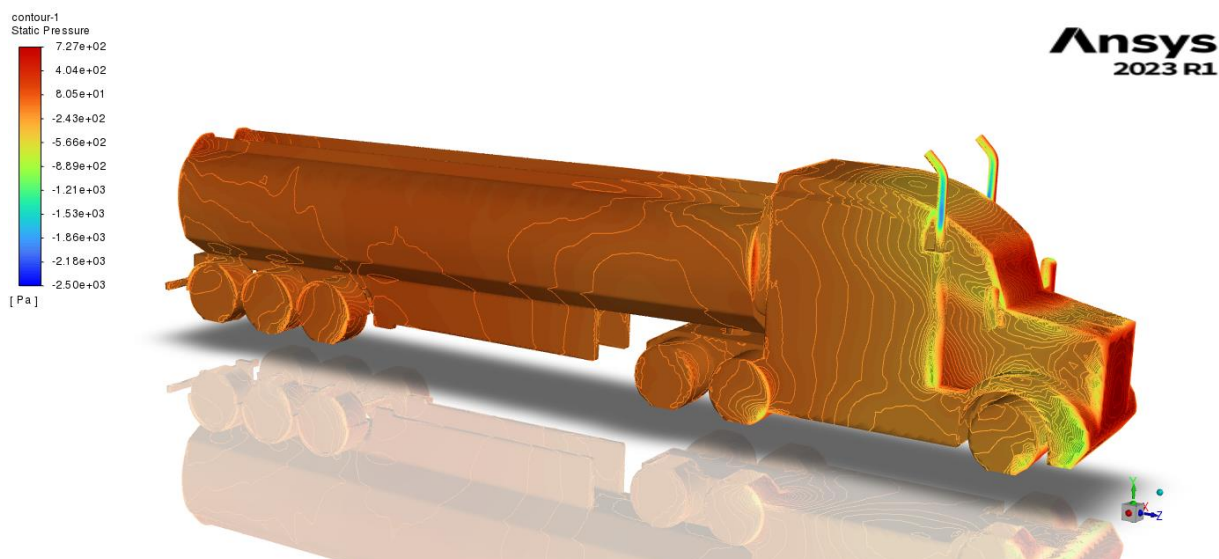


Figure 5.5.2-117: Static Pressure on the Leeward Side of Aerodynamic Tanker 15-degree crosswind angle



❖ Total Pressure Distribution on both tankers 15-degree crosswind angle

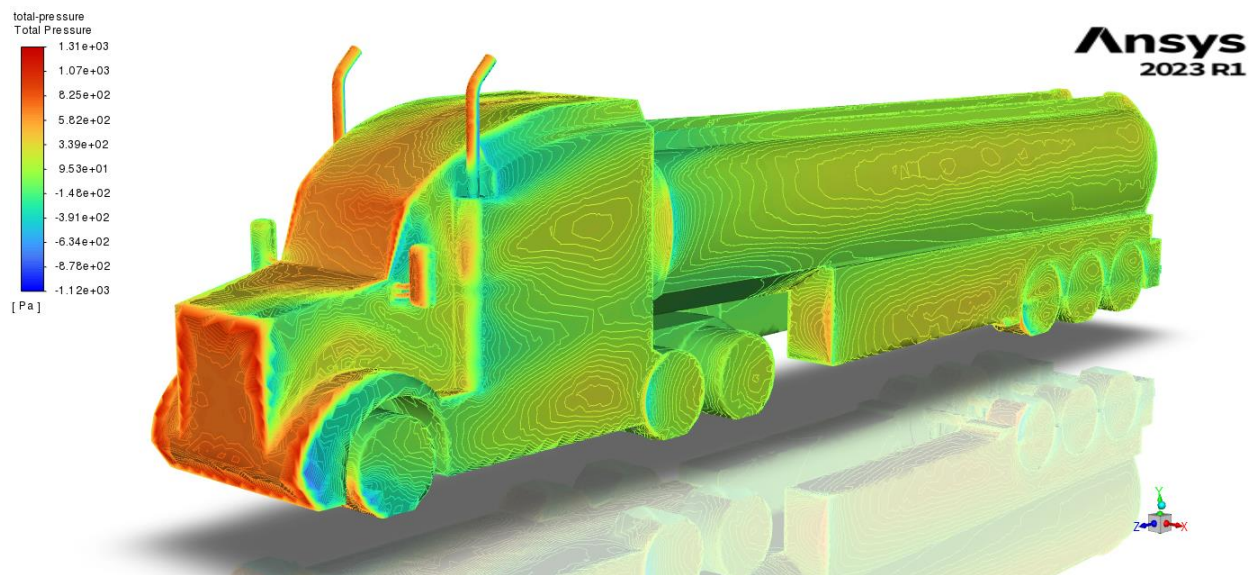


Figure 5.5.2-118: Total Pressure on the Windward Side of Modified Aerodynamic Tanker 15-degree crosswind angle

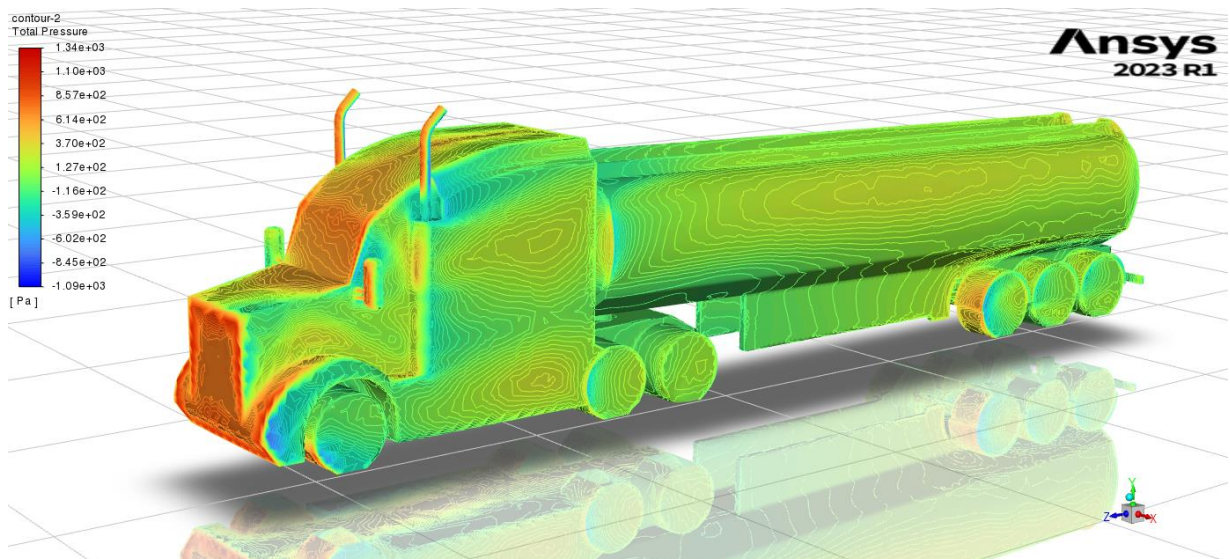


Figure 5.5.2-119: Total Pressure on the Windward Side of Aerodynamic Tanker 15-degree crosswind angle

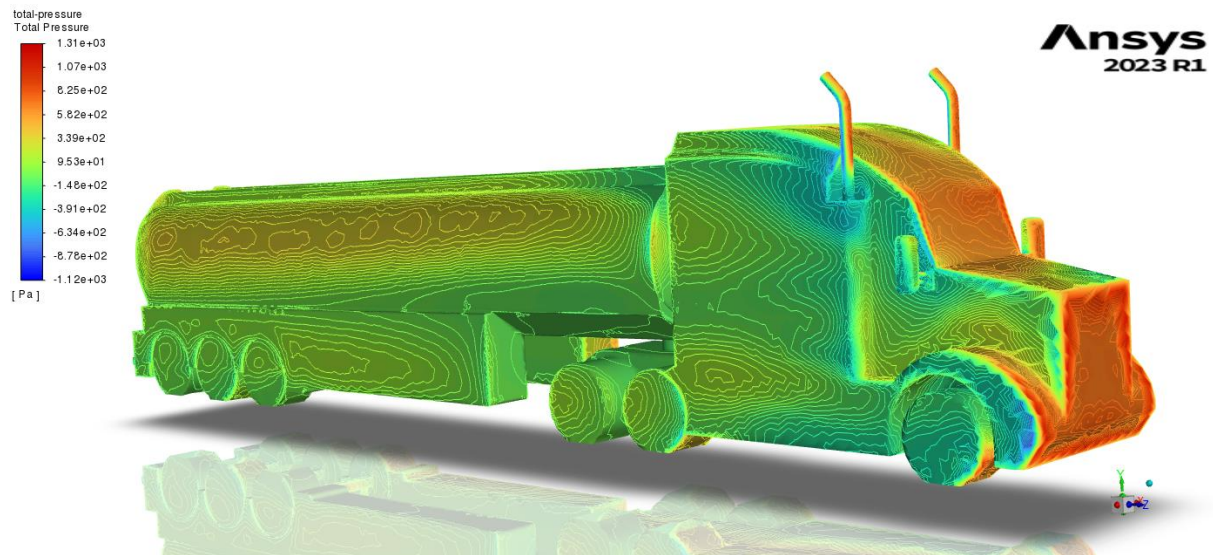


Figure 5.5.2-120: Total Pressure on the Leeward Side of Modified Aerodynamic Tanker 15-degree crosswind angle

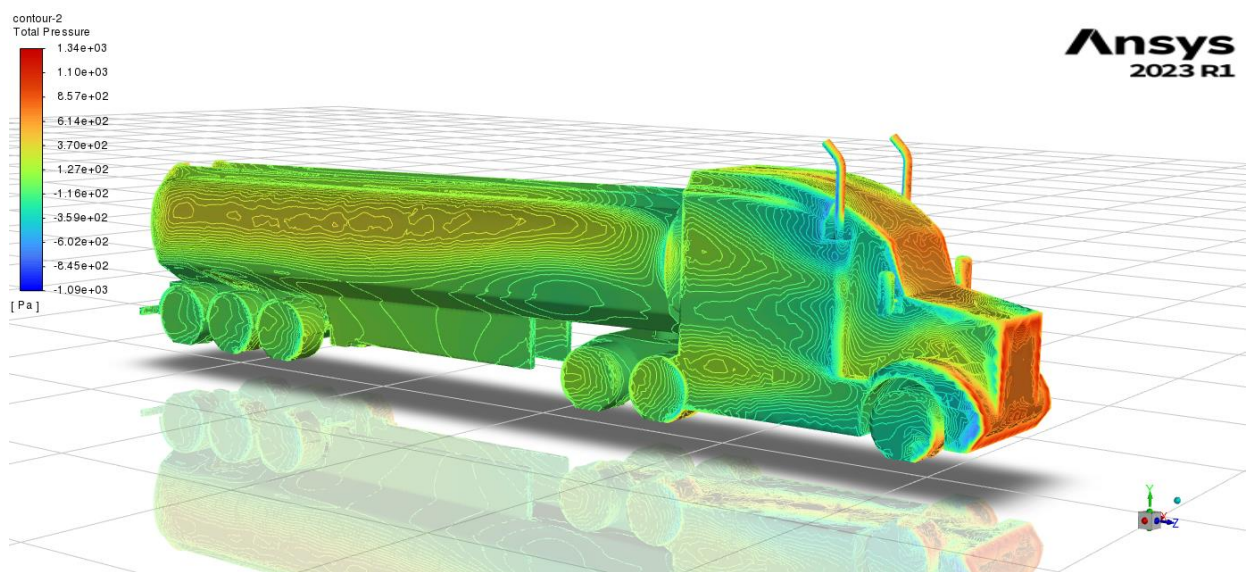
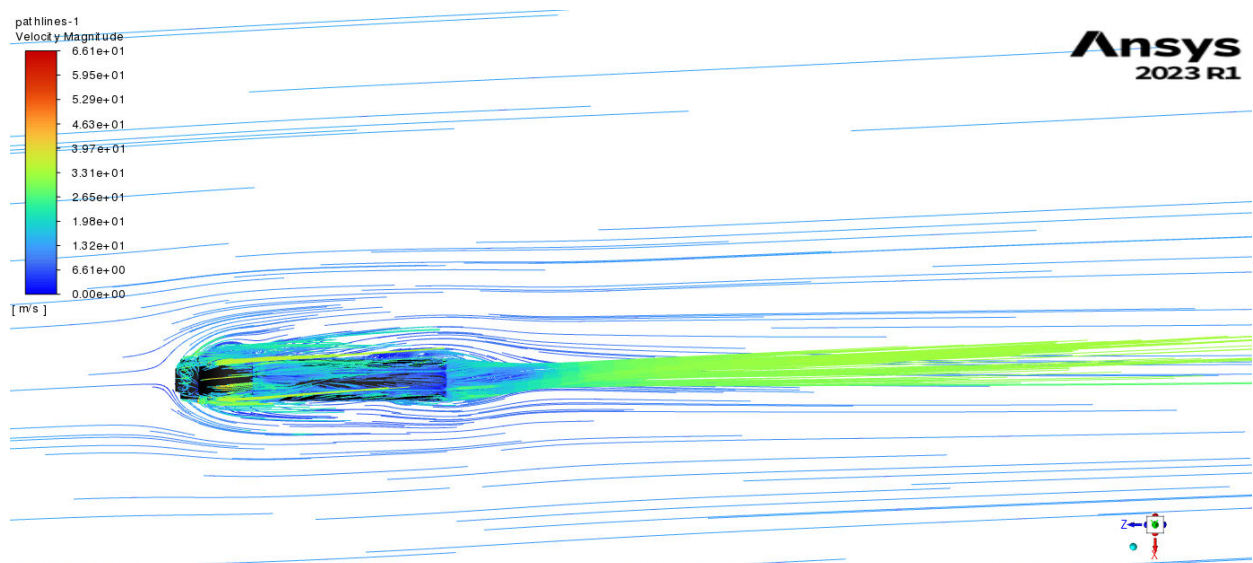


Figure 5.5.2-121: Total Pressure on the Leeward Side of Aerodynamic Tanker 15-degree crosswind angle



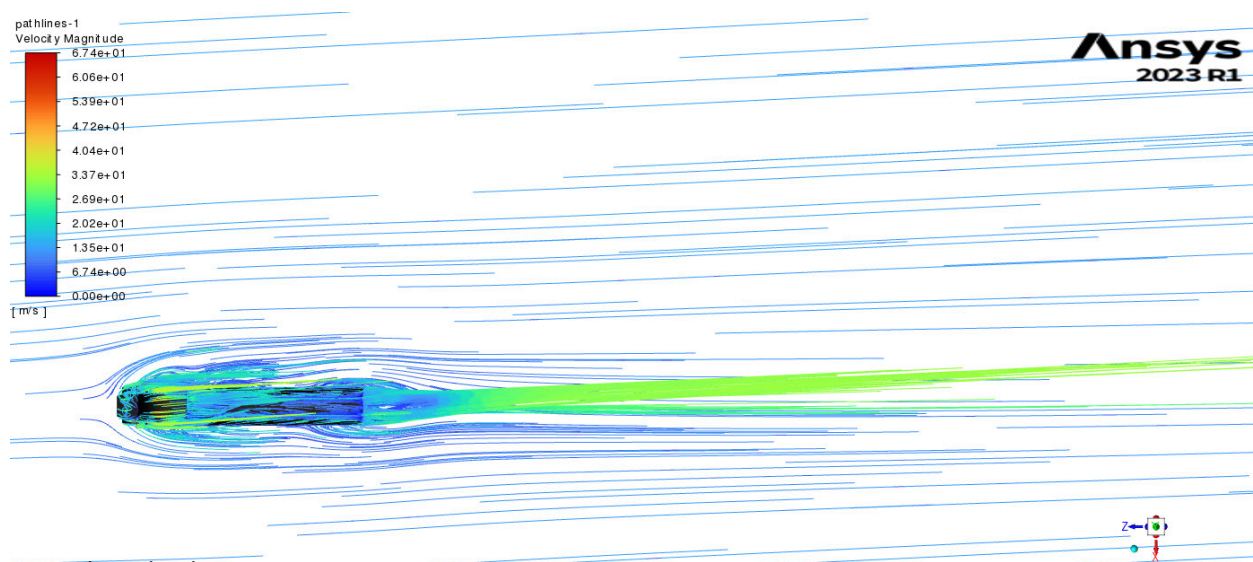
❖ Flow Pathlines of both Tankers 15-degree crosswind angle

○ Overview of Flow Pathlines



Windward Side

Figure 5.5.2-122: Flow Around Modified Aerodynamic Tanker at a 15-degree crosswind angle.



Windward Side

Figure 5.5.2-123: Flow Around Aerodynamic Tanker at 15-degree crosswind angle.



○ Top View of Flow Pathlines

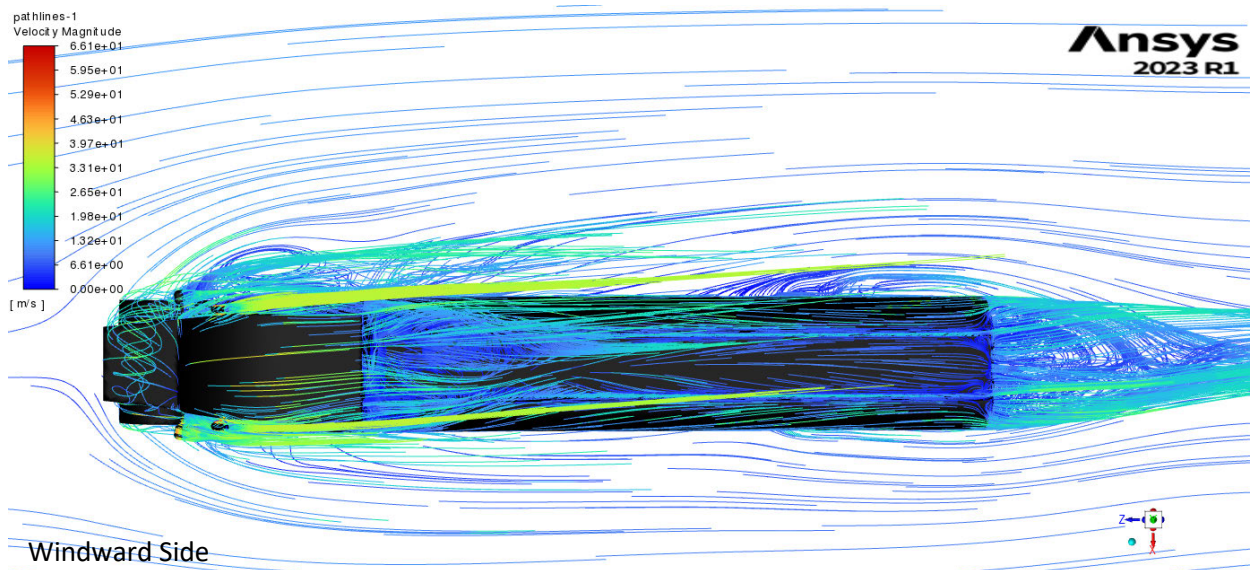


Figure 5.5.2-124: Flow Around Modified Aerodynamic Tanker at 15-degree crosswind angle – Top View.

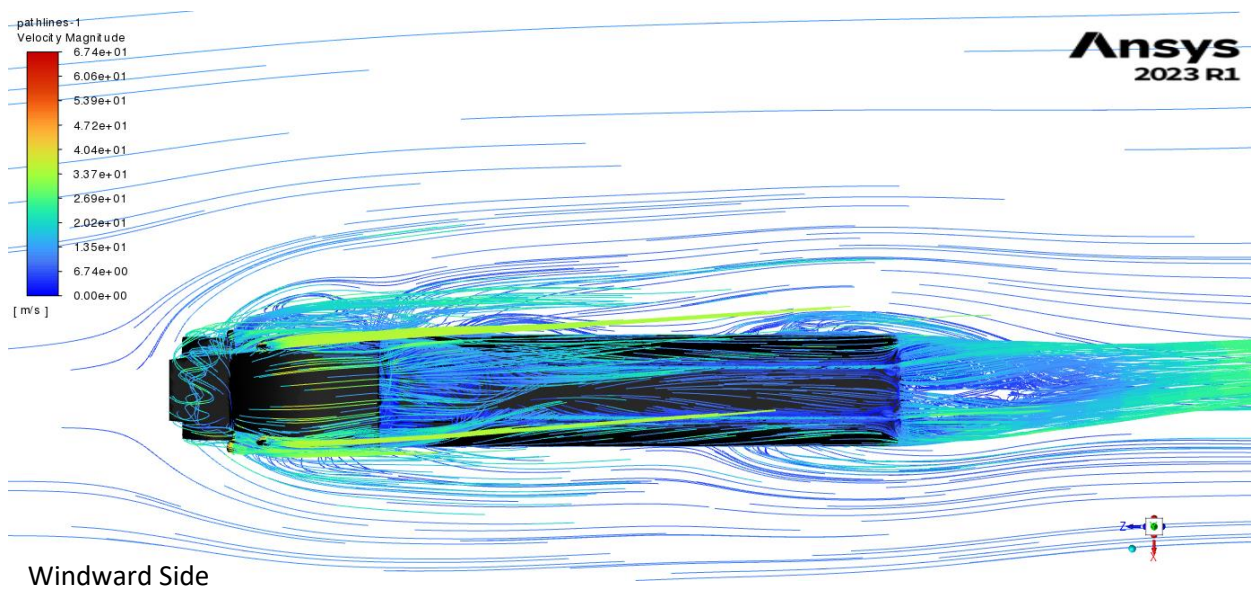


Figure 5.5.2-125: Flow Around Aerodynamic Tanker at 15-degree crosswind angle – Top View.

○ Underside View of Flow Pathlines

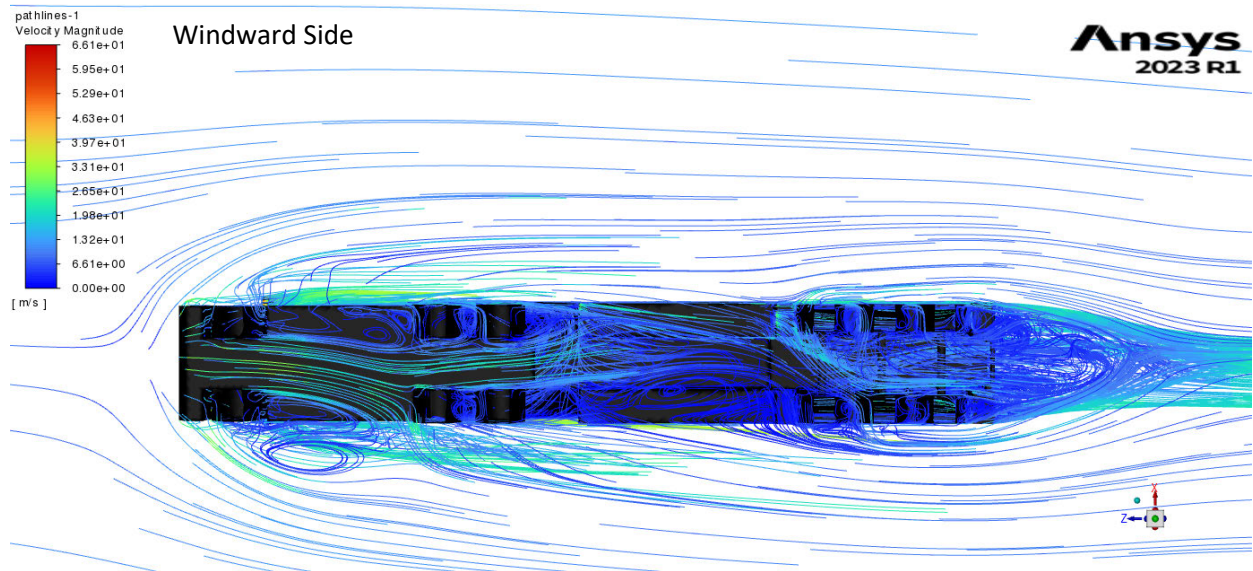


Figure 5.5.2-126: Flow Around Modified Aerodynamic Tanker at 15-degree crosswind angle – Underside View.

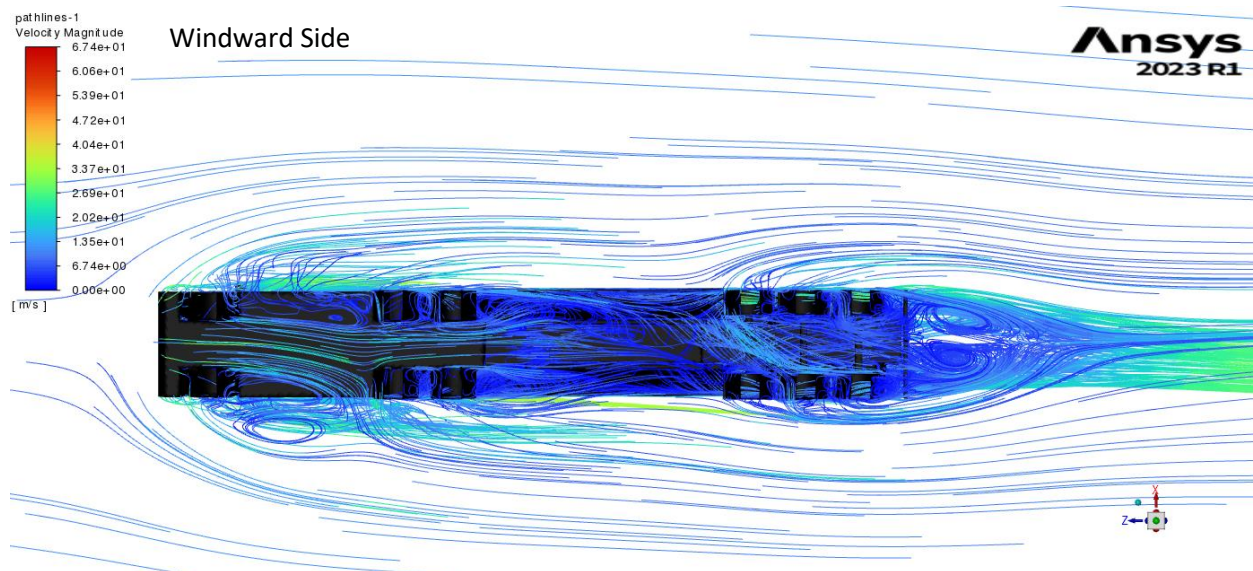


Figure 5.5.2-127: Flow Around Aerodynamic Tanker at 15-degree crosswind angle – Underside View.



○ Elevation View of Flow Pathlines

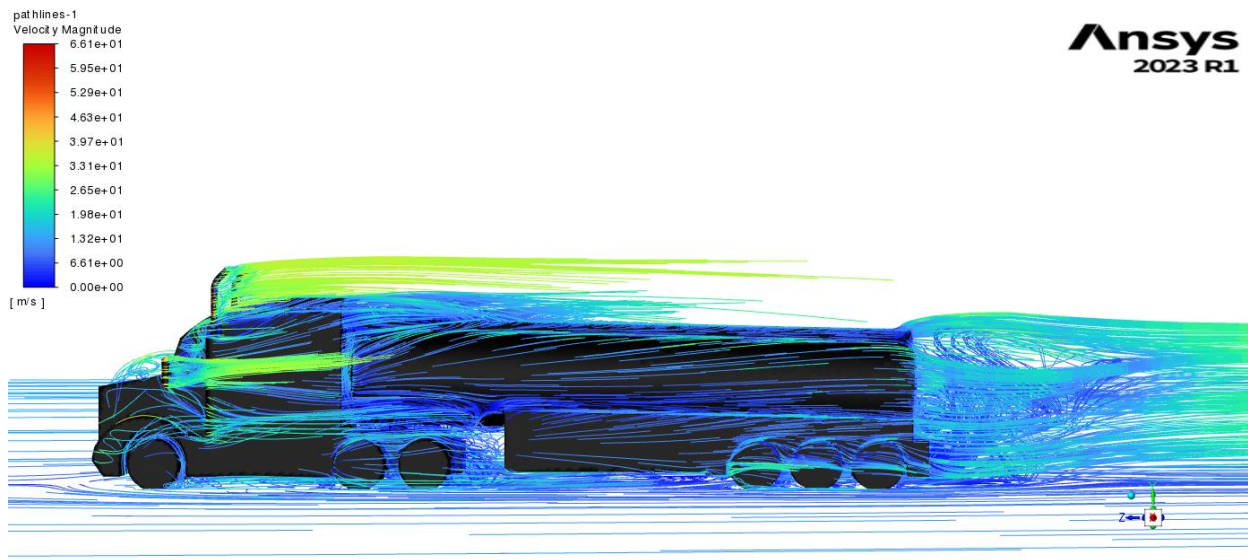


Figure 5.5.2-128: Elevation View of Flow Around Modified Aerodynamic Tanker at 15-degree crosswind angle - Winward Side.

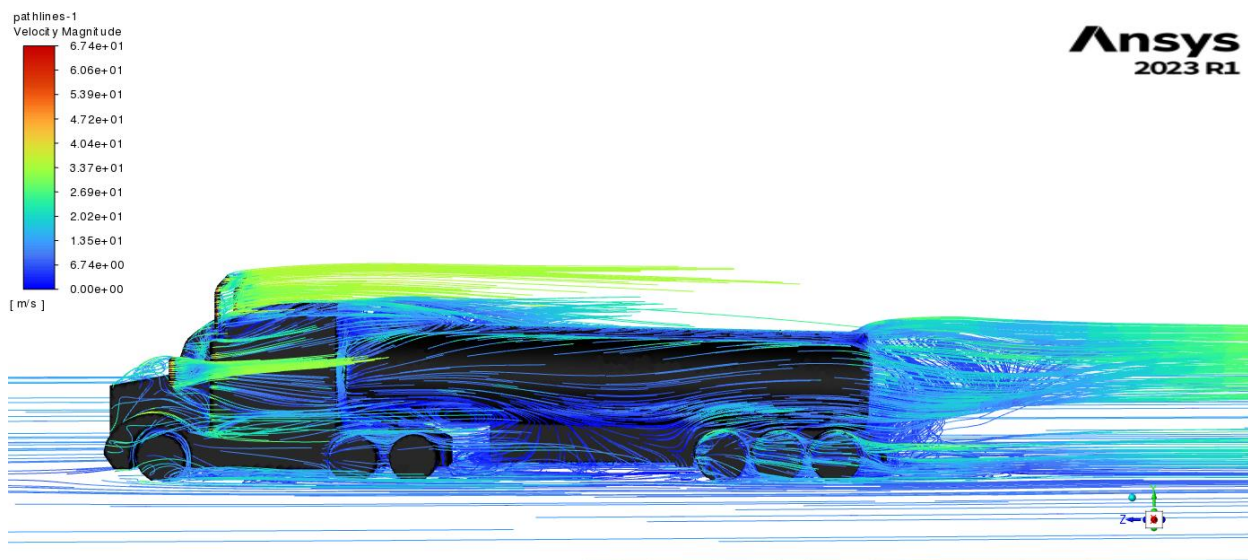


Figure 5.5.2-129: Elevation View of Flow Around Aerodynamic Tanker at 15-degree crosswind angle - Winward Side.

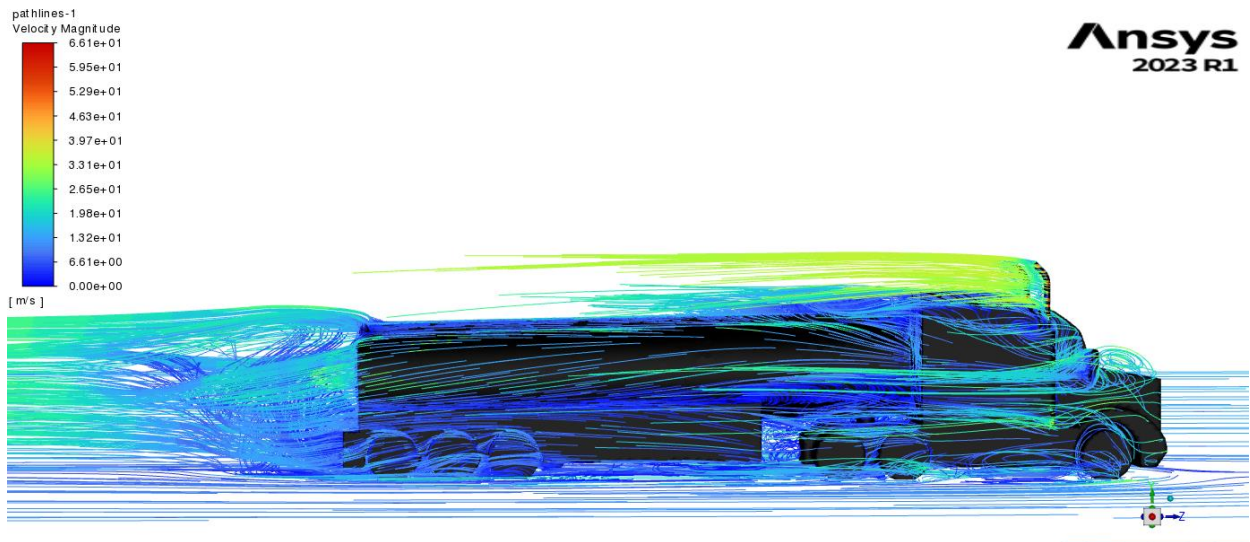


Figure 5.5.2-130: Elevation View of Flow Around Modified Aerodynamic Tanker at 15-degree crosswind angle - Leeward Side.

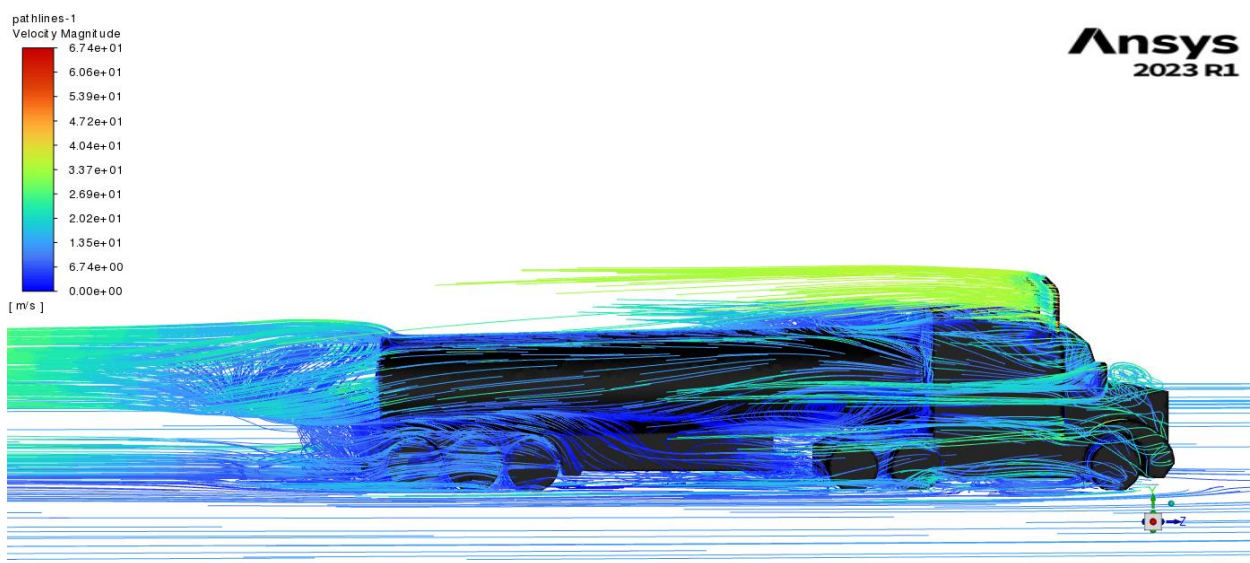


Figure 5.5.2-131: Elevation View of Flow Around Aerodynamic Tanker at 15-degree crosswind angle - Leeward Side



○ Isometric View of Flow Pathlines

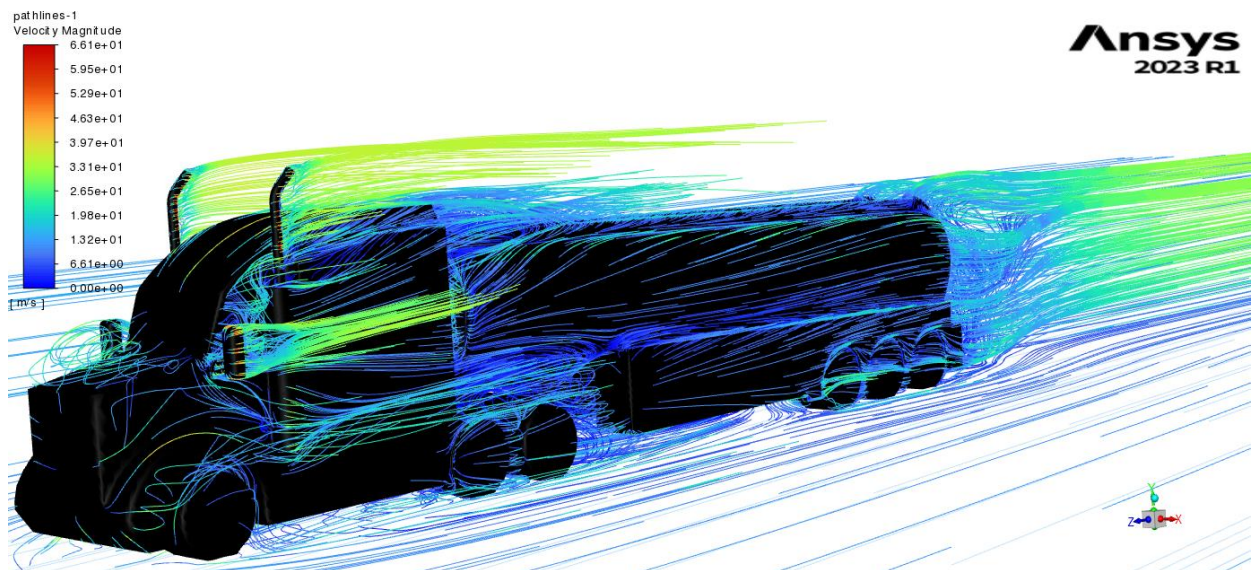


Figure 5.5.2-132: Isometric View of Flow Around Modified Aerodynamic Tanker at 15-degree crosswind angle - Windward Side.

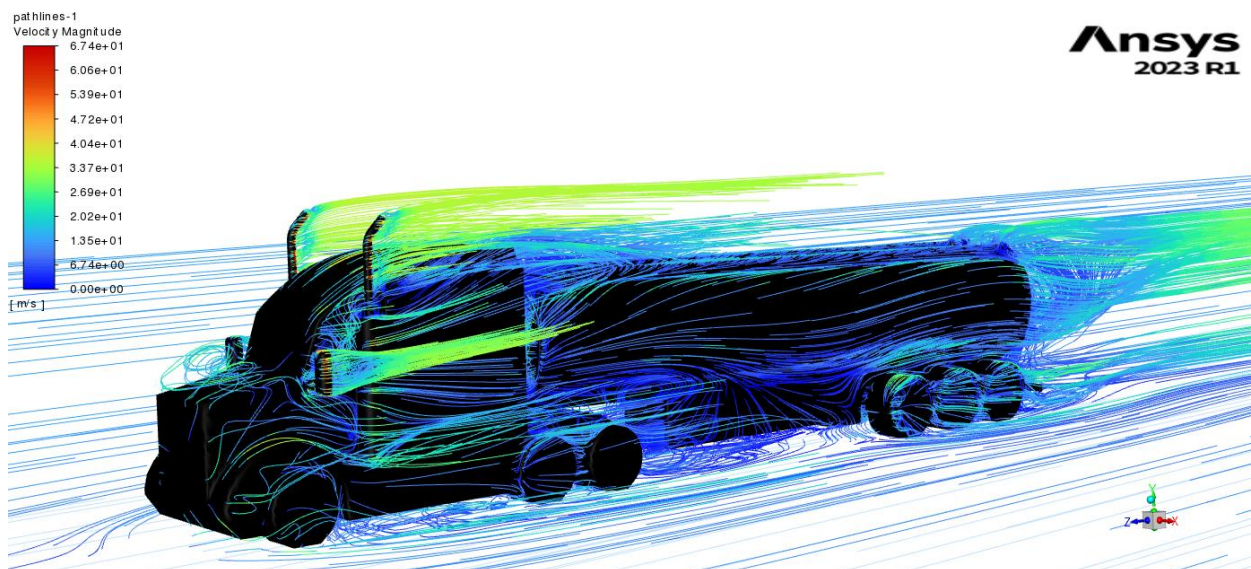


Figure 5.5.2-133: Isometric View of Flow Around Aerodynamic Tanker at 15-degree crosswind angle - Windward Side.

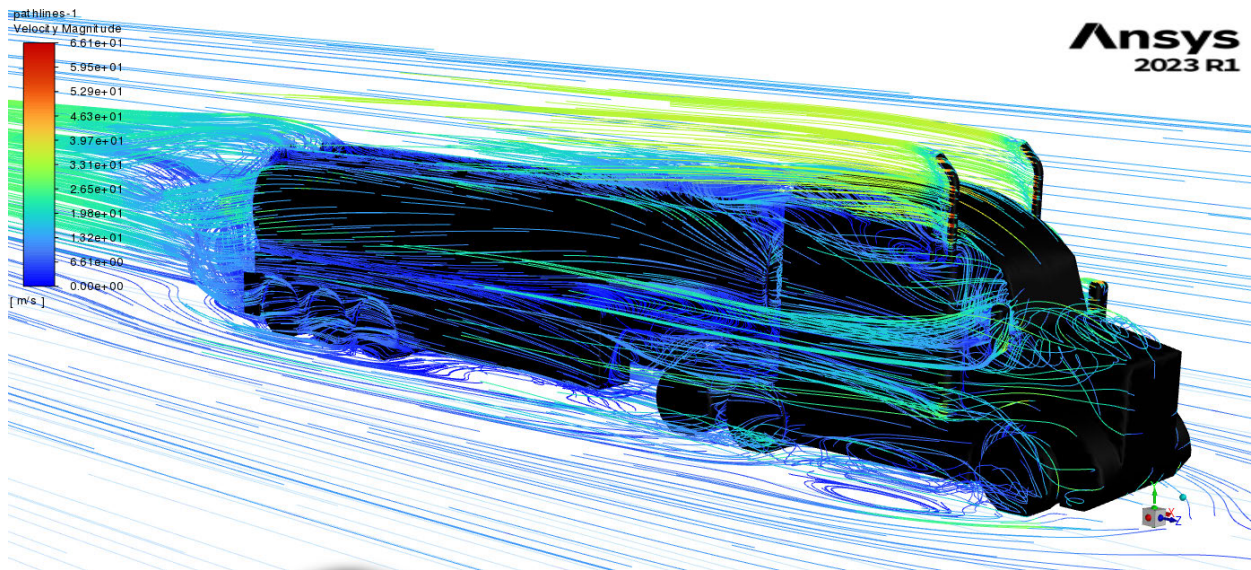


Figure 5.5.2-134: Isometric View of Flow Around Modified Aerodynamic Tanker at 15-degree crosswind angle - Leeward Side.

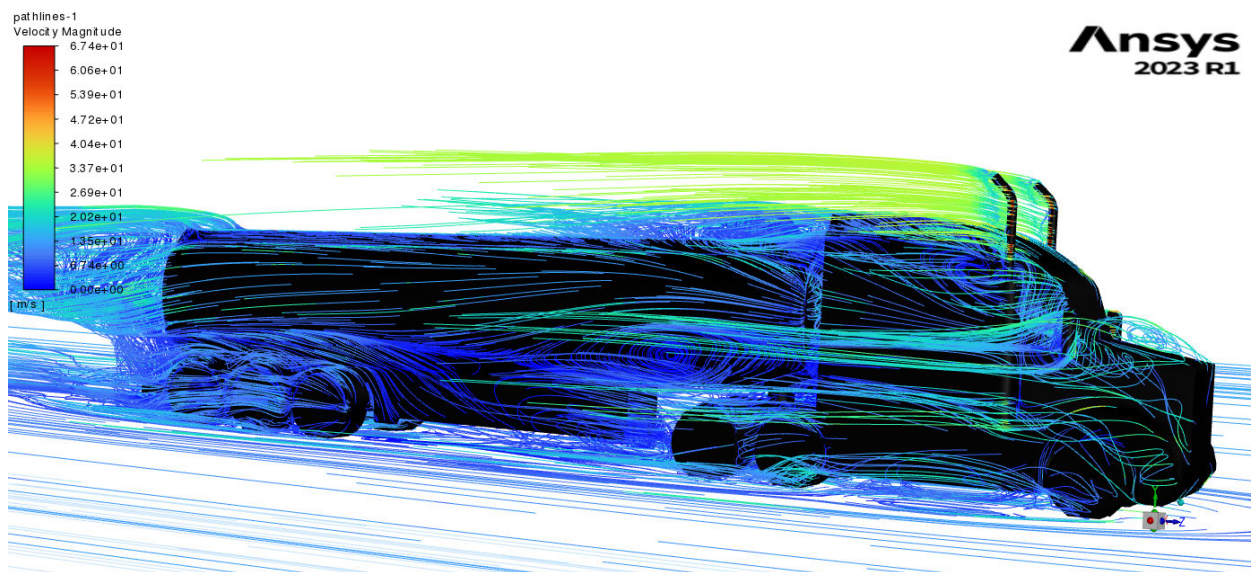


Figure 5.5.2-135: Isometric View of Flow Around Aerodynamic Tanker at 15-degree crosswind angle - Leeward Side.

#### ❖ Contours and Pathlines Comparison Discussion

Figure 5.5.2-114 to Figure 5.5.2-135 illustrate the impact of side skirt modifications on the semitrailer. These modifications result in a decrease in both static and total pressure on the rear wheel group of the trailer. Comparatively, the airflow around the modified aerodynamic tanker (Figure 5.5.2-126 to Figure 5.5.2-135) shows slightly reduced turbulence in comparison



to the original aerodynamic one, leading to a minor decrease in axial drag and rollover moment coefficient.

Additionally, the airflow under and around the modified tanker's sides exhibits less separation and twisting than the original design (Figure 5.5.2-126 to Figure 5.5.2-135), significantly reducing the yawing moment coefficient. This reduction enhances vehicle stability and ease of control, improving stability and predictability when operating the modified aerodynamic tanker in crosswind conditions.

In conclusion, Modifying the trailer side skirts improves vehicle stability and ease of control by significantly reducing lift and yawing moment coefficients while slightly increasing the lateral drag and pitch moment coefficients. Therefore, if yawing stability is a critical concern, the Modified Aero Tanker is the superior choice due to its lower yawing moment coefficients. The choice between these models should be made with specific operational requirements and the trade-offs between lateral and yawing stability in mind.

## CHAPTER 6 – CONCLUSION

### 6.1 Overview

This concluding chapter delves into the study's findings, offering recommendations for implementing the modifications explored in the optimisation study. It also introduces areas for future research to validate these results. Additionally, it addresses the study's limitations and suggests potential solutions.

### 6.2 Conclusion

This research has been dedicated to exploring methods to enhance semitrailer tankers' aerodynamic performance and stability when confronted with crosswind conditions. Several essential findings and conclusions emerge through a comprehensive simulation and analysis process, including investigations into the efficacy of aerodynamic devices and design modifications.

The study's initial phase involved simulating the effects of both headwinds and crosswinds at varying angles. Incorporating specific aerodynamic enhancements, including tractor side skirts, tractor-trailer gap fairings, and trailer side skirts, resulted in a substantially reduced drag coefficient of up to 18%. This alignment with prior research underscores the potential for these enhancements to positively impact fuel efficiency and overall performance, particularly in headwind conditions.

However, as the research delved deeper into the impact of these aerodynamic devices, it became evident that there were trade-offs to consider. Safety assessments uncovered increased lateral drag and the rotational and rollover moments, notably at crosswind angles of 15 and 30 degrees. While it is unlikely that the aerodynamic tanker would experience sideslip, rotation, or rollover accidents under typical crosswind conditions (steady crosswind of 6.5m/s), the increased lateral drag, and yawing moments could compromise vehicle stability.

To address these challenges, a pre-optimization study highlighted the crucial role of side skirts, specifically their design and the issue of flow separation. Proposed modifications, which involved repositioning and redesigning side skirts to mitigate these effects, proved highly effective. Simulations demonstrated significant reductions in rotational moments and axial drag coefficients at crosswind angles of 15 and 30 degrees, thus enhancing vehicle stability and predictability.

This research provides valuable insights for the trucking and transportation industry. The optimization of aerodynamic devices can lead to improved fuel efficiency and overall performance, as evidenced by the reduced drag coefficient. Ultimately, the choice between the baseline, the aerodynamic, or the modified aerodynamic model should be made with specific operational requirements in mind. If lateral stability under crosswind conditions is the primary concern, the baseline model may be preferable. However, due to its lower yawing moment

coefficients, the modified aerodynamic model proves superior for those prioritising yawing stability. This research provides a valuable framework for addressing the complex interplay between aerodynamic enhancements, crosswind conditions, and the performance and safety of tractor-semitrailer tankers, offering practical insights for the transportation industry, where balancing performance and safety is paramount.

The findings from this study contribute to a growing body of knowledge in the field of transportation and vehicle aerodynamics, offering practical solutions for addressing challenges faced by long-haul trucking operations. Future research may focus on further optimizing the design of aerodynamic devices and exploring additional safety measures to ensure semitrailer tankers' optimal performance and safety in diverse environmental conditions.

In conclusion, this research project has effectively addressed its objectives. It has provided insights into the impact of aerodynamic enhancements on tractor-semitrailer tankers in crosswind conditions, highlighting the trade-offs between enhanced performance and potential safety concerns. The study's findings indicate that thoughtful modifications make optimisation possible, offering practical recommendations for improving stability and safety. These findings directly affect the transportation industry and provide valuable guidance for those seeking to balance performance and safety in tractor-semitrailer tanker design and operation.

### 6.3 Limitation and Future Work

As discussed in Section 4.1, several limitations from constraints relate to computational resources, time, and modelling decisions. These limitations have influenced the precision of the findings while also providing a roadmap for future investigations.

One significant limitation was the simplification of tanker geometries, where critical components such as outlets, adaptors, ladders, handrails, landing legs, mudflaps, hose trays, pump frames, and tire carriers were omitted. This simplification was necessary to reduce the computational load and facilitate meshing. Despite these simplifications, we maintained acceptable mesh quality in the tanker domain, skewness at 0.7 and volume mesh quality at 0.24.

Furthermore, convergence issues related to domain mesh quality influenced the selection of the Realizable k-epsilon model with Enhanced Wall Treatment, Curvature Correction, and Production Limiter for the solving stage. This choice was made over the more precise SST k-omega model due to time constraints.

Additionally, the study did not investigate mesh and domain independence or analyse the sloshing effects of liquid loads inside the tanker. These factors collectively contributed to the less precise results obtained.

Therefore, future research and investigation are required as follows:

- Investigate Mesh and Domain Independence: Exploring mesh and domain independence is essential to ensure the robustness of simulation results.

- **Analyse Gusty Crosswinds:** A comprehensive analysis of the impact of gusty crosswinds on tanker aerodynamics is recommended, which can better represent real-world conditions.
- **Simulation of Moving Vehicles:** Expanding the study to simulate a moving vehicle while considering factors like rotating wheels, vehicle acceleration, and deceleration would capture dynamic effects on stability and efficiency more accurately.
- **Investigate Sloshing Effects:** The impact of unfixed loads inside the tanker (sloshing effect) significantly influences road tankers' stability and aerodynamic performance. Therefore, it needs to be carefully investigated.
- **Wind Tunnel Testing:** To validate the results obtained through CFD analysis, conducting wind tunnel tests on the tankers is suggested to get empirical data for comparison.

These proposed avenues for future research hold the potential to yield more accurate and comprehensive results, enhancing our understanding of how crosswinds affect the stability and efficiency of road tankers.

## REFERENCES

1. ABS 2020, *Survey of Motor Vehicle Use*, Australian Bureau of Statistics, Australia, viewed 20 March 2023, <<https://www.abs.gov.au/statistics/industry/tourism-and-transport/survey-motor-vehicle-use-australia/latest-release>>.
2. ADRs 2006a, *Australian Design Rule 42/02 – General Safety Requirements*, ADRs 4202, Department of Infrastructure, Transport, Regional Development, Communication and the Arts, Australia.
3. ADRs 2006b, *Australian Design Rule 65/00 – Maximum Road Speed Limiting for Heavy Goods Vehicles and Heavy Omnibuses*, ADRs 6500, Department of Infrastructure, Transport, Regional Development, Communication and the Arts, Australia.
4. ADRs 2006c, *Australian Design Rule 43/00 – Vehicle Configuration and Marking*, ADRs 4301, Department of Infrastructure, Transport, Regional Development, Communication and the Arts, Australia.
5. ATE\_Tankers 2023, *True Collaboration*, ATE TANKER, Sunshine West Victoria, Australia, <http://atetankers.com.au/>>.
6. Baker, CJ 1987, 'Measures to control vehicle movement at exposed sites during windy periods', *Journal of Wind Engineering and Industrial Aerodynamics*, vol. 25, no. 2, pp. 151-61.
7. Batista, M & Perkovič, M 2014, 'A simple static analysis of moving road vehicle under crosswind', *Journal of Wind Engineering and Industrial Aerodynamics*, vol. 128, pp. 105-13.
8. Brandt, A, Jacobson, B & Sebben, S 2022, 'High speed driving stability of road vehicles under crosswinds: an aerodynamic and vehicle dynamic parametric sensitivity analysis', *Vehicle system dynamics*, vol. 60, no. 7, pp. 2334-57.
9. Çengel, YA, Cimbala, JM & Turner, RH 2017, *FUNDAMENTALS OF THERMAL-FLUID SCIENCES*, 5 edn, McGraw-Hill Education, New York, NY 10121.
10. Chowdhury, H, Moria, H, Ali, A, Khan, I, Alam, F & Watkins, S 2013, 'A Study on Aerodynamic Drag of a Semi-trailer Truck', *Procedia Engineering*, vol. 56, pp. 201-5.
11. Cooper, KR 2003, 'Truck Aerodynamics Reborn - Lessons from the Past', *SAE Transactions*, vol. 112, pp. 132-42.
12. Cummins 2013, *Secrets of Better Fuel Economy - The Ohysic of MPG*, CUMMINS, viewed 30/03/2023, <[https://www.cummins.com/sites/default/files/cummins\\_secrets\\_of\\_better\\_fuel\\_economy.pdf](https://www.cummins.com/sites/default/files/cummins_secrets_of_better_fuel_economy.pdf)>.
13. De Pont, J 2017, *Method for Estimating the SRT of a vehicle*, THE LAND TRANSPORT SAFETY AUTHORITY, Wellington, New Zealand, <https://www.nzta.govt.nz/assets/Vehicles/Method-for-estimating-the-static-roll-threshold-of-a-vehicle.pdf>>.
14. De Pont, J, Baas, P, Hutchinson, D & Kalasih, D 2002, 'Including performance measures in dimensions and mass regulations', *7th International Symposium on Heavy Vehicle Weights and Dimensions*, pp. 349-58.
15. Ervin, R, Winkler, C & Karamihas, S 2002, *A Centrifuge Concept for Measuring the Rollover Threshold of Light-Duty Vehicles*, 0148-7191.
16. Geoscience\_Australia 2023, *Wind Energy*, G Australia, Australian Government, Australia, viewed 20 March 2023, <<https://www.ga.gov.au/scientific-topics/energy/resources/other-renewable-energy-resources/wind-energy>>.
17. Government, A 2023, *Australian Design Rules*, Department of Infrastructure, Transport, Regional Development, Communication and the Arts, Australia, <https://www.infrastructure.gov.au/infrastructure-transport-vehicles/vehicles/vehicle-design-regulation/australian-design-rules>>.
18. Hejdesten, M & Tenstam, A 2022, *Why aerodynamics is important for your trucking business*, Volvo, viewed 30/03/2023, <<https://www.volvotrucks.com/en-en/news-stories/insights/articles/2022/nov/the-importance-of-aerodynamic.html>>.



19. Hendrickson 2023, *INTRAAX® Integrated Axle & Air Suspension System*, Dandenong South Vic 3175, Australia, <https://www.hendrickson-intl.com/en-au/products/intraax/intraax-aat>>.
20. Idealsimulations 2020a, *CFD Computational Domain*, idealsimulations, viewed 2 June, <<https://www.idealsimulations.com/resources/cfd-computational-domain/>>.
21. Idealsimulations 2020b, *Turbulence Models In CFD*, idealsimulations, viewed 2 June, <<https://www.idealsimulations.com/resources/turbulence-models-in-cfd/>>.
22. Kenworth\_AU 2023, *T610 SPECIFICATIONS*, Kenworth Australia, Bayswater Victoria, Australia, <https://www.kenworth.com.au/wp-content/uploads/2020/03/T610-Spec-Sheet-Mar-2020.pdf>>.
23. Kim, JJ, Kim, J, Hann, T, Kim, D, Roh, HS & Lee, SJ 2019, 'Considerable drag reduction and fuel saving of a tractor–trailer using additive aerodynamic devices', *Journal of Wind Engineering and Industrial Aerodynamics*, vol. 191, pp. 54-62.
24. Kirkham, R 2016, *Literature Review of the Effects of Wind on Heavy Vehicles*, Australian Road Research Board, Australia.
25. Malviya, V 2011, 'Effects of a novel aerodynamic intervention for heavy commercial vehicles on fuel saving and stability', ProQuest Dissertations Publishing.
26. Malviya, V, Gundala, N & Mishra, R 2009, 'EFFECT OF CROSS WIND ON AERODYNAMIC COEFFICIENTS OF GROUND VEHICLES', *Proceedings of Computing and Engineering Annual Researchers' Conference*, University of Huddersfield, Huddersfield, UK, <<http://eprints.hud.ac.uk/id/eprint/6856/>>.
27. Mansor, S & Passmore, MA 2013, 'Effect of rear slant angle on vehicle crosswind stability simulation on a simplified car model', *International journal of automotive technology*, vol. 14, no. 5, pp. 701-6.
28. McCallen, R, Salari, K, Ortega, J, Castellucci, P, Pointer, D, Browand, F, Ross, J & Storms, B 2007, *DOE Project on Heavy Vehicle Aerodynamic Drag*, Livermore, California, <https://digital.library.unt.edu/ark:/67531/metadc829871/>>.
29. McCallen, R, Salari, K, Ortega, J, Castellucci, P, Paschkewitz, J, Eastwood, C, Dechant, L, Hassan, B, Pointer, WD, Browand, F, Radovich, C, Merzel, T, Plocher, D, Leonard, A, Rubel, M, Ross, J, Heineck, JT, Walker, S, Storms, B, Roy, C, Whitfield, D, Pankajakshan, R, Taylor, L, Sreenivas, K & Englar, R 2005, *DOE's Effort to Reduce Truck Aerodynamic Drag Through Joint Experiments and Computations*, 0148-7191.
30. Menter, FR 2009, 'Review of the shear-stress transport turbulence model experience from an industrial perspective', *International journal of computational fluid dynamics*, vol. 23, no. 4, pp. 305-16.
31. Menter, FR, Sechner, R & Matyushenko, A 2018, 'Best Practice: RANS Turbulence Modeling in Ansys CFD', no. 1, <https://www.ansys.com/resource-center/technical-paper/best-practice-rans-turbulence-modeling-in-ansys-cfd>>.
32. Miralbes, R & Ferrer, LC 2009, 'Aerodynamic Analysis of a Vehicle Tanker', *Journal of fluids engineering*, vol. 131, no. 4, pp. 0412041-04120417.
33. NHVR 2022, *Performance-Based Standards Scheme – the Standards and Vehicle Assessment Rules*, TNHVR (NHVR), The National Heavy Vehicle Regulator, Brisbane QLD, <https://www.nhvr.gov.au/files/media/document/123/202211-0020-pbs-standards-and-vehicle-assessment-rules.pdf>>.
34. OSTI.GOV 2020, *Technology Roadmap for the 21st Century Truck Program, a government-industry research partnership*, United States, <https://doi.org/10.2172/777307>>.
35. Pacejka, H 2012, '8.3.1 Effective Rolling Radius Variations at Free Rolling', in *Tire and Vehicle Dynamics (3rd Edition)*, Elsevier.
36. R.Miralbes, T 2012, 'Analysis of Some Aerodynamic Improvements for Semi-trailer Tankers', *World Congress on Engineering 2012*, London, U.K.
37. Salari, K 2013, *DOE's Effort to Improve Heavy Vehicle Aerodynamics through Joint Experiments and Computations*, Department of Energy, USA, <https://www.energy.gov/eere/vehicles/articles/does-effort-reduce-truck-aerodynamic-drag-through-joint-experiments-and-3>>.

38. Salari, K 2016, *DOE's Effort to Improve Heavy Vehicle Fuel Efficiency through Improved Aerodynamics*, VS006, Department of Energy, Washington DC, USA, [https://www.energy.gov/sites/prod/files/2016/06/f33/vs006\\_salari\\_2016\\_o\\_web.pdf](https://www.energy.gov/sites/prod/files/2016/06/f33/vs006_salari_2016_o_web.pdf)>.
39. Salati, L, Schito, P & Cheli, F 2017, 'Wind tunnel experiment on a heavy truck equipped with front-rear trailer device', *Journal of Wind Engineering and Industrial Aerodynamics*, vol. 171, pp. 101-9.
40. Service, SF 2018, *A HISTORY OF FUEL DELIVERY TRUCKS*, <https://specialtyfuelservices.com/history-fuel-delivery-trucks/>>.
41. Services, MECF 2014, *THE ROLLOVER RISKS OF TWO-TANK TANKERS ARE TOO GREAT TO CONTINUE TO ALLOW THEM CARRYING HAZARDOUS MATERIALS WITHOUT ADDITIONAL SAFETY MEASURES*, New York, USA, viewed 31/03/2023, <<https://sites.google.com/site/metropolitanenvironmental/the-rollover-risks-of-two-tank-tankers-are-too-great-to-continue-to-allow-them-carrying-hazardous-materials-without-additional-safety-measures>>.
42. Sharma, R, Zhang, J, Langelaar, M, Keulen, F & Aragón, A 2017, 'An improved stress recovery technique for low-order 3-D finite elements', *International Journal for Numerical Methods in Engineering*, vol. 114.
43. SIMSCALE 2023a, *What is CFD | Computational Fluid Dynamics?*, SIMSCALE, viewed 30/05/2023, <<https://www.simscale.com/docs/simwiki/cfd-computational-fluid-dynamics/what-is-cfd-computational-fluid-dynamics/>>.
44. SIMSCALE 2023b, *What Are Boundary Conditions?*, SIMSCALE, viewed 30/05/2023, <<https://www.simscale.com/docs/simwiki/numerics-background/what-are-boundary-conditions/>>.
45. Smith, R 2015, 'CFD Geometry Creation', *Richard Smith's blog*, 19 November, viewed 2 June 2023, <<https://www.symscape.com/blog/cfd-geometry-creation>>.
46. Solmaz, S 2023, 'Turbulence: Which Model Should I Select for My CFD Analysis?', *SIMSCALE Blog*, 30/05/2023, <<https://www.simscale.com/blog/turbulence-cfd-analysis/>>.
47. Standards\_Australia 2020a, *Part 2: Road tank vehicles for flammable liquids*, AS2809.2, The Council of Standard Australia.
48. Standards\_Australia 2020b, *Part 1: General requirement for all road tank vehicles*, AS2809.1, The Council of Standard Australia.
49. Tu, J, Yeoh, GH & Liu, C 2018, *Computational fluid dynamics : a practical approach*, Third edition. edn, Butterworth-Heinemann, an imprint of Elsevier, Oxford, United Kingdom.
50. Versteeg, HK & Malalasekera, W 2011, *An introduction to computational fluid dynamics : the finite volume method*, 2nd edn, Pearson Education, Harlow, England.
51. VicRoads 2010, *Understanding causes of rollover crashes*, DoTa Plaining, Victorian Transport Resources, Victoria, <https://www.vicroads.vic.gov.au/-/media/files/documents/business-and-industry/truckrolloverinformationinformationbulletinmarch2010.ashx>>.
52. WA\_Government 2022, *SRT Calculator*, DoTaM Road, Department of Transport and Main Road, Western Australia, <https://mrwebapps.mainroads.wa.gov.au/srtcalculator/>>.
53. Wandel, A 2021, *MEC5100 Computational Fluid Dynamics*, The University of Southern Queensland, Toowoomba QLD 4350.
54. Winkler, CB & Ervin, RD 1999, *Rollover of Heavy Commercial Vehicles*, UMTRI-99-19, Transportation Research Institute, University of Michigan, viewed 31/03/2023, <<https://deepblue.lib.umich.edu/bitstream/handle/2027.42/1290/93802.0001.001.pdf>>.
55. Wong, JY 2001, 'Theory of ground vehicles', in 3rd edn, Wiley, Hoboken, N.J, ch 1, p. 29.
56. Yokohama 2023, *Understand Your Tires - Tire Dimensions*, Yokohama, viewed 02-July, <<https://www.yokohamatruck.com/tires-101/understanding-your-tires/tire-dimensions>>.

# APPENDICES

## Appendix A – Original Project Specification

### ENG4111/4112 Research Project Project Specification

For: Uy Ngo  
Title: *Numerical simulation and optimisation of the aerodynamic performance of a semi-trailer tanker under crosswind*  
Major: Mechanical Engineering  
Supervisor: Ahmad Sharifian-Barforoush  
Enrolment: ENG4111 – EXT S1, 2023  
ENG4112 – EXT S2, 2023  
Project Aim: To analyse and optimise the aerodynamic performance of a semi-trailer tanker under headwind, tailwind and crosswind conditions.  
Programme: Version 2, 19<sup>th</sup> May 2023

#### A. Phase1- Literature Review

1. Review previous research on the effect of the aerodynamic drag on the performance of trailer tankers to find what has already been done so far and highlight the research gaps
2. Review relevant literature on the effect of crosswind aerodynamic loading on various types of accidents, such as rollover, sideslip and rotation.
3. Research on the existing regulations on semi-trailer[tanker modifications, such as the Australian Design Rules (ADRs) for heavy vehicles, Road tank vehicles for dangerous goods (AS2809.X), the National Heavy Vehicle Regulation (NHVR), the Static Roll Threshold (SRT) and the Performance Based Standards (PBS), etc.
4. Develop a research methodology for studying the effects of crosswind drag forces on the aerodynamic performance of a semi-trailer tanker and developing techniques to perform Computational Fluid Dynamics analysis for the tractor-semitrailer model.

#### B. Phase 2 – Simulation Performance

5. Use ANSYS CFD to simulate the scale 1:20 Kenworth T600A prime mover equipped with tractor-trailer gap fairing and tractor side skirts to determine the drag force and its coefficients under headwind conditions.
6. Validate simulation results using the theoretical drag force equation and the drag coefficient found by the research conducted by McCallen et al. (2007, p32) for this T600A prime mover, as shown in Error! Reference source not found., section 2.3.2.
7. Create two models of tractor-semitrailer tankers combination. One is the base model without any semitrailer's aerodynamic devices, and the other is equipped with full tractor-trailer gap fairing and tractor and trailer side skirts to perform aerodynamic analyses under crosswind conditions.
8. Perform CFD analyses and investigate the dynamic stability of these models under steady crosswind conditions at yaw angles ranging from zero to 90 degrees.
9. Compare the results of these analyses to determine the effect of the aerodynamic devices on the lateral force caused by crosswinds.
10. Modify the trailer tanker aero devices and tractor-trailer gap to minimise the side drag force applied on the semi-trailer.
11. Repeat the simulation for the modified tractor-semitrailer tanker.
12. Compare simulation results between the modified model to the original model and figure out if the modification led to the reduction of drag force and the tanker's instability, as well as establish recommendations on the optimal operating conditions for the tanker, such as setting a maximum speed to minimise the effect of the adverse weather conditions.
13. Discuss further studies on this topic to thoroughly investigate the adverse effects of strong crosswinds on the stability of semi-trailer tankers, such as the effect of gusty crosswinds on non-linear tractor-trailer tankers.

#### C. If time and resources permit:

14. Perform a transient simulation of the modified semi-trailer tanker under crosswind conditions

## Appendix B – Resource Requirements

### ENG4111/4112 Research Project Project Resources

1. Need access to the full license of the ANSYS CFD software, such as to set up an account on the uni's HPC to gain full access to ANSYS CFD.
2. Need access to or purchase 3D modelling software and textbooks, relevant publications and Australian standards, such as:
  - A 3D model with a datasheet of a particular prime mover, such as Kenworth T610 tractor.
  - ANSYS CFD theory and application, etc. ( Access through the ANSYS website)
  - 3D modelling software such as Autodesk Inventor Student (Can be downloaded via the Autodesk website)
  - The Australian Design Rules (ADRs) for heavy vehicles. (Can be downloaded via <https://www.infrastructure.gov.au/>).
  - Australian Standard (AS2809.1, AS2809.2, AS2809.3, AS2809.4) - Road tank vehicles for dangerous goods. (can be found in the USQ library)
  - The National Heavy Vehicle Regulation (NHVR). (Can be accessed via NHVR website)
  - The Static Roll Threshold (SRT) definition, formula and calculation (can be accessed via the NZ Transport Agency website).
  - The Performance Based Standards (PBS). (Can be accessed via NHVR website).

## Appendix C – Project Timelines

### ENG4111/4112 Research Project Project Plan

#### 1. Project Timelines

Numerical simulation and optimisation of the aerodynamic performance of a semi-trailer tanker

Uy Ngo  
0061058598

Project Start: Mon, 2/20/2023

Display Week: 1

				Semester 1/2023																BREAK	Semester 2/2023																	
				WEEK																																		
TASK	ASSIGNED TO	PROGRESS	START	END	1	2	3	4	5	6	7	8	9	10	11	12	13	14	15	16	17	18	1	2	3	4	5	6	7	8	9	10	11	12	13	14	15	16
Phase 1 - Preparation & Progress Report																																						
Project Approval		100%	20-Feb-23	26-Feb-23																																		
Project Specification		50%	27-Feb-23	05-Mar-23																																		
Literature Review & Research Methodology		0%	06-Mar-23	09-Apr-23																																		
Choose a prime mover with know drag and lift forces and perform CFD simulation		0%	10-Apr-23	16-Jun-23																																		
Validate simulation result with the known drag forces & coefficient data. Modify simulation setup if required.		0%	10-Apr-23	16-Jun-23																																		
Progress Report		0%	06-Mar-23	19-May-23																																		
Phase 2 - Continue Performing Simulation																																						
Build semi-trailer tanker model for simulation		0%	19-Jun-23	02-Jul-23																																		
Perform CFD Simulation		0%	03-Jul-23	01-Oct-23																																		
Modify trailer-tanker model to minimise drag forces		0%	03-Jul-23	01-Oct-23																																		
Analyse Results		0%	03-Jul-23	01-Oct-23																																		
Make Correction If Required		0%	03-Jul-23	01-Oct-23																																		
Phase 3 Finalise Dissertation																																						
Draft dissertation			17-Jun-23	01-Oct-23																																		
Finalise dissertation for submission			02-Oct-23	22-Oct-23																																		

#### 2. Communication Method

My supervisor (Dr Sharifian-Barforoush) and I have agreed on taking fortnightly meetings via email, telephone or online. Sometimes more frequent meetings will be held depending on the progress and due dates of the project.

## Appendix D – Risk Management

Eg 1. Enter Consequence

		Consequence				
		Insignificant No Injury 0-\$50K	Minor First Aid \$50K-\$50K	Moderate Med Treatment \$50K-\$100K	Major Serious Injuries \$100K-\$250K	Catastrophic Death More than \$250K
Eg 2. Enter Probability	Almost Certain 1 in 2	M	H	E	E	E
	Likely 1 in 100	M	H	H	E	E
	Possible 1 in 1000	L	M	H	H	H
	Unlikely 1 in 10 000	L	L	M	M	M
	Rare 1 in 1 000 000	L	L	L	L	L
Recommended Action Guide						
E-Extreme Risk - Task MUST NOT proceed						
H-High Risk - Special Procedures Required (See USQSafe)						
M-Moderate Risk - Risk Management Plan/Work Method Statement Required						
L-Low Risk - Use Routine Procedures						

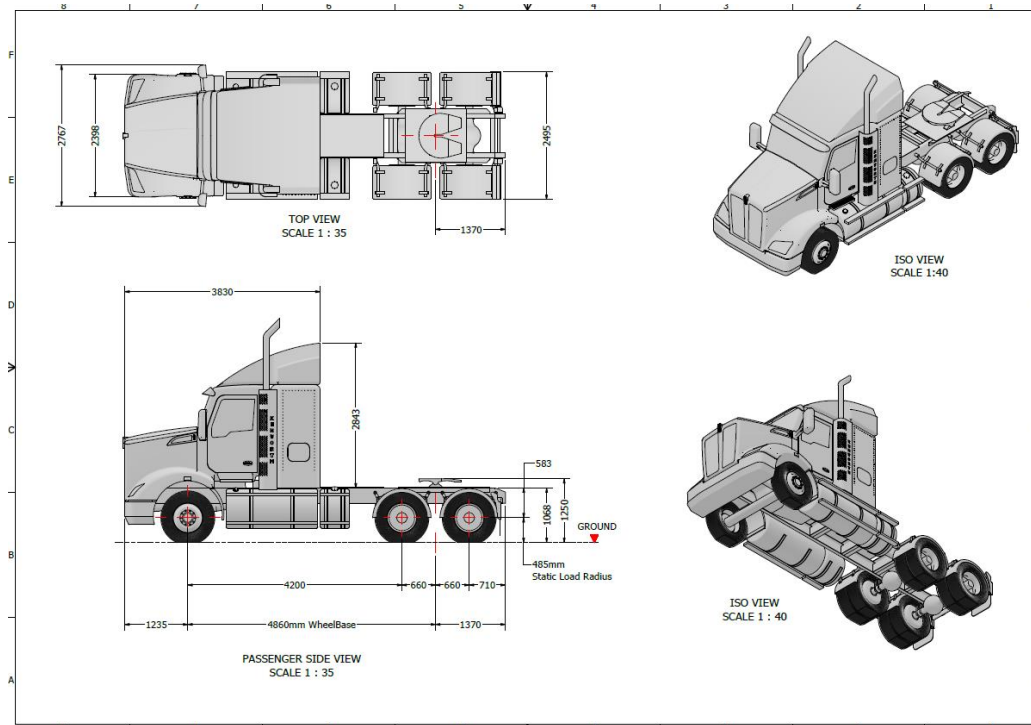
Eg 3. Find Action

Step 1 (cont)	Step 2	Step 2a	Step 2b	Step 3			Step 4				
<i>Hazards:</i> From step 1 or more if identified	<i>The Risk:</i> What can happen if exposed to the hazard without existing controls in place?	<i>Consequence:</i> What is the harm that can be caused by the hazard without existing controls in place?	<i>Existing Controls:</i> What are the existing controls that are already in place?	<i>Risk Assessment:</i> Consequence x Probability = Risk Level			<i>Additional controls:</i> Enter additional controls if required to reduce the risk level	<i>Risk assessment with additional controls:</i>			
				Probability	Risk Level	ALARP? Yes/no		Consequence	Probability	Risk Level	ALARP? Yes/no
<b>Example</b>											
Working in temperatures over 35° C	Heat stress/heat stroke/exhaustion leading to serious personal injury/death	catastrophic	Regular breaks, chilled water available, loose clothing, fatigue management policy.	possible	high	No	temporary shade shelters, essential tasks only, close supervision, buddy system	catastrophic	unlikely	mod	Yes
Long working hours on computer	Back and muscle pain or injuries. Fatigue due to long hours working with computer which leads to personal injuries such as falling off chair, collapsing due to low sugar level.	Minor	Regular breaks, have food regularly and prepare fatigue management plans	Rare	Low	Yes	Set maximum working hours each day	Insignificant	Unlikely	Low	Yes

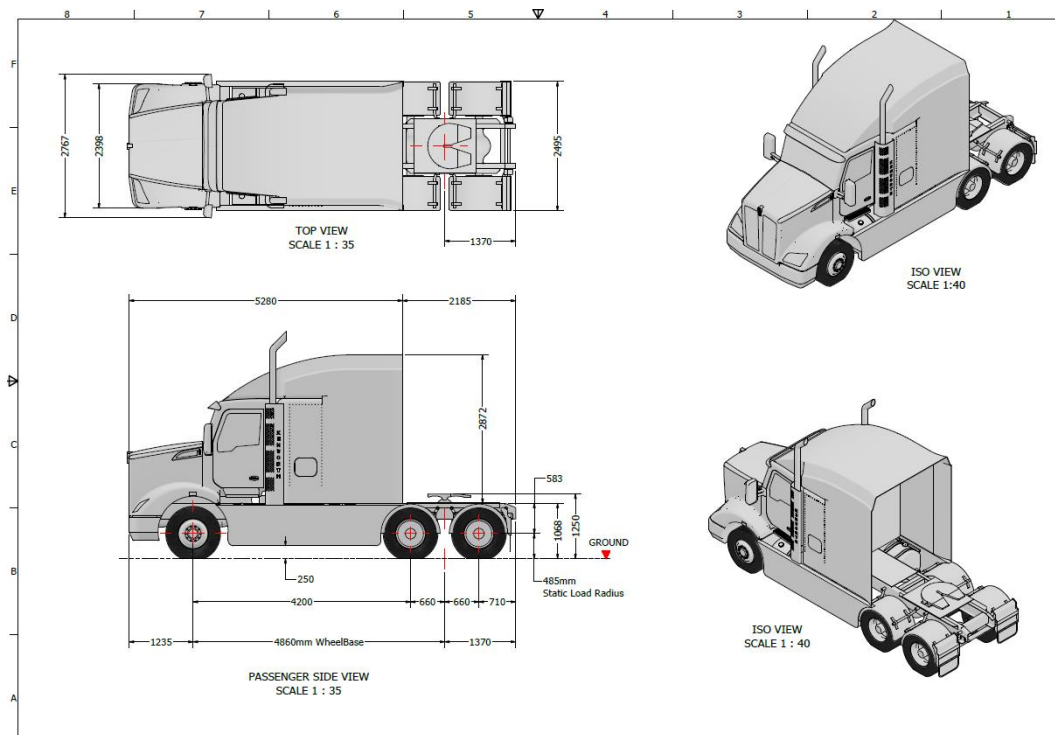


## Appendix E – Semi-Trailer Tanker Specification

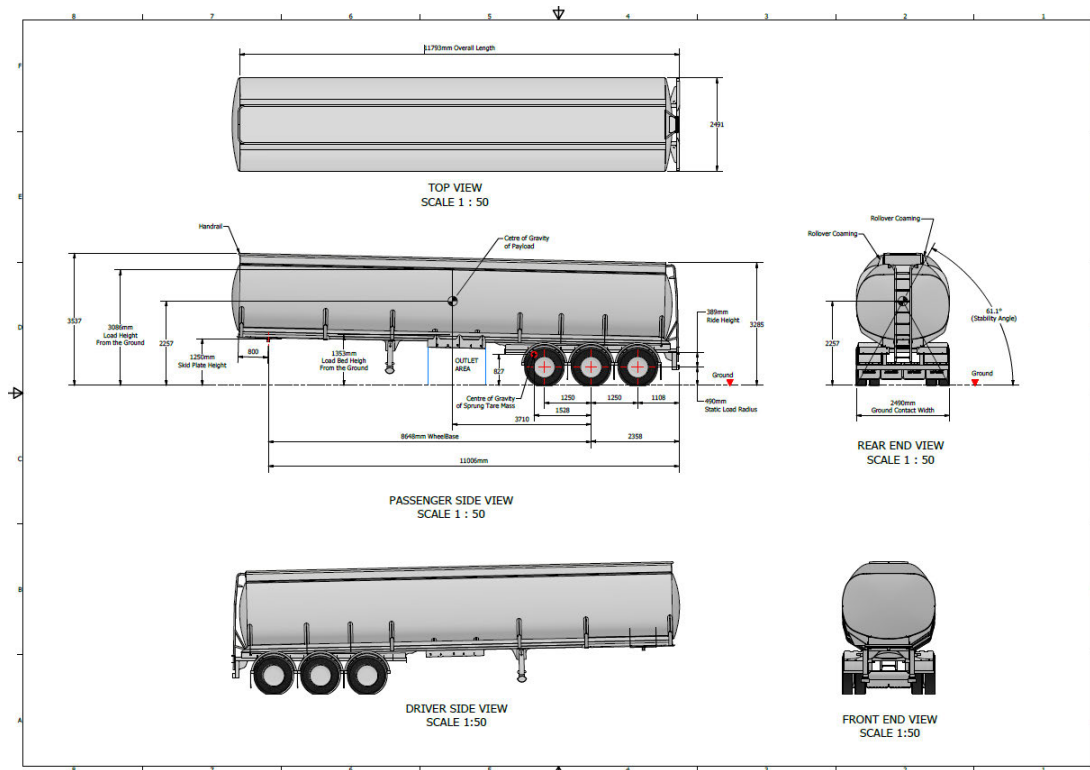
### E.1 Geometry of the Baseline Kenworth 6x4 T610



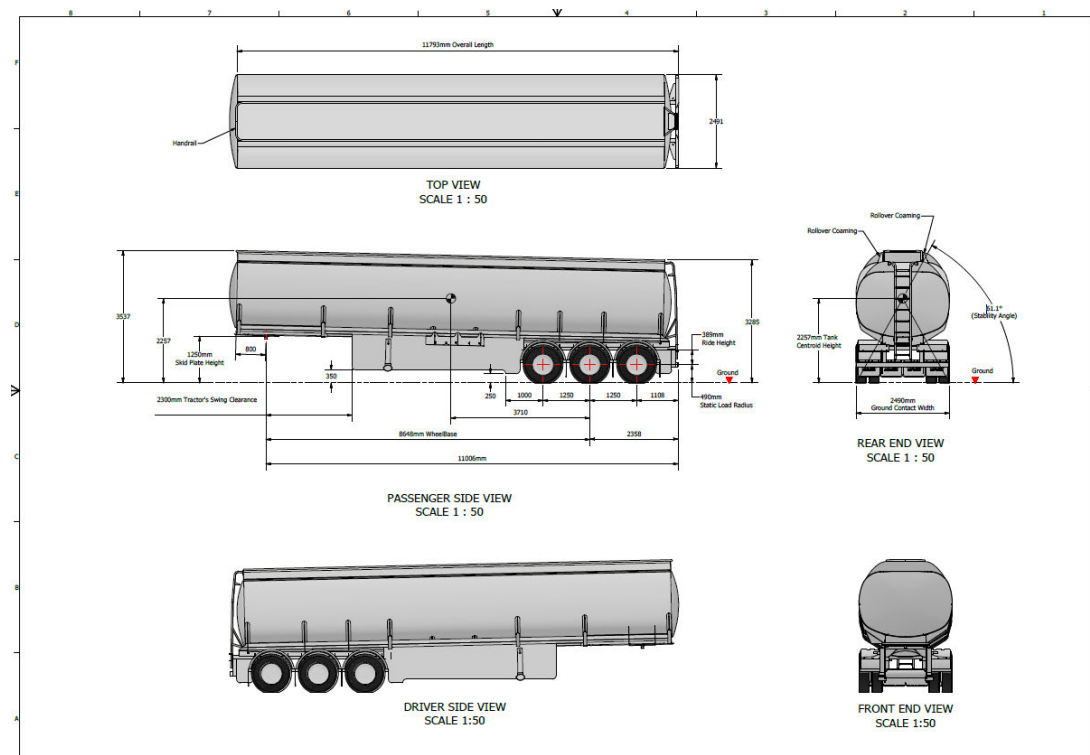
### E.2 Geometry of the Kenworth 6x4 T610 tractor with tractor side skirts and tractor-trailer gap fairing



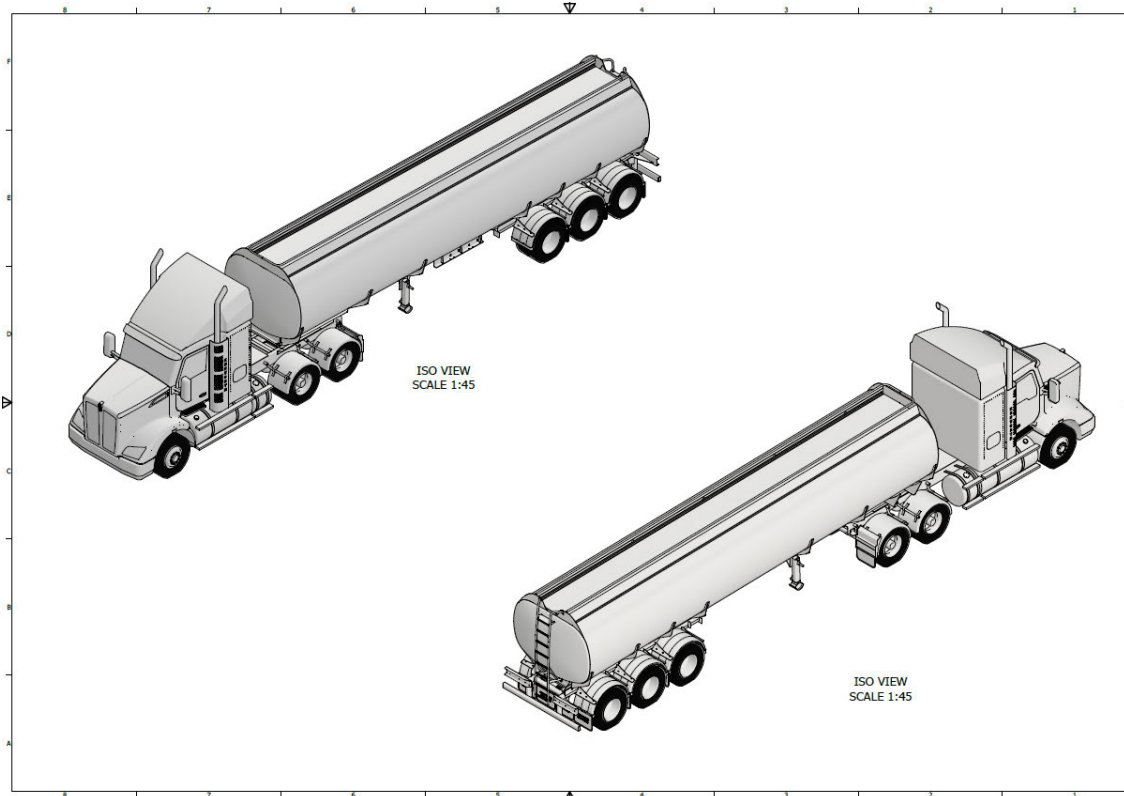
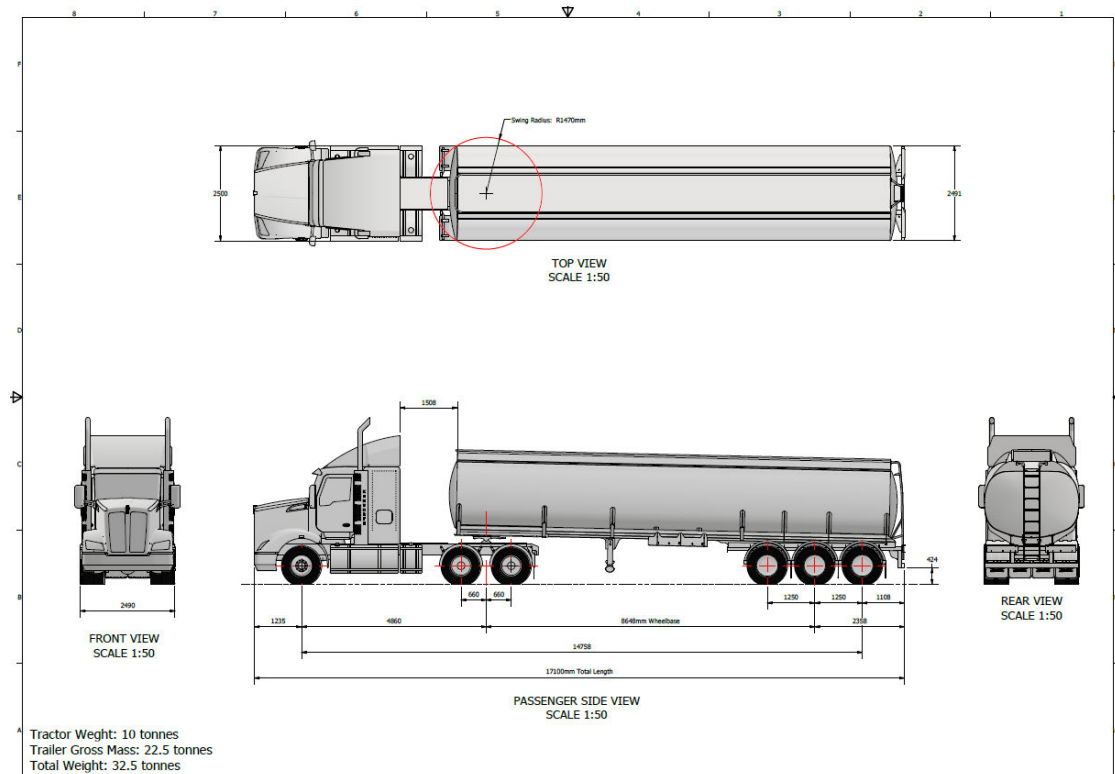
### E.3 The geometry of a baseline semi-trailer tanker



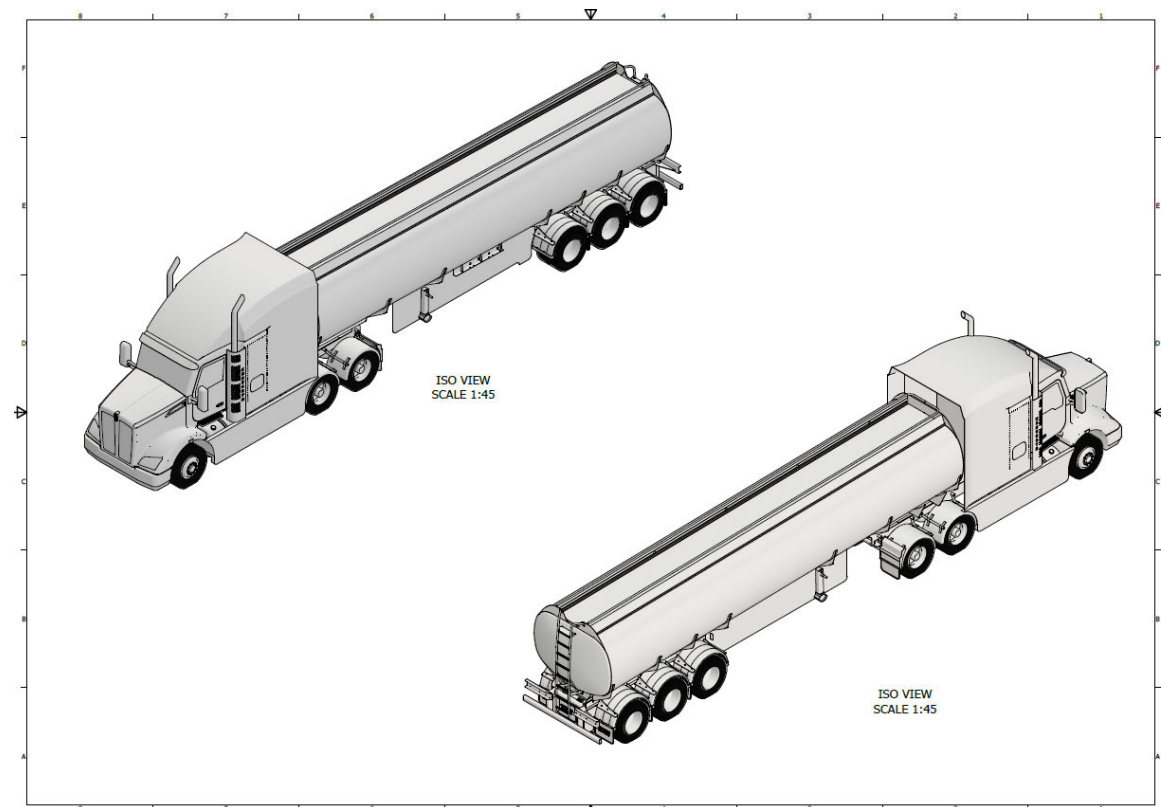
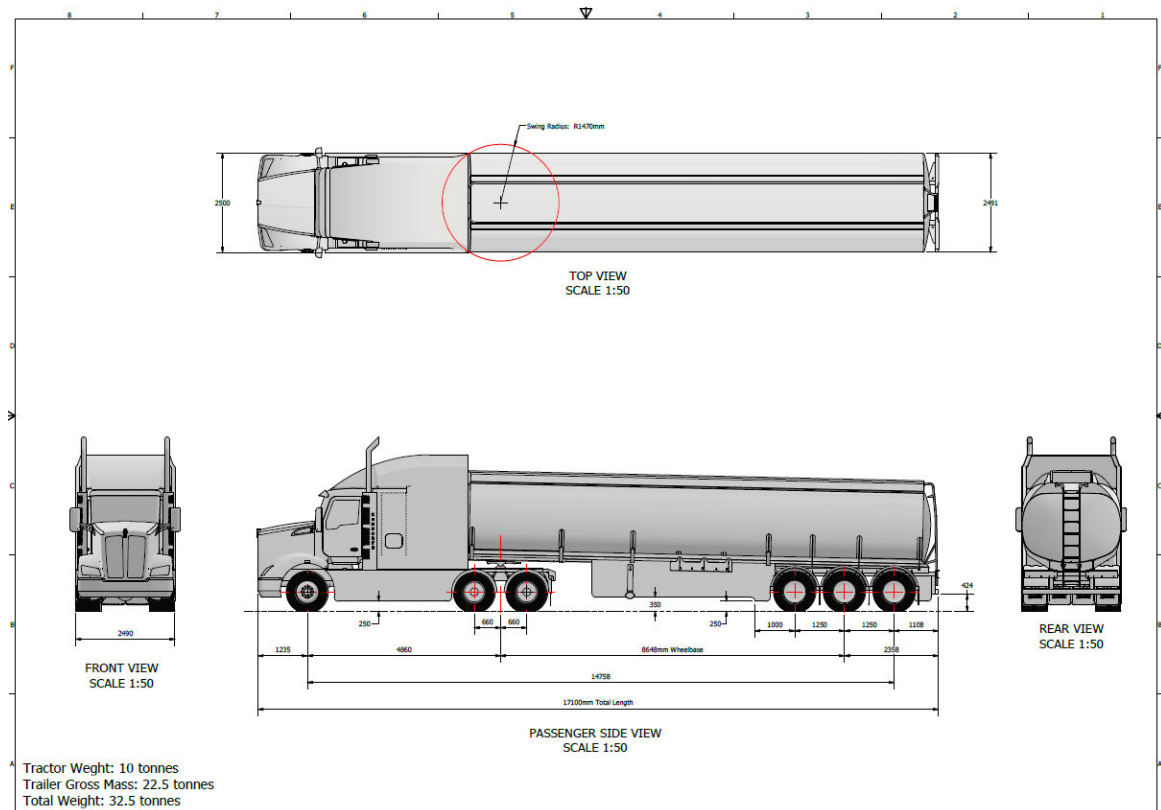
### E.4 The geometry of a semi-trailer tanker with side skirts



## E.5 Geometry of baseline tractor-semitrailer



## E.6 Geometry of tractor-semitrailer tanker equipped with aerodynamic devices

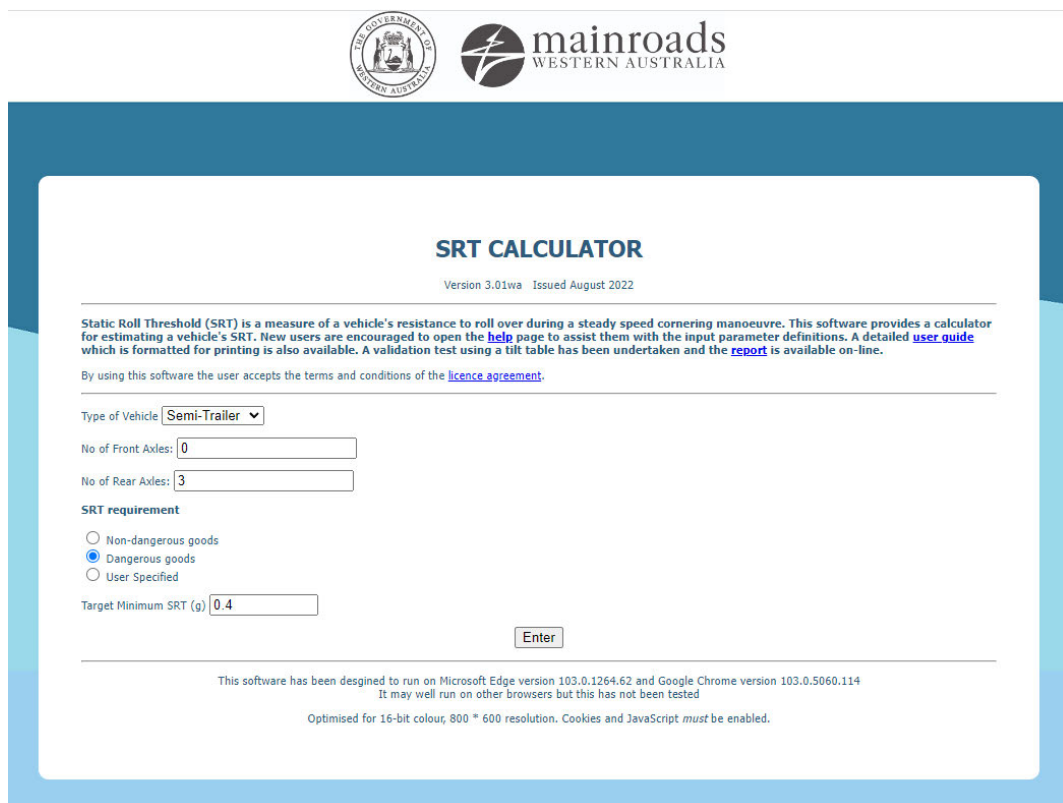


## Appendix F – SRT calculators

### F.1 SRT calculator published by Western Australia Government

(Link: <https://mrwebapps.mainroads.wa.gov.au/srtcalculator/>)

- Starting the SRT calculator opens an input page with the option to select the type of truck, whether a truck, semi-trailer, dog trailer, pig trailer, or other trucks.



The screenshot shows the 'SRT CALCULATOR' web application. At the top, there are logos for the Western Australian Government and Mainroads Western Australia. The title 'SRT CALCULATOR' is centered, with 'Version 3.01wa Issued August 2022' below it. A paragraph explains that the Static Roll Threshold (SRT) is a measure of a vehicle's resistance to roll over during a steady speed cornering manoeuvre. It mentions that new users should open the help page for input parameter definitions, and that a validation test using a tilt table has been undertaken. Below this, a link to the 'licence agreement' is provided. The form includes a 'Type of Vehicle' dropdown menu set to 'Semi-Trailer'. There are input fields for 'No of Front Axles' (0) and 'No of Rear Axles' (3). Under 'SRT requirement', there are three radio buttons: 'Non-dangerous goods', 'Dangerous goods' (which is selected), and 'User Specified'. A 'Target Minimum SRT (g)' input field is set to '0.4'. An 'Enter' button is located below the input fields. At the bottom, a disclaimer states that the software is designed to run on Microsoft Edge version 103.0.1264.62 and Google Chrome version 103.0.5060.114, and that it may not run on other browsers. It also mentions that the software is optimised for 16-bit colour, 800 \* 600 resolution, and that cookies and JavaScript must be enabled.

- Main data entry page. On this page, the first item is the schematic of the chosen truck type, followed by the groups of data input the user must provide to calculate the SRT value. These data include the tyre information, axle load, un-sprung mass, sprung mass, load categories, deck type, load geometry and suspension information.

## SRT CALCULATOR

<

New users are encouraged to open the [help](#) page to assist them with the input parameter definitions.

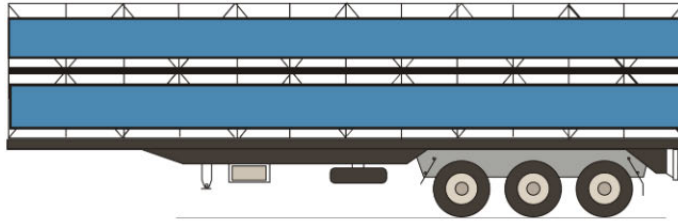


(Diagram as visual aid only :-)

### Tyre Data:

Axle	Tyre Size:	Tyre Configuration:	Maximum Ground Contact Width(m):
1	22.5 ▾	Dual ▾	2.42
2	22.5 ▾	Dual ▾	2.42
3	22.5 ▾	Dual ▾	2.42

### Axle Load Data:

	Rear	Total
Gross Mass:(kg)	<input type="text"/>	<input type="text"/>
Tare Mass:(kg)	<input type="text"/>	<input type="text"/>
Payload Mass:(kg)	<input type="text"/>	<input type="text"/>

### Unsprung Mass Data:

Axle	Unsprung Mass (kg):	Unsprung Mass Cg Height (m):
1	<input type="text" value="800"/>	<input type="text" value="0.49"/>
2	<input type="text" value="800"/>	<input type="text" value="0.49"/>
3	<input type="text" value="800"/>	<input type="text" value="0.49"/>

### Sprung Tare Mass:

Mass (kg)	<input type="text" value="-2400"/>
Centre of Gravity Height from the ground:(m)	<input type="text" value="1.74"/>

### Load Categories:

Mixed Freight ▾

### Deck Style:

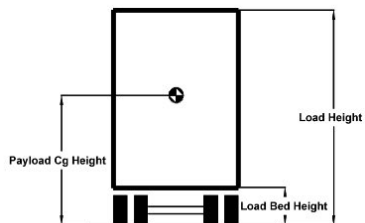
Standard ▾

### Load Geometry:

Load Bed Height from the ground:(m)

Load Height from the ground:(m)

Payload Cg Height from the ground:(m)  
(only required if load type is other)





## Suspension data:

Suspension Type:

### Rear

- ☐ Generic Air  
(low roll stiffness type)
- ☐ Generic Air  
(high roll stiffness type)
- ☒ Generic Steel
- ☐ User Defined:

### Enter data for 'User-Defined', optional for 'Generic':

Suspension Track Width:(m)

0.97

Axle lash:(mm)

30

### Please enter the following details for 'User-Defined':

Suspension brand/model:

Generic

Total Roll Stiffness / axle:(Nm/radian)

520000

Spring Stiffness / spring:(N/m)

1000000

Roll Center Height:(m)

0.2

(from axle center)

Calculate SRT

Reset Form

- The last page is the SRT result, in which the calculator compares the calculated SRT value with the minimum target value set on the first page. The calculator displays the result below if the SRT exceeds the minimum target value.

## SRT CALCULATION:

At a maximum load height of 4.2 metres and a maximum gross mass of 21 tonnes (being the sum of a payload mass of 13 tonnes and a tare mass of 8 tonnes), the SRT is 0.35g

This vehicle meets the minimum SRT standard of 0.35g.

Back

Finish

View Summary

If the calculated SRT is less than the minimum standard, the calculator determines the reduction in payload or the reduction in load height needed to bring the SRT up to the minimum standard. This is displayed as shown below.

## SRT Results

### SRT CALCULATION:

At a maximum load height of 4.2 metres and a maximum gross mass of 21 tonnes (being the sum of a payload mass of 13 tonnes and a tare mass of 8 tonnes), the SRT is 0.33g

This vehicle fails to meet the minimum SRT standard of 0.35g. It will meet the standard if:

- (a) At a maximum load height of 4.2 metres the maximum gross mass is 19.1 tonnes (being the sum of a payload mass of 11.1 tonnes and a tare mass of 8 tonnes)

OR

- (b) At a maximum gross mass of 21 tonnes (being the sum of a payload mass of 13 tonnes and a tare mass of 8 tonnes) the maximum allowable load height is 3.95 metres

The vehicle does achieve the minimum SRT standard of 0.35g at the following weight and height combinations:

Gross Mass (tonnes)	Load Height (m)
21	3.95
20	4.07
19	4.2

Note: Calculated load heights greater than the legal limit of 4.30m have been set to 4.30m

Back

Finish

View Summary

F.2 SRT calculator published by New Zealand Government (Link:  
[https://www.ternz.co.nz/SRT\\_Calculator/main.html](https://www.ternz.co.nz/SRT_Calculator/main.html))



## SRT CALCULATOR

New users are encouraged to open the [help](#) page to assist them with the input parameter definitions.

### Axle Load Data:

Gross Mass:(kg)  
Tare Mass:(kg)  
Payload Mass:(kg)

Front

Rear

Total

### Load Categories:

Uniform Density ▼

### Body Style:

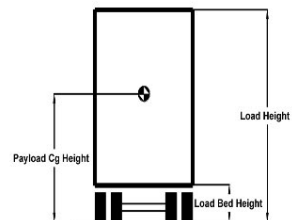
Sloping deck ▼

### Load Geometry:

Load Bed Height from the ground:(m)


Load Height from the ground:(m)

Payload Cg Height from the ground:(m)  
(only required if load type is other)



















### Suspension data:

## Appendix G – Semi-trailer general safety requirements



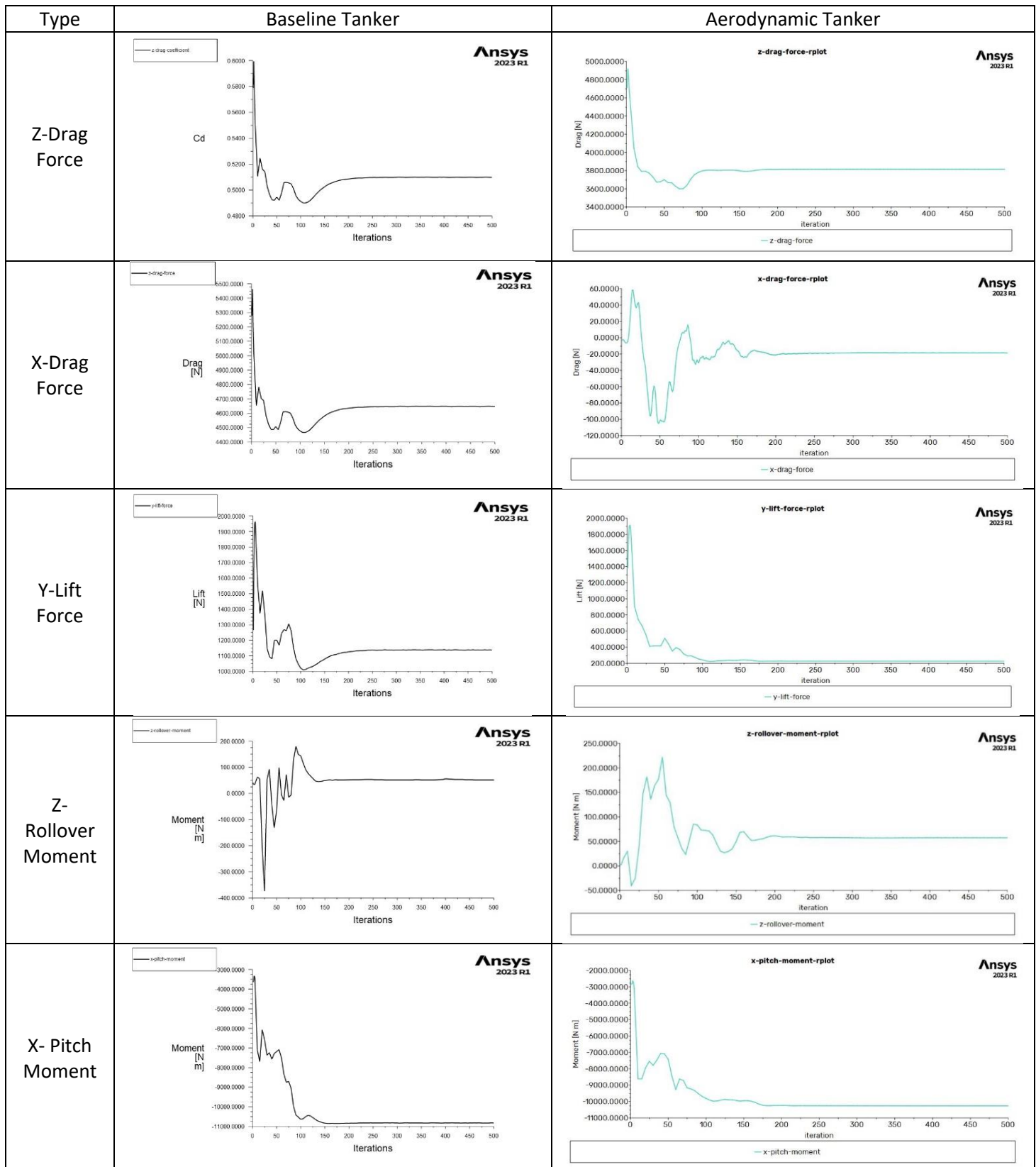
National Heavy Vehicle Regulator  
PBS Vehicle Configurations

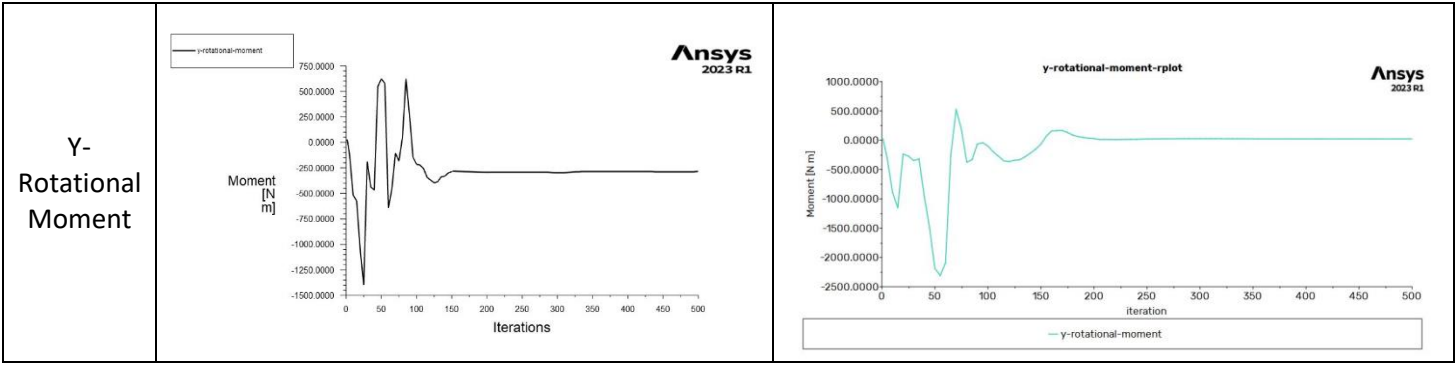
Disclaimer: This chart shows some of the NHVR-approved PBS heavy vehicle combinations used in Australia. Other heavy vehicle configurations may not be represented. The mass and length limits shown are from the Heavy Vehicle (Mass, Dimension and Loading) National Regulation (the MDL Regulation) and are provided for general guidance only. These limits are available only to vehicles that comply with all other regulatory requirements (e.g. width and height limits, tyre width, vehicle standards, load restraint, suspension type etc.). In some circumstances, other mass concessions and length limits may also be available. The NHVR website provides links to the MDL Regulation and to national and state Notices that may apply, depending on individual circumstances. For further information, contact the NHVR on 1300 MYNHVR (1300 696 487) at [info@nhvr.gov.au](mailto:info@nhvr.gov.au) or [www.nhvr.gov.au/contact-us](http://www.nhvr.gov.au/contact-us)

Common PBS vehicle configurations		Description	PBS level	Maximum length <sup>1</sup> (m)	Maximum permitted mass		
					GML (t)	CML (t)	HML (t)
PBS TRUCK AND DOG TRAILERS							
1		3-axle truck and 3-axle dog trailer	1	20.0	48.5	–	–
			2	20.0	48.5	49.5	49.5
2		3-axle truck and 4-axle dog trailer	1	20.0	50.5	–	–
			2	20.0	56.0	57.5	57.5
3		3-axle truck and 5-axle dog trailer	2	26.0	59.5	61.5	63.0
4		3-axle truck and 6-axle dog trailer	2	26.0	63.0	65.0	68.5
5		4-axle truck and 3-axle dog trailer	1	20.0	50.0	–	–
			2	20.0	53.0	54.0	54.0
6		4-axle truck and 4-axle dog trailer	1	20.0	50.0	–	–
			2	20.0	60.5	62.0	62.0
7		4-axle truck and 5-axle dog trailer	2	26.0	64.0	66.0	67.5
8		4-axle truck and 6-axle dog trailer	2	26.0	67.5	69.5	73.0
PBS PRIME MOVER AND SEMITRAILERS							
9		2-axle prime mover and 2-axle semitrailer	1	20.0	32.0	32.5	32.5
10		3-axle prime mover and 2-axle semitrailer	1	20.0	39.5	40.5	40.5
11		3-axle prime mover and 3-axle semitrailer	1	20.0	43.0	44.0	46.0
12		4-axle prime mover and 3-axle semitrailer	1	20.0	47.5	48.5	50.5
13		3-axle prime mover and quad-axle semitrailer	1	20.0	43.0	44.0*	50.5*
14		4-axle prime mover and quad-axle semitrailer	1	20.0	47.5	48.5*	55.0*
15		Prime mover and semitrailer with 2 axle groups (2-1)*	1	20.0	48.0	49.0	49.0
16		Prime mover and semitrailer with 2 axle groups (1-3)*	1	20.0	49.7	50.7	53.5*

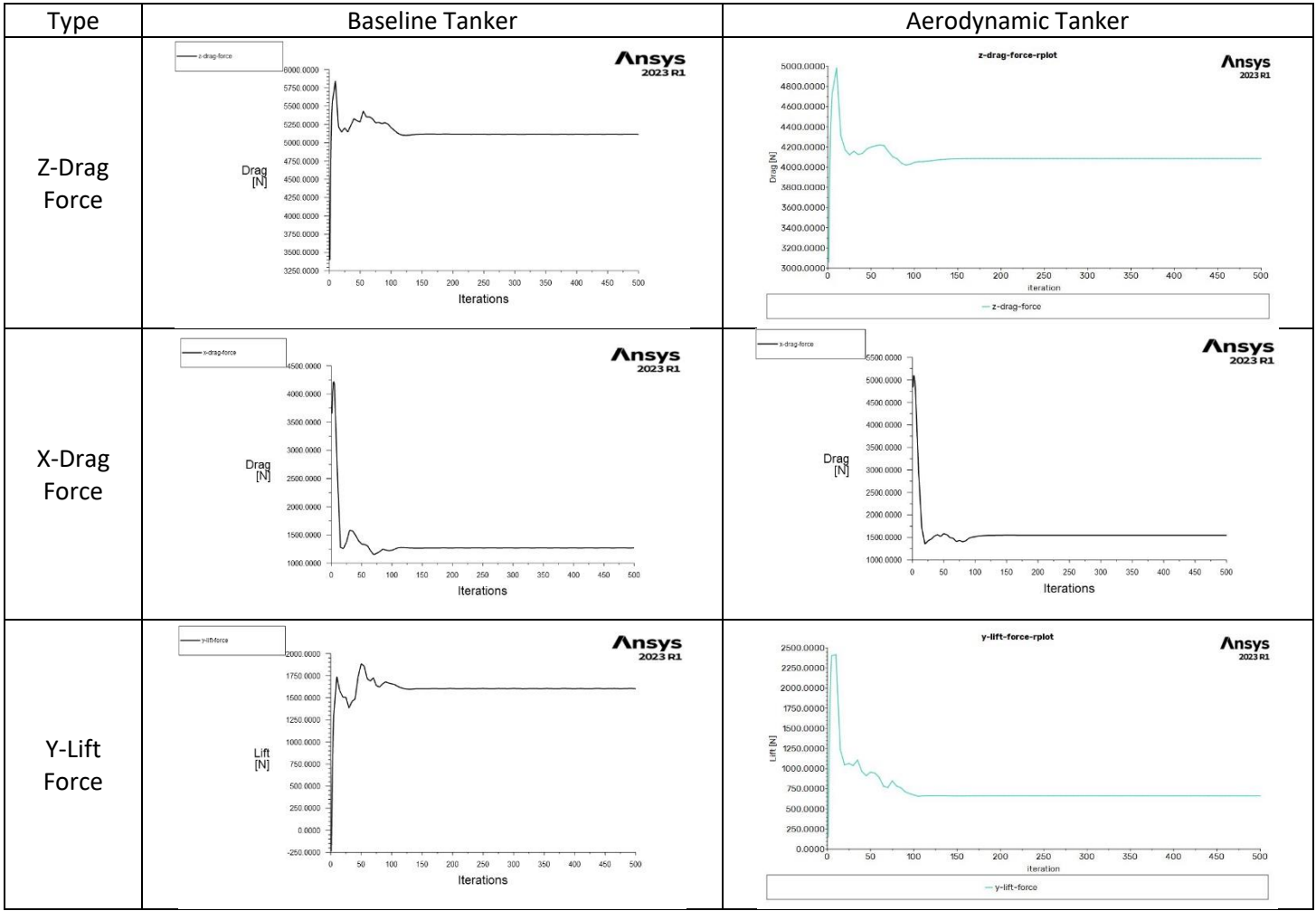
## Appendix H – Baseline and Aerodynamic Tankers Simulation Results Graphs and Contours

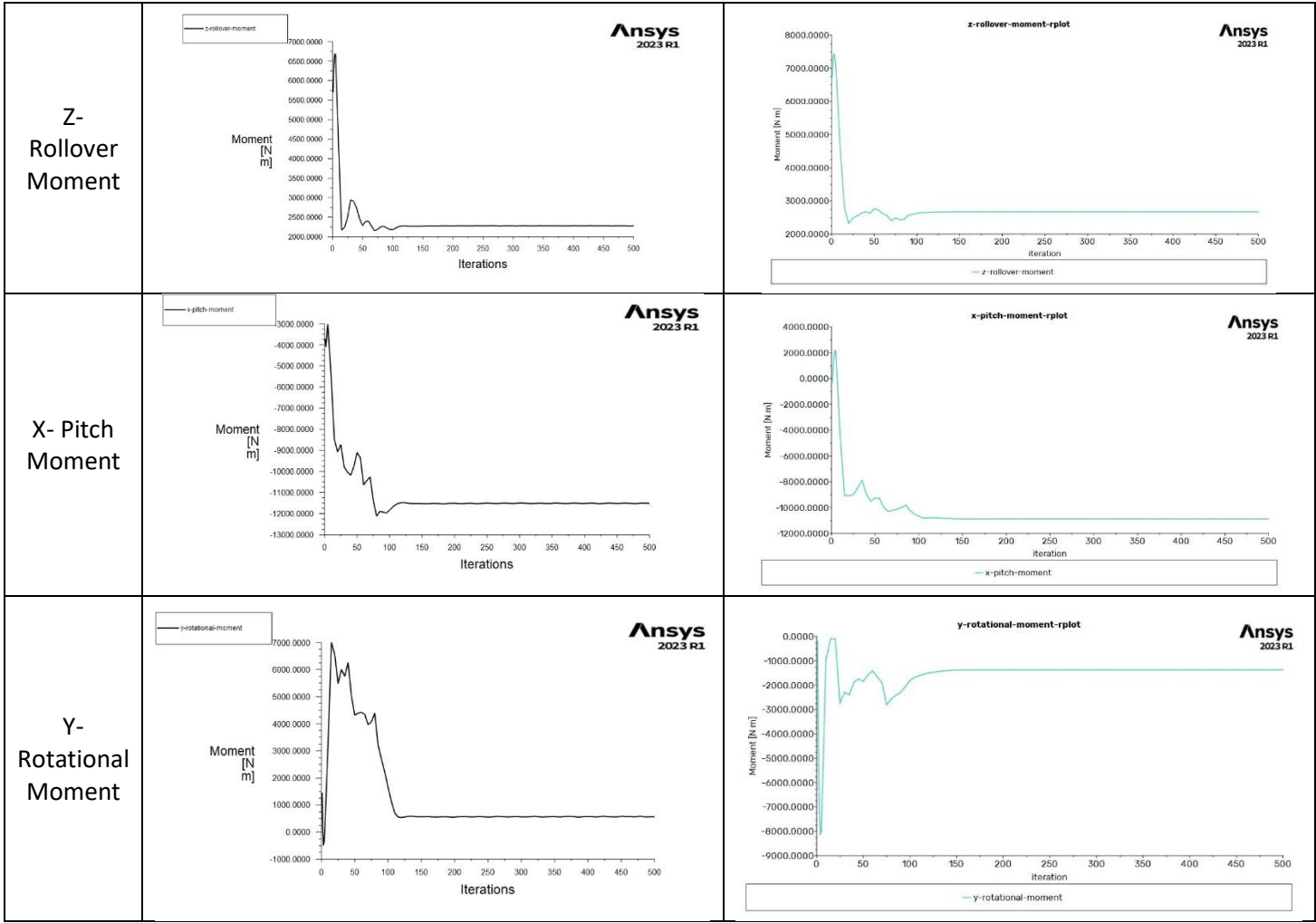
### H.1 X-Y Chart of Headwind Simulation:



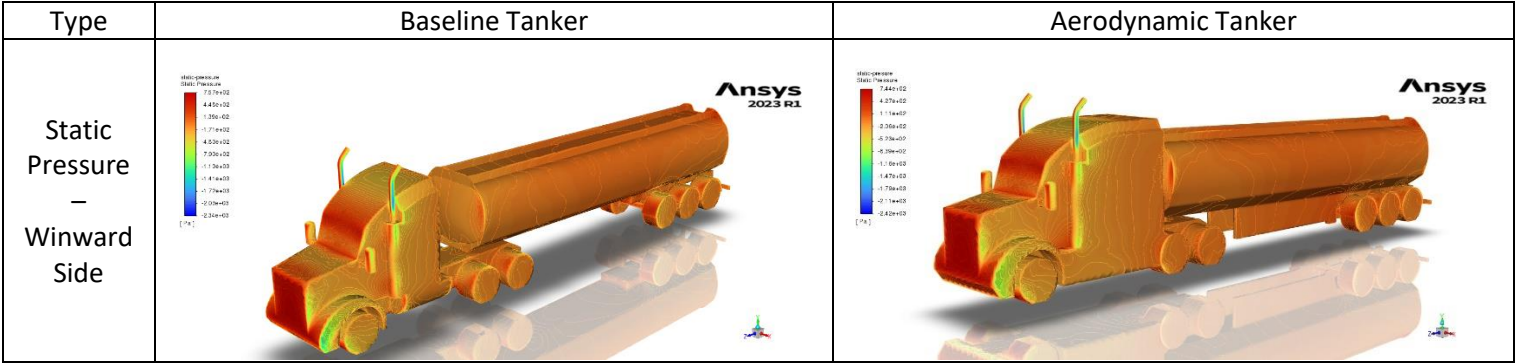


H.2 X-Y Chart of 15-Degree Crosswind Simulation:

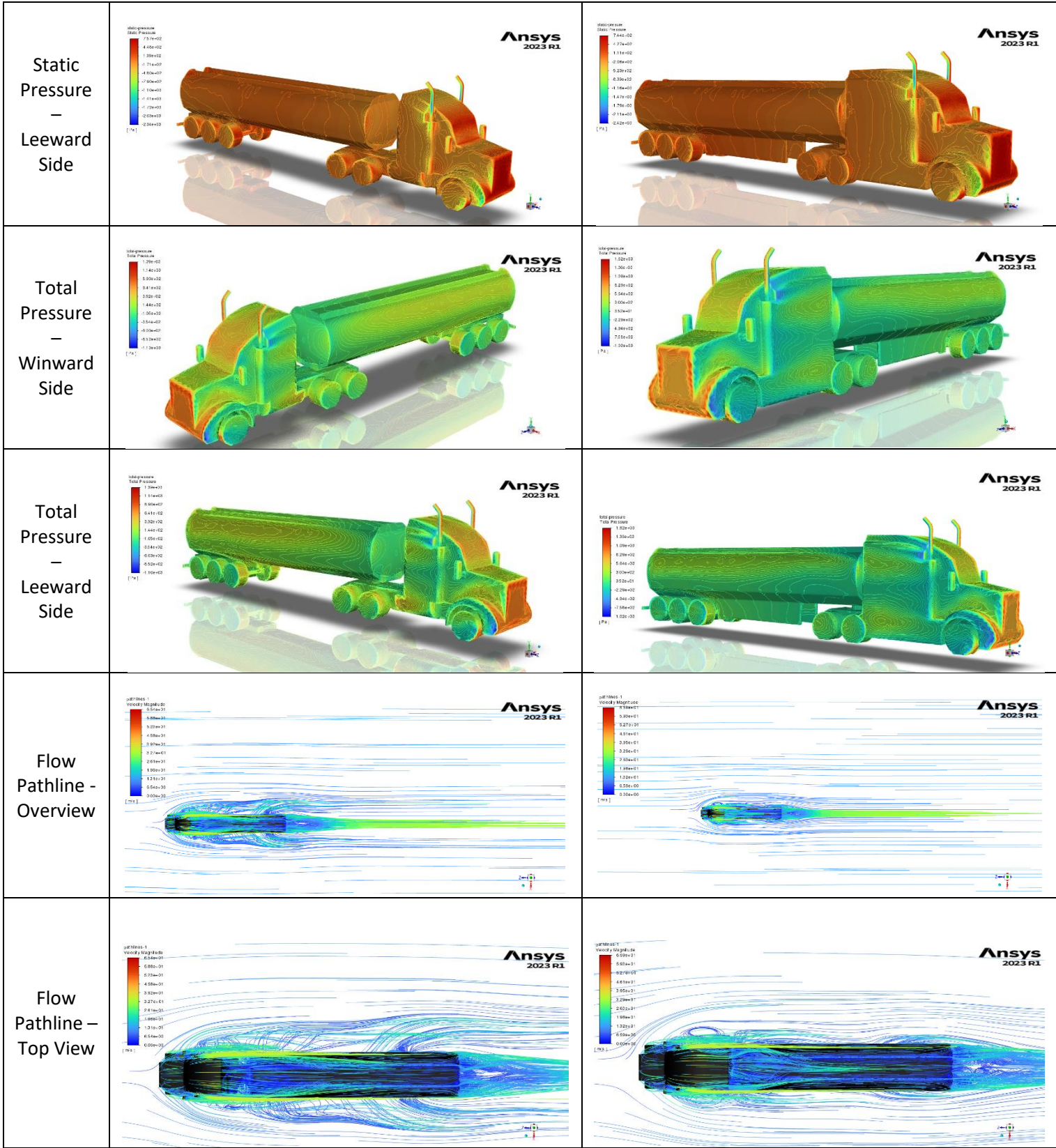




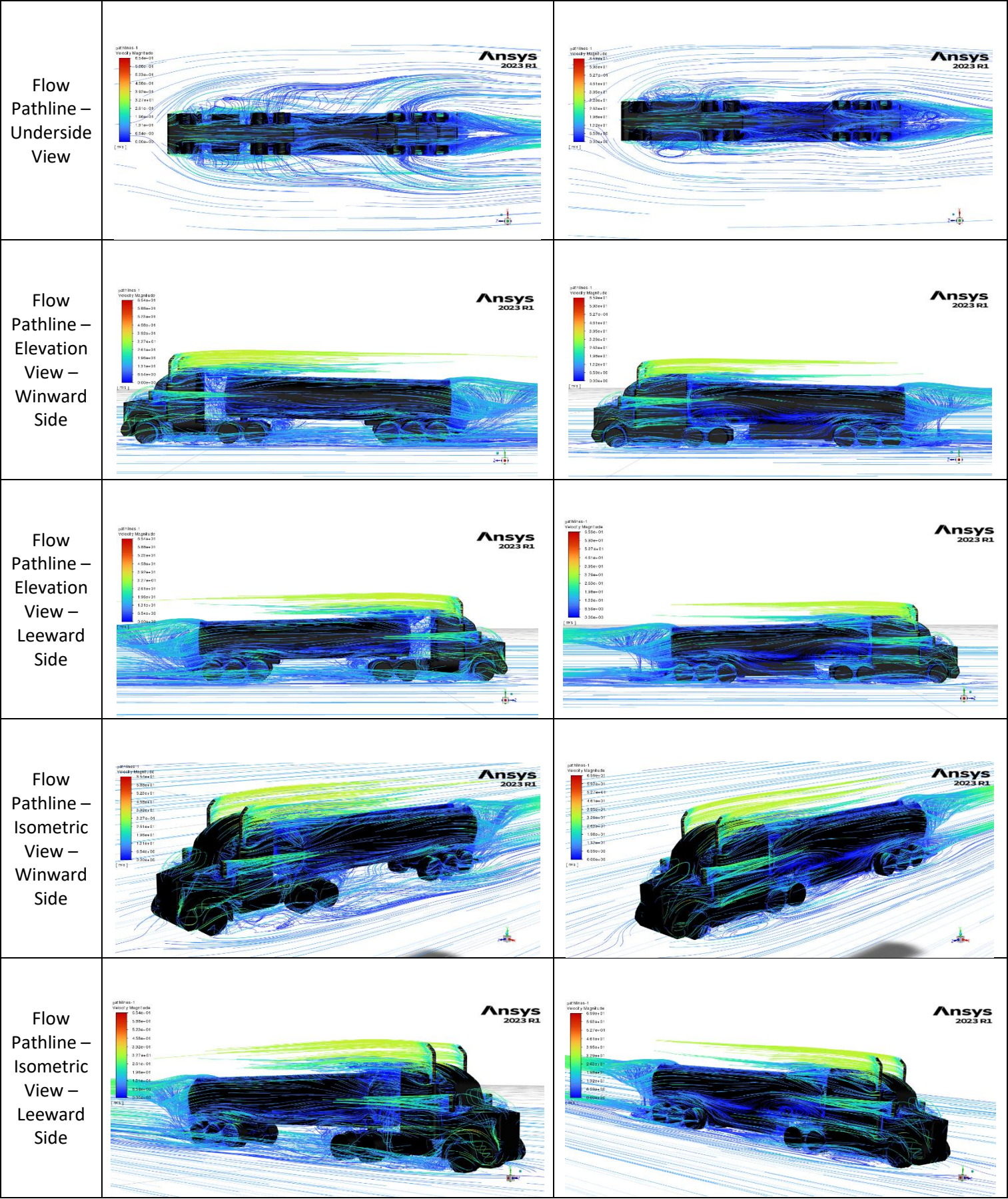
### H.3 Pressure Contours and Flow Pathlines of Baseline and Aerodynamic Tankers at 0-Degree Crosswind Angle





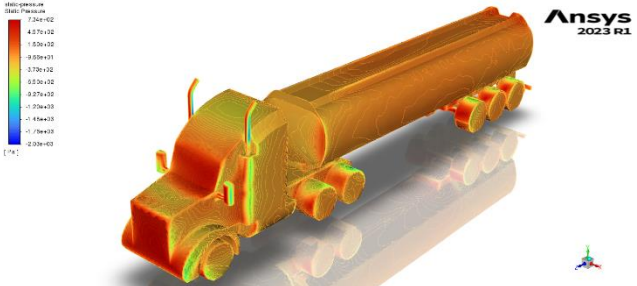
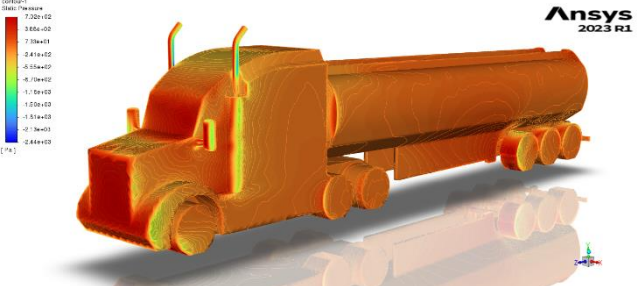
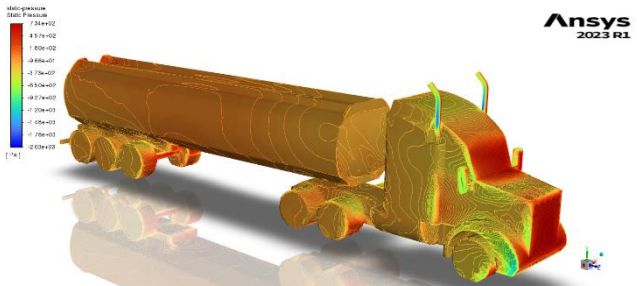
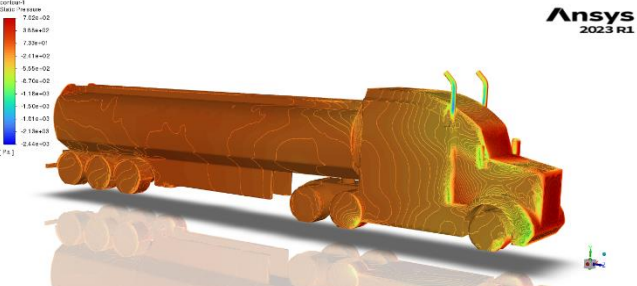
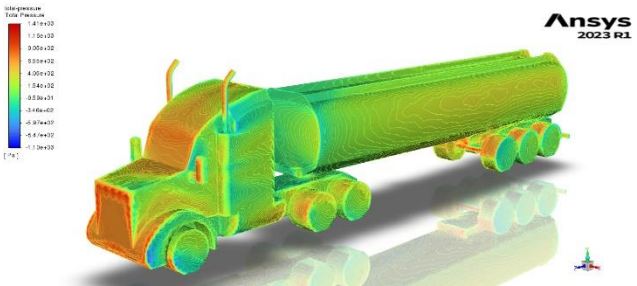
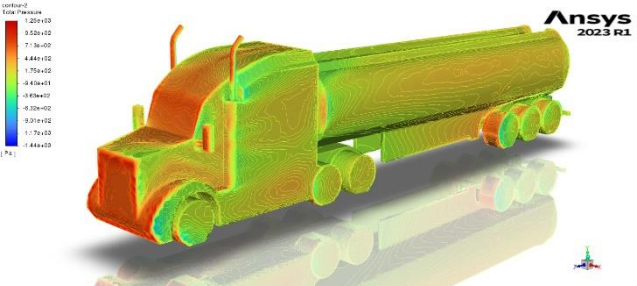
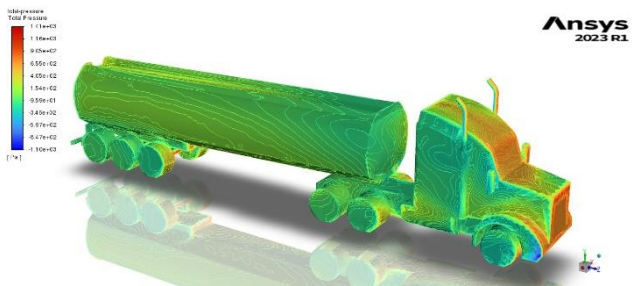
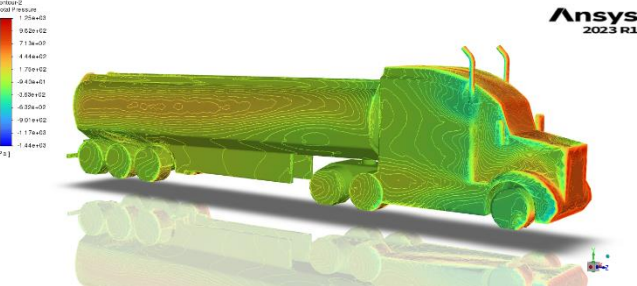
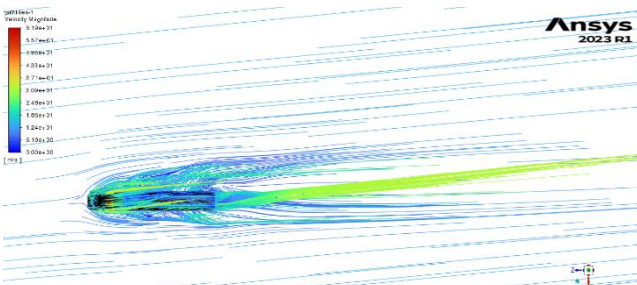
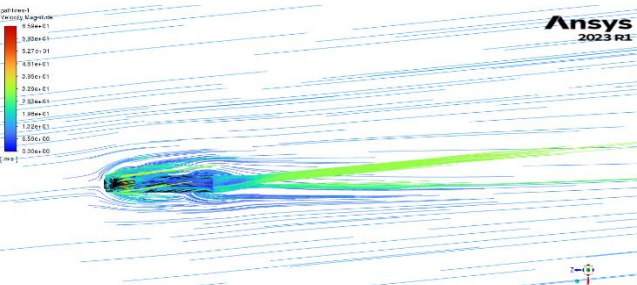




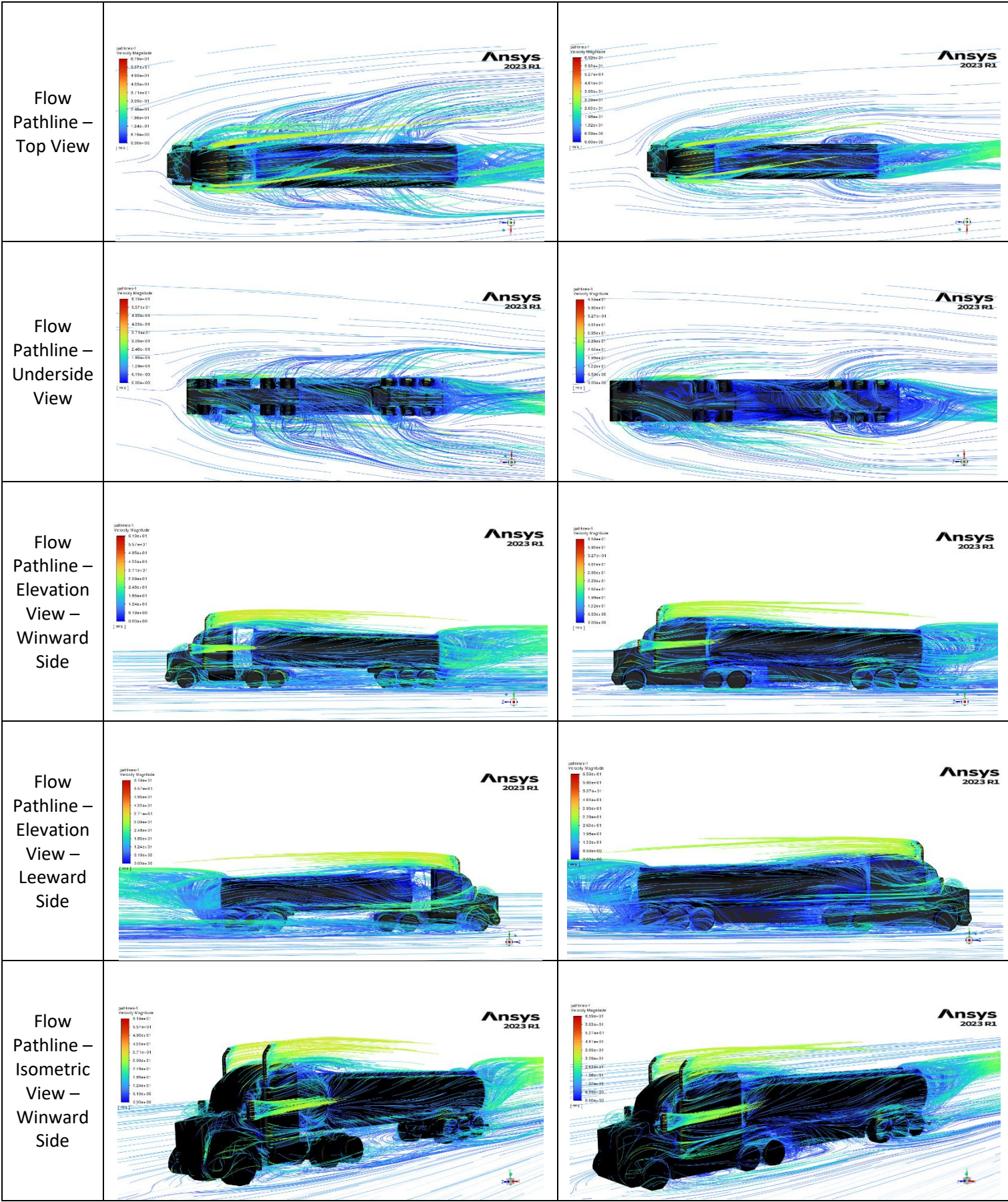




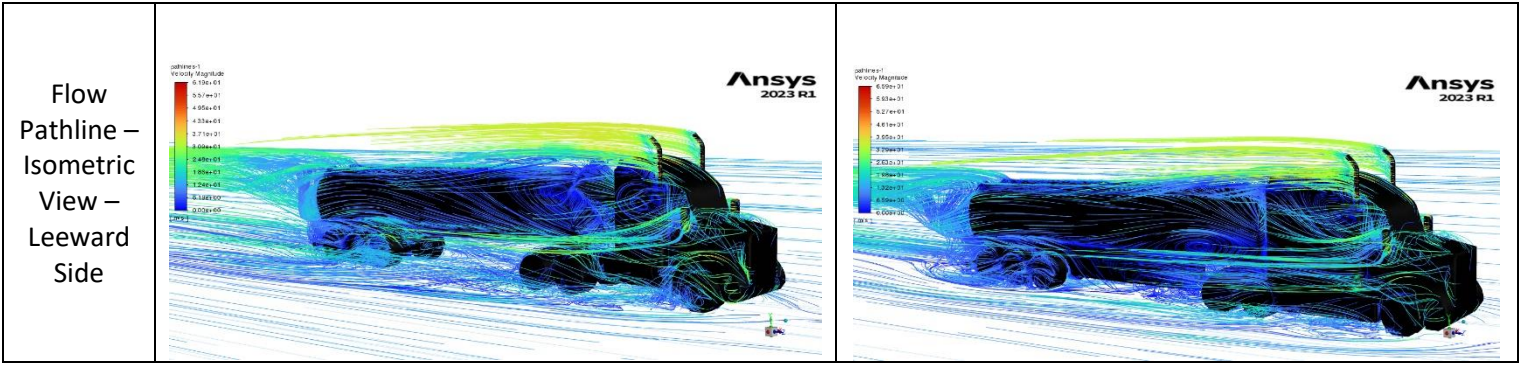
## H.4 Pressure Contours and Flow Pathlines of Baseline and Aerodynamic Tankers at 30-Degree Crosswind Angle

Type	Baseline Tanker	Aerodynamic Tanker
Static Pressure – Winward Side		
Static Pressure – Leeward Side		
Total Pressure – Winward Side		
Total Pressure – Leeward Side		
Flow Pathline - Overview		

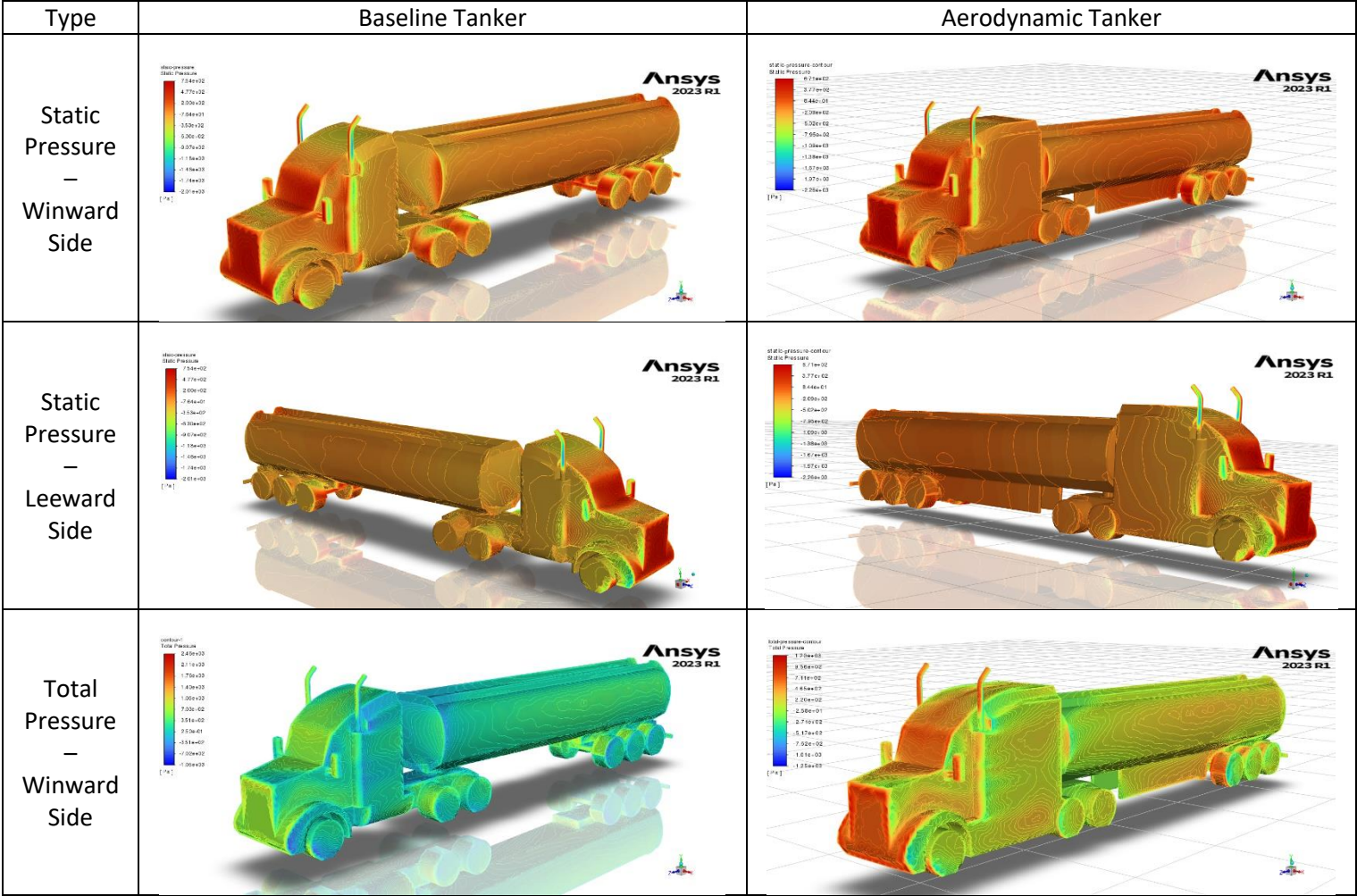




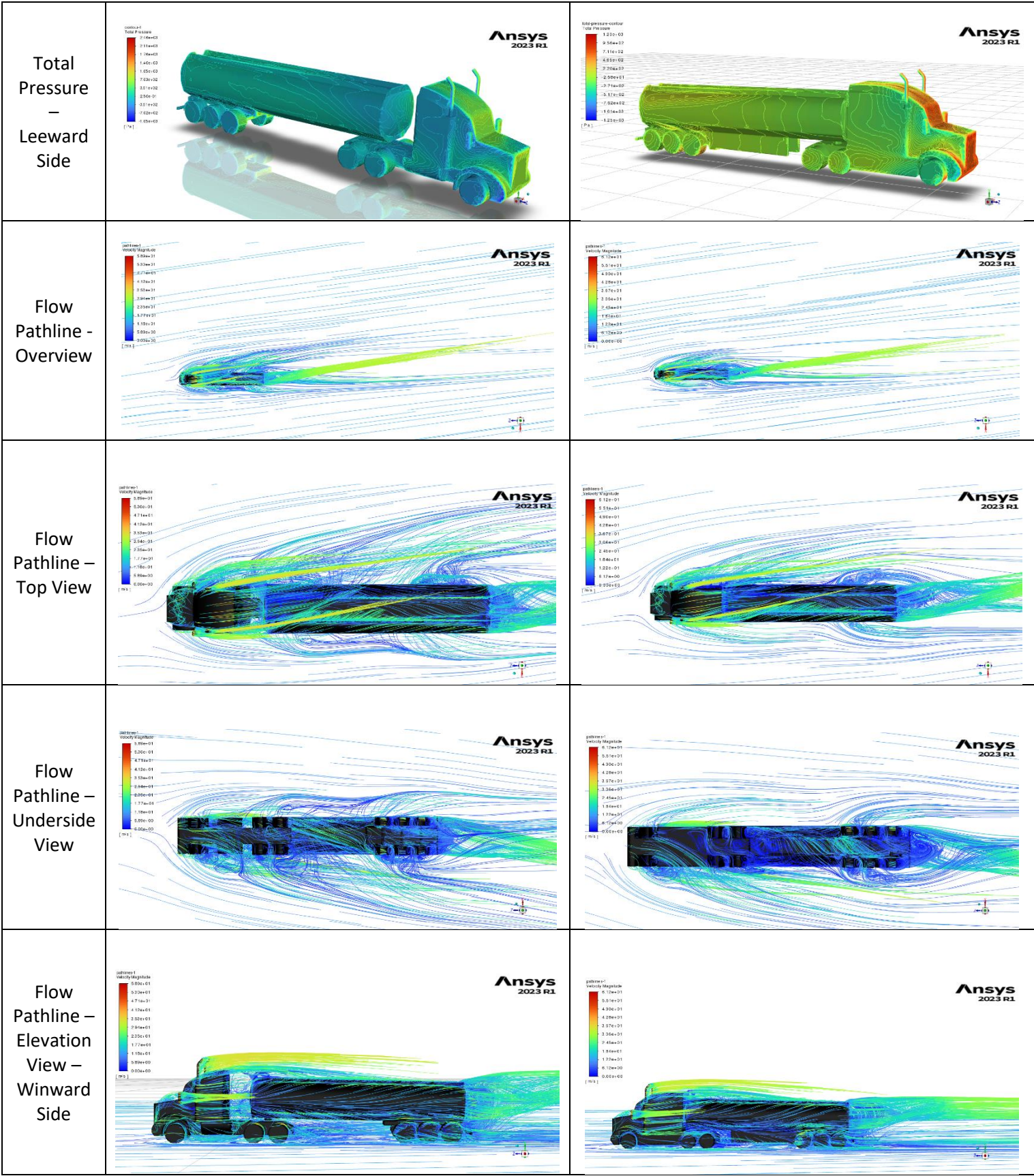




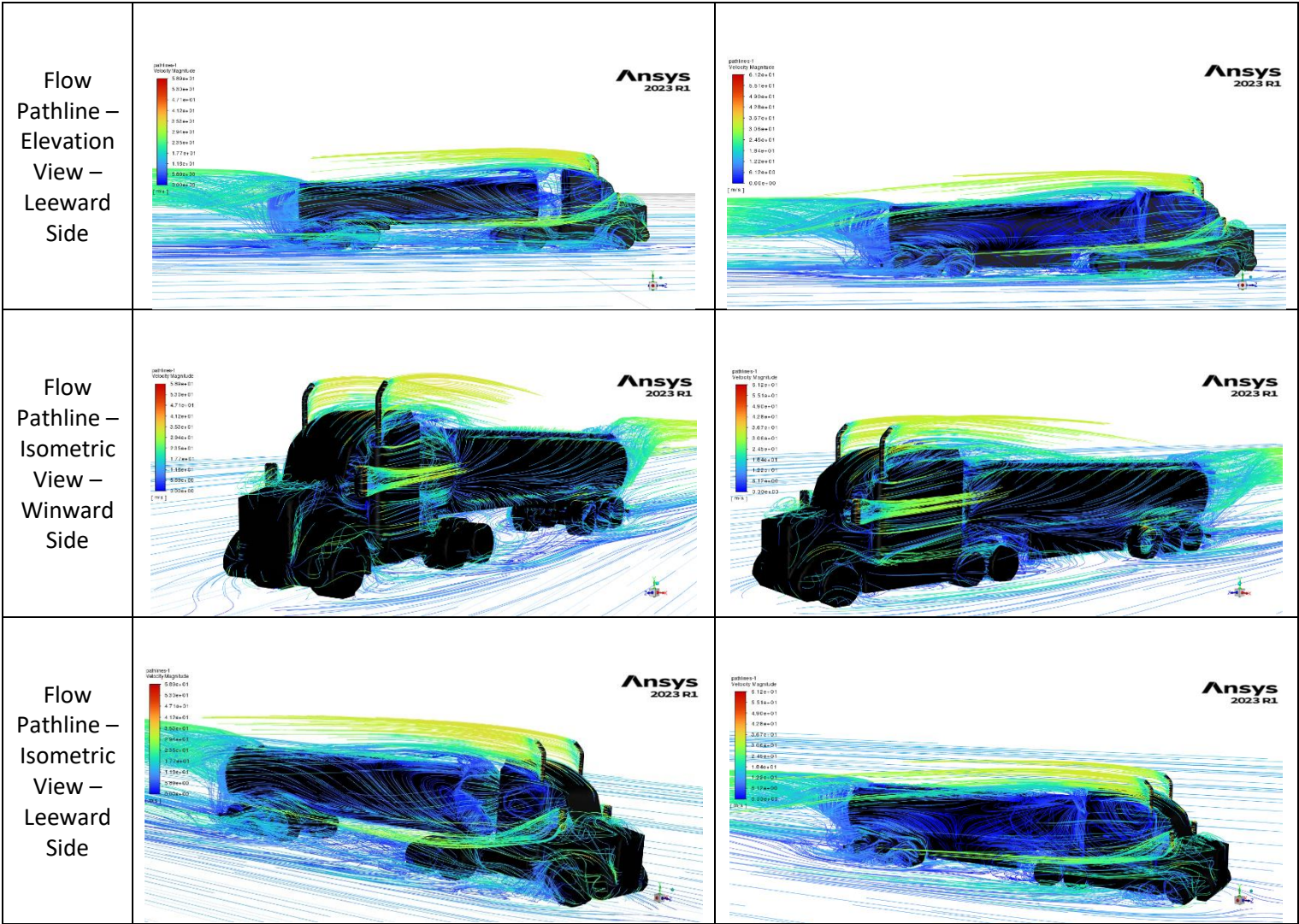
H.5 Pressure Contours and Flow Pathlines of Baseline and Aerodynamic Tankers at 45-Degree Crosswind Angle



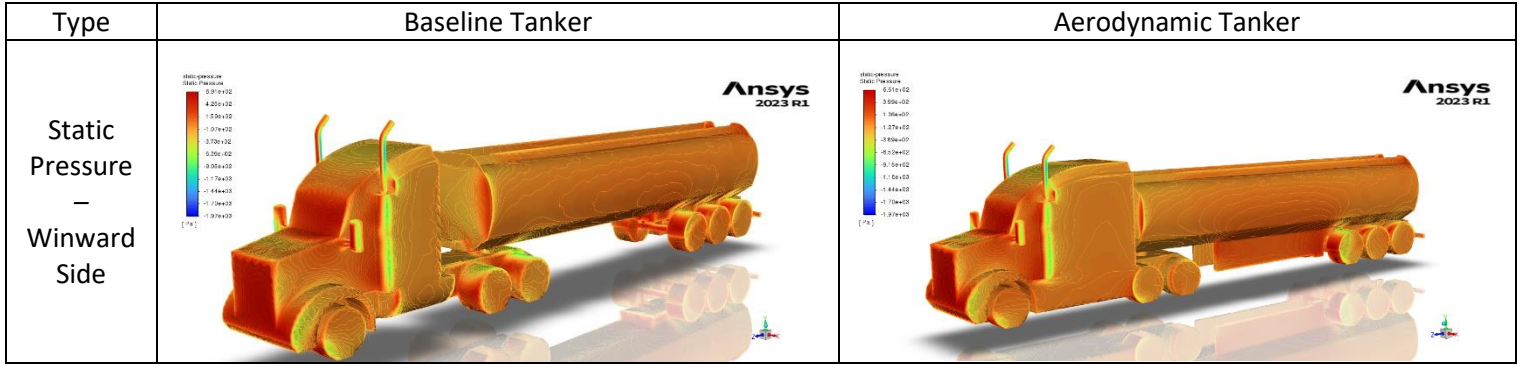




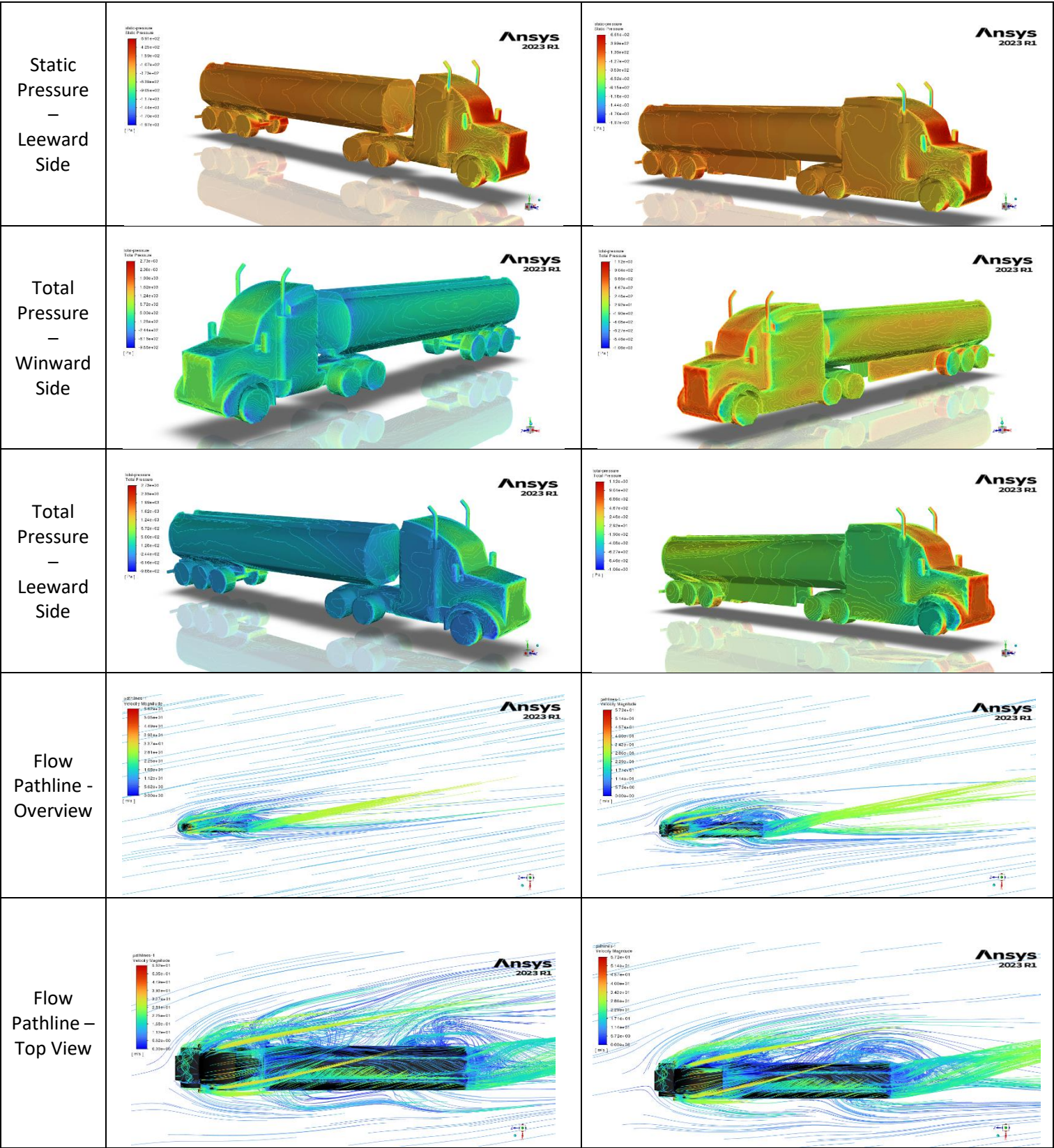




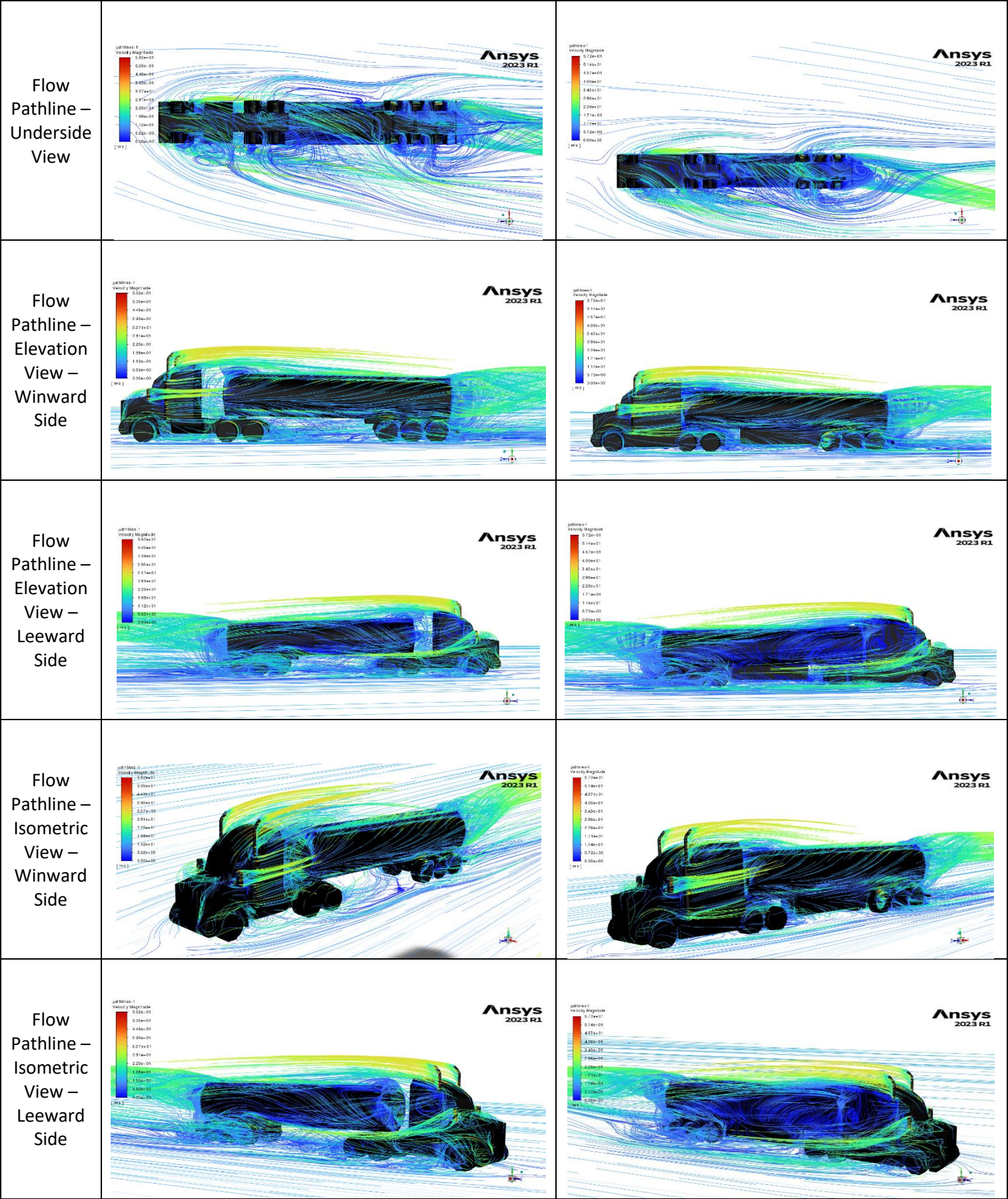
H.6 Pressure Contours and Flow Pathlines of Baseline and Aerodynamic Tankers at 60-Degree Crosswind Angle





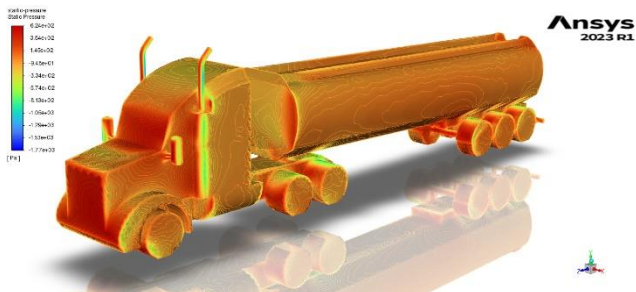
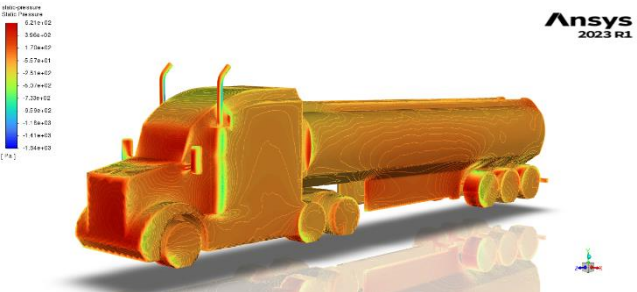
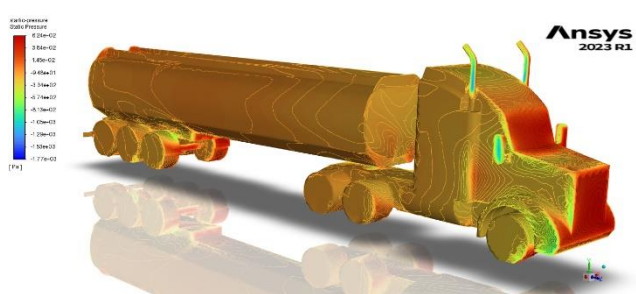
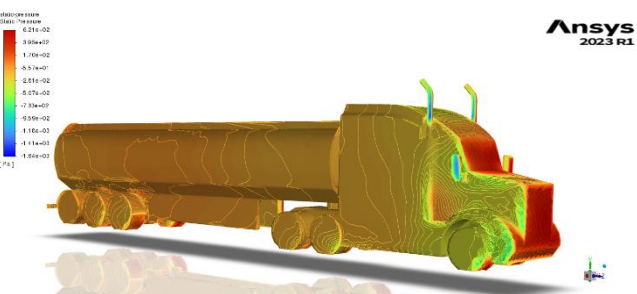
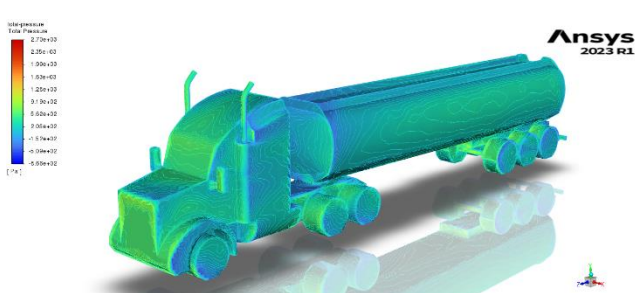
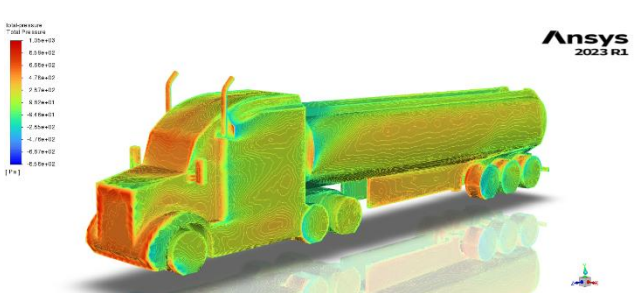
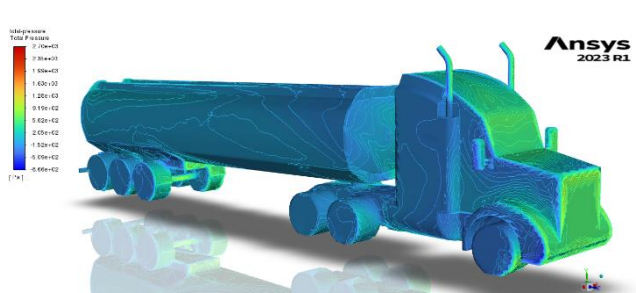
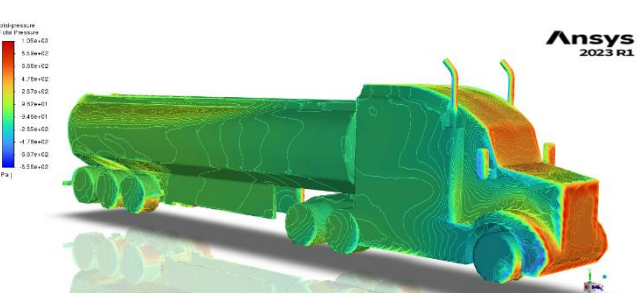
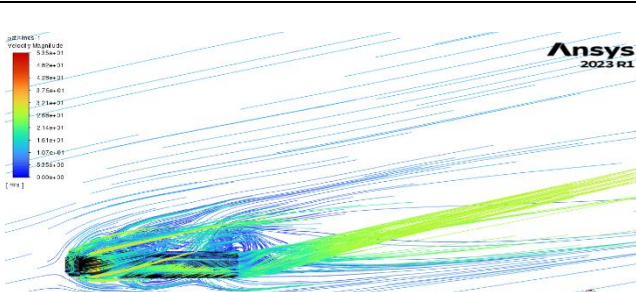
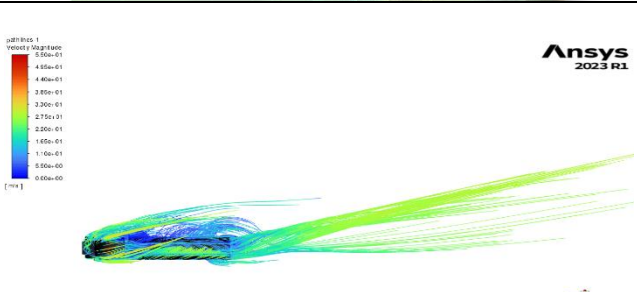




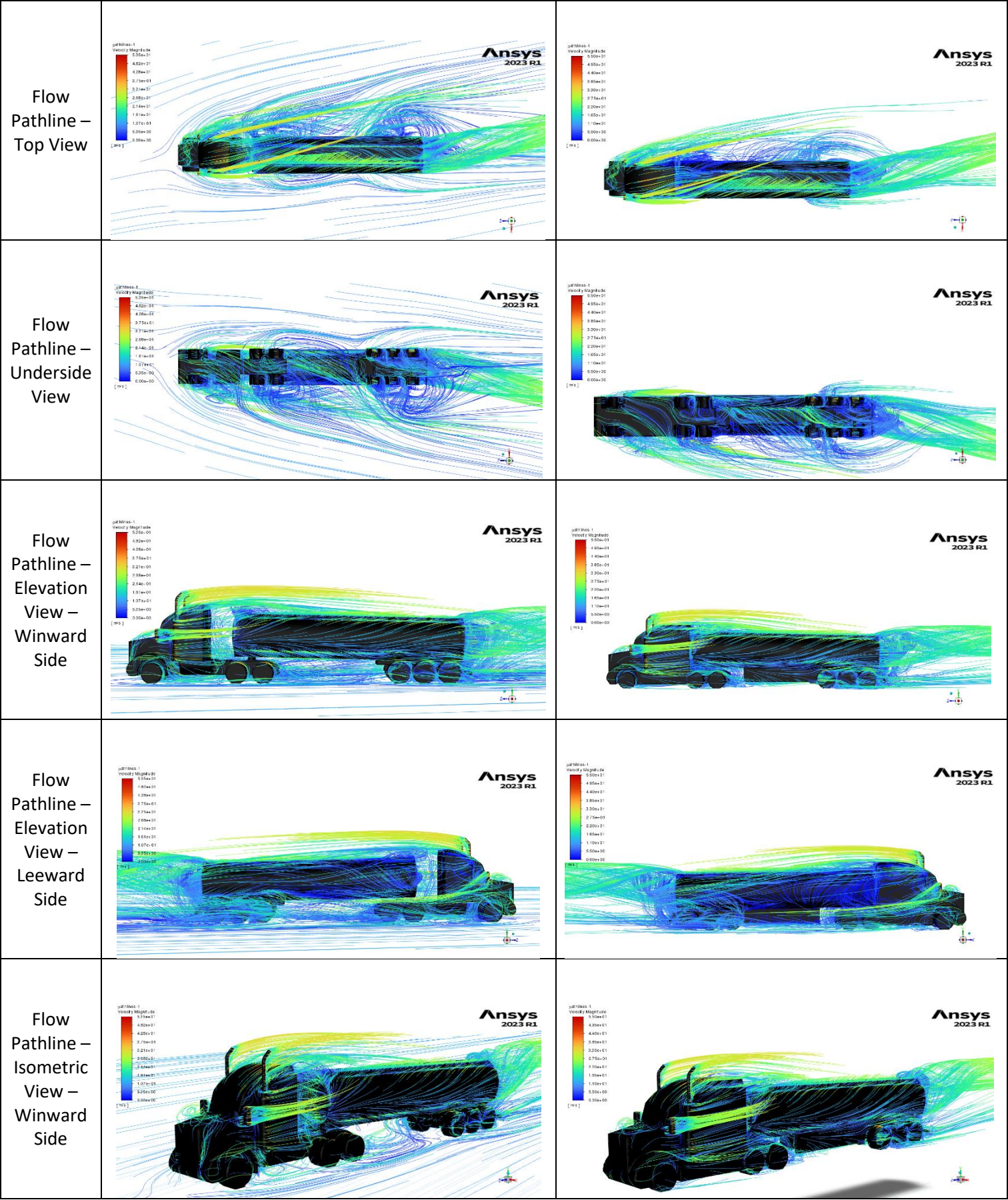




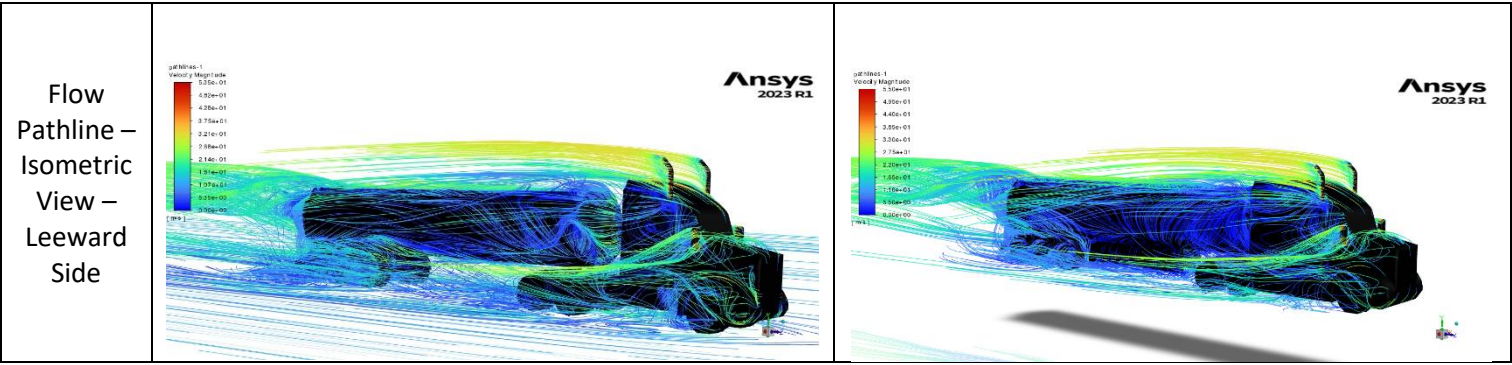
## H.7 Pressure Contours and Flow Pathlines of Baseline and Aerodynamic Tankers at 75-Degree Crosswind Angle

Type	Baseline Tanker	Aerodynamic Tanker
Static Pressure – Winward Side		
Static Pressure – Leeward Side		
Total Pressure – Winward Side		
Total Pressure – Leeward Side		
Flow Pathline - Overview		

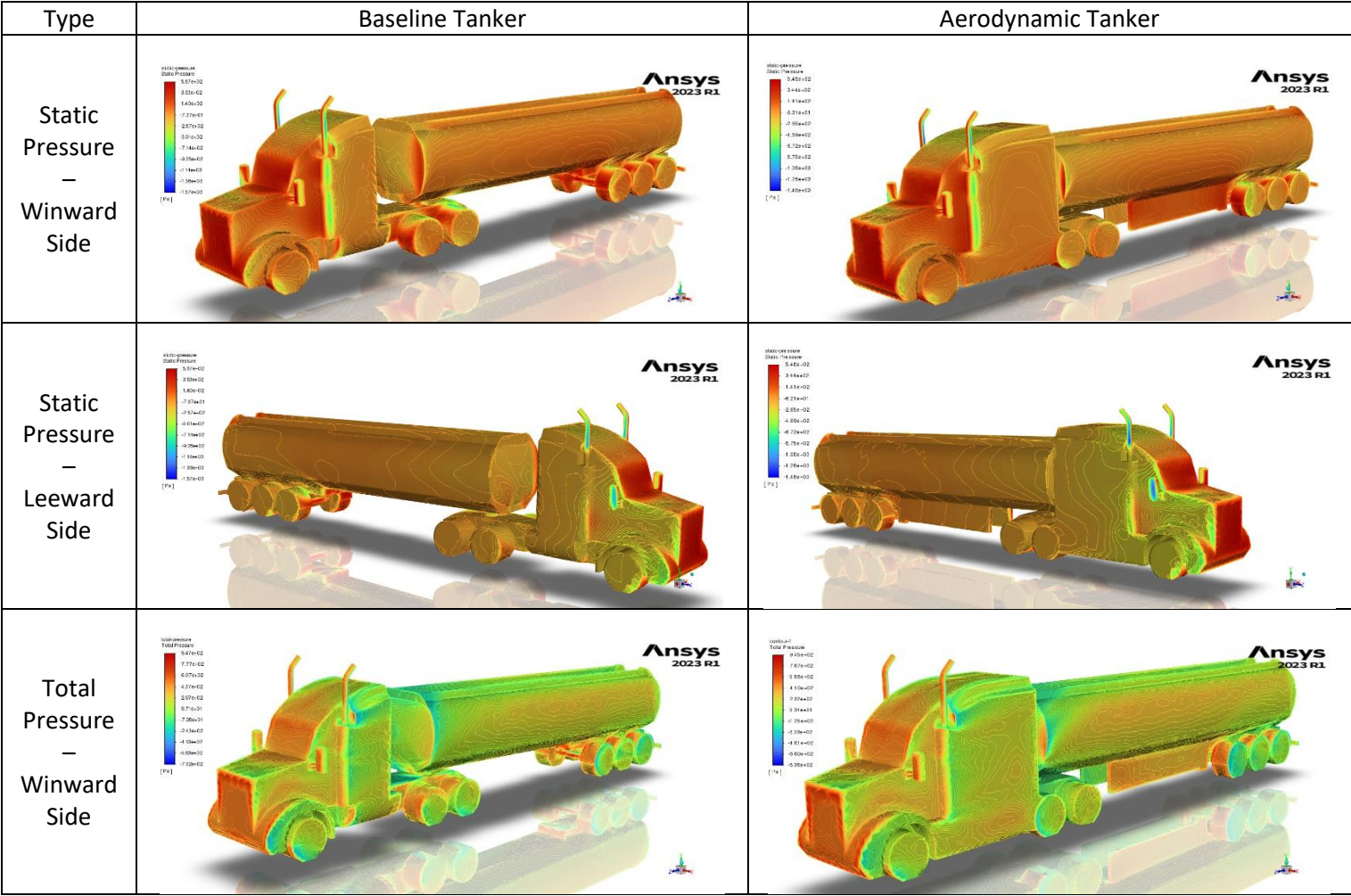




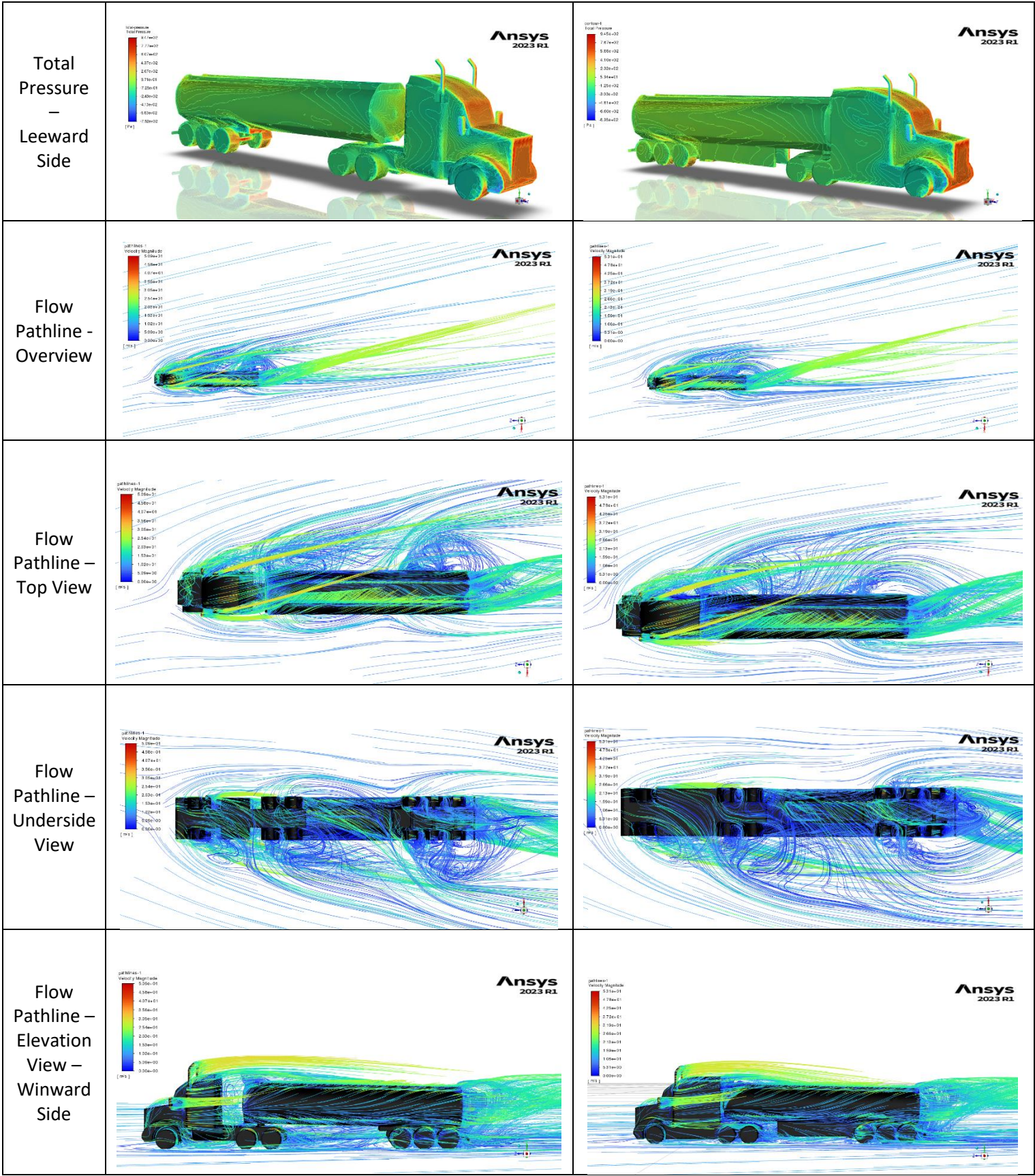




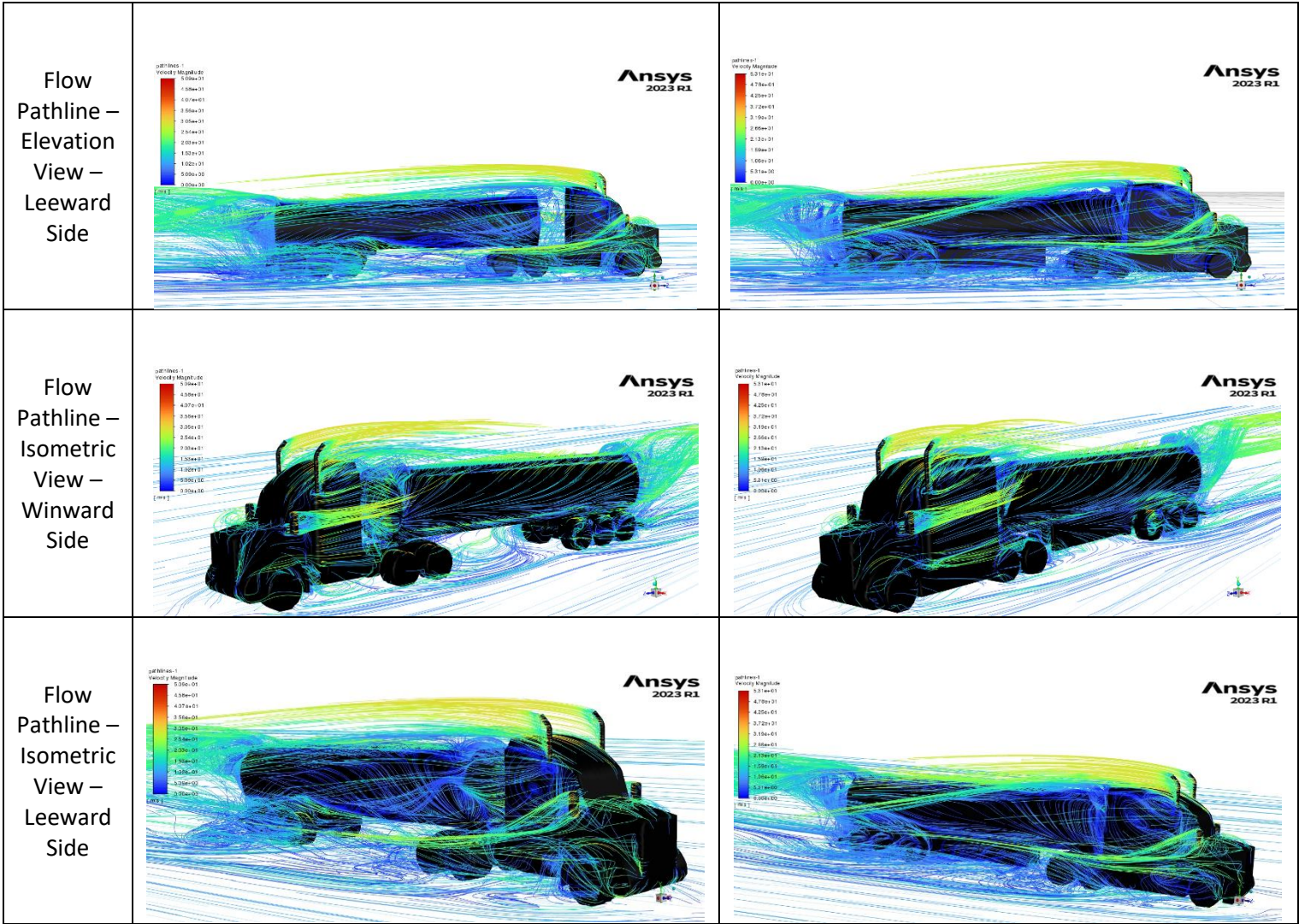
H.8 Pressure Contours and Flow Pathlines of Baseline and Aerodynamic Tankers at 90-Degree Crosswind Angle





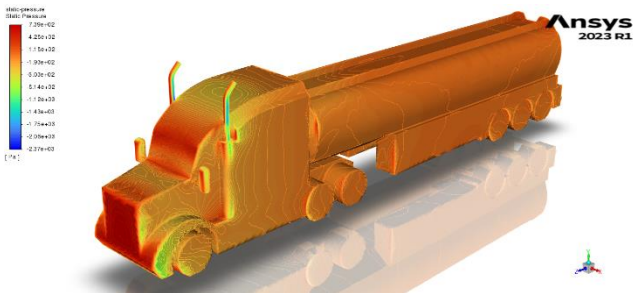
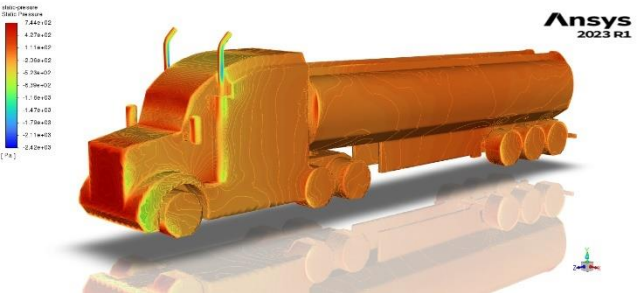
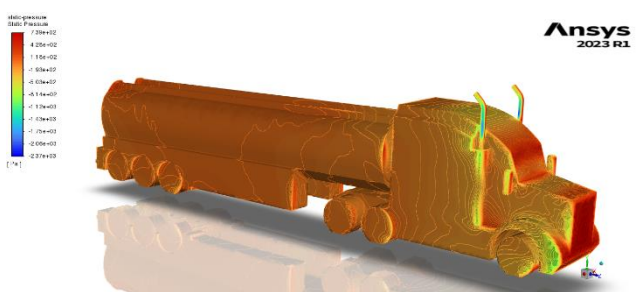
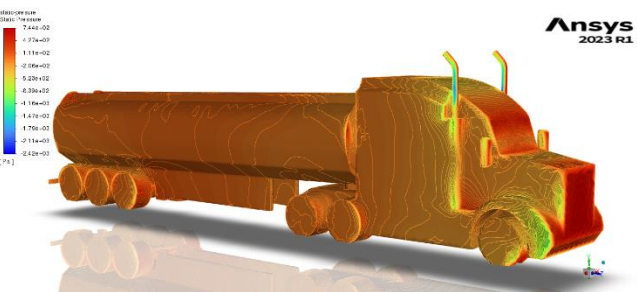
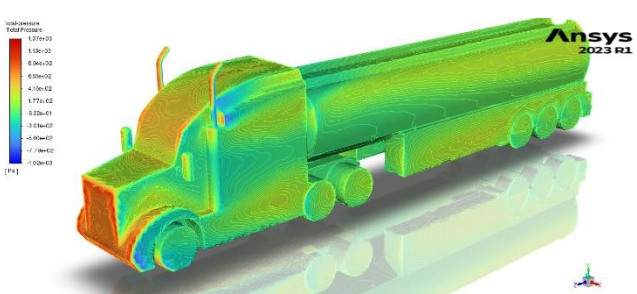
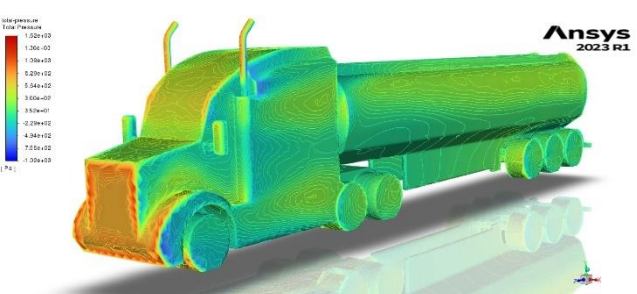
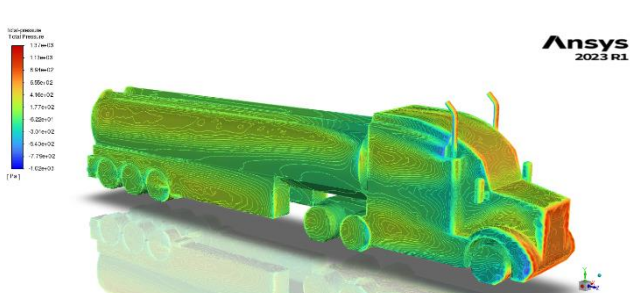
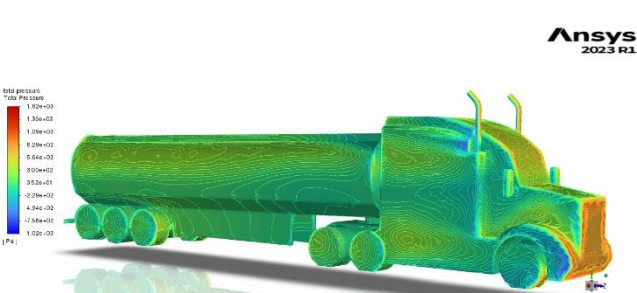




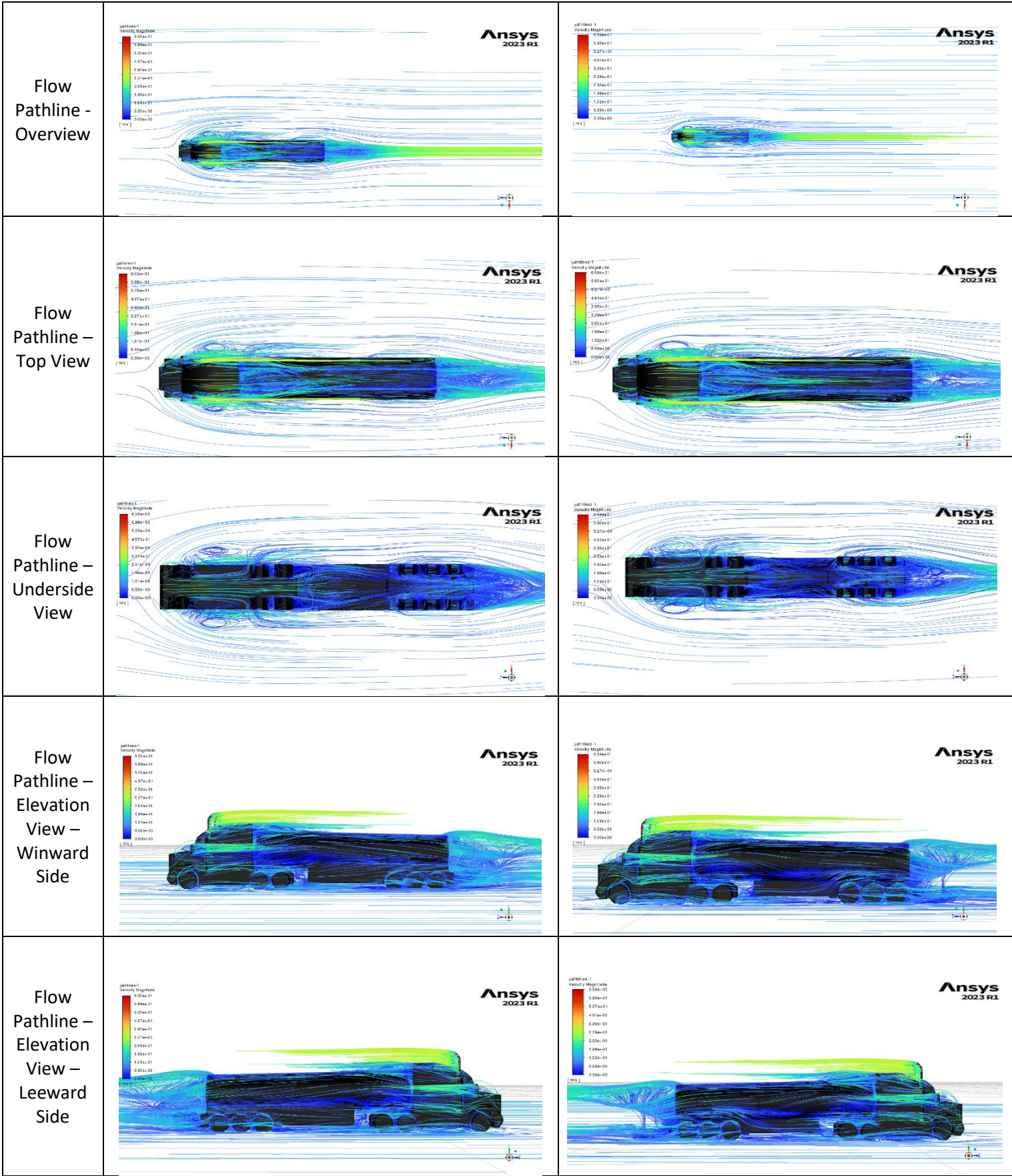


## Appendix I –Modified Aerodynamic and Aerodynamic Tankers Simulation Contours and Pathlines

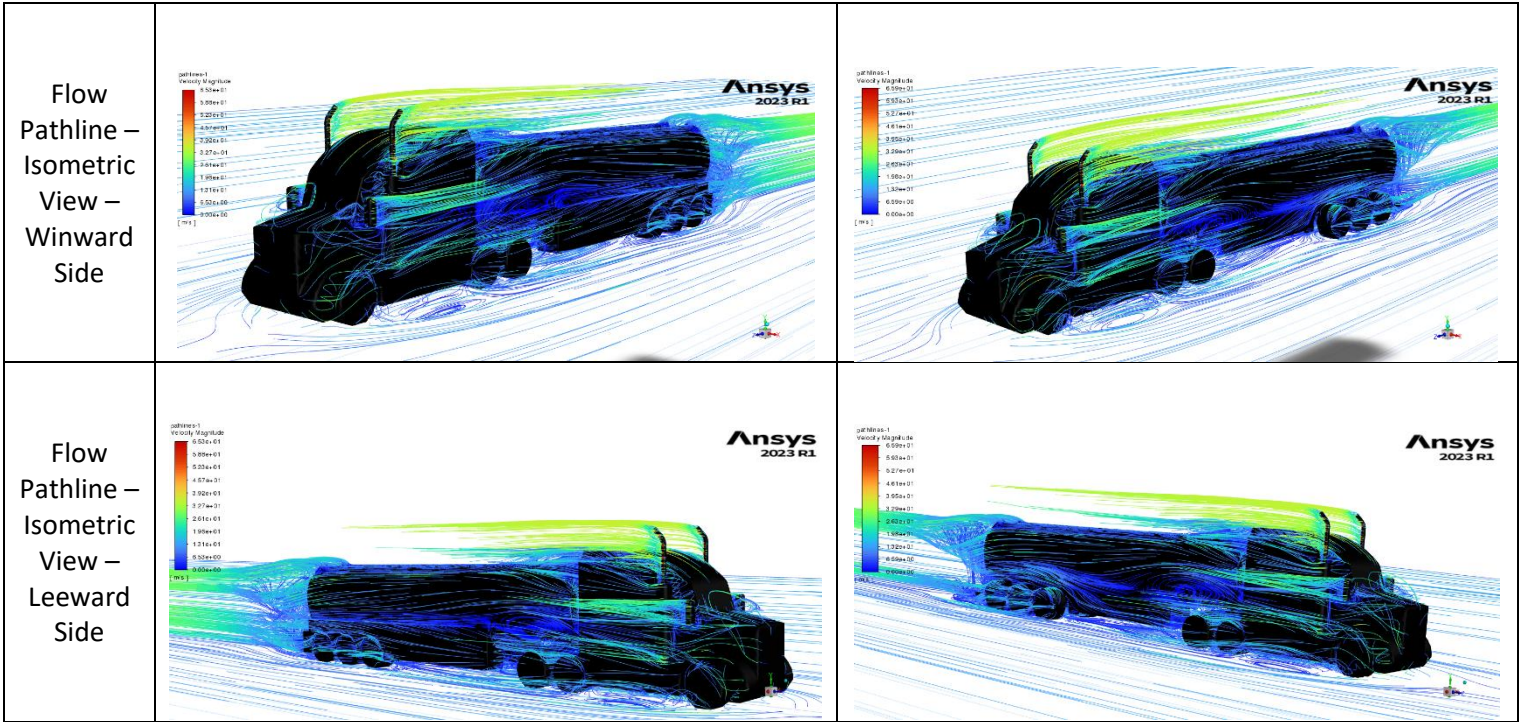
### I.1 Pressure Contours and Flow Pathlines of Modified Aerodynamic and Aerodynamic Tankers at 0-Degree Crosswind Angle

Type	Modified Aerodynamic Tanker	Aerodynamic Tanker
Static Pressure – Winward Side		
Static Pressure – Leeward Side		
Total Pressure – Winward Side		
Total Pressure – Leeward Side		

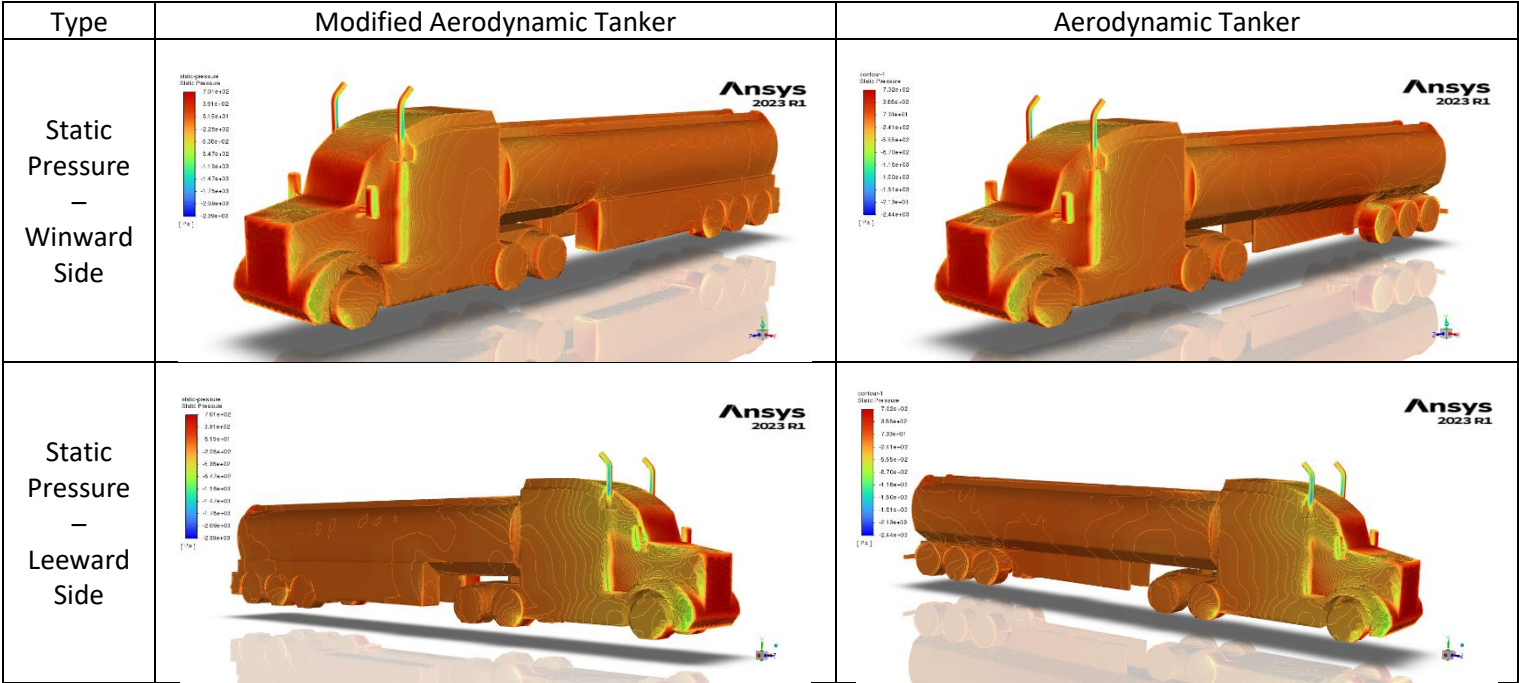




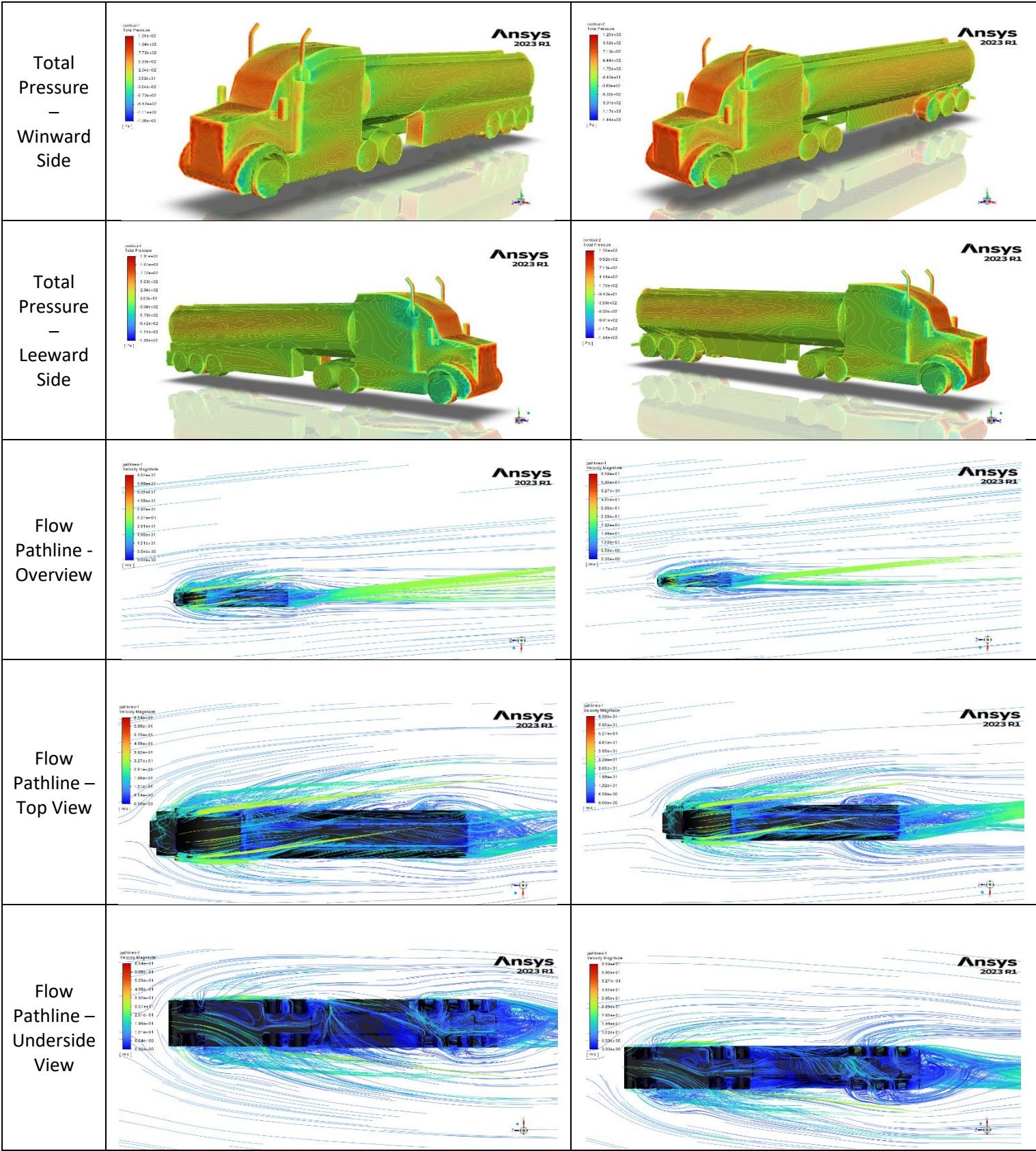




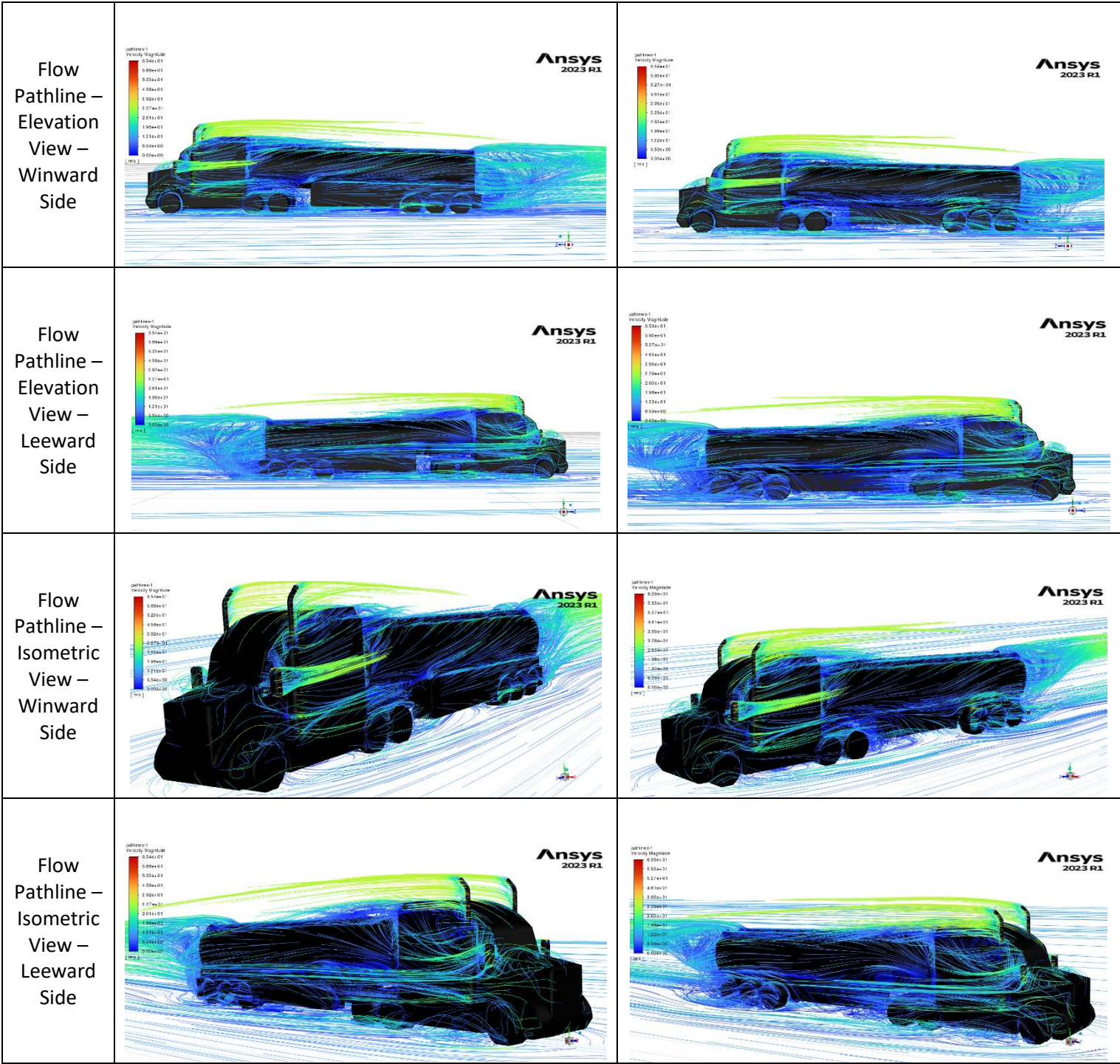
I.2 Pressure Contours and Flow Pathlines of Modified Aerodynamic and Aerodynamic Tankers at 30-Degree Crosswind Angle





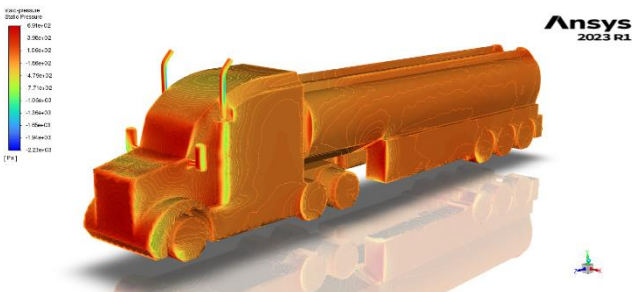
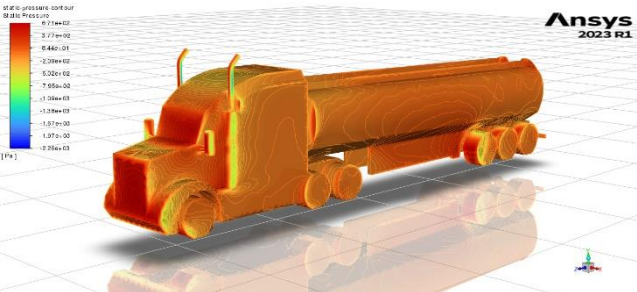
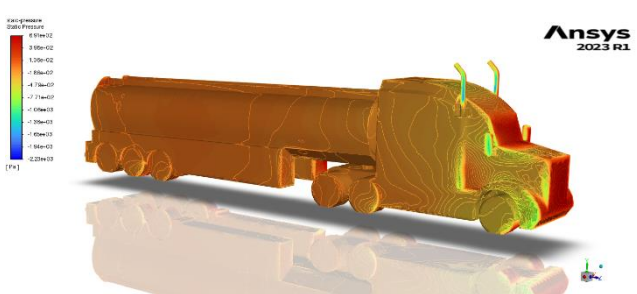
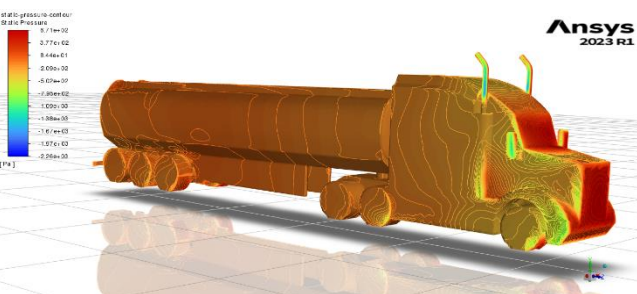
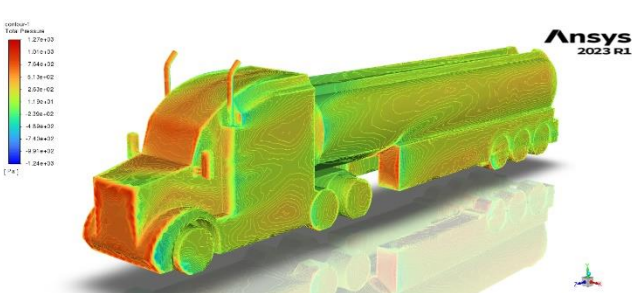
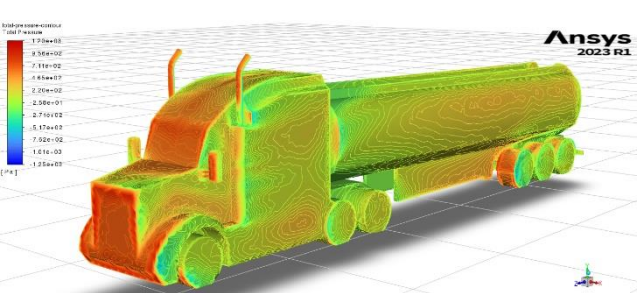
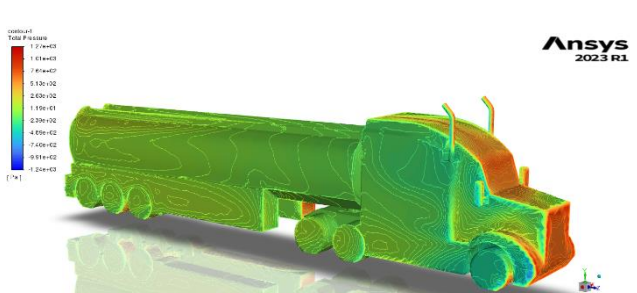
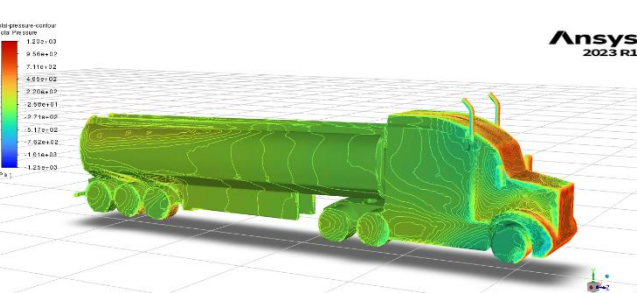
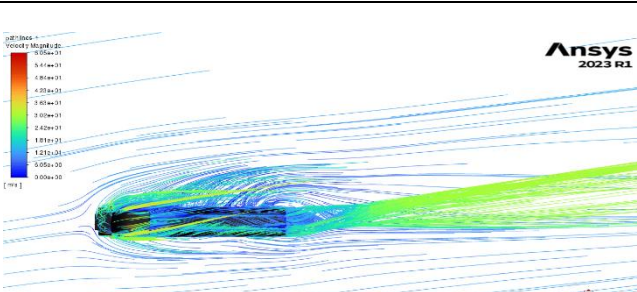
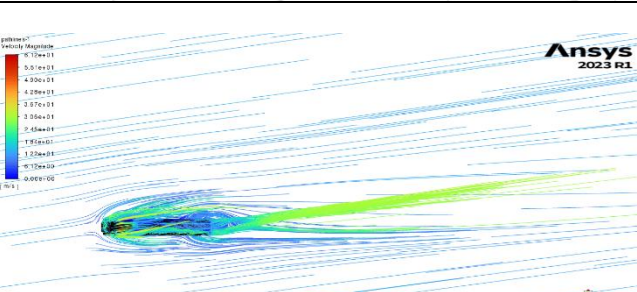




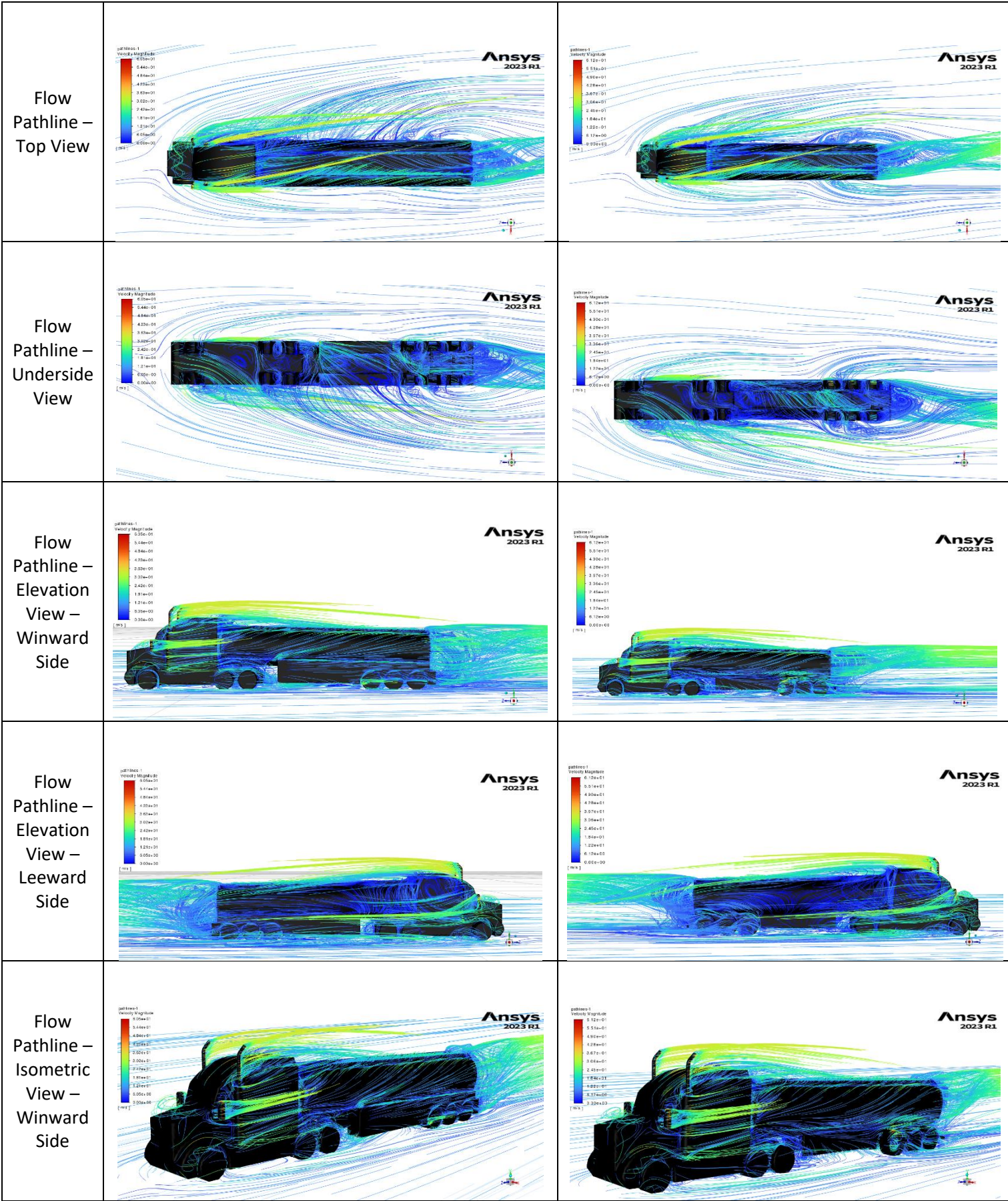




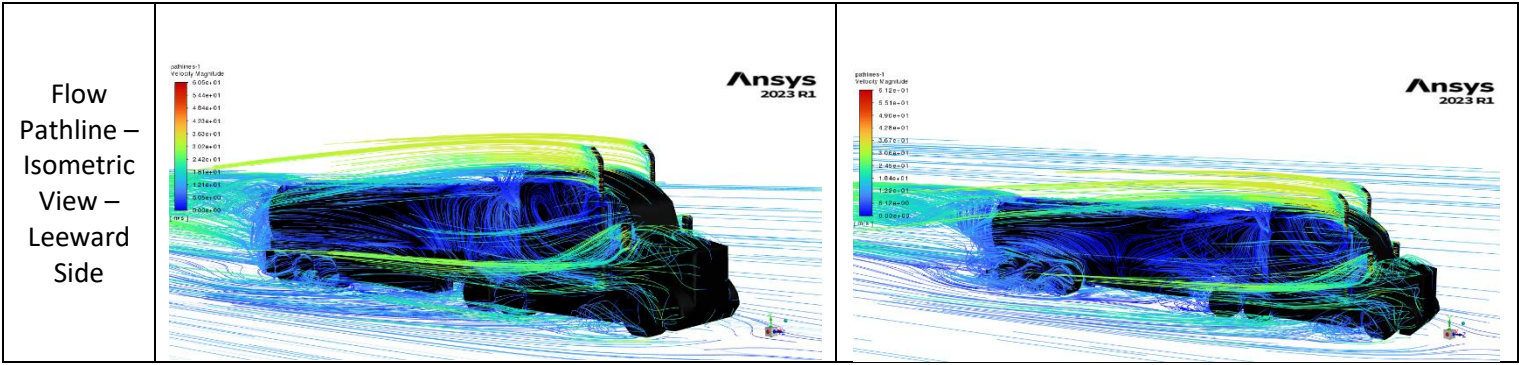
### 1.3 Pressure Contours and Flow Pathlines of Modified Aerodynamic and Aerodynamic Tankers at 45-Degree Crosswind Angle

Type	Modified Aerodynamic Tanker	Aerodynamic Tanker
Static Pressure – Winward Side		
Static Pressure – Leeward Side		
Total Pressure – Winward Side		
Total Pressure – Leeward Side		
Flow Pathline - Overview		





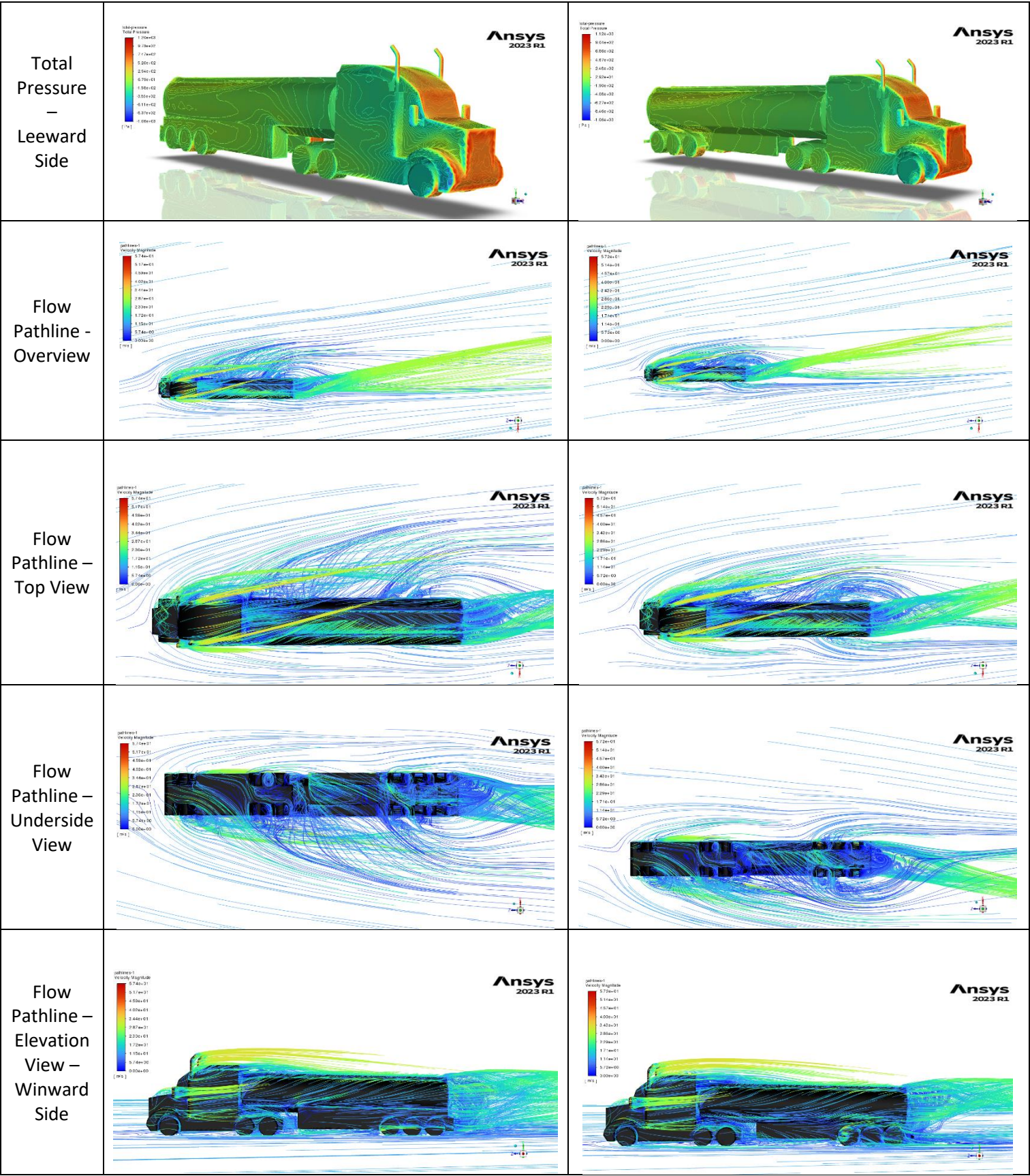




I.4 Pressure Contours and Flow Pathlines of Modified Aerodynamic and Aerodynamic Tankers at 60-Degree Crosswind Angle

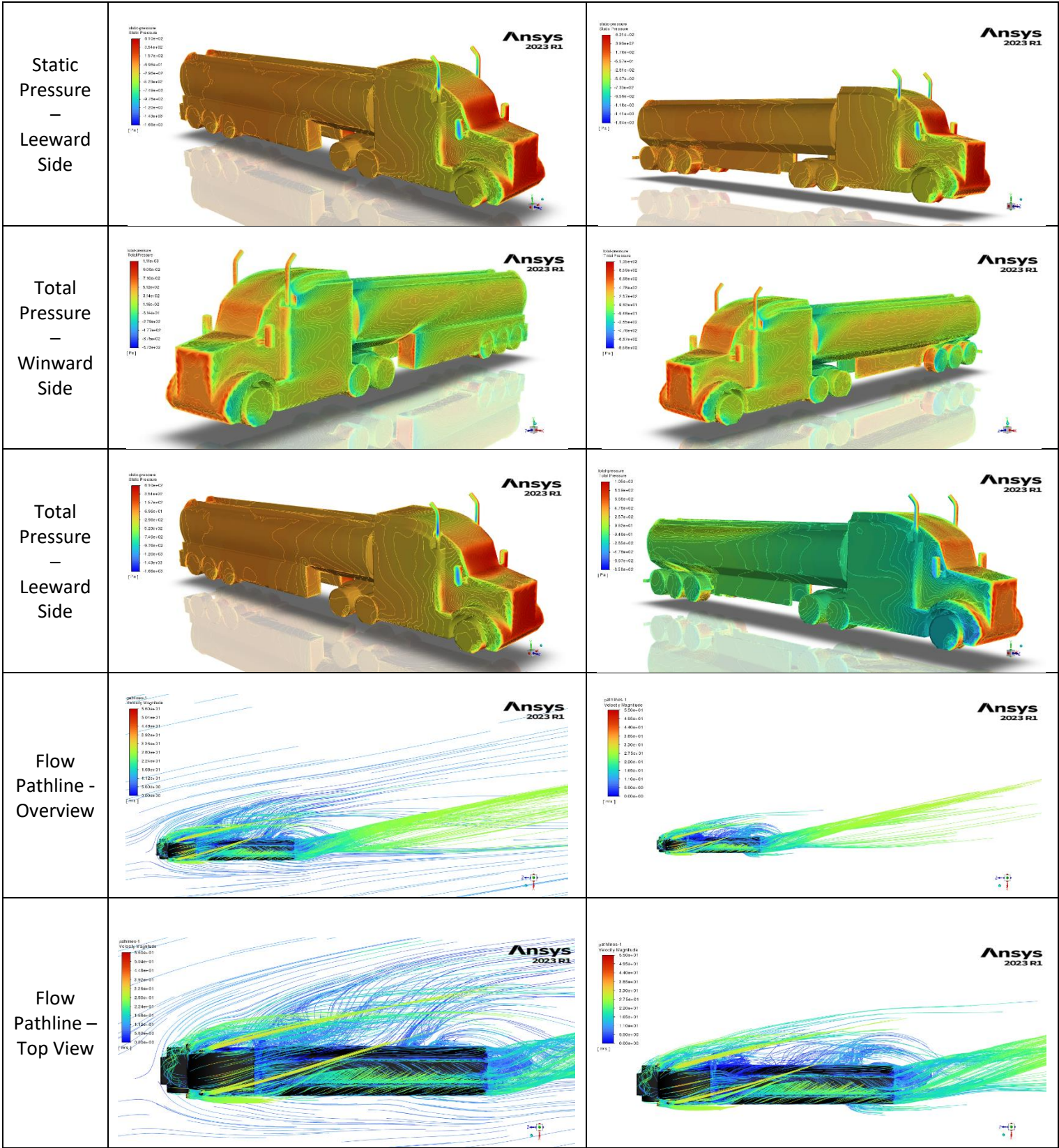
Type	Modified Aerodynamic Tanker	Aerodynamic Tanker
Static Pressure – Winward Side	<p>Ansys 2023 R1</p>	<p>Ansys 2023 R1</p>
Static Pressure – Leeward Side	<p>Ansys 2023 R1</p>	<p>Ansys 2023 R1</p>
Total Pressure – Winward Side	<p>Ansys 2023 R1</p>	<p>Ansys 2023 R1</p>



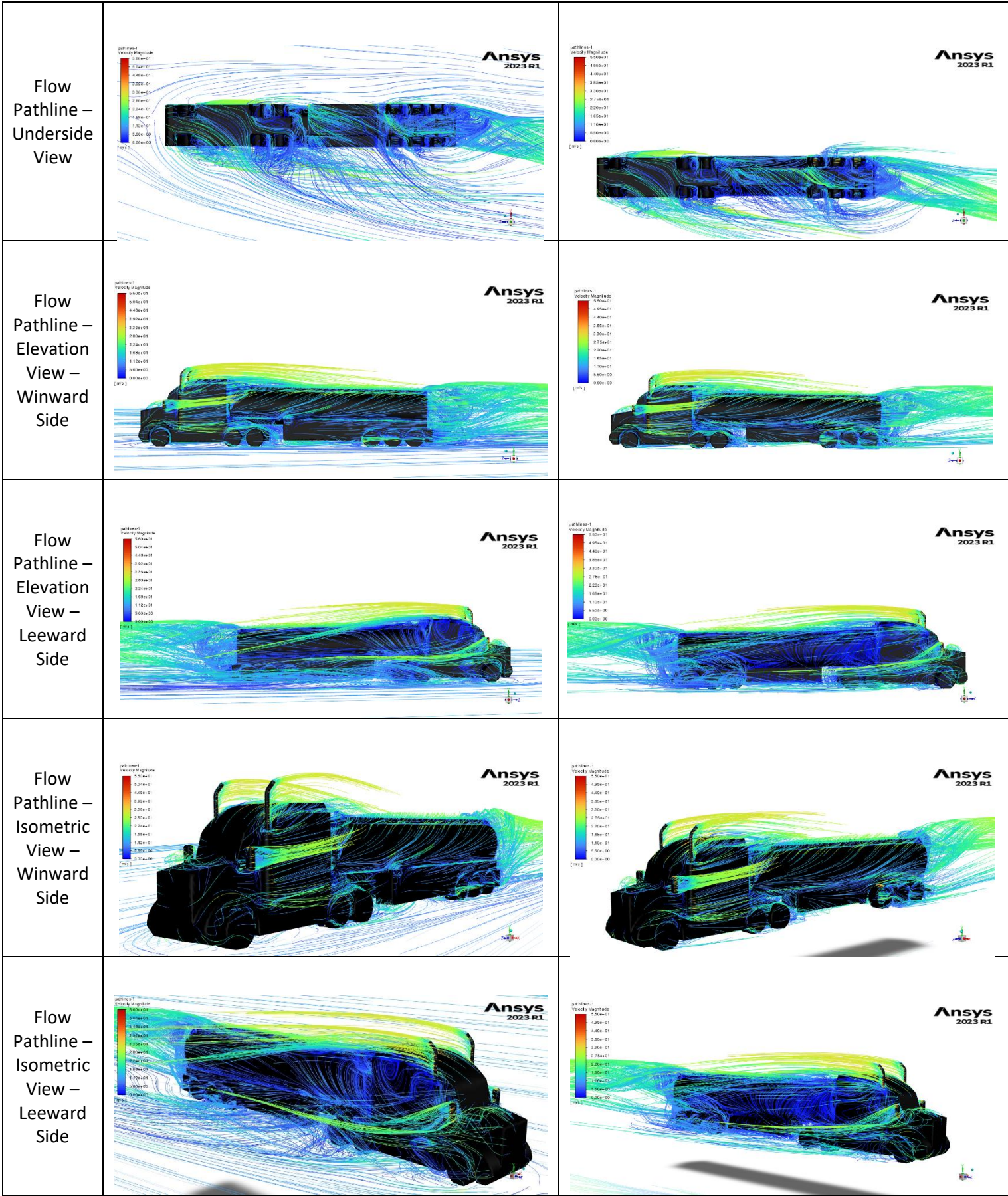




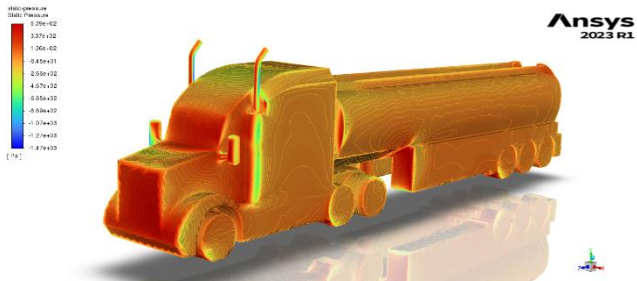
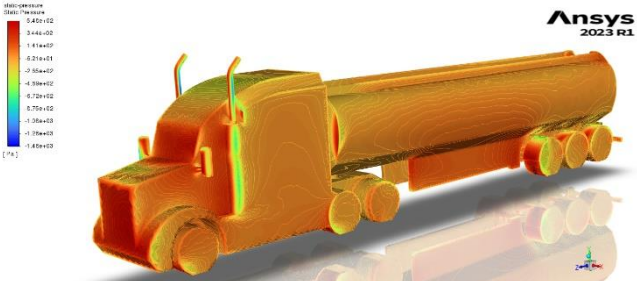
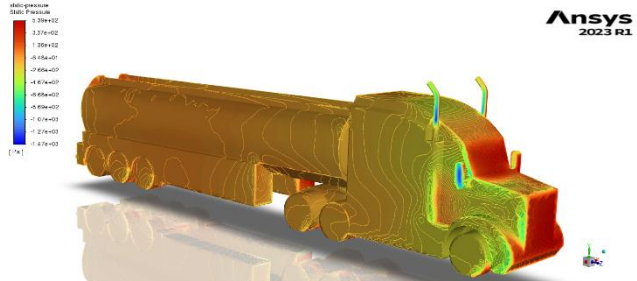
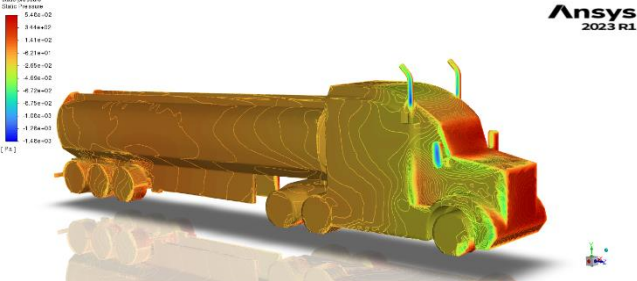
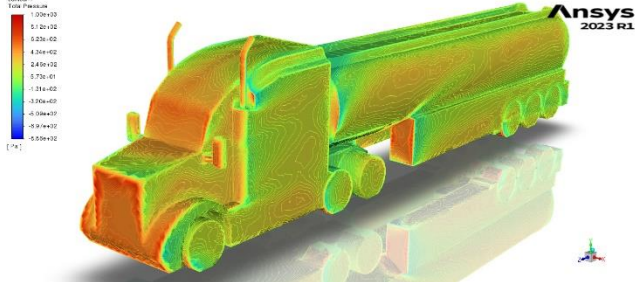
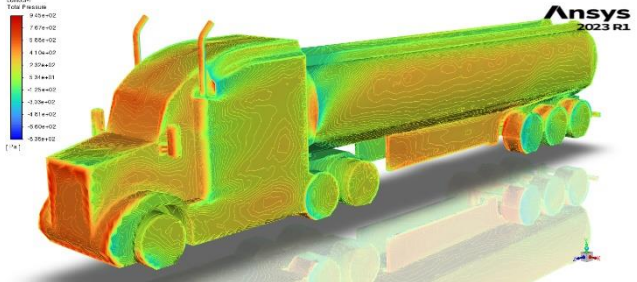
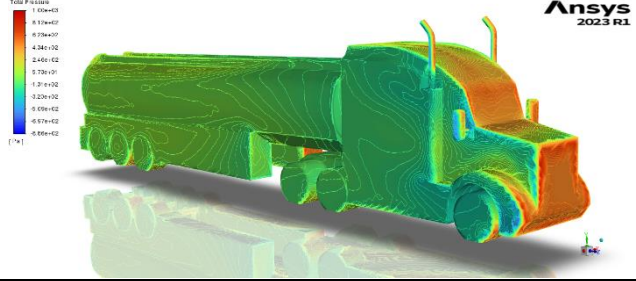
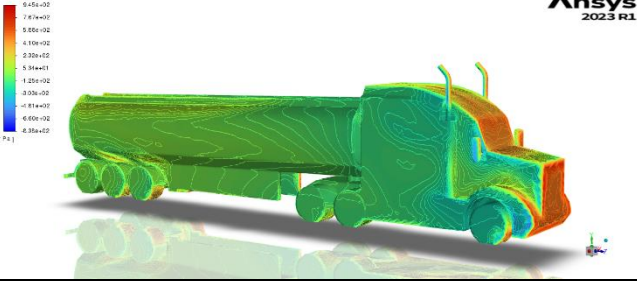




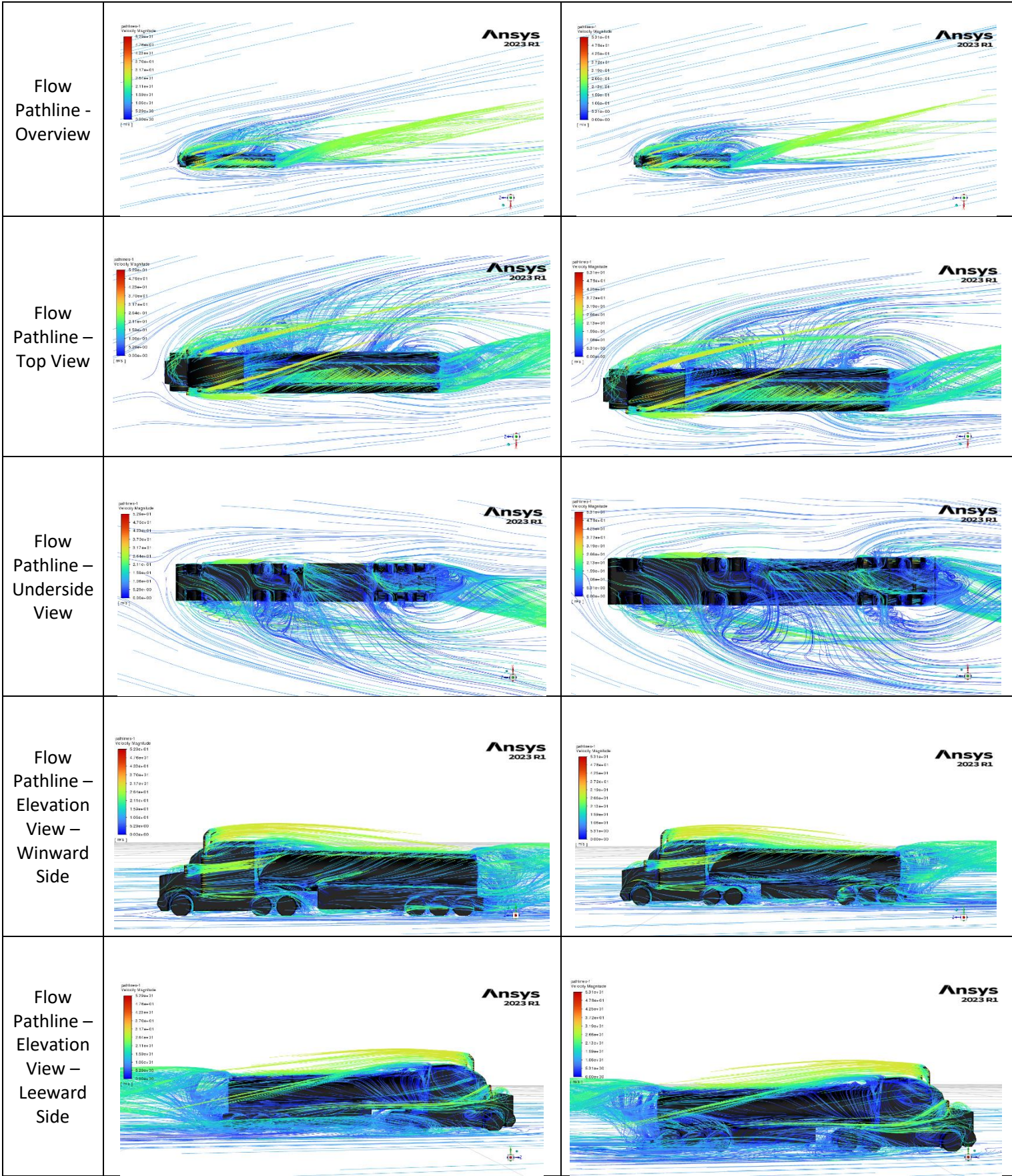




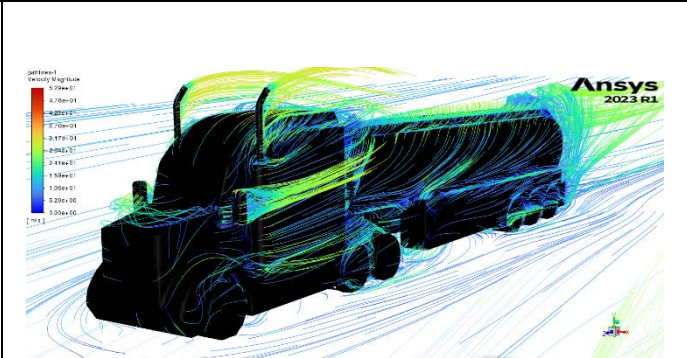
## I.6 Pressure Contours and Flow Pathlines of Modified Aerodynamic and Aerodynamic Tankers at 90-Degree Crosswind Angle

Type	Modified Aerodynamic Tanker	Aerodynamic Tanker
Static Pressure – Winward Side		
Static Pressure – Leeward Side		
Total Pressure – Winward Side		
Total Pressure – Leeward Side		





Flow  
Pathline –  
Isometric  
View –  
Winward  
Side



Flow  
Pathline –  
Isometric  
View –  
Leeward  
Side

